

2004

A MECHANISTIC STUDY TO IDENTIFY PHYSICALLY STABLE AMORPHOUS SOLID DISPERSION

Madhav Vasanthavada
University of Rhode Island

Follow this and additional works at: https://digitalcommons.uri.edu/oa_diss

Terms of Use

All rights reserved under copyright.

Recommended Citation

Vasanthavada, Madhav, "A MECHANISTIC STUDY TO IDENTIFY PHYSICALLY STABLE AMORPHOUS SOLID DISPERSION" (2004). *Open Access Dissertations*. Paper 193.
https://digitalcommons.uri.edu/oa_diss/193

This Dissertation is brought to you by the University of Rhode Island. It has been accepted for inclusion in Open Access Dissertations by an authorized administrator of DigitalCommons@URI. For more information, please contact digitalcommons-group@uri.edu. For permission to reuse copyrighted content, contact the author directly.

A MECHANISTIC STUDY TO IDENTIFY PHYSICALLY STABLE AMORPHOUS
SOLID DISPERSION
BY
MADHAV VASANTHAVADA

A DISSERTATION SUBMITTED IN PARTIAL FULFILLMENT OF THE
REQUIREMENTS FOR THE DEGREE OF
DOCTOR OF PHILOSOPHY
IN
APPLIED PHARMACEUTICAL SCIENCES

UNIVERSITY OF RHODE ISLAND

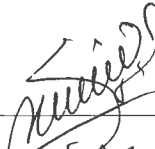
2004

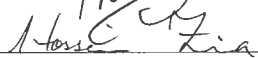
DOCTOR OF PHILOSOPHY DISSERTATION
OF
MADHAV VASANTHAVADA

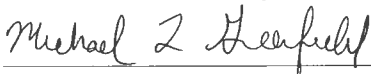
APPROVED:


Dissertation Committee

Major Professor _____









DEAN OF THE GRADUATE SCHOOL

UNIVERSITY OF RHODE ISLAND
2004

ABSTRACT

Amorphous solid dispersions are known to improve the oral bioavailability of poorly water-soluble drugs. However, the physical instability of solid dispersions leading to phase separation and subsequent crystallization is limiting their commercial use. Polymers used in solid dispersions have shown to inhibit drug crystallization by either increasing the glass transition temperature (T_g) of the mixture; and/or by interacting with the drug. To effectively inhibit drug crystallization, the polymer has to remain miscible with the drug. Drug crystallization could occur if drug-carrier miscibility is adversely affected by heat or humidity. It is therefore important to understand the drug-carrier miscibility to define strategies for ensuring the physical stability of amorphous solid dispersions.

In this study, an approach is presented with which one can determine the “solid solubility”, defined as the amount of drug that remains miscible with the carrier under specified heat and humidity condition. Modulated differential scanning calorimeter (MDSC) was used to determine the solid solubility of trehalose, griseofulvin, and indoprofen, in amorphous polymers like PVP and dextran. Solid dispersions that exhibit single T_g , were exposed to accelerated storage conditions and their T_g (s) were monitored periodically. An increase in T_g or the formation of multiple T_g s indicated the phase separation of drug from the polymer. The T_g was monitored until a plateau was reached, indicating an equilibrium state and no further phase separation. The solid solubility of

drug in the polymer was determined from the calibration plot of T_g of freshly prepared solid dispersion vs. drug-polymer ratio.

The mechanism of solid solubility was elucidated and hydrogen bonding was shown to play a critical role in enhancing the solid solubility. Indoprofen that hydrogen bonds to PVP had solid solubility of 13%w/w, whereas griseofulvin which had no hydrogen bonding to the polymer crystallized completely from the solid dispersions when stored at accelerated conditions of 40°C and 69% relative humidity. In the case of trehalose and dextran miscible solid dispersions the solid solubility of trehalose seemed to decrease with increasing storage temperatures and moisture levels. The kinetic rate of indoprofen and griseofulvin phase separation from the polymer was estimated by fitting the T_g of miscible mixtures, to the first-order rate equation. The phase separation rate of indoprofen was found to be at least 10 times lower than that of griseofulvin.

The effect of surfactants on the drug solid solubility in the polymer was also investigated. To probe into the factors responsible for physical instability of amorphous solid dispersions, the molecular mobility of a model drug-griseofulvin and the polymer-PVP was studied. Isothermal and non-isothermal crystallization studies were conducted on griseofulvin to determine the activation energy for crystallization. Molecular mobility of PVP was studied using thermally stimulated current spectroscopy and the factors influencing the molecular motions were studied.

KEY WORDS: Amorphous, glass transition, molecular mobility, thermal analysis, solid dispersions.

ACKNOWLEDGMENTS

I express my deepest gratitude to Professor M. Serpil Kislalioglu for acting as my major advisor. She has not only guided me during the program with her valuable suggestions but has also encouraged me to plan and implement my research activities independently. She has been very understanding and supportive during my graduate student-life hurdles and I shall always remain thankful to her.

This dissertation was conducted entirely in the research and development laboratories of Novartis Pharmaceuticals Corporation, East Hanover, New Jersey from January 2002 – July 2004. I would like to express my sincere gratitude to Dr. Yatindra Joshi (Vice-President, Pharmaceutical and Analytical Development) who made my Novartis Graduate Research Fellowship possible, and also guided me as a co-advisor. Dr. Joshi is a person with sound fundamental knowledge and an ability to critically evaluate research findings. I admire him for his enthusiasm and dedication to conduct high-quality pharmaceutical research at Novartis. I am extremely delighted for the offer made to me as a Senior Scientist by Novartis Pharmaceuticals.

I very much appreciate the invaluable technical support of Dr. WeiQin (Tony) Tong (Director, Pharmaceutical Development) and thank him for considering me as a part of his team.

I thank Dr. Zeren Wang (presently at Boehringer Ingelheim Corporation) for his valuable support during the initial course of my research. I would also like to thank Dr. Abu Serajuddin, Dr. Alan Royce and Dr. Madhu Pudipeddi for sharing their knowledge with me during my summer internship at Novartis Pharmaceuticals (May '01-Sept. '01). Many thanks to Dr. Sudha Vippagunta for the helpful discussion. I also thank Drs. Erika Zannou, Ping Li, Shoufeng Li, Hanchen Lee, Ms. Sonali Bose, Ms. Yu Cao (Jade), Ms. Jennifer Snyder, Mr. Amol Matharu, and many others in Pharmaceutical Development at Novartis for the wonderful time I was able to share with them.

I will always be thankful for the very-first financial assistance I received from the Department of Chemistry at URI. The teaching assistantship helped me boost my self-confidence in a foreign land. I also would like to thank my friends Satish, Jyothsna, Ravi and Madhu in India who helped making my entry into the United States possible. I miss those golden moments spent with Mangesh, Neelam, Vishwa, and Anasuya in the D-415 graduate village apartment. It was really kind of Kajal and Mangesh to always welcome me to their home during my short visits from NJ to URI, despite short notices! I thank my friends from SVCPS first batch (Satish, Ganesh, Soi, Madhu, Manoj and many) for always cheering in my growth and helping me maintain a positive outlook.

I want to thank Dr. Hossein Zia, (Department of Applied Pharmaceutical Sciences, URI) and Dr. Michael Greenfield (Department of Chemical Engineering, URI) for serving on my Ph.D. dissertation committee. Ms. Kathleen Hayes (Secretary, Department of Applied Pharmaceutical Sciences) for her support whenever I needed.

My heartiest thanks to my loving father V.B.R. Murthi, and my mother V. Girija. It is a result of their sacrifices that has enabled me to receive good standards of education that I am benefiting this day. My brother Keshav, my sister Padmaja, and my brother-in-law Saty, have always showered their love and encouragement. I also consider myself very fortunate for having an ever-loving wife Anasuya. She has stood by me through the thick-and-thin of my Ph.D. program and I cannot thank her enough for that.

I dedicate this thesis to my loving parents and my dearest wife.

Above all, I thank The ALMIGHTY for having given me the power of truth, wisdom, courage, strength and perseverance to face the challenges during this journey.

I shall try to deliver the values I learnt during my program to the best of my abilities!

PREFACE

This work has been prepared in accordance with the manuscript format option for dissertation preparation, as outlined in section 11-3 of The Graduate Manual of The University of Rhode Island. The entire dissertation has been divided into three sections.

Section A contains the introduction of the thesis, which describes the subject of this dissertation, the need to conduct research in the chosen area and the specific objectives of the research.

Section B is comprised of five manuscripts and forms the heart of the dissertation. It contains the significant findings of the research and discusses them in detail. Each manuscript has been presented in the format required by the journal to which they have been accepted, or they will, or have been submitted. Each manuscript has an abstract pertaining to that chapter, followed by introduction, the materials and methods used and have a conclusion along with the cited references. The figures and tables have been provided at the end of respective manuscript.

Section C contains six appendices. Except for the first appendix, the last five appendices provide additional information that is essential to, but not usually included for publications in the manuscripts. Each appendix contains supporting data corresponding to individual manuscript chapter and has been designated accordingly. This dissertation closes with a complete listing of all the works cited in this dissertation, arranged in alphabetical order by the author's last name.

<u>TABLE OF CONTENTS</u>	<u>PAGE</u>
ABSTRACT.....	ii
ACKNOWLEDGMENTS.....	iv
PREFACE.....	vii
TABLE OF CONTENTS.....	viii
LIST OF TABLES.....	xi
LIST OF FIGURES.....	xiii
 <u>SECTION A</u>	
OVERALL THESIS INTRODUCTION.....	1
SPECIFIC OBJECTIVES.....	10
 <u>SECTION B</u>	
MANUSCRIPT I:	
PHASE BEHAVIOR OF AMORPHOUS MOLECULAR DISPERSIONS I: DETERMINATION OF THE DEGREE AND MECHANISM OF SOLID MISCIBILITY.....	19
 MANUSCRIPT II:	
PHASE BEHAVIOR OF AMORPHOUS MOLECULAR DISPERSIONS II: ROLE OF HYDROGEN BONDING IN SOLID SOLUBILITY AND PHASE SEPARATION KINETICS.....	50

<u>TABLE OF CONTENTS</u>	<u>PAGE</u>
MANUSCRIPT III:	
PHASE BEHAVIOR OF AMORPHOUS MOLECULAR DISPERSIONS III: CHARACTERIZATION OF THE SURFACTANT EFFECT ON THE SOLID SOLUBILITY OF A DRUG IN A SOLID DISPERSION.....	81
MANUSCRIPT IV:	
MOISTURE EFFECT ON THE KINETICS OF GRISEOFULVIN CRYSTALLIZATION.....	112
MANUSCRIPT V:	
MEASUREMENT OF SUB-GLASS TRANSITION MOLECULAR MOTIONS OF POLY(VINYLPYRROLIDONE); COMPARISON OF THE UTILITY OF THERMALLY STIMULATED CURRENT (TSC) AND MODULATED DIFFERENTIAL SCANNING CALORIMETER (MDSC).....	155
<u>SECTION C</u>	
APPENDIX A.....	197
APPENDIX B.....	202
APPENDIX C.....	248
APPENDIX D.....	273
APPENDIX E.....	277
APPENDIX F.....	294
BIBLIOGRAPHY.....	302

LIST OF TABLES

<u>TABLE</u>	<u>TITLE</u>	<u>PAGE</u>
<u>SECTION A:</u>		
A-I	Nature of drug dispersed in the polymeric matrix.....	16
A-II	Physical Stability of Solid Dispersions.....	17
<u>SECTION B:</u>		
MANUSCRIPT I		
B-I-I	Effect of storage conditions on thermal behavior of selected trehalose-dextran mixtures.....	39
B-I-II	Solid solubility of trehalose in the polymers used as a function of storage condition.....	40
MANUSCRIPT II		
B-II-I	Physical chemical properties of griseofulvin and indoprofen.....	72
B-II-II	Drug-to-polymer ratio and kinetics of phase separation of drugs from solid dispersions at 40°C/69%RH.....	73
MANUSCRIPT III		
B-III-I	Surfactant effect on the morphology and thermal properties of griseofulvin and PVP solid dispersions.....	96

<u>TABLE</u>	<u>TITLE</u>	<u>PAGE</u>
MANUSCRIPT IV		
B-IV-I	Methods used in isothermal crystallization studies.....	137
B-IV-II	HPLC assay to assess griseofulvin degradation during melt-quench process.....	139
B-IV-III	List of various solid-state transformation kinetic rate mechanisms and their equations.....	140
B-IV-IV	Hancock-Sharp fit of the experimental data and the Isothermal crystallization rate constants as a function of relative humidity.....	141
MANUSCRIPT V		
B-V-I	Characterization of relaxation temperatures in PVP.....	178
B-V-II	Average relaxation time constants obtained from enthalpy relaxation measurements.....	179

LIST OF FIGURES

<u>FIGURE</u>	<u>TITLE</u>	<u>PAGE</u>
<u>SECTION A:</u>		
A-1	Depiction of glass transition temperature in amorphous solids.....	18
<u>SECTION B:</u>		
MANUSCRIPT I		
B-1-1	DSC total heat flow scans of trehalose and dextran.....	41
B-1-2	MDSC scans of trehalose-dextran and trehalose-PVP mixtures.....	42
B-1-3	MDSC scans of trehalose-dextran mixtures exposed to 50°C/ 75% RH conditions.....	44
B-1-4	Plot of T_{g2} of trehalose-dextran mixtures: at different storage conditions.....	46
B-1-5	Percent crystalline trehalose dihydrate present in trehalose-dextran mixtures.....	47
B-1-6	Hypothetical depiction of solid solubility between trehalose and dextran	48
B-1-7	Enthalpy of mixing (ΔH_{mix}) and free energy of mixing (ΔG_{mix}) of trehalose-dextran and trehalose-PVP.....	49

<u>FIGURE</u>	<u>TITLE</u>	<u>PAGE</u>
MANUSCRIPT II		
B-II-1	Chemical structures of griseofulvin, indoprofen and PVP.....	74
B-II-2	MDSC scans of solid dispersions of PVP- griseofulvin and PVP- indoprofen.....	75
B-II-3	Infrared spectra of solid dispersions and physical mixtures of griseofulvin-PVP and indoprofen-PVP.....	76
B-II-4	MDSC scans of solid dispersions exposed to 40°C / 69% RH for different time intervals.....	77
B-II-5	Changes in the glass transition temperatures of griseofulvin-PVP and indoprofen-PVP solid dispersions.....	79
B-II-6	X-ray diffraction patterns of solid dispersions and physical mixtures of griseofulvin-PVP and indoprofen-PVP.....	80
MANUSCRIPT III		
B-III-1	Chemical structures of griseofulvin, PVP and Sucrose Stearate.....	97
B-III-2	MDSC scans of solid dispersions of sucrose stearate and PVP.....	98
B-III-3	FT-IR spectra of solid dispersions and physical mixtures of sugar ester and PVP.....	99
B-III-4	MDSC heat flow scans of solid dispersions of griseofulvin and sucrose stearate.....	100

<u>FIGURE</u>	<u>TITLE</u>	<u>PAGE</u>
B-III-5	FT-IR spectra in solid dispersions and physical mixtures of sugar ester and griseofulvin.....	101
B-III-6	X-ray diffraction pattern of griseofulvin-PVP solid dispersions.....	102
B-III-7	X-ray diffraction pattern of ternary solid dispersion of PVP / griseofulvin/ sucrose stearate.....	103
B-III-8	MDSC scans of ternary solid dispersions of PVP, griseofulvin and sucrose stearate.....	105
B-III-9	T _g values of ternary solid dispersions.....	108
B-III-10	Ternary phase diagram of PVP, griseofulvin and sucrose stearate.....	109
B-III-11	Determination of solid solubility of griseofulvin in PVP in the presence of sucrose stearate.....	110
MANUSCRIPT IV		
B-IV-1	Chemical structure of griseofulvin.....	142
B-IV-2	X-ray diffraction patterns of griseofulvin untreated (crystalline) and melt-quench treated (amorphous).....	143
B-IV-3	X-ray diffraction patterns of repetitions (n=4) of 1:1 physical mixtures of amorphous and crystalline griseofulvin.....	144
B-IV-4	X-ray diffraction calibration plot.....	145

<u>FIGURE</u>	<u>TITLE</u>	<u>PAGE</u>
B-IV-5	DSC heat flow scans of amorphous and crystalline griseofulvin.....	146
B-IV-6	MDSC non-reversing heat flow scans of physical mixtures of crystalline and amorphous griseofulvin.....	147
B-IV-7	DSC calibration plot of percentage amorphous griseofulvin vs. heat of recrystallization.....	148
B-IV-8	MDSC heat flow scans of amorphous griseofulvin as a function of storage time.....	149
B-IV-9	Percentage griseofulvin crystallized as a function of storage time upon storing at 23°C with 43% RH; 32% RH; and 0% RH.....	150
B-IV-10	MDSC non-reversing heat flow scans of amorphous griseofulvin as a function of heating rate.....	151
B-IV-11	Hancock-Sharp fit of the experimental data to determine the <i>m</i> values.....	152
B-IV-12	Fit of the stability data to the KJMA equation to determine the isothermal crystallization rate constant for amorphous griseofulvin...	153
B-IV-13	Determination of the non-isothermal E_{act} values for crystallization of amorphous griseofulvin by using Kissinger analysis.....	154
 MANUSCRIPT V 		
B-V-1	Schematic representation of the glass transition temperature (T_g) and loss in enthalpy of amorphous samples during aging.....	180

<u>FIGURE</u>	<u>TITLE</u>	<u>PAGE</u>
B-V-2	Experimental protocol for conducting enthalpy relaxation (MDSC) and mobility recovery (TSPC) experiments.....	181
B-V-3	Schematic demonstration of the principle of Thermally Stimulated Currents. (b) Schematic demonstration of the glass transition phenomenon in typical thermally stimulated depolarization current experiment.....	182
B-V-4	MDSC heat capacity scans of PVP demonstrating the T_g and the heat- capacity step change at T_g . (b) Thermally Stimulated depolarization currents of PVP K30 demonstrating two different global relaxation peaks: P_1 and P_2	183
B-V-5	MDSC non-reversing heat flow scans demonstrating the enthalpy relaxation of PVP with storage time at 15°C below the respective T_g : for PVP K17; PVP K30; and PVP K90.....	185
B-V-6	Enthalpy relaxation of PVP obtained using MDSC with storage time at 15°C below the respective T_g for PVP K17; PVP K30; and PVP K90.....	188
B-V-7	Variation of logarithm of relaxation time constant (τ) with scaled temperature T_g/T_a , obtained using fitting the enthalpy relaxation data to the empirical KWW stretched non-exponential equation.....	189
B-V-8	Thermally stimulated polarization currents of PVP K17; and PVP K30 undergoing structural relaxation at $T_g-15^\circ\text{C}$	190
B-V-9	Modified experimental protocol for structural relaxation of thermally stimulated polarization currents.....	191

<u>FIGURE</u>	<u>TITLE</u>	<u>PAGE</u>
B-V-10	Thermally stimulated polarization currents following the modified experimental protocol for PVP K17, PVP K30 and PVP K90 that wwere aged at Tg-15°C.....	192
B-V-11	TSC net current plotted against the storage time for PVP aged at respective Tg-15°C for PVP K17, K30 and K90.....	195
B-V-12	Relationship between the enthalpy recovery measurements from MDSC and mobility recovery measurements from modified TSPC...	196

SECTION A

Overall Thesis Introduction

Pharmaceutical solid dispersion technology is generally accepted as a technique to enhance the dissolution characteristics of drugs with poor water solubility [1-3]. The drug substance is dispersed in a water soluble inert polymer matrix, sometimes at the molecular level, and the higher surface area due to the presence of polymer may increase the drug solubility and dissolution rate [4]. If the drug is not dispersed on a molecular scale, it is often physically modified from its crystalline to amorphous form during processing [5]. The presence of high-energy amorphous state leads to enhanced dissolution rate and hence bioavailability owing to the lack of crystalline lattice [6]. The prime reason for the increasing popularity of solid dispersion technology for oral solid dosage formulations is the improvement in the solubility and bioavailability of poorly water soluble drugs [7].

Solid dispersion technology: an attractive alternative

For over centuries the water solubility of pharmaceutical drugs was improved by techniques like particle size reduction through grinding [8]. Eventually sophisticated techniques like modification of the chemical structure of drug molecule via pro- drug formation, selection of suitable salt form, and complexation with solubilizing agents generated increasing attention [9]. Lately however, increasing number of highly

lipophilic drug molecules are being synthesized through combinatorial chemistry synthesis program and the conventional techniques are unable to enhance the drug dissolution rate and bioavailability of such hydrophobic drugs [10]. Majority of the drug molecules that are recently entering into the pharmaceutical company pipeline have intrinsic water solubility of less than 1 $\mu\text{g}/\text{mL}$ when compared to conventional 100 $\mu\text{g}/\text{mL}$. Therefore there is a need for newer formulation approaches that could help meet the challenge of providing adequate drug plasma concentration for therapeutic efficacy. Solid dispersion technology proves to be an attractive alternative for such drug molecules.

Conventionally, converting the physical state of drug substance from crystalline to its high-energy amorphous state was used as an approach to improve the drug dissolution performance. This was primarily done since the aqueous solubility of amorphous drug can be as high as 1000 fold greater than the crystalline form [11]. Such an amorphous state, however, is thermodynamically unstable and under certain conditions of temperature and relative humidity during storage it could crystallize [12]. Solid dispersion formulation could be an attractive alternative to stabilize such amorphous drug substances while improving the drug dissolution rate and bioavailability [13].

Solid dispersions: challenges and opportunities

Although solid dispersion technique has generated several research contributions for over four decades, the number of marketed formulations that use this technique is rather disappointing. Only a griseofulvin-poly (ethylene glycol) solid dispersion (Gris-PEG,

Novartis) and a nabilone-povidone solid dispersion (Cesamet, Lilly) were commercially available during the past four decades. There can be various subjective reasons for such a scenario. A drug candidate that is suitable to be formulated via this technique can 'die' during the pharmaceutical pipeline due to reasons like toxicity manifestation, low therapeutic efficacy, chemical instability, extremely low water solubility, and various formulation challenges. However in the case of solid dispersion, the challenges have been on a more generalized scale to prevent commercial products for several years. One of the challenges associated with this technology is the physical instability of the amorphous drug substance dispersed in the polymeric matrix during shelf life storage [14]. Other challenges include the inability to scale-up the solid dosage formulation from the typical small-scale melt-quench, or solvent-evaporation technique; inadequate knowledge of the mechanism of dissolution of drugs from the dosage forms, prevention of crystallization of some drug substances in the gastric fluids; and poor understanding of the *in vitro* /*in vivo* correlation in these dosage forms [7, 15].

The purpose of this dissertation is to address the physical instability of the amorphous drug substance dispersed in the polymeric matrix. Specifically, to understand the crystallization behavior of the amorphous component from solid dispersions during their storage, and to evaluate the factors that could improve the physical stability of these dosage forms.

In this chapter an extensive literature review on the field of solid dispersion is provided, more specifically relating to physical stability issues of amorphous components. The

purpose of this chapter is to increase the appetite of the reader for this field and to get familiarized with some of the latest developments.

Physical state of drug dispersion: amorphous solid solutions

Solid dispersions have been traditionally formulated by heating the physical mixture of drug and carrier to the molten state and solidifying by cooling it either rapidly or slowly. Alternate methods involved dissolving the physical mixtures in a common volatile solvent and evaporating the solvent to obtain the residual dispersion. The solvent can also be spray-dried (organic volatile solvent) or freeze dried (aqueous) to obtain the solid dispersion. Recently supercritical fluid processing and hot melt extrusion are being explored extensively for a large-scale manufacturing of solid dispersion by pharmaceutical companies [16, 17]. Although there are several approaches to formulate solid dispersions, the effect of processing conditions on the physicochemical properties of the overall formulation and the exact physical state of the drug that is dispersed through the polymer is yet to be ascertained. The nature of the drug dispersion i.e. molecular vs. phase segregation, amorphous vs. crystalline and the presence of polymer can influence the overall free energy and the physical stability of the product.

In 1961, Sekiguchi and Obi performed the initial work on pharmaceutical solid dispersion [18]. They classified the physical state of active components in the inert matrix into several groups as depicted in table A-I. The group under which a solid dispersion product would belong is entirely dependent upon the intrinsic property of the drug and carrier. Historically solid dispersions have been preferred in their eutectic form in which the drug

and carrier are dispersed as fine crystalline particles in close proximity to each other. At the eutectic composition, as indicated by the depression in melting temperature of the fused material, the active component and the carrier have the maximum possible interface with each other. At this composition the active component experiences a maximum increase in the surface area and hence the dissolution rate is enhanced. However with storage time, crystal growth of active component has been reported leading to reduction in surface area and hence dissolution rate [19]. The crystal growth could possibly be inhibited if the carrier is dispersed on a molecular level with the active component. The molecular dispersion is achieved through formation of solid solution. Since a crystalline solid solution is very rare and difficult to formulate, amorphous solid solutions are being investigated as a means for drug crystal inhibition. In amorphous solid solution, the drug and carrier is dispersed on a molecular level leading to an amorphous product that exhibits a single glass transition temperature (T_g). The glass transition temperature is the characteristic feature of the miscible mixture and is generally considered as an indicator of the degree of molecular mobility. In the following sections some fundamental information relating to amorphous forms that is needed to address physical stability aspects is provided.

Glass transition temperature (T_g)

In order to elaborate the glass transition phenomenon, let us examine closely into the thermodynamics of molecular motion of a crystalline material that is liquefied and is maintained above its melting temperature (T_m). Fig A-1 describes the changes in specific

volume of the liquid as it is cooled from high temperatures. Upon cooling, the molecules of the liquid may come in close proximity and be bound, resulting in crystalline material at T_m . Melting or crystallization is a first order phase transition, where there is a change in the first derivative of Gibbs free energy with respect to temperature, and the process of crystallization results in a drastic reduction in the specific volume (water is an exception). If the liquid manages not to crystallize at T_m , then its specific volume continues to decrease with corresponding increase in the viscosity. The system is now termed as a 'supercooled liquid' and is considered to be in 'equilibrium' with properties similar to linear extrapolation of enthalpy of a liquid. As a supercooled liquid is cooled to lower temperatures, the molecules move more and more slowly and at some temperature they do not have a chance to significantly rearrange or to mobilize themselves. At this point the system is thrown out of equilibrium and this temperature is termed as the glass transition temperature (T_g). At temperatures lower than the T_g , the time scales of molecular motion become drastically long and the material is essentially considered in a frozen state and is termed as 'amorphous' or 'glass'. Glass transition temperature is a second order transition in which there is no change in the free energy of the system, but changes in enthalpy, entropy or viscosity of the material do occur.

Solid solutions or miscible dispersions are characterized based on their single glass transition temperature since both polymer and drug undergo the transformation from liquid state to corresponding unique amorphous phase simultaneously upon cooling. The presence of two T_g s in the mixtures represents a phase separated product. Interested

readers on the thermodynamics of amorphous materials are referred to an excellent review and references therein by Ediger and co-authors [20].

Molecular mobility in amorphous phase

Molecular mobility in amorphous phase is typically described in terms of relaxation time (τ). Relaxation time is the time taken for one molecular motion i.e. rotational or translational to occur. In molecular liquids near T_g , it may take minutes or hours for a molecule less than 10^9 \AA in diameter to reorient [21]. Although the molecules in amorphous state at temperatures below the T_g are in a frozen state, they do possess mobility in the order of hundred of hours. The temperature dependence of relaxation time for supercooled liquids is often described at least approximately by the Vogel-Tammann-Fulcher (VTF) equation:

$$\tau = \tau_0 \exp\left(\frac{B}{T - T_\infty}\right)$$

where τ_0 can be considered as a pre-exponential factor, if the equation is considered as Arrhenius equation (i.e. when $T_\infty = 0$). B is then equal to E/k where E is the energy of activation for molecular motion and k is the Boltzmann constant. When $T_\infty > 0$, the temperature dependence of relaxation time is non-Arrhenius and the relaxation time is predicted to become infinite at T_∞ . In other words, the molecular mobility is very low at temperatures well below the T_g . The primary cause of such slow dynamics is due to high viscosity and low kinetic energy at such low temperatures. However the slow dynamics

of amorphous state could in some cases be significant enough for the molecules to orient and transform to the low free energy crystalline state [22].

Factors influencing physical stability of solid solutions

In amorphous solid solutions, the presence of polymer having a higher glass transition temperature has been suggested as an approach to inhibit drug crystallization [23]. Typically a storage temperature of 50°C below the T_g of amorphous system is considered suitable to minimize the crystallization tendency of the material [24]. When the drug substance is mixed molecularly with the polymer, the T_g of the molecular dispersion is increased relative to the T_g of drug alone and hence the molecular mobility of the drug that is needed for crystallization is reduced. It has also been shown, in specific cases, that presence of drug-polymer interactions e.g. hydrogen bonding, could play a role in delaying or preventing the drug crystallization from molecular dispersions [25]. However mechanism of prevention of drug crystallization from such dispersions is not yet fully understood in the presence of moisture and elevated temperature conditions. Moisture is a well known plasticizer and is naturally present in the atmosphere. It has a tendency to be absorbed by the amorphous materials and reduces the glass transition temperature, thereby increasing the molecular mobility and the crystallization tendency of drug components [26-28]. The exact extent of increase in the molecular mobility by moisture and crystallization rate is not yet clear. Also the effect of moisture on the extent of drug-polymer interaction is poorly understood.

The storage temperature is also believed to play a role in crystallization. It is generally known that increasing the storage temperature leads to enhanced crystallization kinetics. Temperature could also influence the extent of drug-polymer interactions, by decreasing the strength of interaction with its increase. Therefore all the issues suggest that molecular dispersions are kinetically stable and their physical stability is largely influenced by storage conditions i.e. temperature and relative humidity, choice of polymer i.e. less hygroscopic polymer is better, absence of nuclei or seed crystals to prevent secondary nucleation of drug, nature of drug product packaging i.e. presence of desiccants, etc. All of these restrictions make it nearly impossible to formulate a successful physically stable molecular dispersion.

Determination of solid solubility to improve physical stability

In this thesis, I address the issue of physical stability of solid dispersions by resolving the problem into two categories: kinetic stability and thermodynamic stability. A list of factors that differentiate the two have been tabulated (table A-II). When a drug is formulated as a miscible solid dispersion with a carrier, although it is miscible initially, i.e. under low moisture content levels, its extent of miscibility may not be retained in the presence of moisture that can be gained by samples during shelf-life storage. Under such conditions, the drug or polymer could phase separate from the mixtures thereby making the drug vulnerable to crystallization.

If a solid dispersion system can be designed where the drug concentration is such that the presence of moisture cannot cause phase separation and hence drug crystallization,

physical stability can be assured. The concentration of the drug that remains miscible with the polymer in the presence of accelerated stress conditions i.e. high relative humidity and temperature is defined as the “solid solubility” of drug in the polymer. To characterize such solid solubility is indeed challenging, as stated by Duncan Q. M. Craig in one of his recent reviews on solid dispersions [4],

“... unequivocal demonstration of solid solubility is not as simple as one may imagine.”

The concept of solid solution has been addressed for several years in the metallurgy and polymer science fields [29]. However, techniques to characterize solid solubility are very limited and restricted to specific fields. Calorimetric techniques are utilized in characterizing drug-polymer miscibility [30], and can be of valuable support to quantify drug solid solubility as performed in the present research.

Specific objectives of this thesis

1. To design and evaluate a screening technique to identify the “solid solubility” of drug substances in commonly employed polymeric carriers using calorimetric approaches. Also to verify if solid dispersions prepared at solid solubility levels are physically stable by storing them under accelerated stability conditions for at least six months.

2. To investigate the influence of factors like storage temperature, moisture content drug-polymer interactions, drug loading etc. on the solid solubility and drug crystallization from solid dispersions.
3. To validate the universal applicability of the screening technique by employing different hydrophobic drug models and using various analytical tools like X-ray diffraction and Fourier transform infrared spectroscopy.
4. To understand the mechanism of drug crystallization from solid miscible dispersions and performing extensive literature review to substantiate the findings theoretically.
5. To characterize the physical stability of model amorphous hydrophobic compounds by conducting crystallization studies to investigate the influence of moisture and storage temperature on the crystallization kinetics. Eventually compare the drug crystallization rate with the kinetics of drug phase separation and crystallization from solid dispersions.
6. If circumstances allow, to design formulation approaches like addition of surfactant or complexing agents to decrease the kinetics of drug phase separation or crystallization and to enhance the drug solid solubility in the carrier.
7. Finally, to employ a newer sensitive thermally stimulated current spectroscopy (TSC) measurement to characterize the molecular mobility of commonly employed polymer in solid dispersion. To evaluate the potential of TSC in characterizing amorphous formulations and comparing the results with experimental results obtained using modulated differential scanning calorimeter (MDSC).

References:

1. W. L. Chiou, and S. Riegelman. Pharmaceutical applications of solid dispersion systems. *Journal of Pharmaceutical Sciences*. 60:1281-1302 (1971).
2. J. L. Ford. The current status of solid dispersions. *Pharmaceutica Acta Helvetica*. 61:69-88 (1986).
3. C. Leuner and J. Dressman. Improving drug solubility for oral delivery using solid dispersion. *European Journal of Pharmaceutics and Biopharmaceutics*. 50:47-60 (2000).
4. D. Q. M. Craig. The mechanism of drug release from solid dispersions in water soluble polymers. *International Journal of Pharmaceutics*. 231:131-144 (2002).
5. G. Verreck, K. Six, G. V. Mooter, L. Baert, J. Peeters, and M. E. Brewster. Characterization of solid dispersions of itraconazole and hydroxypropylmethylcellulose prepared by melt extrusion-part I. *International Journal of Pharmaceutics*. 251:165-174 (2003).
6. L. Yu. Amorphous pharmaceutical solids: preparation, characterization and stabilization. *Advanced Drug Delivery Reviews* 48:27-42 (2001).
7. A. T. M. Serajuddin. Solid dispersion of poorly water-soluble drugs: early promises, subsequent problems, and recent breakthroughs. *Journal of Pharmaceutical Sciences*. 88:1058-1066 (1999).
8. G. Levy. *American Journal of Pharmaceutics*. 135:78- 83 (1963).
9. N. J. Medlicott, K. A. Foster, K. L. Audus, S. Gupta and V. J. Stella. Comparison of the effects of potential parenteral vehicles for poorly water soluble anticancer drugs (organic cosolvents and cyclodextrins solutions) on cultured endothelial cells (HUV-EC). *Journal of Pharmaceutical Sciences*. 87:1138-1143 (1998).

10. A. T. M Serajuddin. Recent advances in the formulation of solid dispersion systems for poorly water-soluble drugs. Abstract for symposium at the 2004 American Association of Pharmaceutical Scientists Annual Meeting and Exposition, Baltimore, MD November 7-11, 2004.
11. B. C. Hancock, and M. Parks. What is the true solubility advantage for amorphous pharmaceuticals? *Pharmaceutical Research*. 17:397-404 (2000).
12. Y. Matsuda, and S. Kawaguchi. Physicochemical characterization of oxyphenbutazone and solid-state stability of its amorphous form under various temperature and humidity conditions. *Chemical and Pharmaceutical Bulletin*. 34:1289-1298 (1986).
13. K. Khougaz, and S. D. Clas. Crystallization inhibition in solid dispersions of MK-0591 and poly(vinylpyrrolidone) polymers. *Journal of Pharmaceutical Sciences*. 89:1325-1334 (2000).
14. I. Sugimoto, A. Kuchiki, and H. Nakagawa. Stability of nifedipine-polyvinylpyrrolidone coprecipitate. *Chemical and Pharmaceutical Bulletin*. 29:1715-1723 (1981).
15. P. C. Sheen, V. K. Khetarpal, C. M. Cariola, C. E. Rowlings. Formulation studies of a poorly water-soluble drug in solid dispersions to improve bioavailability. *International Journal of Pharmaceutics*. 118:221-227 (1995).
16. S. Sethia, and E. Squillante. Physicochemical characterization of solid dispersions of carbamazepine formulated by supercritical carbon dioxide and conventional solvent evaporation method. *Journal of Pharmaceutical Sciences*. 91:1948 (2002).
17. A. Forster, T. Rades, and J. Hempenstall. Selection of suitable drug and excipient candidates to prepare glass solutions by melt extrusion for immediate release oral formulations. *Pharmaceutical Technology Europe*. October:27-37 (2002).

18. K. Sekiguchi, and N. Obi. Studies on absorption of eutectic mixture. I. A comparison of the behavior of eutectic mixture of sulfathiazole and that of ordinary sulfathiazole in man. *Chemical and Pharmaceutical Bulletin*. 9:866-872 (1961).
19. S. K. Dordunoo, J. L. Ford, and M. H. Rubinstein. Physical stability of solid dispersions containing triamterene or temazepam in polyethylene glycols. *Journal of Pharmacy and Pharmacology*. 49:390-396 (1997).
20. M. D. Ediger, C. A. Angell, and S. R. Nagel. Supercooled liquids and glasses. *Journal of Physical Chemistry*. 100:13200-13212 (1996)
21. I. Chang, F. Fujara, B. Geil, G. Heuberger, T. Mangel, H. J. Sillescu. Translational and rotational molecular motion in supercooled liquids studied by NMR and forced Rayleigh scattering. *Journal of Non Crystalline Solids* 172-174: 248-255 (1994)
22. Y. Aso, S. Yoshioka, and S. Kojima. Explanation of the crystallization rate of amorphous nifedipine and Phenobarbital from their molecular mobility as measured by ¹³C nuclear magnetic resonance relaxation time and relaxation time obtained from the heating rate dependence of the glass transition temperature. *Journal of Pharmaceutical Sciences*. 90:798-806 (2001).
23. M. Yoshioka, B. C. Hancock and G. Zografi. Inhibition of indomethacin crystallization in poly(vinylpyrrolidone) coprecipitates. *Journal of Pharmaceutical Sciences*. 84:983-986 (1995).
24. B. C. Hancock, S. L. Shamblin and G. Zografi. Molecular mobility of amorphous pharmaceutical solids below their glass transition temperatures. *Pharmaceutical Research*. 12:799-806 (1995).
25. L. S. Taylor, and G. Zografi. Spectroscopic characterization of interactions between PVP and indomethacin in amorphous molecular dispersions. *Pharmaceutical Research*. 14:1691-1698 (1997).
26. B. C. Hancock, and G. Zografi. The relationship between the glass transition temperature and the water content of amorphous pharmaceutical solids. *Pharmaceutical Research*. 11:471-477 (1994).

27. C. A. Oksanen, and G. Zografi. Molecular mobility in mixtures of absorbed water and solid poly(vinylpyrrolidone). *Pharmaceutical Research*. 10:791-799 (1993).
28. S. L. Shamblin, and G. Zografi. The effects of absorbed water on the properties of amorphous mixtures containing sucrose. *Pharmaceutical Research*. 16:1119-1124 (1999).
29. E. Coleman. A study of the crystallization of some binary metallic glasses. M. Sc. Thesis, *Rutgers, The State University of New Jersey*. (1979).
30. Q. Lu, and G. Zografi. Phase behavior of binary and ternary amorphous mixtures containing indomethacin, citric acid, and PVP. *Pharmaceutical Research*. 15:1202-1206 (1998).

Table A- I: Nature of drug dispersed in the polymeric matrix

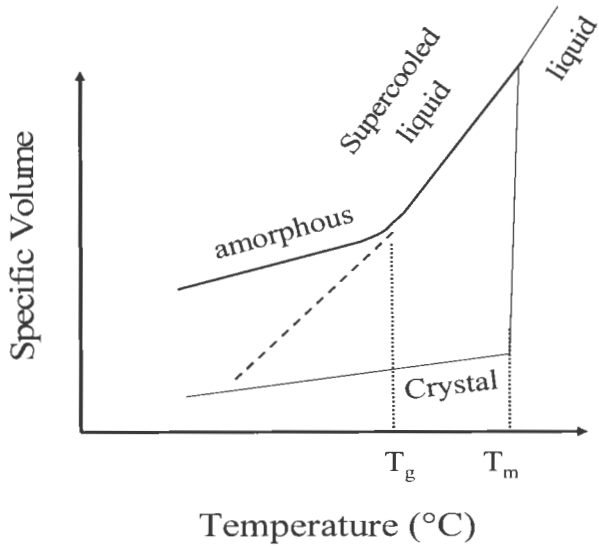
Group	Dispersion type
1	simple eutectic mixtures
2	solid solutions
3	amorphous (glass) solutions and glass suspensions
4	amorphous precipitation of a drug in crystalline carrier
5	compound or complex formations between drug and carrier
6	any combinations among groups 1-5

Table A-II: Physical Stability of Solid Dispersions

Kinetic Stability	Thermodynamic Stability
Kinetic stability is possessed by the system initially but not during regular handling and storage of drug product	Thermodynamic stability can be possessed by the system for prolonged period and it is a definite value at a specified temperature and moisture content
Possessed by supersaturated systems	Possessed by saturated or under-saturated systems
Usually characterized by initial drug miscibility levels	It can be characterized by drug solid solubility levels
Choice of storage temperature and moisture content is restricted	Less likely influenced by storage temperature and moisture content
Unpredictable crystallization of drug could occur from the solid dispersions	No crystallization of drug can occur from solid dispersions
Kinetic stability can be influenced by method of solid dispersion preparation i.e. rate of cooling, extent of mixing with carrier etc.	Thermodynamic stability can be improved by suitable selection of polymer i.e. hydrogen bonding, addition of surfactants or complexing agents etc.
Most systems possess kinetic stability	Very few systems could possess thermodynamic stability

Figure A-1

Depiction of glass transition temperature in amorphous solids



SECTION B

MANUSCRIPT I

PHASE BEHAVIOR OF AMORPHOUS MOLECULAR DISPERSIONS I: DETERMINATION OF THE DEGREE AND MECHANISM OF SOLID SOLUBILITY

Madhav Vasanthavada¹, WeiQin Tong², Yatindra Joshi², and M. Serpil Kislalioglu^{1,3}

ABSTRACT

Purpose: To understand the phase behavior, and the degree and mechanism of the solid miscibility in amorphous molecular dispersions by the use of thermal analysis.

Methods: Amorphous molecular dispersions of trehalose-dextran and trehalose- PVP were prepared by co-lyophilization. The mixtures were exposed to 23°, 40° and 50°C

¹ Department of Applied Pharmaceutical Sciences, The University of Rhode Island, Kingston, RI 02881.

² Pharmaceutical & Analytical Development, Novartis Pharmaceutical Corporation, East Hanover, NJ 07936.

³ To whom correspondence should be addressed. (Telephone: (401) 874 5017; Email: skis@uri.edu), Fax: (401)874-2181

(75% relative humidity (RH)) and 23°C (69% RH) storage conditions respectively. Thermal analysis was conducted by Modulated Differential Scanning Calorimeter (MDSC).

Results: Upon exposure to moisture, two glass transition temperatures (T_g s), one for phase separated amorphous trehalose (T_{g1}) and the other for polymer-trehalose mixture (T_{g2}) were observed. With time, T_{g2} increased and reached to a plateau (T_g^{eq}), whereas T_{g1} disappeared. The disappearance of T_{g1} and the appearance of T_m , i.e. melting endotherm for trehalose dihydrate was attributed for the crystallization of the phase-separated amorphous trehalose. It was observed that T_g^{eq} was always less than T_g of pure polymer. The lower T_g^{eq} when compared to T_g of pure polymer may be the result of solubility of a fraction of trehalose in the polymers chosen. The miscible fraction of trehalose was estimated to be 12% and 18% w/w in dextran at 50°C / 75% RH and 23°C / 75% RH respectively, and 10% w/w in PVP at 23°C/ 69% RH.

Conclusions: Mixing behavior of trehalose-dextran and trehalose-PVP dispersions were examined both experimentally and theoretically. A method determining the “extent of molecular miscibility”, referred to as “solid solubility”, was developed, and mechanistically and thermodynamically analyzed. Solid dispersions prepared at trehalose concentrations below the “solid solubility limit” were shown to be physically stable even under accelerated stability conditions.

KEY WORDS: glass transition, solid dispersions, miscibility, phase separation, thermal analysis

INTRODUCTION

In the pharmaceutical literature, publications on the use of solid dispersions to enhance the dissolution rate and bioavailability of poorly water-soluble compounds are in abundance [1]. However, despite the extensive R&D efforts only a few solid dispersion products are commercially available. One of the reasons for this rarity is the thermodynamic instability of amorphous active component in dispersed systems [2,3]. Although recrystallization of amorphous drugs from solid dispersions is reported in several publications, the exact mechanism of such recrystallization is not clear. The investigators, who extensively evaluated the physical stability of amorphous materials, attributed the recrystallization phenomenon mainly to the molecular motions of amorphous components even below the glass transition temperature (T_g) [4-8].

It is generally understood that polymers improve the physical stability of amorphous drugs in solid dispersions by either: a) increasing the T_g of the miscible mixture, thereby reducing the molecular mobility at regular storage temperatures, or b) specifically interacting (e.g. hydrogen bonding) with functional groups of amorphous drug substance [9-11]. For a polymer to be effective in preventing crystallization by either of these mechanisms, it has to be molecularly miscible with the amorphous substance. For complete miscibility, interactions between the two components are necessary [12]. A miscible system can phase-separate and become unstable if specific interactions between the components are adversely affected by a third component like water. The extent of moisture uptake depends upon factors like hygroscopicity of the drug and/or carrier, the

concentration of the active substance in the drug product and the storage temperature. Due to this complexity, the prediction of physical stability of a drug substance in a solid dispersion becomes challenging. In order that the solid dispersion systems can be effectively utilized by the pharmaceutical industry, it is critical to understand the role of time, temperature, and humidity in determination of the physical stability of solid dispersion during its shelf-life.

The objective of this study was two-fold: The first was to study the phase behavior of the selected solid dispersions via thermal analysis, in order to determine the extent of solid state miscibility under accelerated stability conditions, and the second was to understand the mechanism of physical stability of these amorphous molecular dispersions.

Molecular dispersions of trehalose-dextran and trehalose- poly (vinylpyrrolidone) (PVP) were chosen as models to understand the phase behavior of a crystallizable amorphous substance that was molecularly mixed with a polymer. Trehalose is a well characterized compound [13]. Amorphous trehalose, which is highly susceptible to moisture, crystallizes to a stable dihydrate that can be characterized thermally [13]. Although hydrogen-bond interactions between trehalose and PVP have been cited [14], the influence of water on these interactions, the phase behavior of the mixtures and the solid-state miscibility has not yet been demonstrated in the literature.

MATERIALS AND METHODS

Materials

Dextran (polymer containing sucrose having α -1, 6-glucosidic linkage), with M_n of 70 KDa, and trehalose (α -D-Glucopyranosyl α -D-glucopyranoside) dihydrate were purchased from Sigma Chemical Co., (St. Louis, MO). Poly (vinylpyrrolidone) (PVP-K29/32), (M_w of 58 KDa) was obtained from ISP Technologies (Wayne, NJ). Sodium chloride (Fisher Chemicals Co., Fair Lawn, NJ), was used to prepare saturated salt solution providing 75% RH conditions.

Methods

Preparation of Amorphous Mixtures by Lyophilization:

Dextran and PVP-K29/32 were dried in a vacuum oven overnight at 105°C until a constant weight was obtained. Trehalose dihydrate was used without any further treatment. Physical mixtures of each polymer and trehalose dihydrate were made in dry glove bags (RH<15%) to obtain weight proportions of trehalose dihydrate in the polymer from 0% to 100% at 10% w/w intervals. These mixtures were dissolved in purified water to obtain 10% w/v concentration and stirred overnight at 35°C. Aqueous solutions (2 mL) were freeze-dried using a commercial freeze dryer (Dura-Stop μ P, FTS System, Stone Ridge, NY). Vials containing solutions were transferred onto pre-cooled shelves (-45°C). Primary drying was carried out at shelf temperature of -27°C for 22-24 hrs, followed by drying at -12°C for 2 hrs, 0°C for 16 hrs, and secondary drying at 30°C for 20 hrs.

Vacuum pressure of 15 mTorr was applied throughout the drying. All samples were stored over anhydrous calcium sulfate at room temperature, after capping the vials. X-ray analysis of these samples showed that all the mixtures were amorphous.

Isothermal Stability Studies:

Lyophilized amorphous mixtures of dextran containing 10, 20, 30, 40 and 70% by weight of trehalose were accurately weighed (8-12 mg) in standard DSC pans in a glove bag (RH<15%). These pans were placed in desiccators containing saturated sodium chloride solution (75% RH) to expose the miscible mixtures to excess humidity. The desiccators were kept at room temperature ($23 \pm 1^\circ\text{C}$) and incubators (Precision Scientific Inc., Chicago, IL) at $40 \pm 1^\circ\text{C}$ and $50 \pm 1^\circ\text{C}$. Saturated NaCl solution provides relative humidity of $75 \pm 0.5\%$ over the temperature range of 23° to 50°C [15]. By storing the samples in discrete DSC pans, the reproducibility of all measurements was ascertained without any interference of sample handling. Samples were taken out for analysis at pre-determined time intervals for a period of up to six months. They were crimped with aluminum lids having 10 pinholes to facilitate removal of absorbed and bound water liberated upon melting of any recrystallized trehalose.

Thermal Analysis:

Modulated Differential Scanning Calorimeter (MDSC) (TA Instruments 2920, New Castle, DE), with a liquid nitrogen cooling accessory was used for thermal analysis. The analysis was performed under a purge of dry nitrogen gas (60cc/min). High purity indium

and sapphire were used frequently to calibrate for the heat flow and heat capacity of the instrument. Samples were initially cooled to -30°C for 10 minutes and were heated to 245°C at $1^{\circ}\text{C}/\text{min}$ with modulations of 0.266° every 50 seconds.

MDSC offers an advantage over conventional DSC because it can detect reversible glass transition phenomenon in the presence of several other non-reversible relaxation processes. Heat capacity changes can be resolved from moisture removal endotherm, thereby improving the signal to noise ratio and improving the elucidation of the T_g .

RESULTS

Modulated DSC Analysis of Trehalose and Trehalose-Polymers Mixtures:

Characterization of trehalose:

DSC scans of trehalose before and after lyophilization are shown in Fig. B-1-1a. A heating rate of $1^{\circ}\text{C}/\text{min}$ was employed to minimize polymorphic conversion of trehalose dihydrate during heating [16]. Upon heating trehalose dihydrate, an endotherm at $96^{\circ} \pm 1^{\circ}\text{C}$ (T_h) was observed. This was followed by a T_g at 122°C and recrystallization at 171°C . The recrystallized anhydrous trehalose melted at 212°C . Thermo-gravimetric analysis (TGA) performed on trehalose dihydrate showed a 9.5% weight loss at 96°C confirming that the endotherm at $96^{\circ} \pm 1^{\circ}\text{C}$ was due to the removal of water of hydration. Hot-stage microscopy was conducted on trehalose dihydrate by heating at $1^{\circ}\text{C}/\text{min}$ and it was observed that water removal from trehalose resulted in a structural collapse and loss of birefringence (indicating amorphous state). At approximately 135°C , trehalose

liquefied and recrystallized to the anhydrate form. These results agreed with DSC characterization and with observations of Taylor and York [13].

Lyophilized trehalose was amorphous as determined by X-ray diffraction. DSC scan of lyophilized trehalose (Fig. B-I-1a) showed no endotherm at 96°C, indicating the absence of crystalline hydrate structure. For verification, amorphous trehalose that was exposed to 50°C and 40°C with 75%RH were heated in DSC and examined. One would expect the amorphous trehalose to crystallize upon storage and indeed as seen in Fig. B-I-1b, the thermograms are similar. In conclusion, the water-loss endotherm observed at 96°C is the characteristic of crystalline trehalose.

Molecular dispersions of trehalose and polymer:

All the freshly prepared co-lyophilized mixtures of trehalose-dextran or trehalose-PVP were amorphous exhibiting a composition-dependent single T_g indicating their molecular miscibility. The T_g of the mixtures decreased with increasing concentration of trehalose as shown in Fig. B-I-2a,b, indicating the plasticizing effect of trehalose on the polymers. The T_g values were plotted as a function of weight fraction of trehalose in polymer and are shown in Fig. B-I-2c,d for the determination of solid solubility.

Trehalose-dextran and Trehalose-PVP molecular mixtures: physical stability studies

MDSC reversing heat flow scans of mixtures containing 40% w/w trehalose-in-dextran, which were stored at 50°C/ 75% RH for a period of 2 – 50 days are shown in Fig. B-I-3a. A freshly prepared sample showed a single T_g at 169°C, indicating miscibility.

Amorphous miscible mixtures when exposed to 50°C/ 75% RH absorbed moisture, and the plasticized T_g of such a system, from the total heat flow scan (data not shown), was detected at $22^\circ \pm 3^\circ\text{C}$. The absorbed moisture was removed from the mixtures as the samples were heated in MDSC. As opposed to a single T_g of 169°C in the original mixture, two distinct T_g s were observed in the 2 and 4-day old samples; T_g values at 123° and 121°C (referred to as T_{g1}), and T_g at 203°C (T_{g2}). In the 16 – 34 day samples, T_{g1} was not observed. However a water-loss endotherm at $96^\circ \pm 1^\circ\text{C}$ (T_h), characteristic of crystalline trehalose, had appeared. In addition, T_{g2} values had increased and seemed to plateau, which is termed as equilibrium T_g ($T_{g^{eq}}$). There was also a distinct reduction in the heat capacity step change, (ΔC_p) at T_{g2} . These values decreased initially and seemed to reach a plateau as seen from data in Table B-I-I. The thermal events in dextran mixtures containing 30% w/w trehalose were also similar to those that were observed for 40% w/w mixtures when stored at 50°C/ 75%RH (Fig. B-I-3b).

MDSC reversing heat flow scans of mixtures containing 20% and 40% w/w trehalose-in-PVP which were stored at 23°C/ 69% RH are shown in Fig. B-I-3c. With this polymer, the phase separation of amorphous trehalose was observed (T_{g1} at 120°C) in the 190, 195 and 200 day old samples. A water-loss endotherm at $96^\circ \pm 1^\circ\text{C}$ (T_h) was also observed. For 20% w/w samples, the T_{g1} and T_h were not noticeable even after 200 days of storage. A reduction in ΔC_p values at T_{g2} (given within brackets in Fig. B-I-3c) followed by a plateau was noticed in these systems as well. The heat flow scans that are depicted in Fig. B-I-3d are to demonstrate the presence of T_{g1} & T_{g2} values for some selected mixtures.

A plot of T_{g2} values of dextran mixtures containing different weight fraction of trehalose, stored at 50°, 40° and 23°C with 75% RH is shown in Fig. B-I-4. It should be noted from the figure that T_g^{69} is always less than 225°C, which is the T_g of pure amorphous dextran (dotted line). This reduction in T_g indicated that a fraction of trehalose remained miscible with the polymer even after being exposed to excessive temperature and humidity conditions for up to six months. This fraction was identified as the “solid solubility” of trehalose in dextran. The T_g^{69} of all amorphous mixtures ranged from 207° - 210°C, when they were stored at 40° and 50°C with 75% RH, and within 196° - 203°C for mixtures stored at 23°C/75% RH conditions. These findings suggested that, at equilibrium, irrespective of the initial trehalose-concentrations, the solid solubility limit of trehalose in dextran was the same for a specified storage condition. For instance, when stored at 50°C/ 75% RH, 70% w/w trehalose mixture which was initially miscible with dextran, formed a dihydrate and demonstrated T_{g2} values at 207°-210°C upon “equilibrium”. This concentration was accepted as its solid solubility limit.

To exclude the possible interference of moisture on reduction of T_{g2} , amorphous dextran that was equilibrated at 50°C / 75%RH for a month and contained 11% w/w water was heated in MDSC. The T_g of the sample was 225°C, which was identical to the T_g of the original sample with 3% w/w water content. These findings proved that moisture was not the cause of T_{g2} reduction.

On the other hand, trehalose that was liquefied above its T_g of 118°C could plasticize dextran and lower the T_g below 225°C. Such a possibility was suggested by Six *et al.* [17] for HPMC- itraconazole dispersions. The MDSC scan of 1:1 physical mixture of

amorphous trehalose and dextran, demonstrated T_g s at $119^\circ \pm 0.5^\circ\text{C}$ and $223^\circ \pm 0.9^\circ\text{C}$ ($n=3$) upon heating at $1^\circ\text{C}/\text{min}$ rate. The two T_g values coincided with the T_g s of pure trehalose and dextran respectively indicating that heating in MDSC did not cause any mixing. The reduction in T_{g2} values from 225°C to T_g^{eq} , is indicating the presence of the miscible fraction of trehalose in the polymer.

Crystallization of trehalose:

A plot of percent crystallinity of trehalose from the miscible mixtures containing 40% and 30% w/w trehalose as a function of storage time is shown in Fig. B-I-5. The amount of trehalose crystallized as the dihydrate was calculated from the heat of fusion under the water-loss-endotherm (T_h) of the total heat flow scan. Amorphous trehalose by itself when exposed to 75% RH had enthalpy of fusion equal to untreated crystalline trehalose dihydrate indicating 100% crystallization (Fig. B-I-1b). On the other hand, solid dispersion samples showed a maximum of 84% crystallization for samples stored at $50^\circ\text{C}/75\%$ RH for six months. It was also seen that the rate of crystallization, after an initial rapid increase, was much less in 30%w/w dispersions when compared to 40%w/w dispersions. These findings are consistent with results which suggest that a fraction of trehalose remains miscible with the polymer.

Quantifying the limit of solid solubility:

To determine the molecularly-dispersed trehalose concentration in the polymer, the plot of T_g of the mixtures against the % w/w trehalose concentration was utilized (Fig. B-I-

2c,d). In this graph, the T_g^{69} values were used to determine the fraction of trehalose that remained miscible with dextran (Fig. B-I-2c) and PVP (Fig. B-I-2d). In these graphs, the solubility limits are shown by arrows. The corresponding value on the x-axis represented the solid solubility of trehalose in the polymer. Table B-I-II demonstrates the solid solubility limits of trehalose in dextran at different storage conditions. In this table the difference between the storage temperature and the plasticized T_g due to presence of moisture (T_g^w) is shown as ΔT_g . It is important to note that the samples were stored at temperatures above their plasticized T_g . At this region, the system has a high degree of molecular mobility and consequently, a higher rate of destabilization. The solid solubility of trehalose-in-dextran decreased from 18% w/w at 23°C to 12% w/w at 50°C, whereas the total water content decreased from 16.5% w/w to 11% w/w. However, no appreciable difference in solid solubility was observed between 40°C and 50°C storage conditions, although total water content decreased from 13% to 11%.

DISCUSSION

Mechanism of Phase Separation & Solid Solubility:

The hypothesized mechanism for phase separation and solid solubility is depicted schematically in Fig. B-I-6 for a dextran-trehalose model. The repeat units of dextran and trehalose are labeled as 1D, 2D, and 1T, 2T, etc respectively.

In the absence of moisture, freshly prepared mixtures have high T_g values and hence the molecular mobility is very low at the storage temperatures. Trehalose, therefore, remains

in a kinetically frozen state of miscibility. Upon exposure to moisture, the mixtures are plasticized, and the molecular mobility increases. The exact role of water is not clear yet. Water may either weaken the H-bond interaction (between –OH of trehalose and –OH or –O- groups in dextran, or C=O groups in PVP) by bridging with polymer and trehalose structural units, or may merely increase the molecular mobility by plasticizing the mixtures. In either case, diffusion of trehalose through the polymeric matrix could result in separation of trehalose into an amorphous phase, and subsequent crystallization. As more and more trehalose phase separates, increasing amounts of “free” polymer units are left to interact with the remaining trehalose. Such units possibly orient around and arrest the non-diffused trehalose molecules by satisfying their H-bond requirements (1T, in Fig. B-1-6). At equilibrium, localized pockets of trehalose molecules are almost entirely bonded to the polymer, reaching solid solubility as characterized by T_{g2} .

Thermodynamic Interpretation of Solid Solubility:

To analyze the solid-solubility of trehalose in the polymers thermodynamically, the energetics of interactions between trehalose and polymers were calculated using the Couchman & Karasz theoretical equations [18]. Similar approach was used by Shamblyn *et al.* to determine the excess thermodynamic properties of mixing in the binary mixtures [19]. Using the equations described in detail in the appendix, the enthalpy (ΔH_{mix}) and free energy (ΔG_{mix}) of mixing as a function of trehalose weight fraction were calculated and plotted in Fig. B-1-7.

Since the influence of water on the free energy of mixing is not understood, water was not taken into consideration in the thermodynamic analysis. The enthalpy of mixing (ΔH_{mix}) shown in Fig. B-I-7 was positive for the entire composition range and was similar in magnitude to those reported for mixtures of sucrose-PVP or sucrose-dextran [19]. The positive ΔH_{mix} at all compositions indicates that greater numbers of H-bonds are broken between trehalose-trehalose and polymer-polymer than are formed between trehalose-polymer during mixing. Since lesser number of bonds was formed between trehalose and polymer when compared to the bonds that they had in their individual states, the positive ΔH_{mix} would favor trehalose and polymer to self-associate or phase separate. The excess entropy of mixtures was positive (not shown) throughout the trehalose composition favoring mixing. The negative free energy values for low trehalose-containing mixtures are thus driven by the excess entropy. Although the dextran-trehalose mixtures studied contained moisture, and a three-phase system could be significantly different from the two-phase system, the analysis conducted supports the hypothesis that a component dispersed in a solid dispersion with certain solubility can be thermodynamically favored.

Mechanism of crystal growth:

Upon phase-separation, amorphous trehalose, as characterized by T_{g1} crystallizes in the presence of water, and is characterized by T_h (Fig. B-I-3). The crystallization is

dependent upon the initial concentration of trehalose in the mixture and the storage conditions employed (Fig. B-I-5).

The portion of polymer located at the amorphous-crystalline interface has low molecular mobility and is termed as “rigid amorphous fraction” as suggested by Lee and Kim [20]. This fraction does not contribute significantly to the heat capacity step change values at T_{g2} (ΔC_p) [20-22]. The fraction of amorphous bulk distant from crystalline region is the “mobile amorphous phase” and could be responsible for the ΔC_p at T_{g2} as indicated by Craig *et al.* (21). As the phase separated trehalose crystallizes, the fraction of polymer in close contact with the crystalline surface increases. This explains for the reduction in the ΔC_p values at T_{g2} (Table B-I-1), until no more “rigid amorphous fraction” is formed.

Formation of rigid amorphous fraction may also explain the decrease in the rate and extent of crystallization in 30% and 40% w/w mixtures with time (Fig. B-I-5). As suggested by Crowley and Zografí [23], the rigid amorphous fraction impedes the kinetics of crystallization of trehalose that has already phase separated. This kinetic phenomenon is different from the solid solubility, which is characterized by T_{g2} , as described in the previous section.

Effect of temperature and moisture on solid solubility:

Table B-I-II demonstrates the effect of storage temperature and moisture content on the solid solubility of trehalose. Reduction of solid solubility limit with an increase in the temperature is probably due to the higher molecular mobility of the system at elevated

temperatures, leading to an enhanced phase separation and crystallization. In addition, at 50°C, thermal expansion of the mixtures may reduce the degree of interaction between the sugar and polymer thereby decreasing the miscibility limit as suggested by Tang *et al.* [24]. Finally, since the miscible mixtures have a higher enthalpy and free energy, it is not surprising to see that at higher temperatures, the system proceeds for de-mixing causing trehalose to crystallize. Although with an increase in temperature from 23°C to 40°C solubility reduction was seen, no difference in solubility was noticed between 40°C and 50°C. This is possibly due to an associated reduction in water content, where the reduced water level compensates the temperature effects. Therefore, water seems to have an indirect effect on T_{g2} reduction and hence solid solubility. Overall, the data obtained suggest that both temperature and moisture affect the phase behavior and extent of solid solubility.

CONCLUSIONS

In this paper, we have shown application of MDSC in monitoring the phase separation and crystallization behavior of trehalose from its amorphous miscible mixtures, at ambient temperature and accelerated stability conditions. Upon exposure to moisture, trehalose separated as an intermediate amorphous phase which later crystallized to the dihydrate form. Based on the experimental data and thermodynamic as well as mechanistic assessment, it is postulated that a fraction of trehalose remained miscible with the polymers due to extensive hydrogen bonding between the two components. This

fraction was analyzed by the changes in the glass transition temperatures and was referred to as the “solid solubility” of trehalose in the polymer. Molecular mixtures containing 10% w/w trehalose (i.e., trehalose concentration below solid solubility) did not phase separate or crystallize during the six months storage at accelerated stability conditions, which substantiated our findings. We also propose that the MDSC technique described can be applied to determine the phase behavior and solid solubility limits of the hydrophobic drugs that are dispersed in water-soluble carriers. This method can be useful in identifying the solid dispersions that will remain physically stable during the shelf-life.

ACKNOWLEDGMENTS

This study is a part of Ph.D. research of M. Vasanthavada who is a Novartis Graduate Research Fellow and has conducted his research at Novartis R&D facility. He wishes to acknowledge the fellowship and also thank Dr. M. Greenfield of Department of Chemical Engineering, University of Rhode Island for helpful discussions on thermodynamic calculations. Dr. Zeren Wang, presently working with Boehringer Ingelheim Corporation, is acknowledged for his helpful discussion during the early phase of this work.

REFERENCES

1. A. T. M. Serajuddin. Solid dispersion of poorly water-soluble drugs: early promises, subsequent problems, and recent breakthroughs. *Journal of Pharmaceutical Sciences* **88**:1058-1066 (1999).
2. C. Doherty, and P. York. Accelerated stability of an X-ray amorphous furesemide-poly (vinyl pyrrolidone) solid dispersion. *Drug Development and Industrial Pharmacy* **15**:1969-1987 (1989).
3. H. Suzuki, and H. Sunanda. Some factors influencing the dissolution of solid dispersions with nicotinamide and hydroxypropylmethylcellulose as combined carriers. *Chemical and Pharmaceutical Bulletin* **46**:1015-1020 (1998).
4. E. Y. Shalaev, and G. Zografi. How does residual water affect the solid-state degradation of drugs in the amorphous state? *Journal of Pharmaceutical Sciences* **85**:1137-1141 (1996).
5. V. Andronis, M. Yoshioka, and G. Zografi. Effects of sorbed water on the crystallization of indomethacin from the amorphous state. *Journal of Pharmaceutical Sciences* **86**:346-351 (1997).
6. K. Khougaz, and S. D. Clas. Crystallization inhibition in solid dispersions of MK-0591 and poly (vinylpyrrolidone) polymers. *Journal of Pharmaceutical Sciences* **89**:1325-1334 (2000).
7. Y. Aso, S. Yoshioka, and S. Kojima. Relationship between the crystallization rates of amorphous nifedipine, Phenobarbital, and flopropione, and their molecular mobility as measured by their enthalpy relaxation and ¹H NMR relaxation times. *Journal of Pharmaceutical Sciences* **89**:408-416 (2000).
8. M. Yoshioka, B. C. Hancock, and G. Zografi. Crystallization of indomethacin from the amorphous state below and above its glass transition temperature. *Journal of Pharmaceutical Sciences* **83**:1700-1705 (1994).

9. M. Yoshioka, B. C. Hancock, and G. Zografi. Inhibition of indomethacin crystallization in poly(vinylpyrrolidone) coprecipitates. *Journal of Pharmaceutical Sciences* **84**:983-986 (1995).
10. T. Matsumoto, and G. Zografi. Physical properties of solid molecular dispersions of indomethacin with poly(vinylpyrrolidone) and poly(vinylpyrrolidone-co-vinylacetate) in relation to indomethacin crystallization. *Pharmaceutical Research* **16**:1722-1728 (1999).
11. L. S. Taylor, and G. Zografi. Spectroscopic characterization of interactions between PVP and indomethacin in amorphous molecular dispersions. *Pharmaceutical Research* **14**:1691-1698 (1997).
12. M. M. Coleman, J. F. Graf and P. C. Painter. *Specific interactions and the miscibility of polymer blends*. Technomic Publishing, Lancaster, Basel, 1991.
13. L. S. Taylor and P. York. Characterization of phase transitions of trehalose dihydrate on heating and subsequent dehydration. *Journal of Pharmaceutical Sciences* **87**:347-355 (1998).
14. L. S. Taylor and G. Zografi. Sugar-polymer hydrogen bond interactions in lyophilized amorphous mixtures. *Journal of Pharmaceutical Sciences* **87**:1615-1621 (1998).
15. H. Nyqvist. Saturated salt solutions for maintaining specified relative humidities. *Int. J. Pharm. Tech. & Prod. Mfr.* **4**:47-48 (1983).
16. F. Sussuch, R. Urbani, F. Princivale, and A. Cesaro. Polymorphic amorphous and crystalline forms of trehalose. *Journal of American Chemical Society* **120**:7893 – 7899 (1998).
17. K. Six, H. Berghmans, C. Leuner, J. Dressman, K. V. Werde, J. Mullens, L. Benoist, M. Thimon, L. Meublat, G. Verreck, J. Peeters, M. Brewster, and G. V.

- Mooter Characterization of solid dispersions of itraconazole and hydroxypropylmethylcellulose prepared by melt extrusion, part II. *Pharmaceutical Research* **20**:1047-1054 (2003).
18. P. R. Couchman, and F. E. Karasz. A classical thermodynamic discussion on the effect of composition on glass-transition temperatures. *Macromolecules* **11**:117-119 (1978).
 19. S. L. Shamblin, L. S. Taylor, and G. Zografi. Mixing behavior of colyophilized binary systems. *Journal of Pharmaceutical Sciences* **87**:694-701 (1998).
 20. H. S. Lee, and W. N. Kim. Glass transition temperatures and rigid amorphous fraction of poly(ether ether ketone) and poly (ether imide) blends. *Polymer* **38**:2657-2663 (1997).
 21. D. Q. M. Craig, V. L. Kett, J. R. Murphy, and D. M. Price. The measurement of small quantities of amorphous material – should we be considering the rigid amorphous fraction? *Pharmaceutical Research* **18**:1081-1082 (2001).
 22. Y. S. Chun, Y. S. Han, J. C. Hyun, and W. N. Kim. Glass transition temperatures and rigid amorphous fraction of poly (ether ether ketone) and polyarylate blends. *Polymer* **41**:8717-8720 (2000).
 23. K. J. Crowley, and G. Zografi. The effect of low concentrations of molecularly dispersed poly(vinylpyrrolidone) on indomethacin crystallization from the amorphous state. *Pharmaceutical Research* **20**:1417-1422 (2003).
 24. X. C. Tang, M. J. Pikal, and L. S. Taylor. The effect of temperature on hydrogen bonding in crystalline and amorphous phases in dihydropyridine calcium channel blockers. *Pharmaceutical Research* **19**:484-490 (2002).
 25. K. K. Chee. Thermodynamic study of glass transitions in miscible polymer blends. *Polymer* **36**:809-813 (1995).

Table B-I-I: Effect of storage conditions on thermal behavior of selected trehalose-dextran mixtures

Storage condition	Percent trehalose (w/w)	Storage period (days)	T _h * (J/g)	T _{g2} [†] (°C)	ΔC _p [‡] at T _{g2} (J/g/°C)
50°C/ 75% RH	40	0		169	0.3727
		2		203	0.1710
		4		203	0.1564
		13	17.7	209	0.1095
		23	28.6	206	0.1189
		34	34.9	207	0.0981
	30	0		182	0.3329
		5		200	0.2428
		8	12.9	202	0.1314
		19	13.8	207	0.1214
31		14.7	208	0.1176	
40°C/ 75% RH	40	0		169	0.3727
		6	7.6	196	0.1807
		13	23.9	213	0.1076
		23	27.0	207	0.1136
		34	30.6	207	0.0741
	30	0		182	0.3329
		8	6.2	192	0.1579
		19	9.5	202	0.0971
		31	12.2	206	0.1913
		52	12.5	203	0.1192
	90	17.9	205	0.1620	

* Heat of fusion of water-loss-endotherm for recrystallized trehalose dihydrate.

[†] Glass transition temperature of polymer-trehalose mixtures.

[‡] Heat capacity change

Table B-I-II: Solid solubility of trehalose in the polymers used as a function of storage condition

Polymer	Storage condition °C / %RH	Water content at equilibrium* %w/w	$(T_{\text{storage}} - T_{\text{g}}^{\text{w}}) = \Delta T_{\text{g}}^{\text{s}}$ (°C)	T_{g}^{eq} °C	Solid solubility [‡] % w/w trehalose
Dextran	23 / 75	16.5% ± 1.0	1	197.8 ± 4.4	18 ± 2.9
	40 / 75	13% ± 1.0	18	208.7 ± 3.8	12 ± 2.5
	50 / 75	11% ± 0.8	28	208.3 ± 1.0	12 ± 0.7
PVP	23 / 69	19.9 ± 1.1	5-15	158 ± 2.1	10 ± 2.5

* Determined by thermogravimetric analysis by heating the sample at 5°C/min.

§ ΔT_{g} is the difference between storage temperature and the plasticized T_{g} due to presence of moisture (T_{g}^{w}), when the samples were exposed to stability conditions.

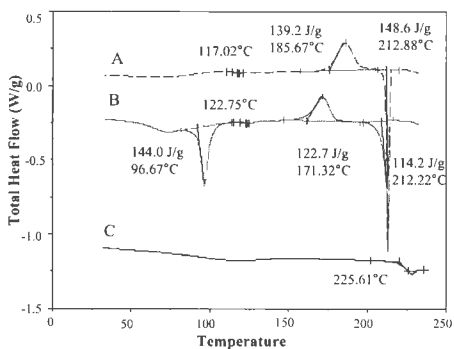
† Mean value of $T_{\text{g}2}$ (i.e., T_{g} of polymer-trehalose mixture) after $T_{\text{g}2}$ reaches a steady state.

‡ Calculation of solid solubility limit is described in Fig. B-I-2c,d and the text.

Figure B-I-1

DSC total heat flow scans of (a) **A**: lyophilized trehalose; **B**: untreated trehalose dihydrate and **C**: lyophilized dextran; (b) heat flow due to recrystallization of amorphous trehalose by storing it at **A1**: 50°C/ 75% RH; and **A2**: 40°C/ 75% RH and **B**: untreated trehalose dihydrate.

a)



b)

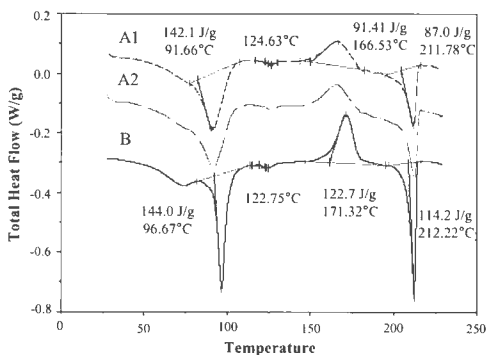


Figure B-I-2

MDSO reversing heat flow scans of mixtures of trehalose with (a) dextran and (b) PVP, showing a composition dependent single T_g . Plots of T_g of mixture of trehalose with (c) dextran and (d) PVP as function of trehalose composition. Arrows represent the solid-solubility limits of trehalose in the polymers as explained in the text.

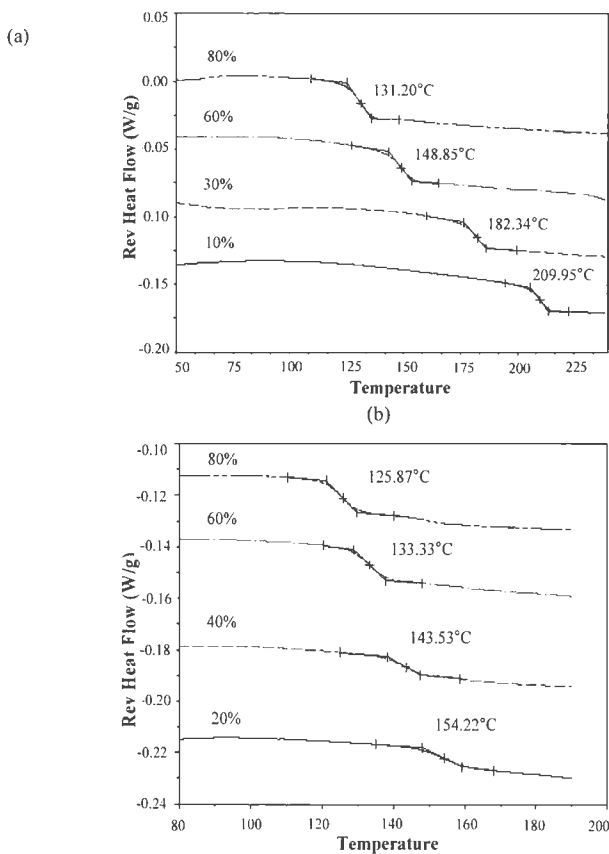


Figure B-I-2 (contd.)

MDSC reversing heat flow scans of mixtures of trehalose with (a) dextran and (b) PVP, showing a composition dependent single T_g . Plots of T_g of mixture of trehalose with (c) dextran and (d) PVP as function of trehalose composition. Arrows represent the solid-solubility limits of trehalose in the polymers as explained in the text.

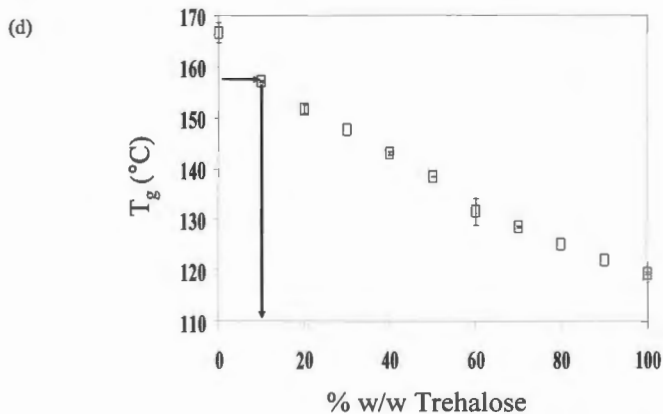
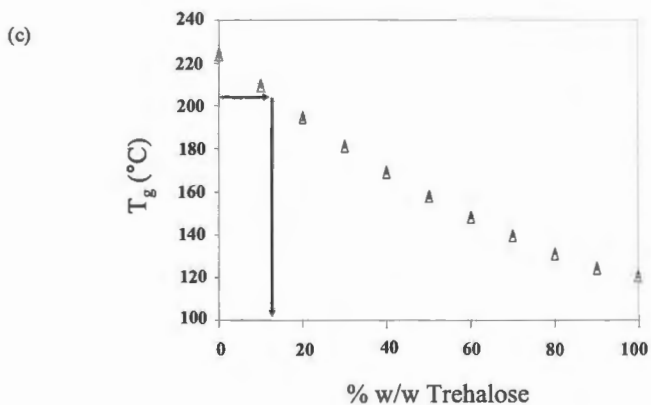


Figure B-I-3

MDSC reversing heat flow scans of trehalose-dextran mixtures exposed to 50°C/ 75% RH conditions for different time intervals: (a) 40% w/w trehalose (A: 0 days, B: 2 days, C: 4 days, D: 13 days, E: 23 days, F: 34 days) (b) 30%w/w trehalose (G: 0 days, H: 5 days, I: 8 days, J: 19 days, K: 31 days, L: 50 days) (c) trehalose-in-PVP stored at 23°C/ 69%RH (O: 40% w/w, 0 days; P: 20%w/w, 0 days; Q: 0% w/w, 0 days; R: 20% w/w, 200 days; S: 40% w/w, 190 days; T: 40% w/w, 195 days; U: 40% w/w, 200 days) and (d) 40% w/w trehalose at M: 4 days, N: 34 days [T_{R1} : T_g of phase separated amorphous trehalose; T_{R2} : T_g of polymer-trehalose mixture; T_h : water-loss endotherm of crystalline trehalose. The numbers within the brackets in Fig. B-I-3c represents the change in heat capacity (ΔC_p) at T_{R2}].

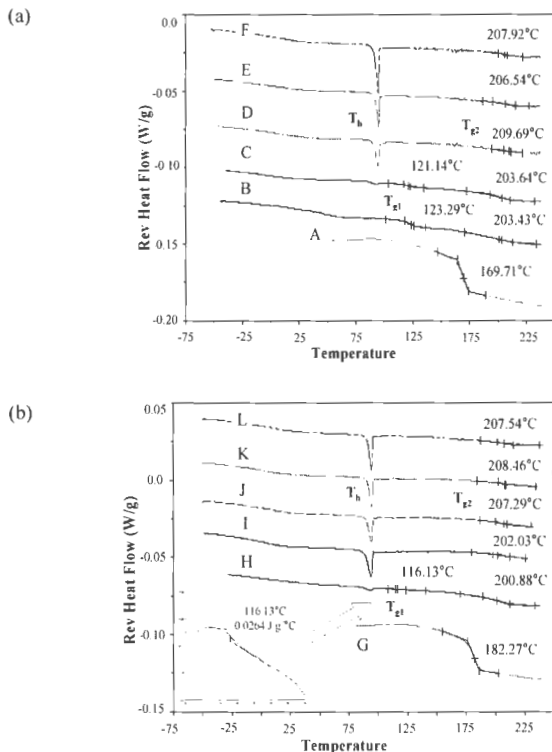
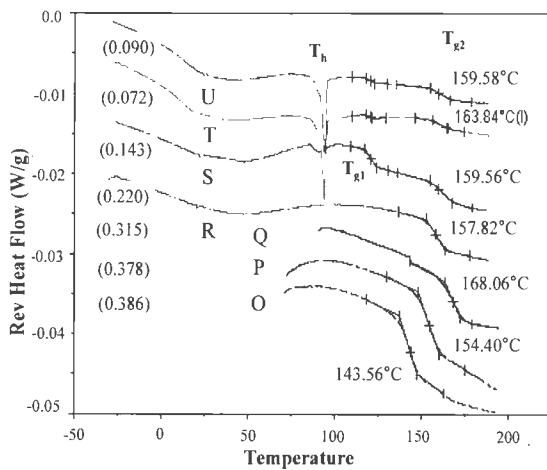


Figure B-I-3 (contd.)

(c)



(d)

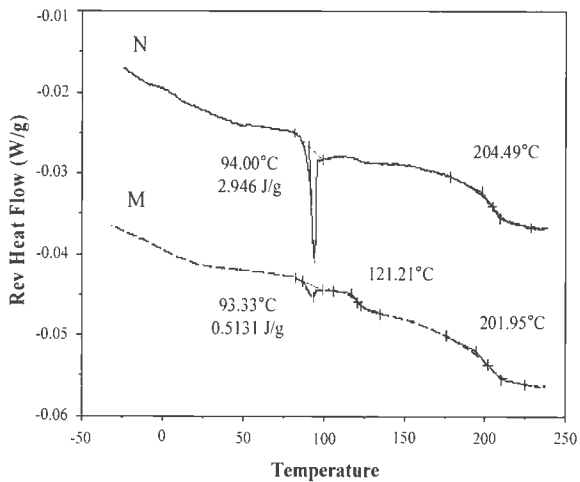


Figure B-I-4

Plot of T_{g2} of trehalose-dextran mixtures: 70% w/w (\square), 40% w/w (Δ), 30% w/w (\blacksquare), and 20% w/w (\blacktriangle) at (a) 50°C/ 75% RH; (b) 40°C/ 75% RH; (c) 23°C/ 75% RH. Dotted line indicates the T_g of pure dextran.

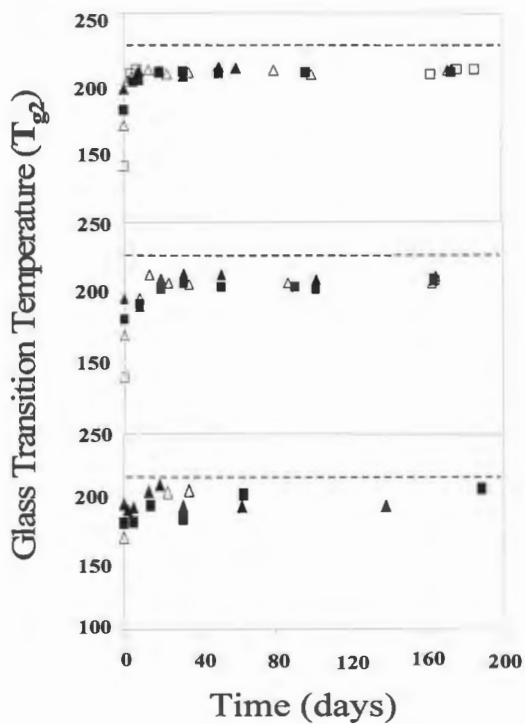
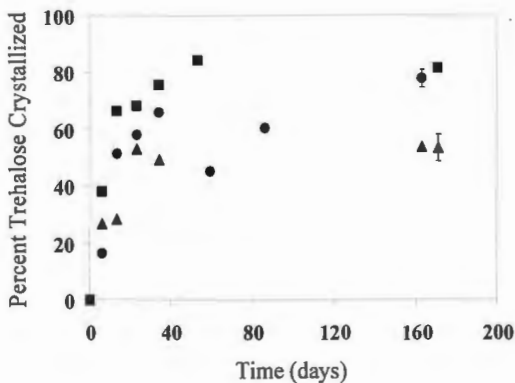


Figure B-1-5

Percent crystalline trehalose dihydrate present in trehalose-dextran mixtures containing (a) 40% w/w trehalose and (b) 30% w/w trehalose under storage conditions: 50°C/ 75% RH (■), 40°C/ 75% RH (●), and 23°C/ 75% RH (▲). Error bars represent the range for (n=3) measurements whenever shown. The percent crystallinity was calculated from the heat of fusion values of water-loss endotherm of the total heat flow and has been adjusted for the differences in initial trehalose content.

a)



b)

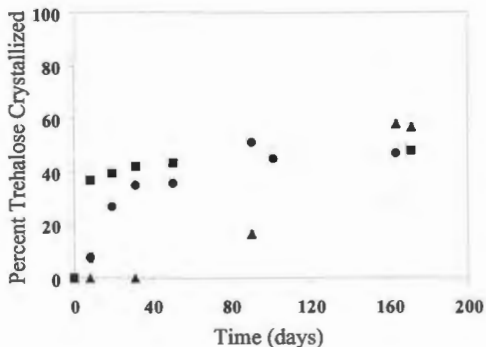


Figure B-I-6

Hypothetical depiction of solid solubility between trehalose (1T, 2T, 3T, 4T) and dextran (repeat units: 1D, 2D, 3D, 4D). Bridging cylinders represent the hydrogen bonds between the acceptor and donor groups of the components.

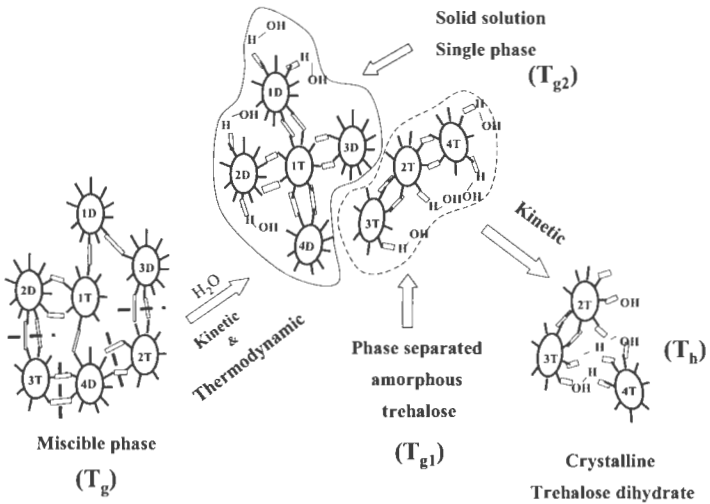
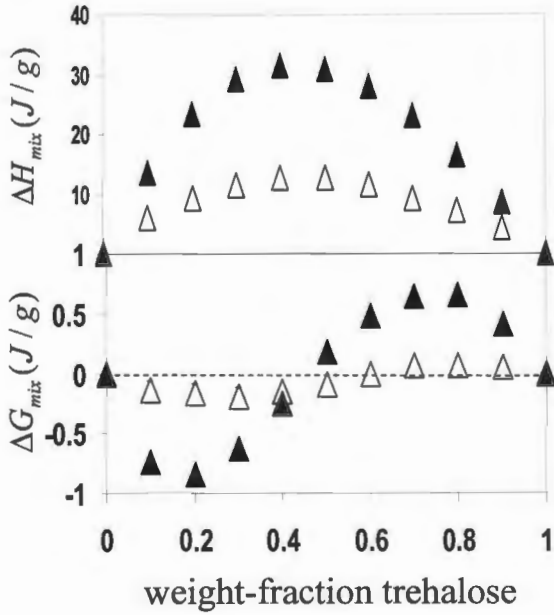


Figure B-I-7

Enthalpy of mixing (ΔH_{mix}) and free energy of mixing (ΔG_{mix}) of trehalose with dextran (\blacktriangle) and PVP (\triangle). The broken line indicates zero ΔG_{mix} .



MANUSCRIPT II

PHASE BEHAVIOR OF AMORPHOUS MOLECULAR DISPERSIONS II: ROLE OF HYDROGEN BONDING IN SOLID SOLUBILITY AND PHASE SEPARATION KINETICS

Madhav Vasanthavada¹, WeiQin Tong², Yatindra Joshi², and M. Serpil Kislalioglu^{1,3}

ABSTRACT

Purpose: To study the factors influencing the 'solid solubility' and phase separation kinetics of drugs from solid dispersions using modulated DSC (MDSC).

Methods: Solid dispersions of PVP with griseofulvin and indoprofen were prepared using solvent evaporation technique. MDSC was used to quantify the drug-polymer miscibility, the drug solid solubility and the rate of drug-polymer phase separation at

¹ Department of Applied Pharmaceutical Sciences, The University of Rhode Island, Kingston, RI 02881.

² Pharmaceutical & Analytical Development, Novartis Pharmaceutical Corporation, East Hanover, NJ 07936.

³ To whom correspondence should be addressed. (Telephone: (401) 874 5017; Email: skis@uri.edu)

40°C/69%RH. Characterization of drug-polymer interactions was performed using FTIR spectroscopy. X-ray diffractometry (XRD) was used to detect the levels of crystallinity in the solid dispersions.

Results: In the freshly prepared solid dispersions, both griseofulvin and indoprofen were molecularly miscible with PVP up to 30% w/w drug concentration. FTIR demonstrated the presence of hydrogen bonding in indoprofen-PVP dispersions, but not in griseofulvin-PVP dispersions. When exposed to 40°C/69%RH for 15 days, griseofulvin-PVP mixtures resulted in complete phase separation and crystallization which was monitored by the changes in their T_g . A complete phase separation indicated absence of solid solubility. XRD detected crystallinity in 10%w/w griseofulvin dispersions, supporting the MDSC analysis. On the other hand, the solid solubility of indoprofen in PVP was determined as 13% w/w and no crystallinity could be detected around this concentration using XRD. The rate of phase separation of drug from the polymer was estimated by fitting the fraction of drug phase separated from the polymer as determined by analyzing the T_g of drug-polymer miscible phase to the use of first order kinetics. The rate constants for 10%, 20% and 30% w/w griseofulvin-in-PVP were 4.66, 5.19, and 12.50 ($\times 10^2$) [day^{-1}] respectively. Indoprofen-PVP dispersions had rate constants of 0.62, and 1.25 ($\times 10^2$) [day^{-1}] for 20% and 30%w/w solid dispersions respectively. 10%w/w indoprofen solid dispersions did not phase separate.

Conclusions: Although both indoprofen and griseofulvin formed amorphous solid dispersions with PVP at 30%w/w initial drug concentration, the hydrogen bonding ability

of indoprofen to PVP improved its solid solubility and hence physical stability. The phase separation rate was seen to decrease by decreasing drug-to-carrier ratio.

KEY WORDS: miscibility, hydrogen bonding, amorphous, PVP, crystallization

INTRODUCTION

Currently the development of a successful solid dispersion product is dependent upon the ability to stabilize the metastable amorphous form of the drug substance. Because amorphous form offers high solubility, it is important of retain this form of the drug in the solid dispersion [1-3]. Several studies have however demonstrated the unpredictable crystallization of amorphous drugs by itself and from solid dispersions, which is limiting its commercial potential [4-7]. Water soluble polymers have been proposed as a means to inhibit or delay the drug crystallization by forming a miscible phase with the drug. In the miscible phase, the drug and polymer are molecularly dispersed and crystallization inhibition is possible via drug-polymer hydrogen bonding, and/or the anti-plasticizing effect (i.e. increase in T_g of solid dispersions) by the polymer [8, 9]. A detailed evaluation of the factors influencing the physical stability of amorphous solid dispersions reveals the presence of two opposing forces. On one hand, polymer helps in retaining the miscibility and prevents the drug crystallization. On the other hand, the uptake of moisture and/or exposure to elevated temperatures increases the molecular mobility, thereby increasing

the potential for phase separation (de-mixing) and crystallization. The physical integrity of the miscible solid dispersion would therefore depend upon the relative magnitude of the two opposing forces.

In an earlier study, we demonstrated that depending upon the nature of drug-polymer interactions, a fraction of the drug can remain dissolved in the polymer in the solid-state even under high heat and humidity conditions [10]. This fraction is termed as the “solid solubility” and one of the factors influencing the solid solubility is the affinity between the two components of the dispersion.

In view of the earlier findings, the purpose of this paper is to provide further evidence to substantiate the importance of hydrogen bonding in the solid solubility and physical stability of solid dispersions. The solid solubility of two different hydrophobic drugs, namely griseofulvin and indoprofen in poly (vinyl pyrrolidone) (PVP), were determined. Griseofulvin and indoprofen are highly crystalline in nature as indicated by their high melting temperatures and heats of fusion and therefore serve as good model compounds. In addition, based on their chemical structures, griseofulvin cannot hydrogen bond with PVP whereas indoprofen can participate in hydrogen bonding, thus enabling assessing the impact of drug-polymer affinity on the solid solubility.

The second objective of this study was to determine experimentally the kinetics of phase separation of the drug from the polymer. One may intuitively expect that for a drug to crystallize from a miscible solid dispersion, it would have to phase separate first from the polymer matrix. Therefore determining the rate of phase separation of drug would serve to provide valuable information on the overall rate of physical instability since

crystallization of drug substance is often complex to predict. In some cases the solid solubility of the drug in the solid dispersion may need to be very low in order to formulate a physically stable miscible solid dispersion that would meet the high therapeutic dose requirement. By understanding the drug phase separation and crystallization kinetics one can possibly formulate miscible solid dispersions that are above the drug's solid solubility and retain their physical stability by either defining the shelf life or by choosing appropriate storage conditions. In this study we have employed a theoretical rate equation that is typically used in determining crystallization kinetics, to analyze the phase separation rate of griseofulvin and indoprofen from their solid dispersions.

MATERIALS AND METHODS

Materials:

Plasdone (Poly (vinylpyrrolidone)) PVP K29/32 with M_w 50 KDa was obtained from ISP Technologies Inc., (Wayne, NJ). Samples were dried at 105°C under vacuum for 20 hours prior to preparing solid dispersions. Griseofulvin ((2S)-trans-7-Chloro-2',4,6-trimethoxy-6'-methylspiro(benzofuran-2[3H], 1'-[2]cyclohexene)-3,4'-dione)) and indoprofen (α -Methyl-p-(1-oxo-2-isoindolinyl)benzenacetic acid) were purchased from Sigma Chemical Company (St. Louis, MO) and were used as received to prepare the solid dispersions. Copper chloride that was used to prepare saturated salt solution to

obtain 69% RH was purchased from Fisher Chemicals Co., Fair Lawn, NJ [11]. The chemical structures of all the materials involved in the study are shown in Fig. B-II-1.

Methods:

Preparation of solid dispersions using solvent evaporation technique:

Solid dispersions of drug (10-50% w/w) in PVP were prepared using solvent evaporation technique. Crystalline griseofulvin and crystalline indoprofen were dissolved (0.3 – 1.5g) in dichloromethane and methanol respectively by stirring the solution in a waterbath at 37°C for about 15 minutes. PVP was added to the drug solution to make the total weight of solids as 3g. After all the PVP was dissolved, as determined visually, the solvent was evaporated using a rotary vacuum evaporator (Rotavap[®]) by heating the solution at 37°C in a water bath. The residual solid dispersions thus obtained were further dried in a vacuum oven at room temperature for 24 hours to remove the remaining residual solvent. They were ground with a mortar and pestle and were sifted through sieve # 70 to result in particle size $\leq 210\mu\text{m}$. The solid dispersions were stored in vials over anhydrous CaSO_4 in a freezer when not being studied in order to minimize the molecular mobility of the system.

Determination of solid solubility

To determine the solid solubility of drugs in the polymer, solid dispersions containing 10, 20, and 30% w/w of griseofulvin and indoprofen in PVP were accurately weighed (8-12mg) in standard DSC pans. The pans were placed in desiccators containing saturated copper chloride solution (69% RH) and an oven at $40 \pm 1^\circ\text{C}$ (Precision Scientific Inc.,

Chicago, IL). The 69% RH was chosen in order to prevent deliquescence of PVP at higher moisture levels and yet to provide an accelerated storage condition. By storing the samples in discrete DSC pans, the reproducibility could be assessed without disturbing the bulk properties of the aging samples. Samples were taken out from the desiccators for analysis at regular intervals for up to 90 days. They were crimped with aluminium lids having five pinholes to facilitate the removal of absorbed water during heating. The resulting thermal scans were analyzed for their changes in the drug-polymer phase compositions by measuring the glass transition temperatures (T_g). An increase in the T_g of the miscible phase implied phase separation of drug from the solid dispersion since lesser fraction of drug is present in the polymer phase to plasticize the system (provided the T_g of drug is less than T_g of polymer). The increase in T_g of the solid dispersion was monitored as a function of storage time until no further increase in the T_g was observed. To quantify the solid solubility, the equilibrium T_g value was utilized to identify the percentage of drug that would provide the same T_g value in a freshly prepared solid dispersion.

Modulated differential scanning calorimeter (MDSC):

Thermal analysis was performed using MDSC 2920 (TA Instruments, New Castle, DE), with a liquid nitrogen cooling accessory. The analysis was performed under a purge of dry nitrogen gas (60cc/min). High purity indium and sapphire were used frequently to calibrate the heat flow and heat capacity of the instrument. Thermal history of the samples was not erased. The events were recorded and analyzed during the first heating

scan. Samples (~ 8-12 mg) were initially cooled to -10°C for 10 minutes and were heated to 245°C at $1^{\circ}\text{C}/\text{min}$ with modulations of 0.266° every 50 seconds. The specified amplitude and period were optimized to provide the best results for analysis. Each measurement was repeated three times at every time point to ascertain the reproducibility of the experiments.

X-ray Powder Diffraction (XRPD):

The X-ray powder diffractometer (Rigaku RINT (D/Max) 2200 that was equipped with an Ultimagoniometer) consisted of a 40 KV, 40mA generator with a Cu K_{α} radiation anode tube. XRD pattern was used to test the presence of crystallinity in the solid dispersions. The samples were sifted through 70-mesh and placed on a 0.5 mm quartz plate holder prior to exposure to X-rays. They were scanned over a 2θ range between 2° and 40° at a scan rate of 2° per minute in 0.02° step size. The divergence and scattering slits were set at 1.00° , receiving slit at 0.15mm and monochromator was used at 0.45mm.

Fourier Transform Infra-red Spectroscopy (FTIR):

Nicolet spectrometer equipped with a KBr beam splitter was used to obtain the infrared spectra. Calibration for wavenumber accuracy was performed by using polystyrene sample. Dry nitrogen gas was used to purge the beam splitter and the sample compartment. IR spectra were obtained using an attenuated total reflectance (ATR) accessory (single reflection bounce diamond crystal; Golden Gate accessory). For each spectrum, 32 scans were performed and a resolution of 4 cm was chosen. The ATR accessory enabled to obtain the spectra by pressing the solid material onto the diamond

crystal. This accessory eliminates the use of KBr and yet produces comparable results [12]. All samples were dried under vacuum for 20 hrs prior to obtaining any spectra, to remove the influence of residual moisture.

RESULTS

Characterization of drug substance

A comparison of the physical-chemical properties of griseofulvin and indoprofen is provided in Table B-II-1. Both compounds were seen to have high melting temperatures and heats of fusion. The glass transition temperature was obtained by heating the amorphous drug substance in DSC at 1°C/min. The amorphous drug was formed by rapidly cooling the molten crystalline drug. Upon heating both the amorphous drugs underwent recrystallization at temperatures above their T_g , indicating their propensity to crystallize.

Characterization of amorphous molecular dispersions

Griseofulvin-PVP and indoprofen-PVP solid dispersions showed a composition-dependent single T_g for up to 30% w/w drug concentrations (Fig. B-II-2). This behavior indicated the presence of molecularly dispersed drug in the polymer at these concentrations. Above 30%w/w, multiple T_g s were observed in the solid dispersions of griseofulvin-PVP, indicating a phase-separated mixture. In the indoprofen-PVP dispersions, the T_g of 40%w/w dispersion was higher than the T_g of 30%w/w dispersion

thus indicating immiscibility in the sample. For both the drug solid dispersions no crystalline peaks were seen at drug levels of 30%w/w or less using x-ray diffraction. Although x-ray pattern revealed crystallinity for 40%w/w solid dispersions, no significant melting endotherm was detected at this composition for the crystalline drug using MDSC (Fig. B-II-2). This could most likely be due to the solubilizing effect of polymer on the crystalline drug while heating in the MDSC.

In order to probe the interactions between the drug and PVP, the FTIR spectra of freshly prepared solid dispersions were compared with the drug – PVP physical mixtures. In Fig. B-II-3a, the carbonyl stretching of a 30%w/w griseofulvin-in-PVP solid dispersion is compared with the corresponding physical mixture of amorphous griseofulvin and PVP. No significant differences were observed between the two spectra, indicating the absence of interactions between griseofulvin and PVP in the solid dispersions. Even with an increase in griseofulvin concentration from 10 to 30%w/w in solid dispersions, the peak carbonyl position of PVP did not shift significantly from 1667cm^{-1} . Only a slight broadening of the peak and a shift in the wave numbers towards values of pure amorphous griseofulvin was seen most likely due to the presence of higher concentrations of griseofulvin.

For indoprofen-PVP solid dispersions, addition of 10% and 30%w/w indoprofen caused a significant shift in the carbonyl stretching of PVP from 1667cm^{-1} to 1654cm^{-1} (Fig. B-II-3b), suggesting the presence of hydrogen bonding between the two components. The spectrum of a 30%w/w solid dispersion, which had the maximum miscibility as suggested by MDSC, was clearly different from the corresponding physical mixture. The

physical mixtures were prepared using crystalline indoprofen and PVP, because of the rapid tendency of indoprofen to crystallize during the preparation and characterization of physical mixtures. Pure amorphous indoprofen was however scanned immediately after its preparation as was confirmed amorphous even after the scan using optical microscopy. To ensure that the crystalline nature of indoprofen in the physical mixture did not contribute to the peak shift, the spectra of amorphous and crystalline indoprofen were compared and no significant differences were observed in the peak region of interest (i.e. 1667cm^{-1} to 1654cm^{-1}).

Determination of solid solubility

Griseofulvin and PVP solid dispersions

Solid dispersions of griseofulvin and PVP that were exposed to accelerated stability conditions of $40^{\circ}\text{C}/69\%\text{RH}$ were analyzed periodically by monitoring their T_g , to determine any alteration in the miscible phase composition. MDSC reversing heat flow scans of 30% w/w griseofulvin and PVP solid dispersions, which were stored at $40^{\circ}\text{C}/69\%\text{RH}$ for a period of 1 – 15 days are shown in Fig. B-II-4a. While a freshly prepared solid dispersion showed a single T_g at 131°C , two T_g s referred to as T_{g1} and T_{g2} , were observed in the stability samples during the 5 day-storage period. T_{g1} corresponded to the T_g of PVP-in-griseofulvin dispersions and T_{g2} corresponded to the T_g of griseofulvin-in-PVP dispersions.

The formation of two T_g s indicates the phase separation of griseofulvin and PVP. Upon storage, the heat capacity change at T_{g1} decreased and that of T_{g2} increased in a time-

dependent manner. The T_{g1} and T_{g2} values were seen to increase with storage time, indicating a progressive phase separation, except for the 1 day-old sample, where a decrease in T_{g1} was noticed. While T_{g1} disappeared in the 9 day-old or older samples, T_{g2} values increased and seemed to reach a plateau at $166^{\circ} \pm 1.5^{\circ}\text{C}$. This plateau value was termed as equilibrium T_g (T_g^{eq}).

The thermal events for 20%w/w griseofulvin and PVP solid dispersions followed the same pattern when they were exposed to $40^{\circ}\text{C}/69\%\text{RH}$ (Fig. B-II-4b). However, unlike 30% w/w dispersions, the T_{g1} decreased during the first 4 days and then disappeared subsequently. Such a decrease in T_{g1} is possibly due to the increased plasticization of griseofulvin in the griseofulvin-rich fraction of solid dispersion. The T_{g1} disappears after reducing to a certain value suggesting a threshold level of griseofulvin in the griseofulvin-rich phase above which crystallization would occur. Indeed as expected the T_{g1} of 20% and 30%w/w solid dispersions reach the same value before disappearing, indicating the threshold composition needed for crystallization. This possibility may also explain the crystallinity in a freshly prepared 40%w/w solid dispersion which is most likely above the threshold drug level.

Indoprofen and PVP solid dispersions

MDSC scans of 30% w/w indoprofen-in-PVP solid dispersions, which were stored at $40^{\circ}\text{C}/69\% \text{RH}$ for a period of 1 – 90 days are shown in Fig. B-II-4c. In contrast to the phase behavior of griseofulvin-PVP solid dispersions, a single T_g was detected in the indoprofen-PVP solid dispersions throughout the 90 day storage period. The T_g values of

the solid dispersions increased with storage time, although at a much slower rate, when compared to the griseofulvin-PVP solid dispersions. The T_g values reached a plateau at T_g^{eq} of $142 \pm 1.3^\circ\text{C}$ after about 70 days of storage period. The 20%w/w indoprofen solid dispersions also showed a similar shift in the T_g values representing similar changes in phase composition when stored at $40^\circ\text{C}/69\%\text{RH}$.

Quantification of solid solubility

A plot of T_g values of 10%, 20% and 30% w/w solid dispersions of griseofulvin-in-PVP and indoprofen-in-PVP that were subjected to $40^\circ\text{C}/69\% \text{RH}$ for 3 months is shown in Fig. B-II-5. For griseofulvin-PVP solid dispersions (Fig. B-II-5a), the T_{g2} values of all the solid dispersions reached a plateau (T_g^{eq}) at $166^\circ \pm 1.5^\circ\text{C}$ during the 90 days storage period, which is close to the T_g of pure PVP (167°C). Since the entire drug phase separated from PVP as seen from the increase in T_g to $\sim 167^\circ\text{C}$, the solid solubility of griseofulvin in PVP was determined as $\sim 0\% \text{w/w}$ at the employed storage condition. The solid solubility limit was found to be independent of the initial concentration of griseofulvin-in-PVP since the T_g^{eq} was independent of the T_g values of freshly prepared solid dispersions.

On the other hand, the solid dispersions of indoprofen and PVP behaved very differently as seen from Fig. B-II-5b. During the 70 days storage period, the T_g values reached a plateau at T_g^{eq} of $142 \pm 1.3^\circ\text{C}$. As seen clearly from Fig. B-II-5b, the T_g^{eq} for indoprofen-PVP solid dispersions is significantly lower than the T_g of pure PVP (167°C). The solid

solubility of indoprofen in PVP at storage conditions of 40°C/69% RH was quantified as 13% w/w.

X-ray diffraction analysis

In order to determine if the phase separation and/or crystallization of drugs from the solid dispersions indeed resulted in crystallization of drug substance, X-ray diffraction was utilized. MDSC was unable to detect a melting endotherm of crystalline drug substance possibly due to the solvent effect of polymer at high temperatures as described earlier. Hence X-ray diffraction was chosen to validate the experimental solid solubility values. Fig. B-II-6a shows the X-ray patterns of solid dispersions containing 10% and 20% w/w griseofulvin-in-PVP after 10 days of exposure to 40°C/69% RH. The X-ray patterns at the same composition of physical mixtures of the crystalline drug and PVP were used for comparison. From Fig. B-II-6a, crystallinity is seen within 10 days even for the 10%w/w solid dispersions. Moreover, the peak intensity of the 10% and 20%w/w solid dispersions, after exposure to stability conditions, was similar to the corresponding physical mixtures thus supporting ~0%w/w drug solid solubility.

In Fig. B-II-6b, the X-ray diffraction patterns of 10% and 20% w/w indoprofen and PVP solid dispersions that were exposed to 40°C/69% RH for 90 days are compared with the corresponding physical mixtures. No crystallinity in the 10%w/w solid dispersions was noticed even at the end of 90 days storage period. However 20% w/w solid dispersion had small fraction of crystalline drug, as indicated by the smaller peak height in the solid dispersion when compared to the corresponding physical mixtures. These findings

support the solid solubility of 13%w/w of indoprofen-in-PVP that was determined using MDSC.

DISCUSSION

Hydrogen bonding and solid solubility

The data presented in this study suggests that the presence of hydrogen bonding facilitated phase miscibility between indoprofen and PVP even under accelerated stability conditions. Griseofulvin and indoprofen are easily crystallisable drugs as seen from their high melting temperatures, high heats of fusion and recrystallization. Further both drugs demonstrate relatively low glass transition temperatures in their amorphous states and recrystallized instantaneously when exposed to relative humidity greater than 57%. Therefore to maintain the drugs in their amorphous form in the solid dispersions under stability conditions is indeed a challenging and an important task.

If the chemical structures of PVP, griseofulvin and indoprofen, illustrated in Fig. B-II-1, are examined, it is seen that PVP can act only as a proton acceptor through either the O or N atoms of the pyrrolidone ring. However due to the steric constraints, the N atom may not participate actively in hydrogen bonding [13]. The chemical structure of griseofulvin reveals two carbonyl and three methoxy groups which can actively participate in hydrogen bonding as proton acceptors. On the other hand, indoprofen has four hydrogen bond acceptors namely the carbonyl group of $-COOH$, oxygen atom of hydroxyl group of $-COOH$, the carbonyl group of the pyrrolidone ring and the N atom of the pyrrolidone

ring. Indoprofen also has one proton donor which is the proton of the hydroxyl group of –COOH. Since hydrogen bonding occurs between a hydrogen bond acceptor and a donor, for two components to interact one of them should have at least one donor and the other at least one acceptor [14].

When griseofulvin and PVP are molecularly mixed, no hydrogen bonding between the two components is demonstrated through the FTIR spectra since neither component have hydrogen bond donor. On the other hand, a hydrogen bond interaction between the hydroxyl group of –COOH of indoprofen and the carbonyl group of the pyrrolidone ring in PVP is likely to occur. This is evidenced by a decrease in the carbonyl stretching of the carbonyl group of PVP from 1667cm^{-1} to 1654cm^{-1} in the 10% and 30%w/w solid dispersions.

Despite the absence of hydrogen bonding in griseofulvin and PVP solid dispersions, a 30% w/w initial miscibility is seen in these dispersions, similar to the indoprofen-PVP solid dispersions that demonstrate hydrogen bonding. Such miscibility in the absence of interactions is possibly favored through gain in the entropy of the system. Griseofulvin is dispersed in PVP in its amorphous phase, which is entropically favored when compared to its crystalline form. The solid dispersions thus formed remained miscible at regular storage temperature most likely due to the lack of molecular mobility, due to their high T_g values. In the presence of moisture however, plasticization of solid dispersion could lead to an increase in the molecular mobility and thereby induce de-mixing and crystallization. One of the factors offering resistance for physical instability could be the extent of drug-polymer affinity. Although indoprofen and PVP solid dispersions have moisture levels

comparable to those of griseofulvin and PVP solid dispersions, the presence of hydrogen bonding between indoprofen and PVP could possibly explain for the enhanced solid solubility.

Kinetics of phase separation

Often times the therapeutic dose requirements of the drug substance is very high and the solid solubility of drug in the solid dispersions may not be high enough to formulate a physically stable solid dispersion. In such a case, it is important to understand the rate of drug phase separation under the regular storage conditions. Such estimation should provide a general understanding as to how various storage conditions influence the phase separation process. Phase separation of drug from the miscible phase could be the very first step towards drug crystallization and hence monitoring this process is very essential to better define physical stability. It is evident from Fig. B-II-5 that both the solid dispersions clearly had different rates of phase separation despite having similar moisture contents, same storage temperatures, same polymer and similar initial and moisture-plasticized T_g values. In order to determine and explain for the differences in various rates with which griseofulvin and indoprofen reach their solid solubility limit, the kinetic rate constants for phase separation of the drugs from the solid dispersions were calculated by fitting the fraction of drug phase separated to the kinetic rate equations. The phase separated fraction was determined from the shifts in the T_g values of the solid dispersions with storage time. Such a technique to interpret the physical stability of solid dispersions

based on the changes in T_g as an indicator of phase composition has not been demonstrated earlier.

Since griseofulvin and indoprofen have tendency to crystallize instantaneously when stored at 40°C/69%RH, a phase separation would immediately result into crystallization of these drug substances. Therefore, phase separation (i.e. formation of a heterogeneous phase), is considered to be the rate-limiting step for destabilization. Destabilization is defined as the physical state where a two-phase solid dispersion results. In order to estimate the rate constant for destabilization, the Kolmogorov-Johnson-Mehl-Avrami (KJMA) first order equation was used. KJMA equation is typically used to fit experimental crystallization patterns [15] and to obtain their rate constants and is described as:

$$[-\ln(1-\alpha)] = kt \quad (1)$$

where $(1-\alpha)$ is the fraction phase separated, k is the rate constant for phase separation, and t is the storage time.

In equation (1), the fraction crystallized $(1-\alpha)$ was obtained using the following expression:

$$(1-\alpha)_t = 1 - \frac{T_{g(\text{polymer})} - T_{g2(t)}}{T_{g(\text{polymer})} - T_{g(\text{initial})}} \quad (2)$$

The fraction of drug phase separated was obtained by determining the average of triplicate measurements of T_g of the solid dispersions at storage time t and using equation 2. The rate constant for phase separation was obtained using equation 1 and determining the slope of the linear equation. By obtaining the rates of phase separation, the physical

instability (i.e. crystallization) rate can be estimated, since the phase separation step is considered as the rate limiting step ($k_{(\text{crystallization})} \gg k_{(\text{phase separation})}$).

As inferred from the kinetic rate constants provided in Table B-II-II, the phase separation rate is higher for solid dispersions containing higher drug levels. This behavior agrees with the regular solution theory that higher the extent of super-saturation, the greater is the difference in the chemical potential in the supersaturated and saturated state and hence higher would be the driving force for crystallization. For a given drug level, the phase separation rate was found to be higher for griseofulvin-PVP solid dispersions when compared to indoprofen-PVP system. This behavior may be explained on the basis of the differences in the extent of interactions between individual drug and the polymer. Hydrogen bonding therefore seems to influence the solid solubility and thereby affect the kinetic rate of phase separation in amorphous solid dispersions.

CONCLUSIONS

The solid solubility of two crystallizable hydrophobic drugs namely griseofulvin and indoprofen in PVP has been experimentally determined using modulated DSC. Griseofulvin did not provide any solid solubility in PVP whereas a 13%w/w indoprofen remained miscible in the polymer under accelerated stability conditions of 40°C/69%RH. The higher solid solubility of indoprofen in PVP was attributed to the presence of hydrogen bonding between the two components in their solid dispersions. X-ray

diffraction provided supporting results to confirm the MDSC obtained solid solubility values.

The kinetics of phase separation of both drugs from the polymer was obtained by fitting the fraction of drug phase separated, as obtained from the shifts in T_g values of solid dispersions, to the KJMA rate equation. The rate of phase separation was found to be proportional to the extent of drug super-saturation and the strength of drug – polymer interactions. The technique described in this study monitors the very first step of destabilization process i.e., the phase separation that eventually leads to crystallization. Moreover, it does not rely upon the relatively unpredictable crystallization pattern of the drug substance and hence can be a better predictive tool of the physical stability of drugs in amorphous miscible solid dispersions.

ACKNOWLEDGMENTS

This study is a part of Ph.D. research of Mr. Vasanthavada who is a Novartis Graduate Research Fellow and has conducted his research at Novartis R&D facility. He wishes to acknowledge the fellowship and also thank Ms. Marilyn Alvine and Dr. Francis Liu for their support with X-ray scans.

REFERENCES

1. B. C. Hancock, and M. Parks. What is the true solubility advantage for amorphous pharmaceuticals? *Pharmaceutical Research* 17:397-404 (2000).
2. S. Torrado, S. Torrado, J. J. Torrado, and R. Cadomíga. Preparation, dissolution and characterization of albendazole solid dispersions. *International Journal of Pharmaceutics*. 140:247-250 (1996).
3. C. Lin, and T. Cham. Effect of particle size on the available surface area of nifedipine from nifedipine-polyethylene glycol 6000 solid dispersions. *International Journal of Pharmaceutics*. 127:261-272 (1996).
4. H. Ahmed, G. Buckton, and D. Rawlins. Crystallization of partially amorphous griseofulvin in water vapour: determination of kinetic parameter using isothermal heat conduction microcalorimetry. *International Journal of Pharmaceutics*. 167:139-145 (1998).
5. M. Otsuka, and N. Kaneniwa. A kinetic study of the crystallization process of non crystalline indomethacin under isothermal conditions. *Chemical and Pharmaceutical Bulletin*. 36:4026-4032 (1998).
6. G. K. Vudatha, and J. A. Rogers. Oral bioavailability of griseofulvin from aged griseofulvin-lipid co-precipitates: *in vitro* studies in rats. *Journal of Pharmaceutical Sciences*. 81:1166-1169 (1992).
7. S. K. Dordunoo, J. L. Ford, and M. H. Rubinstein. Physical stability of solid dispersions containing triamterene or temazepam in polyethylene glycols. *Journal of pharmacy and pharmacology*. 49:390-396 (1997).
8. K. Khougaz, and S. Clas. Crystallization inhibition in solid dispersions of MK-0591 and poly(vinylpyrrolidone) polymers. *Journal of Pharmaceutical Sciences*. 89:1325-1334 (2000).

9. T. Matsumoto, and G. Zografi. Physical properties of solid molecular dispersions of indomethacin with poly(vinylpyrrolidone) and poly(vinylpyrrolidone-co-vinylacetate) in relation to indomethacin crystallization. *Pharmaceutical Research* 16:1722-1728 (1999).
10. M. Vasanthavada, W. Tong, Y. Joshi and M. S. Kislalioglu. Phase behavior of amorphous molecular dispersions: determination of the degree and mechanism of solid miscibility. *Pharmaceutical Research*. Accepted. *In press*.
11. H. Nyqvist. Saturated salt solutions for maintaining specified relative humidities. *Int. J. Pharm. Tech. & Prod. Mfr.* 4:47-48 (1983).
12. L. S. Taylor and G. Zografi. Spectroscopic characterization of interactions between PVP and indomethacin in amorphous molecular dispersions. *Pharmaceutical Research*. 14:1691-1698 (1997).
13. P. Molyneux. Water-soluble synthetic polymer: properties and behavior, Volume I, CRC Press, Florida. 1983.
14. G. A. Jeffrey, and W. Saenger. Hydrogen bonding in biological structures. Springer-Verlag Berlin Heidelberg, New York. 1991.
15. K. J. Crowley, and G. Zografi. The effect of low concentrations of molecularly dispersed poly(vinylpyrrolidone) on indomethacin crystallization from the amorphous state. *Pharmaceutical Research*. 20:1417-1422 (2003).

Table B-II-1: Physical chemical properties of drug substance

Drug Substance	T _m	ΔH _f	T _g	T _c	ΔH _c	MW	H-bond Acceptors & Donors [§]
Griseofulvin	218	98	86	133	81	352	6 & 0
Indoprofen	214	127	50	75	58	281	4 & 1

MW: Molecular weight; T_m: Melting temperature; ΔH_f: Heat of fusion; T_g: Glass transition temperature of amorphous sample; T_c: Recrystallization temperature upon heating at 1°C/min; ΔH_c: Heat of recrystallization; [§] From the chemical structure (Fig. B-II-1).

Table B-II-II: Drug-to-polymer ratio and kinetics of phase separation at 40°C/69%RH

Solid Dispersion (% w/w drug)	% w/w moisture	Rate constant for phase separation k (days ⁻¹) (x 10 ²)	KJMA linear fit (R ²)	
Griseofulvin	30	6.6 ± 1.5	12.50	0.868
	20	7.8 ± 0.6	5.19	0.958
	10	9.8 ± 0.7	4.66	0.970
Indoprofen	30	6.0 ± 0.5	1.25	0.988
	20	9.3 ± 0.5	0.62	0.968
	10	7.9 ± 3.0	N/A	N/A

Figure B-II-1

Chemical structures of a) griseofulvin; b) indoprofen and c) repeat unit of PVP.

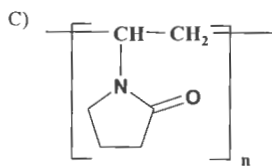
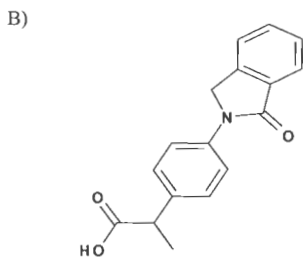
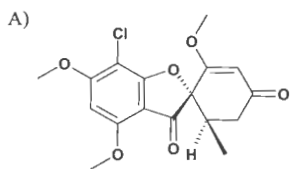
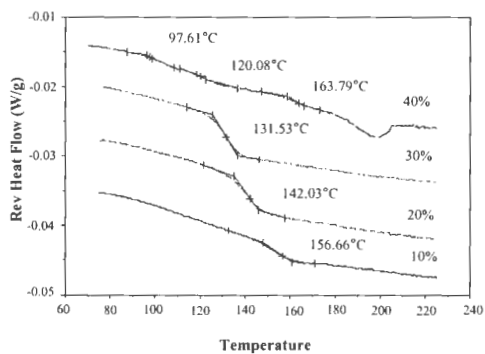


Figure B-II-2

MDSC reversing heat flow scans of solid dispersions of PVP and a) griseofulvin and b) indoprofen. Composition dependent single T_g indicates molecular miscibility for up to 30%w/w of both drugs in PVP.

a)



b)

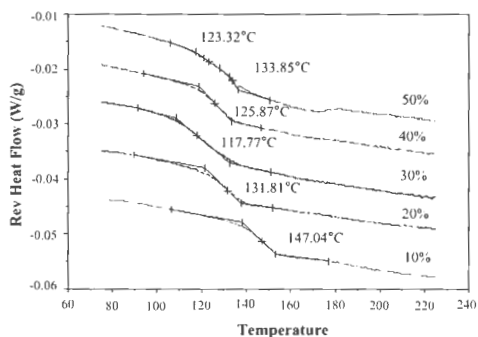


Figure B-II-3

Comparison of the infrared spectra of the carbonyl stretching region of solid dispersions and physical mixtures of (a) griseofulvin & PVP and (b) indoprofen & PVP. The percentages refer to the amounts of drug substance present.

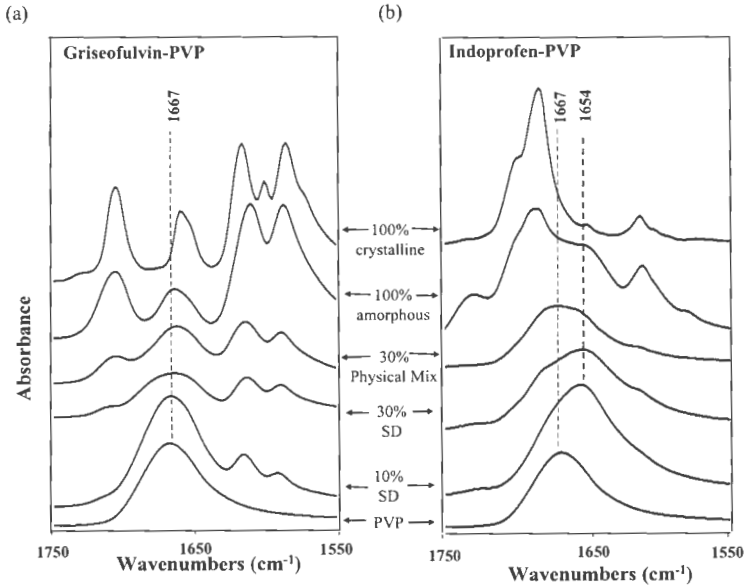
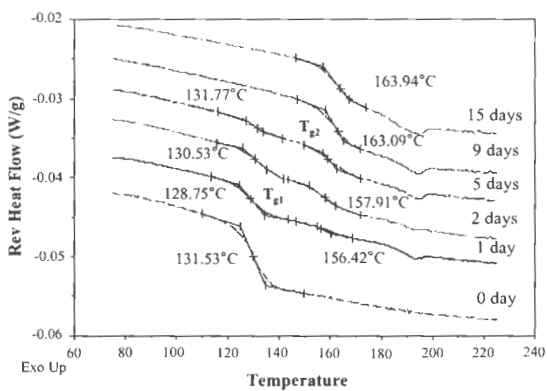


Figure B-II-4

MDSC reversing heat flow scans of solid dispersions exposed to 40°C / 69% RH for different time intervals: (a) 30% w/w griseofulvin-PVP; (b) 20% w/w griseofulvin-PVP; and (c) 30% w/w indoprofen-PVP. [T_{g1} : T_g of phase separated PVP-in-griseofulvin mixture; T_{g2} : T_g of griseofulvin-in-PVP mixture].



b)

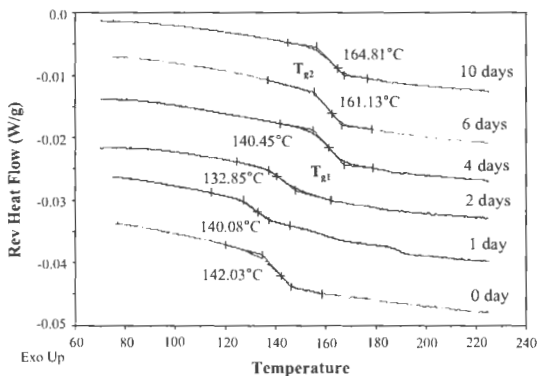


Figure B-II-4 (contd.)

c) 30% Indoprofen-PVP solid dispersions.

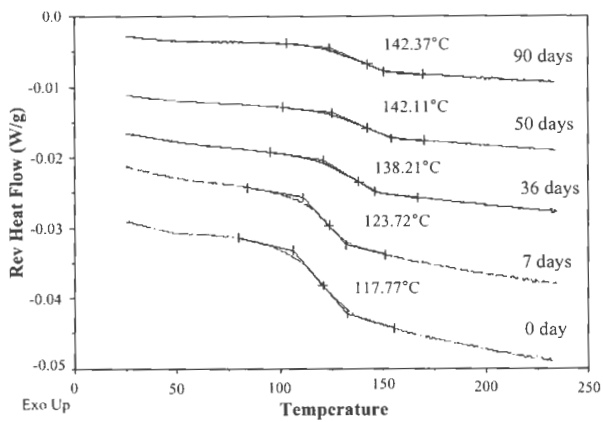


Figure B-II-5

Changes in the glass transition temperatures of 30% w/w (■), 20% w/w (Δ), and 10% w/w (○) of (a) Griseofulvin-PVP and (b) Indoprofen-PVP solid dispersions. The dotted line represents the T_g of PVP (167°C).

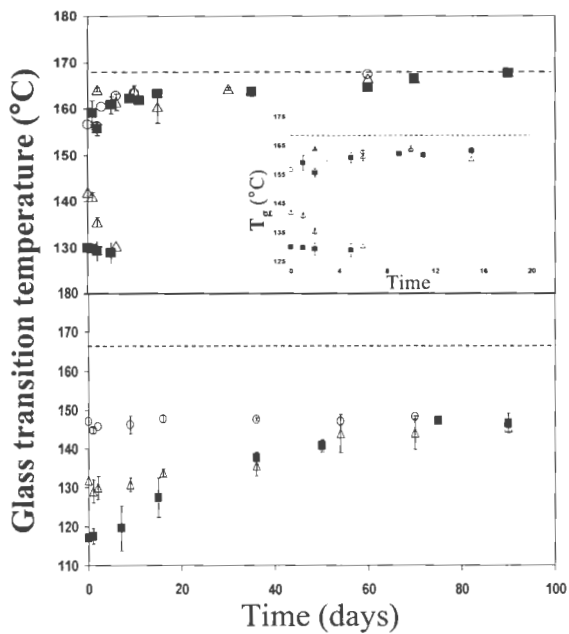
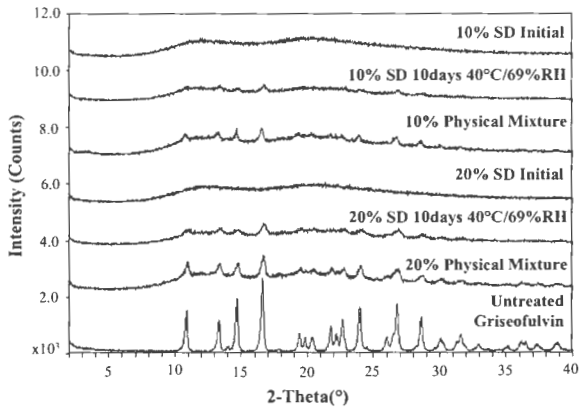
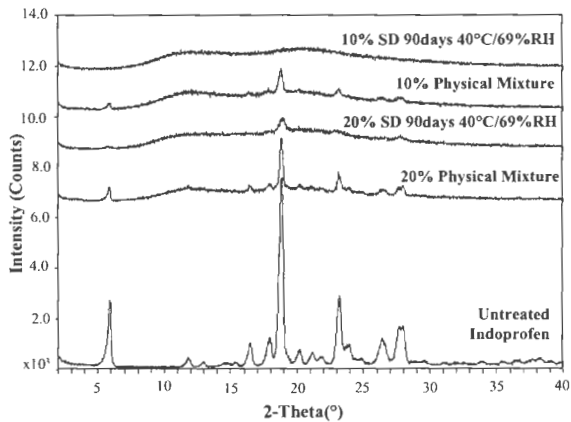


Figure B-II-6

X-ray diffraction patterns of solid dispersions and physical mixtures of (a) griseofulvin-PVP and (b) indoprofen-PVP.



b)



MANUSCRIPT III

PHASE BEHAVIOR OF AMORPHOUS MOLECULAR DISPERSIONS III: CHARACTERIZATION OF THE SURFACTANT EFFECT ON THE SOLID SOLUBILITY OF A DRUG IN A SOLID DISPERSION

Madhav Vasanthavada¹, WeiQin Tong², Yatindra Joshi², and M. Serpil Kislalioglu^{1,3}

INTRODUCTION

Studies conducted in the field of solid dispersions have underlined the significance of drug-carrier interactions in preparation of a miscible and physically stable solid dispersion product [1]. Although the polymer poly(vinylpyrrolidone), used inhibits drug crystallization in solid dispersions, the moisture and temperature variations during its shelf-life storage may adversely impact drug-carrier interactions towards drug crystallization. The physical stability of the drug product would depend upon factors

¹ Department of Applied Pharmaceutical Sciences, The University of Rhode Island, Kingston, RI 02881.

² Pharmaceutical & Analytical Development, Novartis Pharmaceutical Corporation, East Hanover, NJ 07936.

³ To whom correspondence should be addressed. (Telephone: (401) 874 5017; Email: skis@uri.edu)

which include hygroscopicity, glass transition temperature of the product, and the strength of the drug-carrier bonding.

Surfactants may be added in such binary mixtures of drug and polymer to improve the drug-polymer interactions and to create a miscible phase. In the miscible phase, the drug is molecularly dispersed in the carrier and could have a lower tendency to crystallize. Although in pharmaceutical studies surfactants are added in drug-polymer dispersions mainly to improve the solid solubility and dissolution of the poorly soluble drug [2-6], the function and behaviour of the surfactant molecules in the physical stability of the system has never been investigated. The solid solubility of griseofulvin was increased from 3%w/w to 40%w/w in polyethylene glycol 6000 (PEG 6000) by adding 5%w/w of sodium dodecyl sulphate (SDS) [7, 8]. SDS also improved the solid solubility of griseofulvin in PEG 3000 and PEG 20000 in concentrations from 3%w/w to 25%w/w. Pluronic^x F-68 increased the solid solubility and dissolution rate of a poorly water soluble drug, nifedipine, in its solid dispersions [9]. Tween 40 (0.5% w/w) and SDS (0.5% w/w) were incorporated in solid dispersions to double the dissolution rate of 5-lipoxygenase inhibitor [10]. Dissolution studies may be accepted as an indirect measure of the physical stability of solid dispersions. The mechanism suggested for the enhancement of drug solubility in a carrier and its dissolution in the aqueous media is the ability of surfactant to solubilize greater quantity of drug and hence to release it in molecular form during the dissolution process.

Solid solubilities of drugs that have been cited in the literature were investigated in the crystalline polymeric carriers like PEG and quantified by measuring the heat of fusion of the non-solubilized drug in the vehicle. These values were compared to that of the original drug. Although PEG has been shown to enhance the dissolution of hydrophobic drugs to form a solid solution, it has not been able to prolong or retain the physical stability (i.e. amorphous form) of the drug. For instance, upon aging, triamterene and temazepam crystallized from solid dispersions of PEG 1500, PEG 2000, PEG 400 and PEG 6000 [11]. On the other hand, amorphous polymers like PVP have been shown to retain the amorphous nature of the drug, as well as improving its dissolution. The effects of surfactants in amorphous miscible mixtures would therefore be of value to understand whether and how added surfactant would influence the solid solubility of drugs.

Griseofulvin was selected as the model drug compound because it was shown earlier to have no solid solubility in PVP (chapter II thesis of Vasanthavada M.). A linear chain non-ionic surfactant exhibiting axial polarity with its sucrose hydrophilic head and a stearic acid lipophilic chain, was the surfactant used. The presence of hydroxyl units in the sucrose head of the surfactant could interact with the drug as well as the polymer and improve the solid-solubility of the drug. The studies were carried out by determining the morphology and the thermodynamic behaviour of the griseofulvin-PVP solid dispersion in the presence and absence of sucrose stearate. Ternary solid dispersions containing the three ingredients were prepared and characterized by measuring the solid solubility of the drug in the polymer [12]. The effect of surfactants on the solid solubility of the

hydrophobic drug that were dispersed in the amorphous polymers has not yet been reported in the literature.

MATERIALS AND METHODS

Materials:

Plasdone (Poly (vinylpyrrolidone)) PVP K29/32 with M_w 50 KDa was obtained from ISP Technologies Inc., (Wayne, NJ). Samples were dried at 105°C under vacuum for 20 hours prior to preparing solid dispersions. Griseofulvin ((2S)-trans-7-Chloro-2',4,6-trimethoxy-6'-methylspiro(benzofuran-2[3H], 1'-[2]cyclohexene)-3,4'-dione) was purchased from Sigma Chemical Company (St. Louis, MO) and was used as received for the solid dispersion preparation. A sucrose stearate (Ryoto Sugar Ester O1570, a food and pharmaceutical grade surfactant, Mitsubishi-Kagaku Food Corp, Tokyo, Japan) was used as the surfactant. The chemical structures of all the materials used in this study are provided in Fig. B-III-1. The surfactant (sucrose stearate) used was non-ionic and hydrophilic with an HLB value of 14 and was amorphous in nature. We measured its glass transition temperature (T_g) as 34°C.

Methods:

Preparation of Solid Dispersions - Solvent Evaporation Technique:

Solid dispersions of PVP-surfactant, surfactant-drug and PVP-drug-surfactant were prepared using solvent evaporation technique. Ternary solid dispersions were prepared by

dissolving crystalline griseofulvin in dichloromethane. A pre-calculated amount of PVP and surfactant was added to the drug solution. The surfactant concentrations of the batches were increased from 10%w/w to 40%w/w at 10% weight increments and the weight proportion of griseofulvin was altered from 10%w/w of griseofulvin-in-PVP to 60%w/w of griseofulvin-in-PVP. After all three ingredients thoroughly dissolved in dichloromethane, the solution was sonicated for 15 minutes in a water-bath that was maintained at 37°C, to complete clarity. The solvent was removed using a rotary evaporator (Rotavap[®]) at 37°C, leaving the residual drug product. Solid dispersion obtained in this manner was further dried in a vacuum oven at room temperature for at least 24 hours to remove the remaining residual solvent. The batches thus obtained were ground with a mortar and pestle and were sifted through a sieve # 70 to result in particle size $\leq 210\mu\text{m}$. The dispersions were stored in vials over anhydrous CaSO_4 in a freezer until use.

Modulated Differential Scanning Calorimeter (MDSC):

The glass transition temperature (T_g) of the solid dispersions were analyzed using Modulated DSC 2920 (TA Instruments, New Castle, DE), with a liquid nitrogen cooling accessory. The analysis was performed under a purge of dry nitrogen gas (60cc/min). High purity indium and sapphire were used frequently to calibrate for the heat flow and heat capacity of the instrument. Thermal history of the samples was not erased unless mentioned specifically. The events were recorded and analyzed during the first heating scan. Samples (~ 8-12 mg) were initially cooled to -10°C for 10 minutes and were heated

to 245°C at 1°C/min with modulations of 0.266° every 50 seconds. The specified amplitude and period were optimized to provide the best results for analysis.

X-ray Powder Diffraction (XRPD):

The crystallinity of solid dispersions was tested using X-ray powder diffractometer (Rigaku RINT (D/Max) 2200 that was equipped with an Ultimagoniometer). The instrument consisted of a 40 KV, 40mA generator with a Cu K_α radiation anode tube. The samples were sifted through sieve # 70 and placed on a 0.5 mm quartz plate holder prior to exposure to X-rays. They were scanned over a 2θ range between 2° and 40° at a scan rate of 2° per minute in 0.02° step size. The divergence and scattering slits were set at 1.00°, receiving slit at 0.15mm and monochromator was used at 0.45mm.

Fourier Transform Infra-red Spectroscopy (FTIR):

Nicolet spectrometer equipped with a KBr beam splitter was used to obtain infrared spectra. Calibration for wavenumber accuracy was performed by using polystyrene sample. Dry nitrogen gas was used to purge the beam splitter and sample compartment. IR spectra were obtained using an attenuated total reflectance (ATR) accessory (single reflection bounce diamond crystal; Golden Gate accessory). For each spectrum, 32 scans were performed and a resolution of 4 cm was chosen. The ATR accessory enabled to obtain the spectra by pressing the solid material onto the diamond crystal. This accessory eliminates the use of KBr and yet produces comparable results. All samples were dried

under vacuum for 20 hrs prior to obtaining any spectra, to remove the influence of residual moisture.

RESULTS AND DISCUSSION

Thermal and Spectroscopic Analysis of PVP – Sugar ester Solid Dispersions:

The glass transition temperatures of PVP-sucrose stearate solid dispersions are shown in Fig. B-III-2a. The T_g of PVP mixtures decreased from 141°C to 91°C as the surfactant concentration increased from 10% w/w to 50% w/w. Such a composition-dependent single T_g indicates a molecularly miscible mixture. At surfactant concentration of 60% w/w and above, two T_g s were observed, indicating a phase-separated mixture. In Fig. B-III-2b the T_g values have been plotted as a function of weight fraction of the surfactant.

In order to detect the presence of any specific interactions e.g. hydrogen bonding between the polymer and surfactant, FT-IR spectra were obtained. In Fig. B-III-3, the PVP carbonyl stretch in the wave-number region of 1750 cm^{-1} -1550 cm^{-1} is shown. As a control the FT-IR scans of physical mixtures of corresponding weight fractions of surfactant and PVP are provided. It is seen from the spectra that the presence of 10%w/w surfactant decreases the carbonyl stretch of PVP from 1666 cm^{-1} to 1653 cm^{-1} , whereas no such reduction is evident in the corresponding physical mixtures. This suggested the presence of interactions between the polymer and surfactant most likely between the carbonyl group of PVP and the hydroxyl groups of the sucrose moiety of surfactant. Presence of specific interactions could be a cause for the miscibility of surfactant in the polymer. The

importance of interactions for miscibility in macromolecules has been reported earlier [13-18].

Thermal and Spectroscopic Analysis of Griseofulvin-Sugar ester Solid Dispersions:

The MDSC reversing heat flow scans of griseofulvin-sugar ester solid dispersions are shown in Fig. B-III-4a for up to 50% w/w griseofulvin loading. Also the heat flow scans of amorphous griseofulvin and sucrose stearate demonstrating T_g values at 89°C and 34°C respectively are shown as Fig. B-III-4b. In Fig. B-III-4a, the T_g values were recorded for the freshly prepared solid dispersions and for the samples whose thermal history was removed (treated samples), in order to minimize the effect of sample preparation on the T_g values [19]. The thermal history was erased by heating the mixtures to temperatures just below the T_g of pure griseofulvin, to prevent the crystallization of any amorphous drug substance, and rapidly cooled to -10°C. The samples were reheated to record their T_g s. In Fig. B-III-4, the lower T_g is for the freshly prepared solid dispersion and the higher T_g is for the treated samples. A difference of 10°-15°C was seen between the T_g values of freshly prepared and treated samples, possibly due to the differences in the rate of cooling of solid dispersion. Nevertheless, no appreciable difference was observed in the T_g values obtained for the first scan (or the second scans) as a function of drug composition. This behavior indicated minimal or no miscibility between the drug and the surfactant.

In order to investigate the presence of any specific interactions between the two components, i.e. hydrogen bonding or hydrophobic interactions, FT-IR spectra of the

solid dispersions were obtained and were compared with corresponding physical mixtures as seen from Fig. B-III-5. The shift in the wave-number of peak at 1713cm^{-1} to 1700cm^{-1} in the solid dispersions in comparison to shift of 1713cm^{-1} to 1704cm^{-1} in physical mixtures suggested the presence of weak interactive or dispersive forces between the drug and the surfactants.

PVP-drug-surfactant ternary solid dispersions:

It was demonstrated earlier that griseofulvin had a miscibility of up to 30% w/w in PVP. At drug concentration of 40% w/w and higher, the samples were found to be crystalline (Fig. B-III-6). In order to investigate the effects of the surfactant on the extent of miscibility between griseofulvin and PVP, sucrose stearate was added to the binary mixture to provide 10%, 20%, 30% and 40% (w/w) of total sample weight. The T_g values of various mixtures along with the XRD results verifying amorphous or crystalline are shown in Table B-III-I. The raw XRD patterns of the mixtures are also provided in Fig. B-III-7 and 7a.

As seen from Table B-III-I, an increase in the surfactant concentration, from 10% to 20% w/w, increased the amorphous fraction of drug in the solid dispersion. At 20% w/w surfactant concentration, 50% w/w of drug in the polymer can be incorporated in the system in the amorphous form whereas the solid dispersion that contains 10%w/w surfactant facilitates only 30%w/w griseofulvin in the system. However, when the surfactant loading increased from 20% w/w to 30% w/w, the fraction of drug that was present in the amorphous form was dropped from 50% w/w to 40%. Such a

crystallization behavior can be explained by the increased molecular mobility in the system in the presence of higher amounts of low- T_g sucrose ester.

The T_g values of ternary solid dispersions of PVP and griseofulvin containing varying levels of surfactants are shown in Fig. B-III-8. Also the T_g values are plotted in Fig. B-III-9 for different sugar ester containing system as a function of griseofulvin concentration. As it is seen from the figures, at a given surfactant concentration, with an increase in the drug concentration in PVP, the T_g of the mixture decreases. Moreover for a fixed ratio of griseofulvin and PVP, the T_g decreased with an increase in the surfactant concentration indicating a miscible mixture. The ternary phase diagram for PVP, griseofulvin and sucrose stearate system is shown in Fig. B-III-10. It can be seen from the shaded region of the plot that surfactant facilitates the miscibility of griseofulvin in PVP.

Effect of sugar ester on the solid solubility limit of griseofulvin:

To investigate the effect of the sucrose stearate on the solid solubility, the ternary solid dispersions were exposed to accelerated stability conditions of 40°C/69%RH for over 30 days. The MDSC reversing heat flow scans of ternary solid dispersion of PVP: griseofulvin: surfactant in the ratio of 40:40:20 that were subjected to accelerated stability conditions are shown in Fig. B-III-11. It can be seen from the figure that the T_g values increased and after a storage period of 35 days had a T_g of 104°C. This T_g is much less than the T_g of pure PVP of 168°C. Although it is evident that the reduction observed in the T_g value is due to the plasticization of PVP with either griseofulvin or sucrose stearate, it cannot be ascertained as to which of the two components are responsible for

the reduction in T_g . If the plasticization were the result of the solid solubility of drug as well as the surfactant, then a solid dispersion containing a different composition would also provide T_g values of 104°C, upon storage. In order to test this, a ternary solid dispersion containing PVP: griseofulvin: surfactant in the ratio of 45:45:10 were exposed to 40°C/69%RH conditions. A solid dispersion of 45:45:10 was chosen since it had griseofulvin and PVP in 1:1 ratio, which was comparable to 40:40:20 and only the sucrose ester concentration decreased from 20% to 10%w/w. The MDSC scans shown in Fig. B-III-11 demonstrate that the T_g values had reached a plateau at around 125°C, which is significantly different from 104°C, thus suggesting the presence of either griseofulvin or the sucrose stearate alone.

If complete phase separation of griseofulvin is assumed, the concentration of surfactant remaining miscible in PVP would be arithmetically 18% w/w (since 10 parts of surfactant is present in 55 parts of mixture). Therefore, a 20% w/w surfactant dispersed in PVP that contained no griseofulvin was exposed to 40°C/69%RH. The MDSC scans of such a sample are shown in Fig. B-III-11a. At the end of 16 days the T_g values did not change significantly from the initial T_g of 121°C. Based on these results it is assumed that surfactant remains miscible in the polymer and may be lowering the T_g values in the ternary solid dispersions. The fact that the T_g of ternary solid dispersions of 45:45:10 mixtures reaches a value close to 123°C, which corresponds to T_g of soluble fraction of surfactant in PVP, further strengthens the argument that surfactant causes the reduction in the T_g values.

It can be similarly argued in the case of 40:40:20 mixtures that the T_g of 104°C coincides with the T_g of freshly prepared mixture of 30%w/w solid dispersion of surfactant in PVP. The arithmetically calculated value of surfactant in PVP in the absence of griseofulvin is 33%w/w. Therefore it can be concluded that sucrose stearate did not improve the solid solubility limit of griseofulvin in PVP.

CONCLUSIONS

In this study a ternary solid dispersion of drug, polymer and a sugar ester surfactant was prepared and characterized using MDSC and XRD. The surfactant interacted with the polymer through hydrogen bonding and was miscible in it up to 60%w/w concentration. Although the surfactant-drug mixtures did not exhibit composition dependent miscible T_g , FTIR demonstrated the presence of weak interactions between the two components. Therefore, the effect of surfactant on the extent of miscibility between the drug and the polymer was investigated. When present at 20%w/w concentrations, the surfactant increased the extent of miscibility from 30%w/w in PVP to 50%w/w. Such an increase in the miscibility was attributed to the physical interactions between the three components. The effect of surfactant on the solid solubility limit of griseofulvin in PVP was investigated by exposing the mixtures to 40°C/69%RH conditions. From the MDSC analysis of T_g values, it was concluded that this surfactant did not improve the solid solubility limit of griseofulvin in PVP.

ACKNOWLEDGMENTS

This study is a part of Ph.D. research of Mr. Vasanthavada who is a Novartis Graduate Research Fellow and has conducted his research at Novartis R&D facility. He wishes to acknowledge the fellowship and also thank Ms. Marilyn Alvine and Dr. Francis Liu for their support with X-ray analysis.

REFERENCES

1. L. S. Taylor, and G. Zografi. Spectroscopic characterization of interactions between PVP and indomethacin in amorphous molecular dispersions. *Pharmaceutical Research*. 14:1691-1698 (1997).
2. A. T. M. Serajuddin, P. C. Sheen, D. Mufson, D. F. Bernstein, M. A. Augustine. Effect of vehicle amphiphilicity on the dissolution and bioavailability of a poorly water-soluble drug from solid dispersions. *Journal of Pharmaceutical Sciences*. 77:414-417 (1988).
3. A. T. M. Serajuddin, P. C. Sheen, M. A. Augustine. Improved dissolution of a poorly water-soluble drug from solid dispersions in poly(ethylene glycol) polysorbate 80 mixtures. *Journal of Pharmaceutical Sciences*. 79:463-464 (1990).
4. A. T. M. Serajuddin, P. C. Sheen, D. Mufson, D. F. Bernstein, M. A. Augustine. Physicochemical basis of increased bioavailability of a poorly water-soluble drug following oral administration as organic solutions. *Journal of Pharmaceutical Sciences*. 77:325-329 (1988).
5. P. C. Sheen, V. K. Khetarpal, C. M. Cariola, and C. E. Rowlings. Formulation studies of a poorly water soluble drug in solid dispersion to improve bioavailability. *International Journal of Pharmaceutics*. 118:221-227 (1995).
6. J. Aungst, N. H. Nguyen, N. J. Rogers, S. M. Rowe, M. A. Hussain, S. J. White, and L. Shum. Amphiphilic vehicles improve the oral bioavailability of a poorly

- soluble HIV protease inhibitor at high doses. *International Journal of Pharmaceutics*. 156:79-88 (1997).
7. M. Wulff, and M. Alden. Phase equilibria in drug-polymer-surfactant systems. *Thermochimica Acta*. 256:151-165 (1995).
 8. M. Wulff, M. Alden, and D. Q. M. Craig. An investigation into the critical surfactant concentration for solid solubility of hydrophobic drug in different polyethylene glycols. *International Journal of Pharmaceutics*. 142:189-198 (1996).
 9. K. A. Mehta, M. S. Kislalioglu, W. Phuapradit, W. A. Malik and N. H. Shah. Multi-unit controlled release systems of nifedipine and nifedipine:Pluronic[®] F-68 solid dispersion. *Drug Development and Industrial Pharmacy*. 28:275-285 (2002).
 10. Y. Perng, A. S. Kerney, K. Patel, N. R. Palepu, and G. Zuber. Investigation of formulation approaches to improve the dissolution of SB-210661, a poorly water soluble 5-lipoxygenase inhibitor. *International Journal of Pharmaceutics*. 176:31-38 (1998).
 11. S. K. Dordunoo, J. L. Ford, and M. H. Rubinstein. Physical stability of solid dispersions containing triamterene or temazepam in polyethylene glycols. *Journal of Pharmacy and Pharmacology*. 49:390-396 (1997).
 12. M. Vasanthavada, W. Tong, Y. Joshi, and M. S. Kislalioglu. Phase behavior of amorphous molecular dispersions: determination of the degree and mechanism of solid miscibility. *Pharmaceutical Research*. Accepted. *In press*
 13. J. Moskala, D. F. Varnell, and M. M. Coleman. Concerning the miscibility of poly(vinylphenol) blends – FTIR study. *Polymer*. 26:228-234 (1985).
 14. J. Moskala, S. E. Howe, P. C. Painter, and M. M. Coleman. On the role of intermolecular hydrogen bonding in miscible polymer blends. *Macromolecules*. 17:1671-1678 (1984).

15. P. C. Painter, Y. Park, and M. M. Coleman. Hydrogen bonding in polymer blends. 2. Theory. *Macromolecules*. 21:66-72 (1988).
16. S. Shen and J. M. Torkelson. Miscibility and phase separation in poly(methyl methacrylate)/Poly(vinyl chloride) blends: study of thermodynamics by thermal analysis. *Macromolecules*. 25:721-728 (1992).
17. X. Lu and R. A. Weiss. Relationship between the glass transition temperature and the interaction parameter of miscible binary polymer blends. *Macromolecules*. 25:3242-3246 (1992).
18. Brunacci, E. Pedemonte, J. M. G. Cowie, and I. J. McEwen. The thermodynamics of mixing of polystyrene and poly(α -methylstyrene) from a calorimetric viewpoint. *Polymer*. 35:2893-2896 (1994).
19. Q. Lu, and G. Zografi. Phase behavior of binary and ternary amorphous mixtures containing indomethacin, citric acid, and PVP. *Pharmaceutical Research*. 15:1202-1206 (1998).

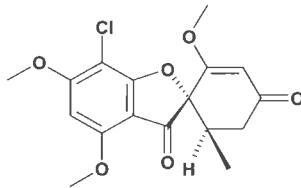
Table B-III-I: Surfactant effect on the morphology and thermal properties of griseofulvin and PVP solid dispersions

W_{PVP}	W_{Gris}	W_{PVP}:W_{Gris}	W_{Surfactant}	T_g of freshly prepared solid dispersion	XRD
72	18	8:2	10	119	Amorphous
63	27	7:3	10	102	Amorphous
45	45	5:5	10	80 ; 96	Crystalline
56	24	7:3	20	97	Amorphous
48	32	6:4	20	92	Amorphous
40	40	5:5	20	84	Amorphous
32	48	4:6	20	80	Crystalline
56	14	8:2	30	93	Amorphous
42	28	6:4	30	80	Amorphous
35	35	5:5	30	77	Crystalline
28	42	4:6	30	88	Crystalline
48	12	8:2	40	99	Amorphous
42	18	7:3	40	83	Amorphous
35	35	5:5	40	73	Crystalline
35	15	7:3	50	79	Amorphous
30	20	6:4	50	73	Crystalline

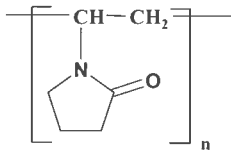
Figure B-III-1

Chemical structures of (a) griseofulvin; (b) repeat unit of poly(vinylpyrrolidone) and (c) Ryoto^x food-grade sugar ester O1570 (sucrose stearate).

(a)



(b)



(c)

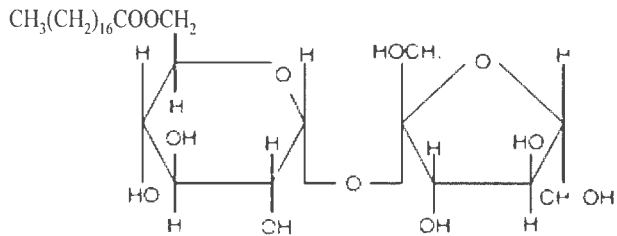


Figure B-III-2

(a) MDSC reversing heat flow scans of solid dispersions of sucrose stearate and PVP demonstrating the composition dependent single T_g indicating miscibility until two T_g s are seen. The percentages refer to the amounts of surfactant (b) Plot of T_g values against the sucrose stearate (o: single T_g values; Δ : second T_g value in a phase separated mixture)

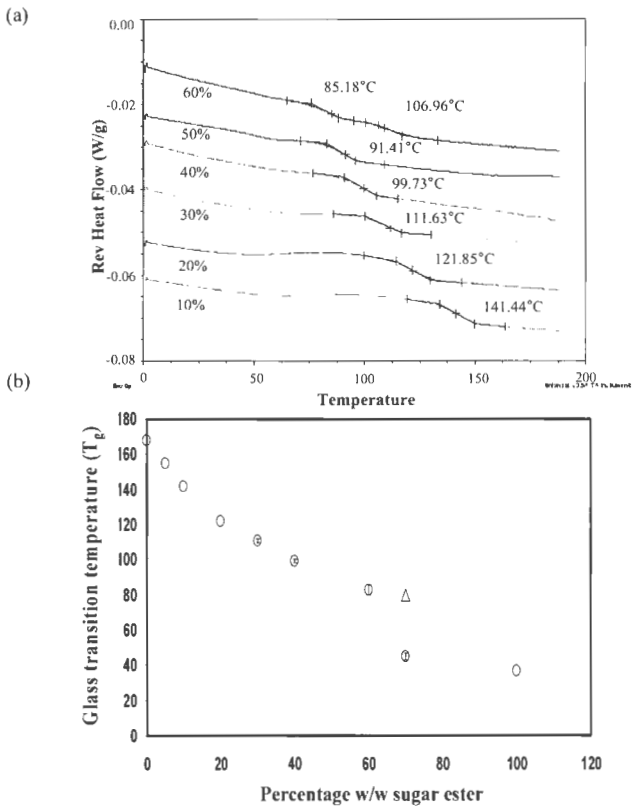


Figure B-III-3

FT-IR spectra showing the carbonyl stretch region of 1750 – 1550 cm^{-1} in solid dispersions and physical mixtures of sugar ester and PVP as a function of changes in the sugar ester composition. The percentages refer to the amounts of sugar ester present.

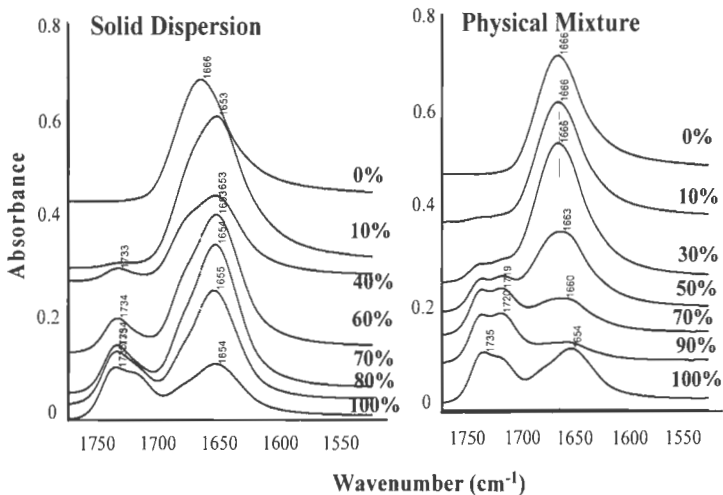


Figure B-III-4

(a) MDSC reversing heat flow scans of solid dispersions of griseofulvin and sucrose stearate. The T_g values shown are for the 'as is' samples and after erasing the thermal history. The higher T_g value at any specific composition is for the samples with thermal history erased. Percentages refer to the amounts of griseofulvin present. (b) MDSC reversing heat flow scans pure sugar ester and amorphous griseofulvin prepared by melt-quench technique.

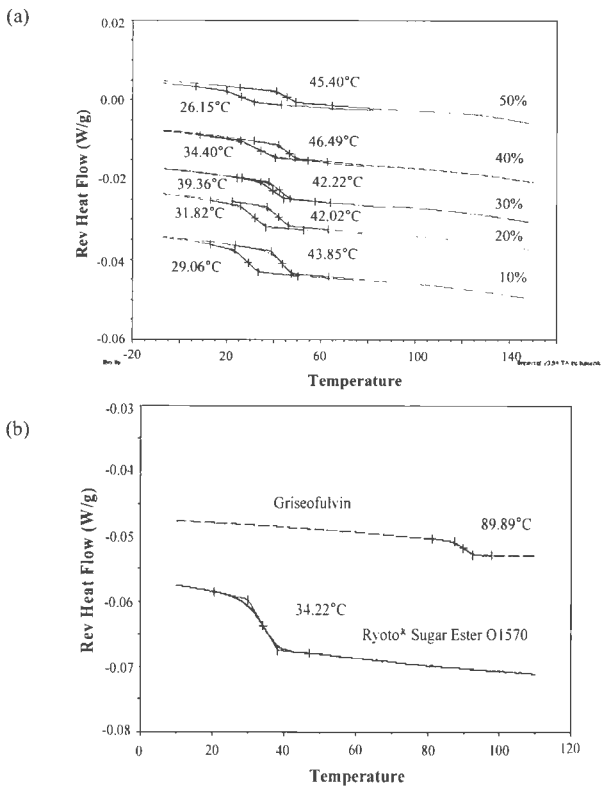


Figure B-III-5

FT-IR spectra showing the carbonyl stretch region of 1750 – 1550 cm^{-1} in solid dispersions and physical mixtures of sugar ester and griseofulvin as a function of changes in the sugar ester composition. The percentages refer to the amounts of sugar ester present.

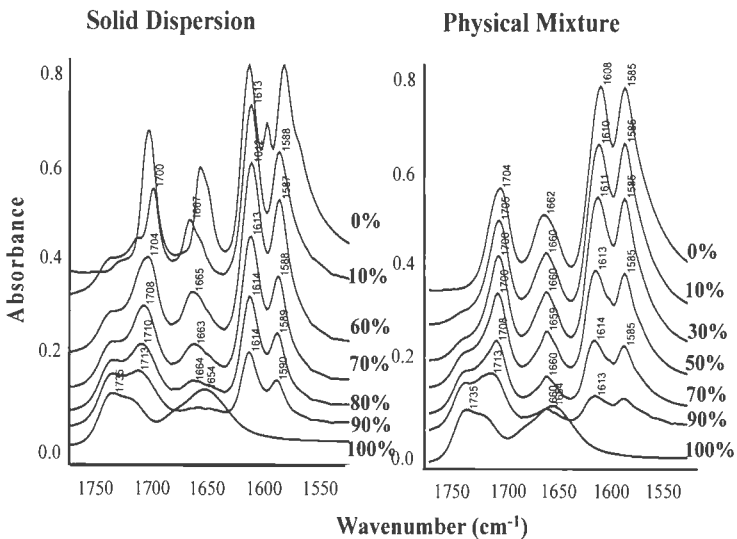


Figure B-III-6

X-ray diffraction pattern demonstrating the presence of crystallinity in 40%w/w griseofulvin-PVP solid dispersions. No crystallinity is seen in the 30%w/w solid dispersions (duplicates).

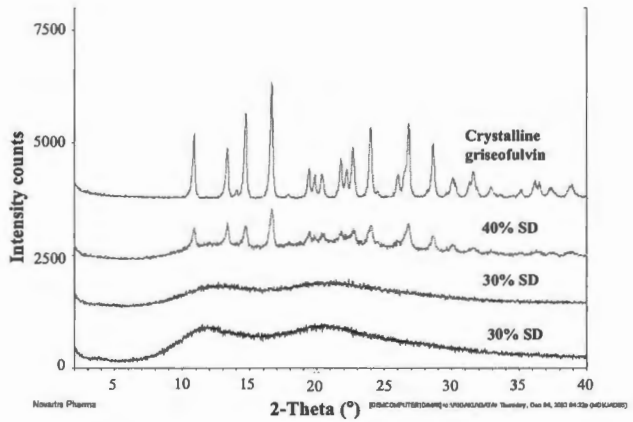


Figure B-III-7

X-ray diffraction pattern of ternary solid dispersion of PVP / griseofulvin / sugar ester showing the presence of crystallinity for 50:50 and 40:60 parts of PVP and griseofulvin in the presence of 30%w/w surfactant

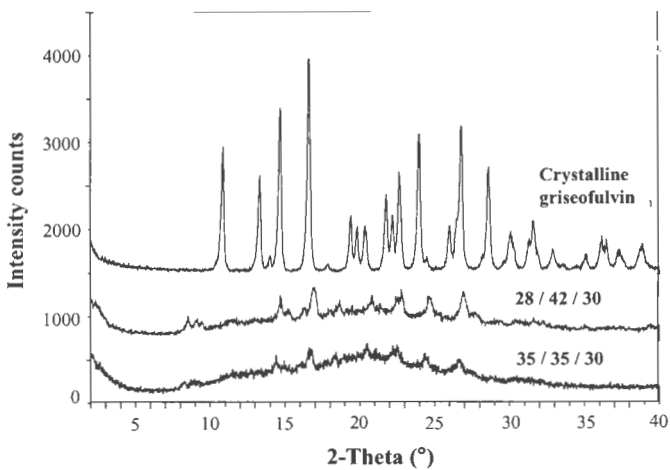
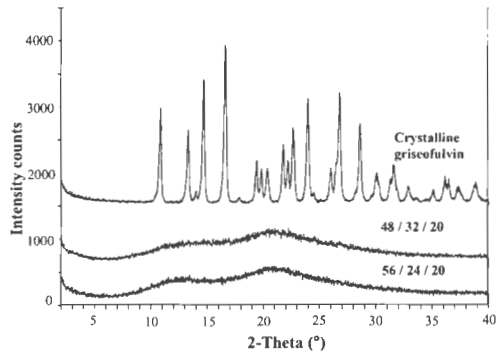


Figure B-III-7a

X-ray diffraction pattern of ternary solid dispersion of PVP / griseofulvin / sugar ester showing the absence of crystallinity for 50:50 parts of PVP and griseofulvin in the presence of 20%w/w surfactant. However 60%w/w griseofulvin in PVP (i.e. 32 / 48 / 20) shows crystallinity.

(a)



(b)

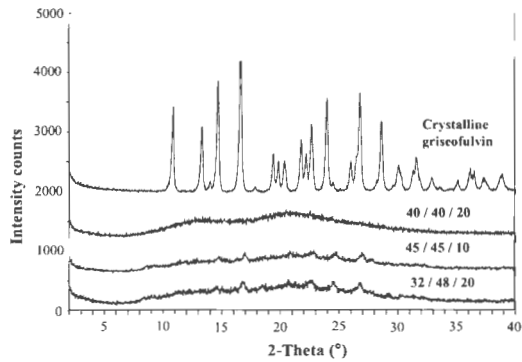


Figure B-III-8

MDSC reversing heat flow scans of ternary solid dispersions of PVP, griseofulvin and sugar ester. The fraction of sugar ester was kept constant at 30%w/w of the total sample weight. The percentages shown are for the fraction of griseofulvin in PVP. A composition dependent single T_g indicates a miscible mixture till 60%w/w limit.

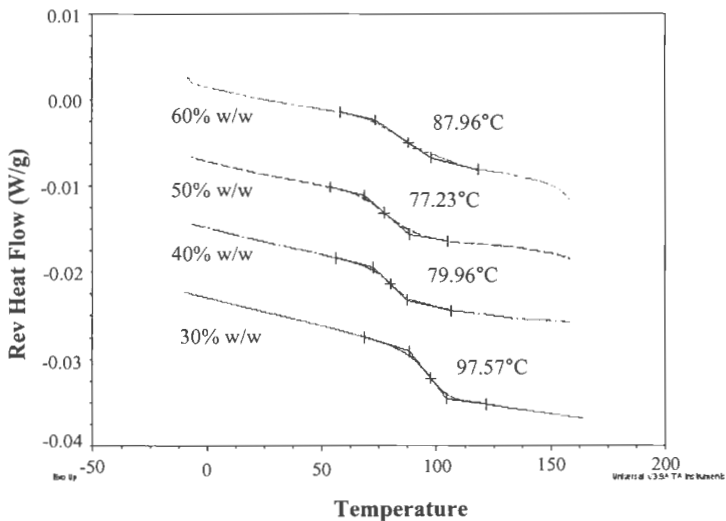


Figure B-III-8a

MDSC reversing heat flow scans of ternary solid dispersions of PVP, griseofulvin and sugar ester. The fraction of sugar ester was kept constant at 20%w/w of the total sample weight. The percentages shown are for the fraction of griseofulvin in PVP. A composition dependent single T_g indicates a miscible mixture till 60%w/w limit.

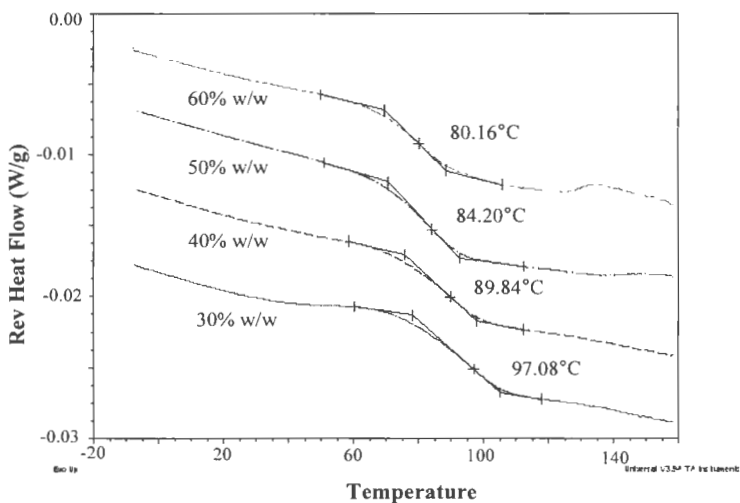


Figure B-III-8b

MDSC reversing heat flow scans of ternary solid dispersions of PVP, griseofulvin and sugar ester containing 50:50 ratio of griseofulvin and PVP, but with sugar ester concentration increasing from 10% to 40%w/w.

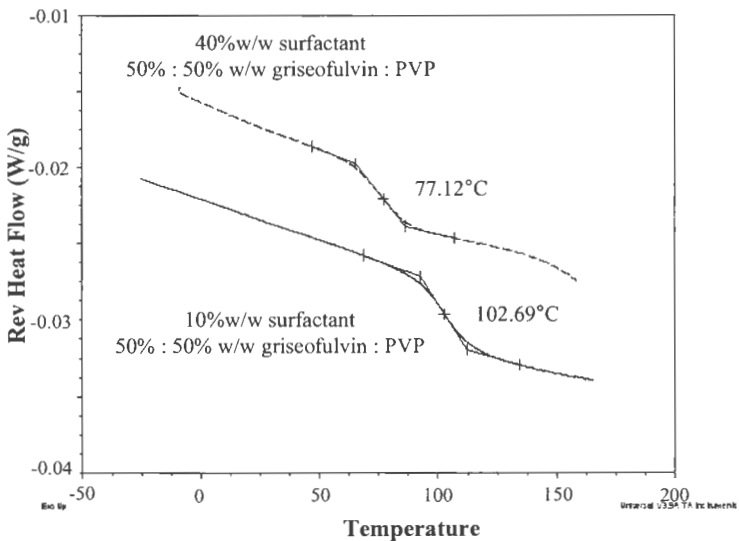


Figure B-III-9

T_g values of ternary solid dispersions as a function of increasing griseofulvin concentration in PVP in the presence of varying levels of sugar ester O1570. Symbols represent the sugar ester concentration: Δ 10% w/w; \bullet 20%w/w; \blacktriangle 30%w/w; and \circ 40%w/w

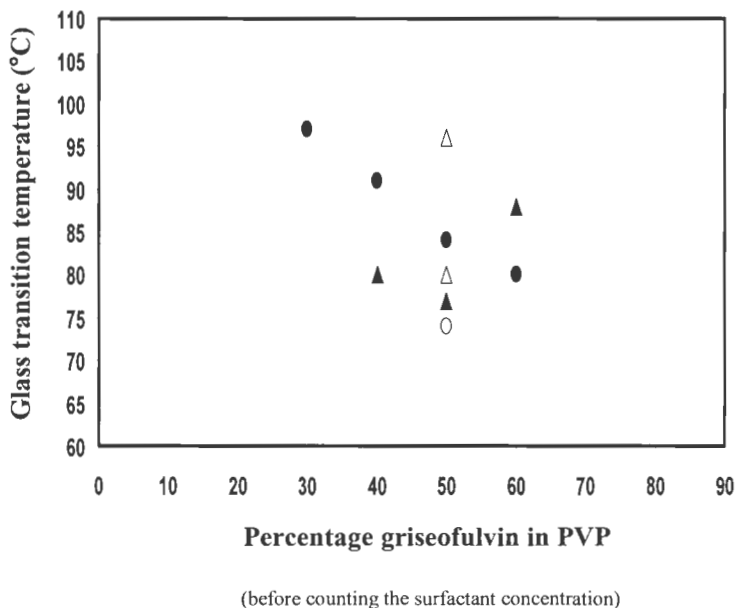


Figure B-III-10

Miscibility of PVP, griseofulvin and sucrose stearate. The shaded zone indicates the enhancement in the miscibility of griseofulvin in PVP achieved by the addition of sucrose stearate. The dotted line represents the possible extrapolation of miscibility region at higher surfactant concentrations.

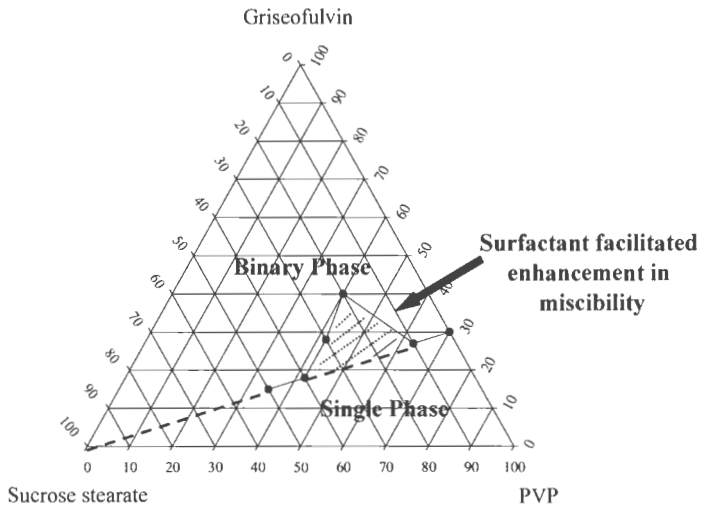


Figure B-III-11

MDSC reversing heat flow scans of PVP / griseofulvin / sugar ester solid dispersions in the ratio 40 / 40 / 20 that were exposed to 40°C / 69% RH conditions. The T_g values increases and reaches a plateau at 104°C.

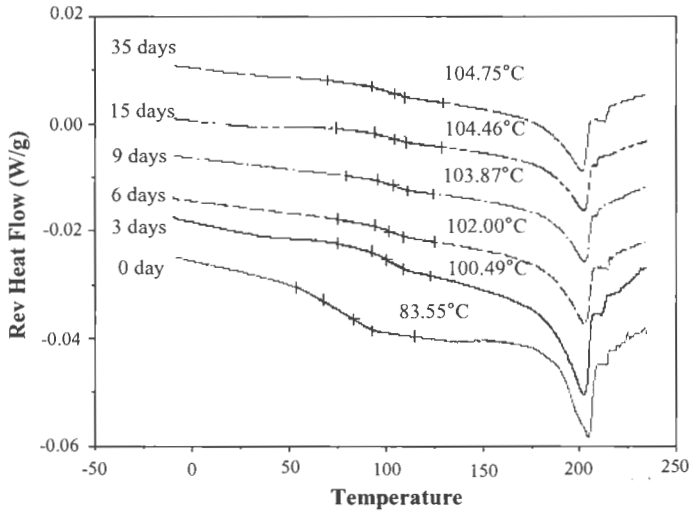
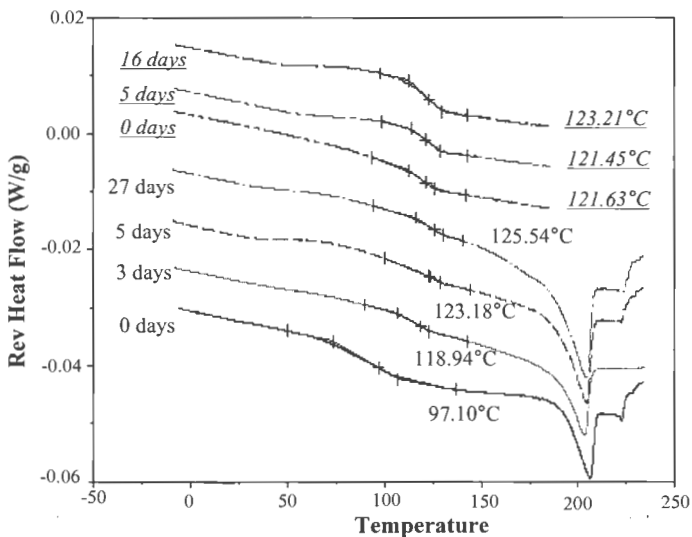


Figure B-III-11a

MDSC reversing heat flow scans of PVP / griseofulvin / sugar ester solid dispersions in the ratio 45 / 45 / 10 that were exposed to 40°C / 69% RH conditions. The upper three scans are for the 20%/w/w sugar ester-PVP solid dispersions exposed to 40°C / 69% RH



MANSUCRIPT IV

MOISTURE EFFECT ON GRISEOFULVIN CRYSTALLIZATION KINETICS

Madhav Vasanthavada¹, WeiQin Tong², Yatindra Joshi², and M. Serpil Kislalioglu^{1,3}

ABSTRACT:

Purpose: To study the isothermal crystallization of griseofulvin at low moisture contents. Also, to determine the energy of activation (E_a) for griseofulvin crystallization using modulated differential scanning calorimeter (MDSC) and non-isothermal crystallization studies.

Methods: Griseofulvin was made amorphous by rapidly cooling from its molten state. X-ray diffraction and MDSC were used to generate the calibration plot for isothermal crystallization studies. Amorphous griseofulvin was exposed to 0%, 32% and 43%

¹ Department of Applied Pharmaceutical Sciences, The University of Rhode Island, Kingston, RI 02881.

² Pharmaceutical & Analytical Development, Novartis Pharmaceutical Corporation, East Hanover, NJ 07936.

³ To whom correspondence should be addressed. (Telephone: (401) 874 5017; Email: skis@uri.edu)

humidity conditions at 23°C using saturated salt solutions. Samples were analyzed periodically using MDSC to quantify the fraction of griseofulvin crystallized based on their heats of recrystallization and the generated calibration plots. The isothermal crystallization rate constants were determined using the established theoretical equations of Hancock-Sharp and Kolmogorov-Johnson-Mehl-Avrami (KJMA). Non-isothermal crystallization kinetics was determined using Kissinger's analysis.

Results: XRD did not prove to be a useful technique because of the large relative standard deviations in the peak height ratios of crystalline griseofulvin and lithium fluoride (internal standard) for the calibration plot. Hence calibration plot was constructed using the MDSC heat of recrystallization values of amorphous griseofulvin. From the Hancock-Sharp experimental fit, the crystallization mechanism was estimated to be as first order rate process. Hence, KJMA equation was employed for the determination of kinetic rate constants. With an increase in relative humidity from 0% to 43%, an increase in the crystallization rate constants was observed from 0.016 to 0.067 days⁻¹. Even at 43% RH, the sample had a total moisture content of < 2%w/w and yet crystallized in a short period of less than 30 days. Crystallization was noticed at 23°C / 0% RH although the glass transition temperature (T_g) of amorphous griseofulvin was found to be at 92°C. The non-isothermal E_a for amorphous griseofulvin was calculated from the Kissinger's analysis as 239 KJ/mol.

Conclusions: Crystallization of amorphous griseofulvin was detected at very low moisture contents and storage temperatures that was 65°C below the T_g of amorphous sample. High molecular mobility of griseofulvin at temperatures well below its T_g is

believed to be the primary cause for griseofulvin crystallization. Kissinger's analysis provides very low crystallization energy of activation, which agrees with the above findings. MDSC proved to be a sensitive technique for the isothermal crystallization of griseofulvin.

Keywords: griseofulvin, crystallization, thermal analysis, XRD, glass transition

INTRODUCTION:

In the manufacturing of pharmaceuticals, commonly employed processes like milling, melt extrusion, spray-drying and freeze-drying may generate partial or complete disorder in the crystalline lattice leading to a metastable amorphous form [1-4]. For drugs with extremely low aqueous solubility in the crystalline state, conversion to amorphous form has been shown to result in its higher solubility [5]. The meta-stable amorphous phase could however interact with moisture during its shelf life storage and undergo crystallization, thus influencing attributes like dissolution, bioavailability and chemical stability of the drugs [6]. Working with amorphous materials, Zografi et. al. [7] have shown that moisture could be selectively absorbed by the disordered regions of amorphous phase, thereby increasing the molecular mobility and inducing crystallization. Crystallization of amorphous drug substances may be prevented by either minimizing exposure to high humidity conditions, or storing them in low temperatures. It is generally understood that storing the amorphous drug substance at 50°C below its glass transition

temperature (T_g) could significantly reduce the molecular mobility that initiates crystallization process although this may not be a feasible approach in many instances [8].

If the drug crystallization cannot be prevented, retention of the drug product attributes in a predetermined period (during the shelf life) may be acceptable. In order to do so one must understand the impact of moisture and temperature on the kinetics of drug crystallization. Crystallization kinetics is typically determined by quantifying the percent crystallinity in the drug substance or a drug product as a function of storage time. There are also reports of conducting non-isothermal crystallization studies [9]. To quantify the fraction of crystalline component in a drug substance, various techniques like X-ray diffraction [10-14], DSC [15, 16], solution calorimetry [17, 18], water vapor sorption [17, 19], thermally stimulated currents [20], density measurements [13, 14, 21], isothermal microcalorimetry [22, 23] etc. have been used. Table B-IV-I summarizes the techniques, their sensitivity level, advantages & disadvantages. Since detection of crystallinity in the early stages of the crystallization process is important, sensitive techniques like solution calorimetry, water vapour sorption, and isothermal micro-calorimetry offer advantages. However these techniques have inherent disadvantages like producing and using an amorphous reference with known energy levels. This was demonstrated in the case of β -lactam antibiotics like cefazolin sodium, cefamandole nafate, cefamandole sodium, and cephaloridine, where the amorphous materials that were prepared by different techniques like freeze-drying and precipitation from solution had different energy contents [17]. Although thermally stimulated currents are very sensitive to molecular mobility, they

may not be able to accurately characterize the crystalline phases. One of the techniques that have been widely used for over three decades is the X-ray diffraction technique [24]. This technique has the advantage of being non-thermal in nature but has a disadvantage of detecting only levels as low as 5 - 10%w/w.

In this study, modulated DSC was used to study the isothermal crystallization kinetics of amorphous griseofulvin at 0%, 32% and 43% relative humidity conditions. Modulated DSC was chosen since it provided greater reproducibility and had ability to differentiate between the effects of slight variations in the amorphous and crystalline griseofulvin ratios when compared to the X-ray diffraction technique. The calibration plot generated using known levels of crystalline and amorphous griseofulvin had higher slope with MDSC when compared to XRD.

Griseofulvin was chosen as the model compound since it is poorly a water-soluble hydrophobic substance and has tendency to crystallize from its amorphous state. It also has a relatively high T_g of 90°C which makes it possible to study the crystallization pattern of the drug well below its T_g , i.e. room temperature (65°C below the T_g), without refrigeration. In addition, since the amorphous samples were exposed to low relative humidity conditions (a maximum of 43%RH), their T_g s were not plasticized to lower values from 90°C. In this study the non-isothermal Kissinger's analysis was used to study the energy of activation for drug crystallization (E_a). A review of the pharmaceutical literature to probe into the mechanism of drug nucleation and crystallization at such low relative humidity and storage temperatures has been provided.

MATERIALS AND METHODS

Materials:

Griseofulvin ((2S)-trans-7-Chloro-2', 4, 6-trimethoxy-6'-methylspiro (benzofuran-2[3H], 1'-[2] cyclohexene)-3, 4'-dione)) was purchased from Sigma Chemical Company (St. Louis, MO). The amorphous form was prepared for the stability studies. Anhydrous calcium sulfate, magnesium chloride and potassium carbonate were purchased from Fisher Chemical Co., Fair Lawn, NJ to prepare saturated salt solutions that would provide 0%, 32% and 43% RH at room temperature respectively. The chemical structure of griseofulvin is shown in Fig. B-IV-1.

Methods:

Preparation of amorphous griseofulvin:

Amorphous griseofulvin was prepared by melt-quenching the crystalline drug substance. The drug was weighed (3g) in a stainless steel beaker and was placed in an oven maintained at 217°C (i.e., 5°C above the melting temperature of drug), for 5 minutes. At the end of 5 minutes, it was ensured that drug was in a complete molten state. The stainless steel beaker was immediately immersed in a pool of liquefied nitrogen to rapidly cool (quench) the molten drug. The solidified drug was then grounded in a mortar and pestle and was sifted through sieve # 70 to result in particle size less \leq 210 μ m. Drug substance obtained this way was stored in a freezer in vials over anhydrous CaSO₄ until use.

Assay for drug degradation:

The melt-quenched drug substance was analyzed using High Performance Liquid Chromatography (HPLC) for any chemical degradation during heating. The HPLC consisted of a pump (Waters model), 15 cm (C₁₈) reversed phase chromatographic column (XTerra™ MS 5µm; Waters, a division of Millipore (Canada) Ltd., Mississauga, ON), a 20-µL injector loop attached to a model 7125 injector (Rheodyne, Cotati, CA), a variable-wavelength UV detector (Waters Lambda Max model 481 LC spectrophotometer) set at 290nm and attached to a Photo Diode Array (PDA) having wavelength ranging from 200nm to 600nm. The experimental running conditions were chosen from previously published method by Vudathala and Rogers [24]. The mobile phase was 45% acetonitrile in 0.1M acetic acid (pH 3.5) at a flow rate of 1 mL/min.

A HPLC calibration plot was first generated before assaying for the drug content. For the calibration plot, untreated crystalline drug substance was dissolved in a mixture of 4:1 parts of methanol: water to result a concentration of 3.33 mg/mL. Several dilutions of this stock solution were made using the solvent. Each solution was analyzed according to the HPLC method described above. A plot of the area under the peak against the 'concentration' of drug substance was generated. Later, a known amount of melt quench drug substance was dissolved in 4:1 methanol: water solution and the percent drug was quantified by obtaining the area under the drug analysis peak and using the calibration plot.

X-ray Powder Diffraction (XRPD):

The X-ray powder diffractometer (Rigaku RINT (D/Max) 2200, equipped with an Ultimagoniometer) consisted of a 40 KV, 40mA generator with a Cu K_α radiation anode tube. XRD pattern was needed to test the presence of any crystalline drug substance in the melt quenched drug substance. The sample was placed on a 0.5 mm quartz plate holder. They were scanned over a 2θ range between 2° and 40° at a scan rate of 2° 2θ per minute and step size 0.02°. The divergence and scattering slits were set at 1.00°, receiving slit at 0.15mm and monochromator was used at 0.45mm. X-ray pattern of melt quenched drug substance showed no crystalline peak indicating an amorphous material (Fig. B-IV-2). In addition no birefringence was seen under a polarized light microscope, thus supporting the X-ray analysis.

Preparation of calibration plot:

X-ray diffraction:

A calibration plot was constructed in order to quantify the percent crystallinity in amorphous sample during stability studies. Conventionally, X-ray diffraction technique is utilized to study isothermal crystallization kinetics [25]. A physical mixture of amorphous griseofulvin, crystalline griseofulvin and an internal reference as lithium fluoride (20% w/w) was prepared in 300mg quantities to fit in entirely on the X-ray slide. Mixing was achieved using Turbula Mixer™ used at 46 rpm for 3 minutes. Each mixture was then X-ray scanned using the method described in triplicate. The peak height ratio of

crystalline griseofulvin and lithium fluoride were then plotted against the weight fraction of amorphous griseofulvin to generate the calibration plot.

Thermal Analysis:

The crystallization kinetics of amorphous griseofulvin was monitored using MDSC. MDSC is a sensitive tool to measure the heat flow associated with thermal events like melting, crystallization, glass transition phenomenon etc. Upon heating, amorphous griseofulvin undergoes a glass transition and crystallizes *in situ* in the DSC pan. The heat of recrystallization (i.e. area under the exothermic area of non-reversing heat flow scan) was found to be experimentally reproducible and was used to obtain a measure of the percent amorphous sample in a given mixture [26]. In order to generate a calibration plot, physical mixtures of crystalline and amorphous griseofulvin, were weighed accurately in known weight proportions in a DSC pan. Calibration plot was constructed by plotting the *in situ* heat of recrystallization of the physical mixture against the percent amorphous griseofulvin.

Modulated Differential Scanning Calorimeter (MDSC):

Thermal analysis was performed using MDSC 2920 (TA Instruments, New Castle, DE), with a liquid nitrogen cooling accessory. The analysis was performed under a purge of dry nitrogen gas (60cc/min). High purity indium and sapphire were used frequently to calibrate for the heat flow and heat capacity of the instrument. Samples (~ 8-12 mg) heated from 0°C to 245°C at 1°C/min with modulations of 0.266° every 50 seconds. The

specified amplitude and period were optimized to provide best results for analysis. The heat of crystallization was obtained by measuring the area under the non reversing heat flow signal of crystallization exothermic peak using the TA Instrument Software for Universal Analysis. Measurement were conducted times n=3 for each time-point to ascertain the reproducibility of experiments.

Isothermal crystallization studies:

Studies were conducted at 23°C with 0%, 32% and 43% relative humidity conditions. The amorphous drug substance was accurately weighed (8-12mg) in standard DSC pans. The pans were exposed to isothermal stability condition by placing them in desiccators containing anhydrous calcium sulfate (0% RH), saturated magnesium chloride solution (32% RH) and saturated potassium carbonate solution (43% RH) [27]. By storing the samples in discrete DSC pans, the reproducibility of the results could be assessed without any interference due to sample handling. Samples were taken out for analysis at pre-determined time intervals for a period of up to seventy days or until near complete crystallization. The sample pans were crimped with aluminum lids having pinholes to facilitate the removal of absorbed water during heating. The heat of recrystallization of the sample was determined and the percent crystallinity at a specific time point was quantified using the calibration plot.

Non isothermal crystallization studies:

The energy of activation E_a for the crystallization of griseofulvin was determined non-isothermally using Kissinger analysis [28, 29].

$$\ln\left(\frac{\beta}{T_c^2}\right) = \left(-E_a/RT\right) + \text{const} \quad (1)$$

In Kissinger's analysis, the energy of activation E_a is determined by measuring the peak crystallization temperature (T_c) at several heating rates (β). The slope of a plot of $\ln(\beta/T_c^2)$ against $1/T_c$ gives $-E_a/R$, where R is the gas constant. Amorphous griseofulvin samples were weighed in DSC pans and were heated at scanning rates of 1, 5, 7.5, 10, 15, 20 and 25°C/min. The peak crystallization temperatures T_c was obtained from the software.

Determination of moisture content:

The moisture content of the sample was analyzed using the Karl Fischer (KF) titration. KF titration detects the bound as well as unbound water present in a sample by dissolving it in the KF reagent. The sample is titrated coulometrically. A small quantity of sample was accurately weighed (15 mg) and was titrated with the Karl Fisher reagent to determine the moisture content. The endpoint, provides the total amount of water present was provided by the instrument.

RESULTS

Chromatographic analysis to assess the drug degradation:

The data pertaining to the calibration plot for HPLC is provided in Appendix I. The test solution concentration used for analysis of melt quenched drug substance was 0.3 mg/mL. Table B-IV-II provides data on the assay for the melt quench drug substance of four different lots. As seen from the assay values, no drug degradation was noticed due to melt quenching of crystalline griseofulvin.

X-ray analysis for the construction of calibration plot:

The X-ray scans for physical mixture of 40%: 40%: 20% w/w of crystalline griseofulvin, amorphous griseofulvin and lithium fluoride respectively four reproducibility scans are shown in Fig. B-IV-3. The peak height ratio of crystalline griseofulvin to lithium fluoride for a specific ratio of 40%:40%:20%w/w of amorphous griseofulvin, crystalline griseofulvin and lithium fluoride were not reproducible. Also, the peak height ratio of crystalline griseofulvin and lithium fluoride, when plotted as a function of percentage w/w of griseofulvin yielded a straight line with very poor slope of 0.0097, as seen in Fig. B-IV-4. The slope obtained was too small to be able to accurately resolve the differences in the percent amorphous griseofulvin in the mixture. Hence X-ray analysis was not chosen as a suitable technique to study isothermal crystallization of griseofulvin.

Thermal analysis of griseofulvin:

The DSC scans of amorphous and crystalline griseofulvin are shown in Fig B-IV-5. The amorphous griseofulvin undergoes a non-reversible exothermic recrystallization during the heating scan with peak maxima at around 81° and 119°C. It appears from the two distinct exothermic peaks that recrystallization occurs in two phases involving a structural transformation from a metastable crystalline form at lower temperature into a stable crystalline one at elevated temperatures. A similar observation in the recrystallization behavior was found in the case of nifedipine and a solid-state transformation was accounted as the reason for two exothermic crystallization peaks [30]. The glass transition event of amorphous griseofulvin was characterized at 92°C from the reversing heat flow scan and is shown as an inset in Fig B-IV-5. After recrystallization, amorphous griseofulvin undergoes melting at 212°C. The heats of fusion and the melting temperatures of the recrystallized and original crystalline griseofulvin were the same, indicating that amorphous griseofulvin undergoes complete crystallization during the heating scan. Overall the heat of recrystallization was used to quantify the fraction of crystalline drug.

Construction of calibration plot: MDSC

Since X-ray diffraction did not prove to be a suitable technique for this compound, MDSC analysis of drug was performed. A calibration plot was generated based on the DSC heat of crystallization of known physical mixtures of amorphous and crystalline griseofulvin. The non-reversing heat flow scans of the physical mixtures are shown in Fig

B-IV-6. It is seen from the figure that with an increase in the weight fraction of amorphous griseofulvin, the heat of recrystallization (i.e. area under both the peaks) increases. To generate the calibration plot, the heat of recrystallization (J/g) that was obtained from the area under the recrystallization peaks was plotted against the percentage of amorphous griseofulvin present (Fig. B-IV-7). As seen from Fig. B-IV-7, the calibration plot has a much higher slope when compared to the plot generated using X-ray analysis and hence was found more suitable to interpret the crystallization studies.

Isothermal stability studies:

Amorphous griseofulvin samples that were exposed to 0%, 32% and 43% RH conditions were analyzed periodically to monitor the changes that occurred in their crystallinity. The MDSC non-reversing heat flow of griseofulvin exposed to 23°C / 43% RH conditions as a function of storage time is shown in Fig B-IV-8. It is seen from the figure that the area under the exothermic peak decreases in magnitude with storage time. This indicates progressive crystallization of amorphous griseofulvin. The percent crystallinity in the sample was obtained using the calibration plot and is shown in Fig. B-IV-9. As can be seen from the plot, the rate and extent of crystallization of the samples stored at 43% RH was much greater than those stored at 32% RH. Even the samples stored at 0% RH showed significant crystallization although at a much smaller rate.

The total moisture absorbed by the samples was obtained using the Karl Fischer titrimetric analysis and are tabulated in Table B-IV-IV.

Non-Isothermal stability studies:

Non isothermal crystallization studies were performed using Kissinger's analysis. The peak crystallization temperature of amorphous griseofulvin was recorded by heating it at different rates. The non reversing heat flow scans of amorphous griseofulvin are shown in Fig B-IV-10.

DISCUSSION

Isothermal crystallization kinetics:

The crystallization kinetics was monitored with time as a function of relative humidity by storing the samples in isothermal stability conditions. The rate and extent of crystallization of griseofulvin have been plotted in Figure 9 and the crystallization kinetics was calculated based on Hancock-Sharp equation [31].

Hancock-Sharp equation:

Unlike the chemical degradation rates in solution, the rate of alteration in the physical state of a powder is difficult to determine from accelerated stability studies. However, predictions of some physical alteration pathways such as crystallization, dehydration, polymorphism etc., have been attempted. The Hancock-Sharp equation is often used to describe the kinetics of reversion of amorphous phase to its crystalline form and is written as follows:

$$\ln[-\ln(1 - \alpha)] = \ln B + m \ln t \quad (2)$$

where α the fraction of drug that has crystallized, t is the storage time, B is a constant and m is a constant relating to the mechanism of griseofulvin crystallization. The kinetic equations for the most common mechanisms that are believed to operate in solid-state decomposition are presented in Table B-IV-III. Upon plotting the experimentally obtained results with Hancock-Sharp equation as $\ln[-\ln(1-\alpha)]$ with the logarithm of storage time t , a linear relationship was obtained as shown in Fig B-IV-11. In order to chose the appropriate mechanism that would fit the experimentally obtained crystallization data, the results were fit to all the equations provided in Table B-IV-III. The results of such fit are provided in Table E-III of Appendix E. Although the same fit to KJMA, and Avrami-Erofeev A2 and A3 were obtained, because of the m value ($m=1.08$) that was obtained by Hancock-Sharp equation we selected KJMA for further modelling.

Kolmogorov-Johnson-Mehl-Avrami (KJMA) equation:

A first order degradation mechanism has often been chosen to plot crystallization kinetic plots [32, 33]. The relationship pertaining to this mechanism is given by the KJMA equation and is described as:

$$-\ln(1-\alpha) = k(t-t_0) \tag{3}$$

where k is the rate constant for crystallization, t is the storage time and t_0 is the induction or the nucleation time. The rate constants for crystallization obtained from the slope of the linear equation are given as a function of relative humidity in Table B-IV-IV. The rate constants were found to be higher at high relative humidity conditions. This was not

surprising because at higher relative humidity, water in the samples could cause an increased molecular mobility and hence increased crystallization rates.

Non-isothermal crystallization:

Non isothermal crystallization was performed using Kissinger's analysis to determine E_a . The E_a value was determined from the slope of the linear plot of $\ln(\beta / T_c^2)$ and $1/T_c$ as shown in Fig. B-IV-13. In this plot, β is the heating rate and T_c is the peak crystallization temperature. With an increase in the heating rate, an increase in the peak crystallization temperature was noticed (Fig. B-IV-10). Although the area under the exothermic crystallization peak appears to increase with an increase in the heating rate, the absolute values were found to be constant (Fig. B-IV-10). This indicated that irrespective of the heating rate employed in this study, amorphous griseofulvin crystallized completely. Similarly at higher heating rates, most of the crystallization probably occurred over a narrow temperature domain and hence, a greater peak appeared compared to the ones obtained with slower heating rates, where crystallization occurred gradually over a larger temperature domain.

The slope of the line in Fig. B-IV-13 provided $-E_a/R$ values, where R is the gas constant, and E_a was calculated as 239 KJ/mol. The E_a value for the crystallization of griseofulvin has not been reported in the literature for comparison with the values obtained in this study. However, the E_a value of griseofulvin was found to be much lower than the E_a of 317 KJ/mol reported for crystallization of lactose by Schmitt et. al [32]. This agrees with

the isothermal crystallization rates which seem to be very high at experimental conditions employed.

Mechanism of crystallization:

The mechanism of crystallization of amorphous materials has been studied extensively in the literature [34-36]. The process of crystallization involves nucleation and crystal growth. It is generally considered that crystallization from amorphous state can occur only at temperatures above the T_g of the material where the viscosity of the amorphous state is low and conducive for nucleation and subsequent crystal growth. However for amorphous indomethacin, crystallization has been shown to occur at temperatures 30°C below the T_g [37]. In our case griseofulvin crystallized at temperatures as low as 65°C below the T_g . The crystallization at this low temperature was expressed by the Turnbull and Fischer equation [20]:

$$\dot{V}^* = -\left(\frac{NkT}{h}\right) \exp\left(-\frac{\Delta G_D + \Delta G_k}{kT}\right) \quad (4)$$

where \dot{V}^* is the nucleation rate per unit volume, N is the number of molecules per unit volume, k is the Boltzman constant, h is Planck's constant, and T is the temperature. The term ΔG_k is the Gibbs free energy change for the formation of nucleus with a critical size and ΔG_D is the free energy associated with transportation of molecules from the amorphous bulk onto the growing nucleus.

It can be seen from the equation shown above that nucleation rate is the result of net effect between two opposing factors: temperature and super-cooling. When temperature

decreases, the degree of super cooling increases. This may correspond to the increase in the temperature difference between the melting temperature and storage temperature. Under such conditions, the nucleation rate would be expected to increase exponentially. However, temperature reduction also causes reduction of the molecular mobility and hence decreases nucleation probability. Although in varying amounts, molecular mobility changes will impact both ΔG_K and ΔG_D . In equation 4, the term ΔG_K is dependent upon the interfacial energy between the nucleus and amorphous bulk as well as degree of super cooling, and is less influenced by the magnitude of changes in the molecular mobility of a system at a constant temperature. ΔG_D on the hand, encompasses the energy of activation for diffusion through the bulk phase and this factor is largely affected by molecular mobility.

For griseofulvin crystallization, it can be assumed that the molecular mobility is still strong even at temperatures as low as 65°C below the T_g and hence nucleation, and crystal growth, results. A similar explanation was provided for the crystallization of amorphous indomethacin at temperatures below T_g and nucleation was explained by the rotational motion of molecules. This assumption can be true for griseofulvin considering its small chemical structure and ease of rotation. The increased moisture content of the drug probably increases the ease of rotation and translational diffusion (Table B-IV-IV). Increased molecular mobility is likely to increase the crystallization rate constant. Interestingly significant crystallization of griseofulvin was observed in the samples containing 0.15%w/w moisture, indicating the high proximity for griseofulvin to crystallize at temperatures as low as 65°C below its T_g .

CONCLUSIONS

In this paper, the isothermal and nonisothermal crystallization of amorphous griseofulvin has been reported. Isothermal crystallization was performed by storing the samples at various relative humidity conditions and monitoring the extent of crystallization of griseofulvin from the heat of crystallization process in DSC heating scan. Nonisothermal experiments were calculated by using Kissinger's analysis and the apparent energy of activation for griseofulvin crystallization (E_a) was calculated as $E_a = 239$ KJ/mol or 57Kcal/mol (1 joule = 0.2388 calories). The isothermal experimental data was treated using the Hancock-Sharp equation and the mechanism of solid-state physical alteration was explained as the first-order random nucleation process. The data was accordingly fit to the KJMA equation, and the kinetic rate constant and induction time for crystallization were calculated. An increase in the rate constant and decrease in the induction time with increasing relative humidity indicated higher molecular mobility at high relative humidities, which enhanced the crystallization process. High molecular mobility was the cause for crystallization at 0% RH and temperatures as low as 65°C below T_g . No crystallization from amorphous phase was noticed in samples stored at -20°C (i.e. 110°C below T_g). The theory of crystallization and the factors affecting the nucleation and crystallization growth rate have also been reviewed. According to the data obtained, it can be concluded that amorphous griseofulvin should be stored at very low temperatures in order to retain its amorphous form.

ACKNOWLEDGMENTS

This study is a part of Ph.D. research of Mr. Vasanthavada who is a Novartis Graduate Research Fellow and has conducted his research at Novartis R&D facility. He wishes to acknowledge the fellowship and also thank Ms. Marilyn Alvine and Dr. Francis Liu for their support with X-ray analysis.

REFERENCES

1. P. York. Solid-state properties of powders in the formulation and processing of solid dosage forms. *International Journal of Pharmaceutics*. 14:1-28 (1983).
2. Y. Nakai, E. Fukuoka, S. Nakajima and J. Hasegawa. Crystallinity and physical characteristics of microcrystalline cellulose. *Chemical and Pharmaceutical Bulletin*. 25:96-101 (1977).
3. M. Mumenthaler and H. Leuenberger. Atmospheric spray freeze-drying: A suitable alternative in freeze-drying technology. *International Journal of Pharmaceutics*. 72:97-110 (1991).
4. M. J. Pikal and S. Shah. The collapse temperature in freeze drying: dependence on measurement methodology and rate of water removal from the glassy phase. *International Journal of Pharmaceutics*. 62:165-186 (1990).
5. B. C. Hancock, and M. Parks. What is the true solubility advantage for amorphous pharmaceuticals? *Pharmaceutical Research* 17:397-404 (2000).

6. V. Andronis, M. Yoshioka and G. Zografi. Effects of sorbed water on the crystallization of indomethacin from the amorphous state. *Journal of Pharmaceutical Sciences*. 86:346-351 (1997).
7. Saleki-Gerhardt, C. Ahlneck and G. Zografi. Assessment of disorder in crystalline solids. *International Journal of Pharmaceutics*. 101:237-247 (1994).
8. C. Hancock, S. L. Shamblin and G. Zografi. Molecular mobility of amorphous pharmaceutical solids below their glass transition temperatures. *Pharmaceutical Research*. 12:799-806 (1995).
9. Saleki-Gerhardt and G. Zografi. Non-Isothermal and Isothermal Crystallization of Sucrose from the Amorphous State. *Pharmaceutical Research*. 11:1166-1173 (1994).
10. M. A. Moustafa, S. A. Khalil, A. R. Ebian and M. M. Motawi. Succinylsulfathiazole crystal forms I: preparation, characterization, and interconversion of different crystal forms. *Journal of Pharmaceutical Sciences* 63:1103-1109 (1974).
11. H. Nakamachi, Y. Wada, I. Aoki, Y. Kodama and K. Kuroda. Effect of a minor component on thermal transformation of crystalline 6-mercaptopurine. *Chemical and Pharmaceutical Bulletin* 29:2956-2965 (1981).
12. M. Otsuka and N. Kaneniwa. A kinetic study of the crystallization process of noncrystalline indomethacin under isothermal conditions. *Chemical and Pharmaceutical Bulletin* 36:4026-4032 (1988).
13. Saleki-Gerhardt, C. Ahlneck and G. Zografi. Assessment of disorder in crystalline solids *International Journal of Pharmaceutics* 101:237-247 (1994).
14. Hendriksen. Characterization of calcium fenoprofen I. Powder dissolution rate and degree of crystallinity. *International Journal of Pharmaceutics* 60:243-252 (1990).

15. E. G. Shami, P. D. Bernardo, E. S. Rattie and L. J. Ravin. Kinetics of polymorphic transformation of sulfathiazole form I. *Journal of Pharmaceutical Sciences* **61**:1318-1320 (1972).
16. M. A. Moustafa and J. E. Carless. Application of differential scanning calorimetry to the study of sulphathiazole crystal forms. *Journal of Pharmacy and Pharmacology* **21**:359-365 (1969).
17. M. J. Pikal, A. L. Lukes, J. E. Lang and K. Gaines. Quantitative crystallinity determinations for β -lactam antibiotics by solution calorimetry: correlations with stability. *Journal of Pharmaceutical Sciences*. **67**:767-773 (1978).
18. D. J. W. Grant and P. York. A disruption index for quantifying the solid state disorder induced by additives or impurities. II. Evaluation from heat of solution. *International Journal of Pharmaceutics* **28**:103-112 (1986).
19. J. T. Carstensen and K. V. Scoik. Amorphous-to-crystalline transformation of sucrose. *Pharmaceutical Research*. **7**:1278-1281.
20. M. Galop and G. L. Collins. Thermally stimulated currents observed in pharmaceutical products. *Thermochemica Acta*. **6436**:1-5 (2000).
21. W. C. Duncan-Hewitt and D. J. W. Grant. True density and thermal expansivity of pharmaceutical solids: comparison of methods and assessment of crystallinity. *International Journal of Pharmaceutics* **28**:75-84 (1986).
22. T. Sebhatu, M. Angberg and C. Ahlneck. Assessment of the degree of disorder in crystalline solids by isothermal microcalorimetry. *International Journal of Pharmaceutics* **104**:135-144 (1994).
23. L. E. Briggner, G. Buckton, K. Bystrom and P. Darcy. The use of isothermal microcalorimetry in the study of changes in crystallinity induced during the processing of powders. *International Journal of Pharmaceutics* **105**:125-135 (1994).

24. G. K. Vudathala and J. A. Rogers. Oral bioavailability of griseofulvin from aged griseofulvin: lipid coprecipitates: *invivo* studies in rats. *Journal of Pharmaceutical Sciences* **81**:1166-1169 (1992).
25. M. A. Moustafa, S. A. Khalil, A. R. Ebian and M. M. Motawi. Succinylsulfathiazole crystal forms I: preparation, characterization, and interconversion of different crystal forms. *Journal of Pharmaceutical Sciences* **63**:1103-1109 (1974).
26. E. G. Shami, P. D. Bernardo, E. S. Rattie and L. J. Ravin. Kinetics of polymorphic transformation of sulfathiazole form I. *Journal of Pharmaceutical Sciences* **61**:1318-1320 (1972).
27. H. Nyqvist. Saturated salt solutions for maintaining specified relative humidities. *Int. J. of Pharm. Tech. & Prod. Mfr.* 4:47-48 (1983).
28. H. E. Kissinger. Reaction kinetics in differential thermal analysis. *Analytical Chemistry* **29**:1702-1706 (1957).
29. H. E. Kissinger. Variation of peak temperature with heating rate in differential thermal analysis. *J. Res. Nat. Bur. Stand.* **57**:217-221 (1956).
30. Y. Aso, S. Yoshioka, T. Otsuka, and S. Kojima. The physical stability of amorphous nifedipine determined by isothermal microcalorimetry. *Chemical and Pharmaceutical Bulletin*. **43**:300-303 (1995).
31. M. Otsuka and N. Kaneniwa. A kinetic study of the crystallization process of noncrystalline indomethacin under isothermal conditions. *Chemical and Pharmaceutical Bulletin* **36**:4026-4032 (1988).
32. E. A. Schmitt, D. Law and G. Z. Zhang. Nucleation and crystallization kinetics of hydrated amorphous lactose above the glass transition temperature. *Journal of Pharmaceutical Sciences* **88**:291-296 (1999).

33. K. J. Crowley and G. Zografi. The effect of low concentrations of molecularly dispersed poly(vinylpyrrolidone) on indomethacin crystallization from the amorphous state. *Pharmaceutical Research* **20**:1417-1422 (2003).
34. D. Turnbull, J. C. Fisher. Rate of nucleation in condensed systems. *Journal of Chemical Physics* **17**:71-73 (1949).
35. E. Woldt. The relationship between isothermal and nonisothermal description of Johnson-Mehl-Avrami-Kolmogorov kinetics. *J. Phys. Chem. Solids* **53**:521-527 (1992).
36. J. W. Mullin. Crystallization; Butterworth Heinemann: Oxford, 1992.
37. M. Yoshioka, B. C. Hancock and G. Zografi. Crystallization of indomethacin from the amorphous state below and above its glass transition temperature. *Journal of Pharmaceutical Sciences* **83**:1700-1705 (1994).

Table B-IV- I

Methods used in isothermal crystallization studies

Technique	Principle	Advantages & Disadvantages	Limit of Detection (amorphous)	Reference
X-ray Diffraction	Peak height ratio of crystalline drug and an internal reference	1. Non-thermal technique 2. Measures average degree of disorder, indirect measure of amorphous material	5 - 10% w/w Model compounds: Succinylsulfathiazole, 6-mercaptopurine, indomethacin,	[10-14]
Differential Scanning Calorimeter	Heat of crystallization of amorphous; heat of fusion of crystalline content	1. Sensitive, no mixing issues 2. Not suitable for thermally sensitive compounds	2 – 3% w/w Model compounds: Lactose, cephalothin sodium, sulfathiazole	[15, 16]
Solution Calorimeter	Heat of solution and energy difference between amorphous and crystalline content	1. Ease of experiment 2. Amorphous standard is difficult to obtain	2% w/w Model compounds: β -lactam antibiotics	[17, 18]
Water vapor sorption	Percent weight loss due to de-sorption when known amount of amorphous material crystallizes	1. Sensitive tool, direct measure of amorphous control 2. Not applicable to all drugs that could form hydrates etc	1-2% w/w Model compound: Sucrose, β -lactam antibiotics	[17, 19]

Table B-IV-I (contd.)

Methods used to detect crystallization in drug products

Technique	Principle	Advantages & Disadvantages	Limit of Detection (amorphous)	Reference
Thermally Stimulated Current	Polarization or depolarization current intensity as a function of amorphous content	1. Very sensitive tool 2. Reproducibility limits the measurements	1% w/w Model compound: undisclosed	[20]
Density Measurements	Density differences between amorphous and crystalline solids.	1. Easy experiments 2. Differences between samples may not be significant	Model compound Adipic acid, acetaminophen, Calcium fenoprofen	[13, 14, 21]
Isothermal Microcalorimetry	Measurement of power-time output as the amorphous component crystallizes and comparison with the amorphous standard	1. Sensitive tool. 2. Direct measure of amorphous content. 3. Not suitable for rapidly crystallizing compounds	0.5-1% w/w Model compounds: Lactose	[22, 23]

Table B-IV-II

HPLC assay to assess griseofulvin stability during melt-quench preparation

Lot	Retention Time (minutes)	Peak Area	Peak Height	Assay	Average Assay
1	5.508	20269286	1802267	98.26	
	5.508	20328777	1804940	98.55	
2	5.508	20629266	1825700	100.01	
	5.508	20633751	1823565	100.03	
3	5.508	21055119	1849861	102.07	100.40 ±
	5.508	21045734	1853770	102.03	1.45
4	5.500	20869814	1833286	101.17	
	5.508	20853720	1832506	101.10	
Standard	5.508	20619686	1824051	99.96	
(Crystalline drug)	5.508	20633751	1823577	100.03	

Table B-IV-III

List of various solid-state transformation kinetic rate mechanisms and their equations

Symbol	Equation	<i>m</i> value	Mechanism
R ₁	$\alpha = kt$	1.24	Zero-order mechanism (Polani - Wigner equation)
R ₂	$1 - (1 - \alpha)^{1/2} = kt$	1.11	Phase boundary reaction; cylindrical symmetry
R ₃	$1 - (1 - \alpha)^{1/3} = kt$	1.07	Phase boundary reaction; spherical symmetry
F ₁	$-\ln(1 - \alpha) = kt$	1.00	Random nucleation, one nucleus on each particle (Kolmogorov-Johnson-Mehl-Avrami (KJMA) equation)
A ₂	$[-\ln(1 - \alpha)]^{1/2} = kt$	2.00	Random nucleation, two dimensional growth of nuclei (Avrami-Erofeev equation)
A ₃	$[-\ln(1 - \alpha)]^{1/3} = kt$	3.00	Random nucleation, three dimensional growth of nuclei (Avrami-Erofeev equation)
D ₁	$\alpha^2 = kt$	0.62	One-dimensional diffusion
D ₂	$(1 - \alpha)\ln(1 - \alpha) + \alpha = kt$	0.57	Two-dimensional diffusion
D ₃	$[1 - (1 - \alpha)^{1/3}]^2 = kt$	0.54	Three-dimensional diffusion (Jander equation)
D ₄	$(1 - 2\alpha/3) - (1 - \alpha)^{2/3} = kt$	0.57	Three-dimensional diffusion (Grinstring-Brounshtein equation)

Table B-IV-IV

Hancock-Sharp fit of the experimental data and the Isothermal crystallization rate constants as a function of relative humidity

Relative humidity	Moisture content (% w/w)	Hancock-Sharp Fit		KJMA Fit (average n=3)		
		<i>m</i> value	R ²	<i>k</i> [days ⁻¹]	<i>t</i> ₀ [days]	R ²
0 %	0.15 ± 0.02%	0.916	0.987	0.016	2.07	0.955
32 %	0.41 ± 0.04%	1.57	0.984	0.051	2.03	0.988
43 %	0.49 ± 0.06%	1.02	0.980	0.067	0.66	0.992

Figure B-IV-1

Chemical structure of griseofulvin ((2*S*)-trans-7-Chloro-2', 4, 6-trimethoxy-6'-methylspiro (benzofuran-2[3*H*], 1'-[2] cyclohexene)-3, 4'-dione)

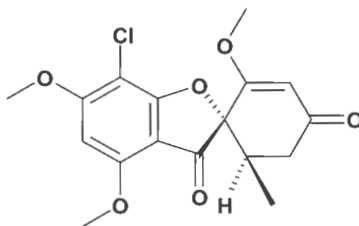


Figure B-IV-2

X-ray diffraction patterns of griseofulvin untreated (crystalline) and melt-quench treated (amorphous)

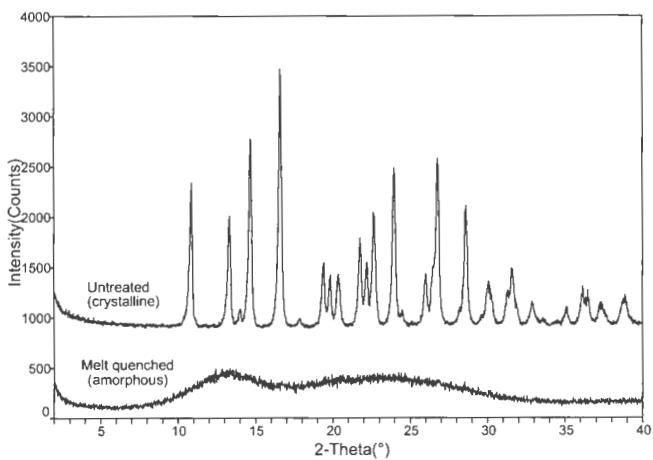


Figure B-IV-3

X-ray diffraction patterns of repetitions ($n=4$) of 1:1 physical mixtures of amorphous and crystalline griseofulvin containing 20%w/w lithium fluoride as an internal standard.

Notice that the peak heights for the griseofulvin ($2\theta = 16.5^\circ$) and lithium fluoride ($2\theta = 39^\circ$) are not of the same height for all the four scans.

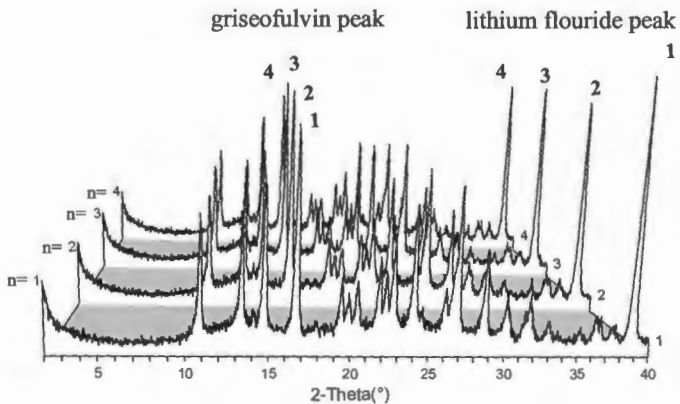


Figure B-IV-4

X-ray diffraction calibration plot of: percentage crystalline griseofulvin vs. peak height ratio of crystalline griseofulvin and lithium fluoride.

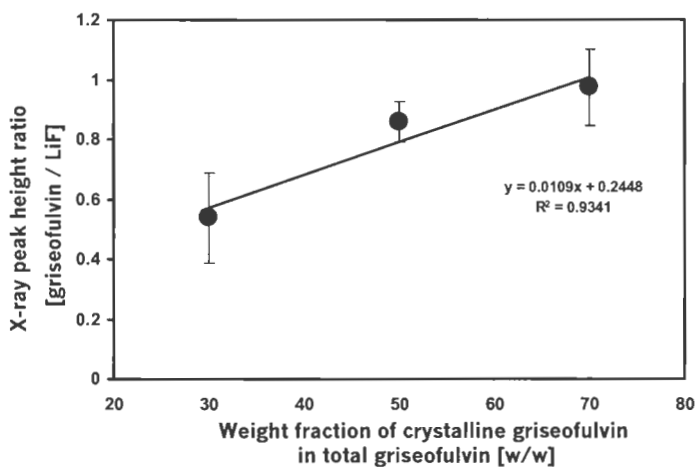


Figure B-IV-5

DSC heat flow scans of griseofulvin amorphous and crystalline. Inset demonstrates the T_g of amorphous sample on the reversing heat flow. Exothermic peak of the amorphous sample indicates its recrystallization. Heats of fusion of the recrystallized and crystalline griseofulvin are similar indicating complete crystallization of amorphous griseofulvin during the heating scan.

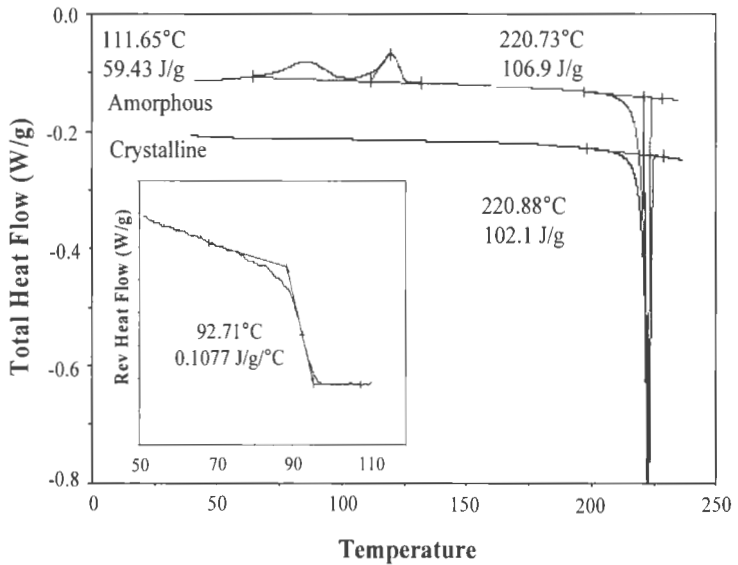


Figure B-IV-6

MDSC non-reversing heat flow scans of physical mixtures of crystalline and amorphous griseofulvin heated at 1°C/min with amplitude of $\pm 0.266^\circ$ every 50 seconds. The percentages refer to the amounts of amorphous griseofulvin present.

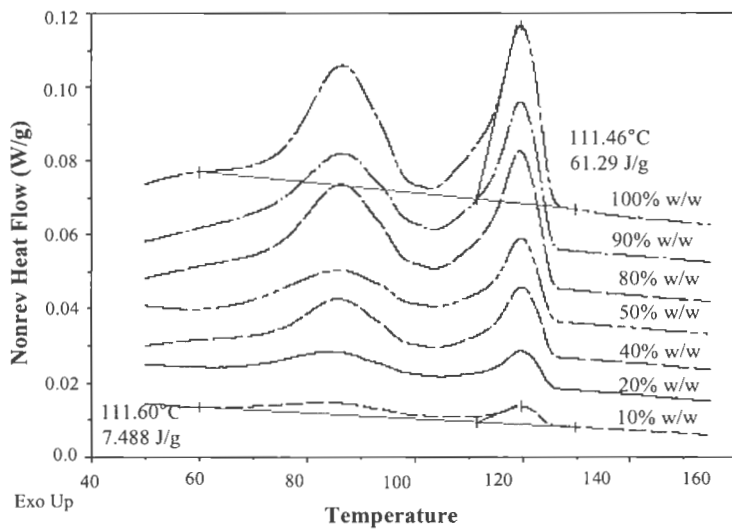


Figure B-IV-7

DSC calibration plot of: percentage amorphous griseofulvin vs. heat of recrystallization
in order to quantify percentage crystallinity in the stability samples.

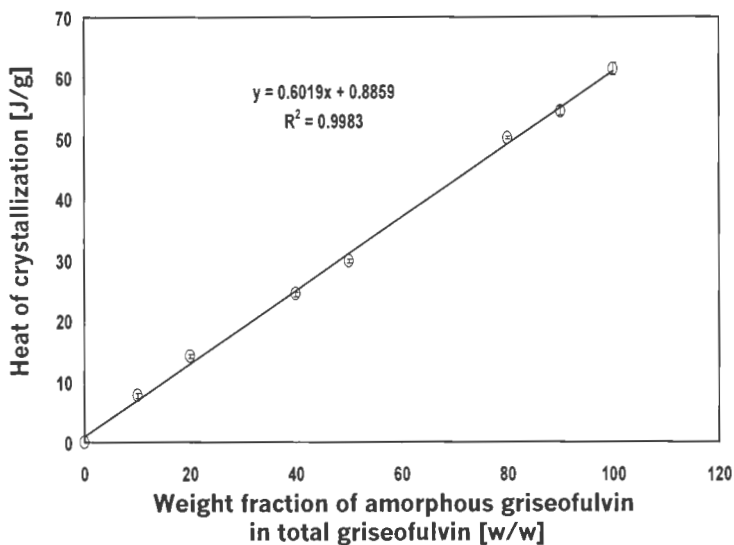


Figure B-IV-8

MDSC non-reversing heat flow scans of amorphous griseofulvin as a function of storage time. Decreasing exothermic peaks of recrystallization indicates increasing crystalline content of the samples.

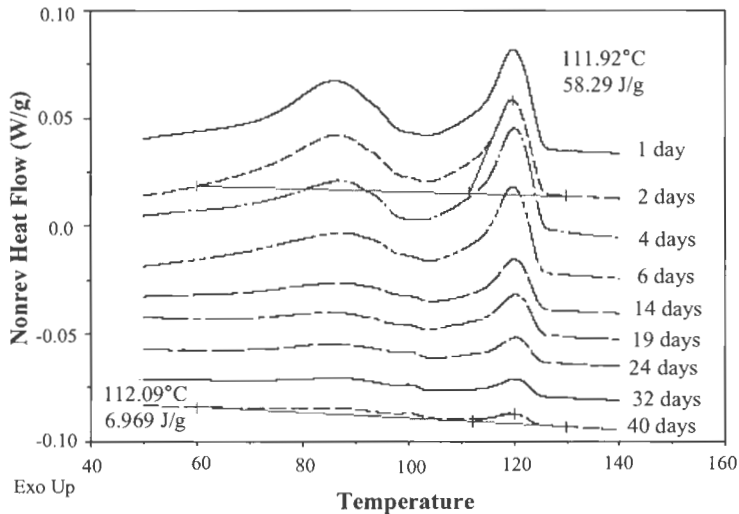


Figure B-IV-9

Percentage griseofulvin crystallized as a function of storage time upon storing at 23°C with 43% RH (■); 32% RH (◆); and 0% RH (●). The percentages are calculated from the heats of crystallization measuring three different batches (n=3) for each time point.

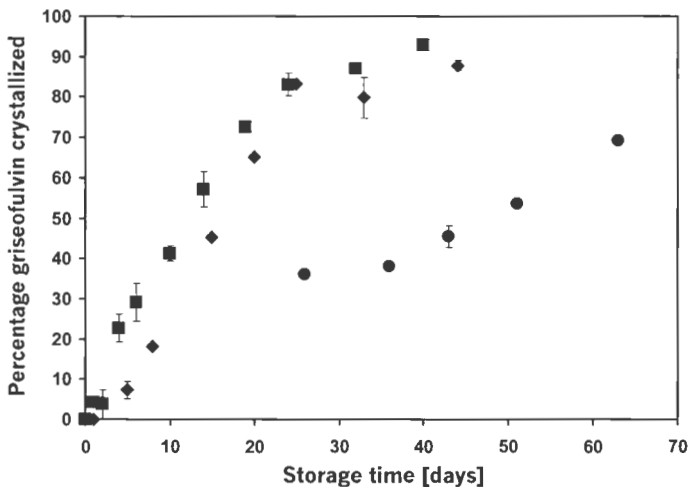


Figure B-IV-10

MDSC non-reversing heat flow scans of amorphous griseofulvin as a function of heating rate. The peak recrystallization temperature increases with an increase in the heating rate, but the total area under the recrystallization peak (J/g) does not change significantly.

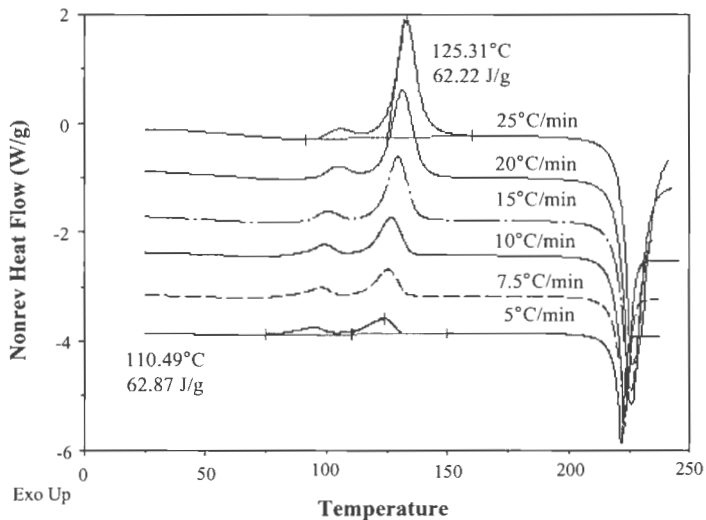


Figure B-IV-12

Fit of the stability data to the first-order KJMA rate equation to determine the isothermal crystallization rate constant for amorphous griseofulvin.

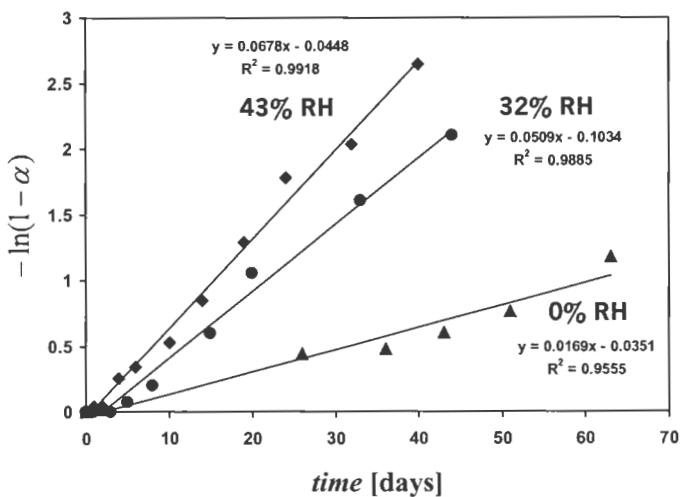
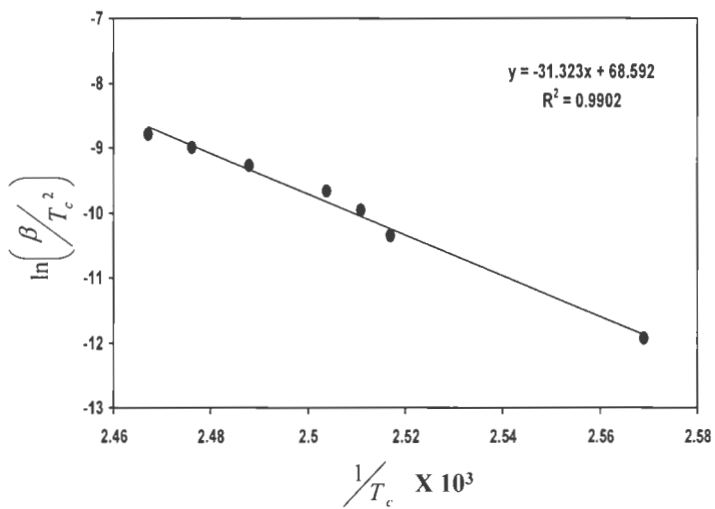


Figure B-IV-13

Determination of the non-isothermal E_{act} values for crystallization of amorphous griseofulvin by using Kissinger analysis.



MANUSCRIPT V

MEASUREMENT OF SUB-GLASS TRANSITION MOLECULAR MOTIONS OF POLY(VINYLPYRROLIDONE): COMPARISON OF THE UTILITY OF THERMALLY STIMULATED CURRENT (TSC) AND MODULATED DIFFERENTIAL SCANNING CALORIMETER (MDSC)

Madhav Vasanthavada¹, Yatindra Joshi², and M. Serpil Kislalioglu^{1,3}

ABSTRACT

Purpose: To compare the utility of Thermally Stimulated Current Spectroscopy (TSC) and Modulated Differential Scanning Calorimetry (MDSC) in determining the effects of the molecular weight on the molecular motions of Poly (vinylpyrrolidone) (PVP).

Methods: PVP of three different molecular weight grades namely PVP K17, PVP K30 and PVP K90 were used as model polymers. TSC was used in the polarization mode. The samples were subjected to a thermal treatment by heating to temperatures 25°C above

¹ Department of Applied Pharmaceutical Sciences, The University of Rhode Island, Kingston, RI 02881.

² Pharmaceutical & Analytical Development, Novartis Pharmaceutical Corporation, East Hanover, NJ 07936.

³ To whom correspondence should be addressed. (Telephone: (401) 874 5017; Email: skis@uri.edu)

their glass transition temperature (T_g), and quench-cooling to 150°C below their T_g . They were then aged at $T_g-5^\circ\text{C}$, $T_g-15^\circ\text{C}$ and $T_g-30^\circ\text{C}$ for different storage periods and reheated at 3°C/min. The aging period extended for up to 16 hours with MDSC with samples analyzed at 1, 2, 4, 8 and 16 hours. For TSC measurements, the samples were aged for up to 8 hours with time points of 0.25, 0.5, 1, 2, 4, 6, and 8 hours. The polarization current was measured at 175 V/mm by heating the samples at 3°C/min.

Results: A reproducible sub- T_g relaxation peak in addition to the T_g peak was observed at $82 \pm 3^\circ\text{C}$ for PVP K17, at $132 \pm 2^\circ\text{C}$ for PVP K30, and at $143 \pm 3^\circ\text{C}$ for PVP K90 using TSC. No such peak was detected using MDSC. Upon aging, the polarization current peak under sub- T_g peak decreased and the area under T_g peak increased with aging time. However no significant change in the “total peak area” was observed. Modified experimental protocols helped to estimate the enthalpy relaxation. From MDSC, the average relaxation time constants were estimated. A linear empirical relation was established between the TSC and MDSC results.

Conclusions: TSC provided additional information about the molecular motions of PVP below T_g when compared with MDSC. The results suggest the rank order of decreasing molecular mobility at a specified temperature below the respective T_g as PVP K17 > PVP K90 > PVP K30. Overall TSC proves to be a powerful, sensitive complimentary tool to characterize the molecular mobility of amorphous solids.

Keywords: *Glass transition temperature, enthalpy relaxation, thermally stimulated current, molecular mobility, modulated differential scanning calorimeter*

INTRODUCTION

Polymers are widely used in the pharmaceutical industry as excipients in several dosage forms like tablets, capsules, trans-dermal dosage forms, inhalation products, suppositories and many other formulation types [1]. They have also been used to modify the drug dissolution profile and to create a sustained or delayed release effect to meet therapeutic requirements [2]. The usage of polymers to improve the aqueous solubility of poorly soluble drugs and to inhibit the drug crystallization has also been reported in the pharmaceutical literature extensively [3-6]. The mechanism of crystallization inhibition by polymers in amorphous solid dispersions has been postulated to be the ability of the polymer to form a miscible phase with the drug [7]. In this molecularly miscible phase, the coupling molecular motions of long chain polymers reduce the net molecular motion of small drug molecules and hence delay the crystallization of the amorphous drug. It is important however to monitor the molecular mobility of the system since the thermodynamic non-equilibrium nature of amorphous drug would always favor crystallization to the lower energy state, which is poorly water soluble.

An amorphous material constantly undergoes structural or enthalpy relaxation to achieve its low-energy super-cooled equilibrium state or a crystalline state as depicted in Fig. B-V-1. Retention of the amorphous state of the solid would therefore depend upon the extent to which the material can structurally relax to lower its enthalpy or heat content. The higher the molecular mobility of the material, the higher would be the rate at which it

will structurally relax. Therefore molecular mobility measurements are necessary to understand the dynamics of crystallization.

It is however, difficult to quantify directly the structural relaxation or the mean relaxation time, which is an indicator of molecular mobility for amorphous solids below their T_g . Such difficulty is due to (a) long time scales of molecular motions and (b) complex relationship between the mean relaxation time and storage temperature [8, 9]. Despite these challenges, various techniques including enthalpy relaxation measurements [10-12], dielectric spectroscopy [13], viscosity measurements [14], and nuclear magnetic resonance [15, 16] have been used to estimate the mean relaxation time.

The purpose of this study was firstly to conduct enthalpy relaxation measurements and to characterize molecular motions to estimate the mean relaxation time of different molecular weight grades of poly (vinylpyrrolidone) (PVP). PVP was chosen as the model compound because it is one of the widely used polymers in the pharmaceutical industry to prepare solid dispersions of the poorly soluble drugs. The molecular mobility of PVP can be characterized with a sensitive thermal technique called thermally stimulated current spectroscopy (TSC). TSC involves heating a sample across its transition temperature in the presence of an electric field. At the solid-transition temperature, the molecular mobility of sample generates an electric current, which is amplified and measured. TSC offers the advantage of being very sensitive to the molecular motions of the sample that it is measuring and, it can measure the molecular mobility recovery.

Comparison and interpretation of the results obtained by molecular mobility recovery (TSC) and those of enthalpy recovery experiments (MDSC) are very useful to gain

insight into the relative extent of molecular mobility of PVP and identify the factors influencing it.

MATERIALS AND METHODS

Materials:

Plasdone[®] (Poly(vinylpyrrolidone)) with K value (as designated by the supplier) 17, 29/32 and 90 having M_w of 10, 58 and 130 KDa respectively, as determined by the supplier from light scattering measurements, was obtained from ISP Technologies Inc., (Wayne, NJ). The molecular weight distribution around each mean molecular weight was 4-6 KDa, as described by the supplier. Samples were dried at 105°C under vacuum for 20 hours prior to running experiments.

Methods:

Modulated Differential Scanning Calorimeter (MDSC):

A Modulated Differential Scanning Calorimeter (MDSC) (TA Instruments 2920, New Castle, DE), with liquid nitrogen cooling accessory was used for the enthalpy recovery measurements. Analysis was performed under a purge of dry nitrogen gas (60cc/min). High purity indium and sapphire were used bimonthly to calibrate for the heat flow and heat capacity of the instrument.

MDSC Experimental Protocol:

The experimental protocol is provided in Fig. B-V-2. The glass transition temperatures of samples (8-12mg) were determined by first heating to 25°C above the T_g (T_f in Fig. B-V-2), to erase the thermal history, and then quench cooling to 150°C below their T_g (T_0). The T_g was detected upon a second heating scan as the midpoint of the inflection in the heat capacity or the reversing heat flow signal. A heating rate of 3°C/min, with modulations of $\pm 1^\circ$ every 60 seconds was used for all analysis. Following the T_g determination, the samples were aged at T_a , which were 5°, 15° and 30°C below the respective T_g for a period (T_s) of 1, 2, 4, 8 and 16 hours. At the end of each aging period, samples were rapidly cooled to 150°C below the T_g and subsequently reheated to 25°C above the T_g . The enthalpy-recovery of the aged samples (ΔH) was obtained as a function of aging time and temperature, from the area under the non-reversing heat flow signal at T_g .

Thermally Stimulated Polarization Current (TSPC):

The principle of TSPC is depicted schematically in Fig. B-V-3. The sample is heated across its transition temperature(s) in the presence of a high voltage electric field and the movement of the polar groups (dipoles) of molecules is measured as they orient to the applied field. The sample is placed between two electrodes of a parallel plane capacitor. As the temperature is increased, the molecular mobility rises and the dipole orients to the applied field when sufficient mobility exists. The motion of the dipole generates a polarization current (I) which is amplified and detected. The intensity of the polarization

current (output signal) provides a direct probe into the degree of molecular mobility of the materials as a function of temperature.

Thermally Stimulated Depolarization Current (TSDC):

The TSDC experiments are similar to TSPC measurements, with an exception that the samples are first heated to temperature above the suspected transition and are then polarized by applying an electric field. The polarization is frozen by rapidly cooling the samples to low temperatures. The depolarization current (opposite in direction to polarization current) is measured in the absence of electric field, by heating the sample across the suspected transition(s). The driving force for molecular motion upon reheating the sample is the restoration of neutrality or the original configuration. The molecular motion causes a depolarization current which is amplified and detected. The glass transition temperature is characterized by the temperature of peak maximum of the broad peak as shown schematically in Fig. B-V-3b.

TSPC Experimental protocol:

In this study, TSPC experiments were performed unless specified. TSPC or TSDC experiments were carried out using TSC/RMA 9000 Instrument (TherMold Partners, Stamford, CT). All experiments were conducted in an atmosphere of high purity helium gas. Samples ($13.5 \pm 0.5\text{mg}$) were placed in aluminium pans, covered with teflon lid and placed between the screw electrodes. This assembly was enclosed in a Faraday cage that was evacuated to 10^{-4} mbar and flushed several times with helium gas prior to experiments. The experimental procedure used to measure enthalpy recovery using TSPC

is depicted in Fig. B-V-2. As seen from Fig. B-V-2, in step 1 and 2, the thermal history of all samples was erased by heating to $T_g + 25^\circ\text{C}$ followed by a rapid cooling to $T_g - 150^\circ\text{C}$. The glass transition temperature of the samples was then determined by heating the samples at $3^\circ\text{C}/\text{min}$ in the presence of electric field (step 4). The samples were kept isothermal at step 5 in the absence of electric field and were quench-cooled (step 6) to form the fresh amorphous sample. Isothermal storage was carried out in step 7 for period of 0-8 hours in the absence of the field and the current produced due to molecular motion of the aged samples were recorded in step 8 in the presence of electric field by heating at $3^\circ\text{C}/\text{min}$. During isothermal storage, the electric field was turned off in order to eliminate any possible effects on enthalpy relaxation of samples and to closely match the treatment with MDSC. As with the MDSC experiments, the T_a was varied from 5° , 10° and 15°C below the respective T_g . An electric field of $175\text{ V}/\text{mm}$ was employed for all TSPC studies. Aging time varied as 0.25, 0.5, 1, 2, 4, 6 and 8 hours.

RESULTS AND DISCUSSIONS

Characterization of poly (vinylpyrrolidone):

MDSC:

The changes in heat capacity for different molecular weight grades of PVP obtained using MDSC are shown in Fig. B-V-4a. Glass transition temperatures T_g , is denoted as the midpoint of inflection in the heat capacity step-change. As seen from the Fig B-V-4a, each molecular weight grade of PVP exhibits a characteristic T_g that increased with an

increase in the molecular weight. In addition, an increase in the heat capacity step-change ΔC_p was also observed with increase in the molecular weight.

TSPC:

In Fig. B-V-4b, thermally stimulated depolarization current (TSDC) profiles for PVP K30 is shown. Unlike the MDSC plots, two distinct global relaxations peaks designated as **P₁** and **P₂** were seen at temperatures near 130°C and 175°C respectively. The depolarization currents were found to be reproducible and are representative of the molecular motions of polymer. The current peak at **P₂** had a peak maximum temperature (**T_{2max}**), that corresponded to the T_g obtained from the MDSC experiments for PVP K30. Similarly the **T_{2max}** of a specified polymer corresponded to respective T_g obtained from MDSC as seen in Table B-V-I. In addition, the current intensity was proportional to the applied electric voltage, indicating that the signal generated was indeed from the sample and not due to any mechanical or charge dissipation.

It was interesting to see that there was a difference of at least 30°C between the two depolarization peaks **P₁** and **P₂** for all molecular weights reported so far. The peak differences may indicate entirely different modes of molecular motion.

It is generally understood that the activation energy (E_{act}) for the relaxation of dipoles is not singular in nature and is a function of temperature [17]. Usually there is no significant difference between the activation energies for dipole relaxations that constitute a specific molecular motion e.g. side chain motion of a polymer, enthalpy relaxation, main chain

relaxation etc. In such cases, the E_{act} of different dipoles that constitute the overall relaxation overlaps to result in a continuous distribution as a function of temperature. The result is a single broad peak in the depolarization or the polarization current output. In the present case, however, a difference of at least 30°C was seen between two peaks indicating that molecular motions from entirely different domains exist. This can be explained further by noting that the dipolar side group – pyrrolidone can rotate locally through its C-N amide linkage, besides moving in union with the main chain. With increase in temperature, a ‘localized cooperative rotational relaxation motion’ of the pyrrolidone side group is possible and this may constitute the β - current peak (**P₁**). A β -relaxation peak has been reported for PVP samples containing 23% w/w water at – 60°C using dielectric analysis [18]. In a different study, PVP was shown to exhibit β -relaxation at approximately -73°C (MW 40 KDa) [19]. A similar explanation for β -relaxation peak was given in the case of polyester liquid crystalline polymer films, polycarbonate phenyl rotation, polystyrene phenyl rotation etc. [20].

The molecular motions of PVP that are believed to be due to the cooperative rotational motion of the side chains did not produce appreciable changes in the heat capacity and therefore remained undetected by MDSC. At higher temperature regions, the main chain motion results in the α - peak (**P₂**) that is characterized by the glass transition temperature by MDSC as well. Moreover, since the two dipole peaks are broad, they can be considered to occur from distribution of E_{act} of several side group and main-chain dipoles. We also observed that with an increase in the applied voltage, the intensity of polarization current increases at **P₁** and **P₂**. This phenomenon further indicated that the

peaks are indeed due to the molecular motions in the sample rather than resulting from dissipation of unknown trapped charges or any other mechanical stress.

Enthalpy relaxation measurements with MDSC and TSPC:

The protocol described in Fig. B-V-2 was followed to understand the structural relaxation behavior in PVP.

Enthalpy relaxation measurements using MDSC:

The non-reversing heat flow signals of different molecular weight grades of PVP that were aged at an aging temperature (T_a) of 15°C below the respective T_g is shown in Fig. B-V-5. An increase in the area under the non-reversing heat flow was observed with aging time for all the three polymers. As the sample was held isothermally at temperature below its T_g , it underwent structural relaxation process, which led to its densification. The increase in the area under the curve is due to the increasing magnitude of heat input that is necessary to overcome the densified state of the polymer and to reach the supercooled equilibrium state. In addition, the temperature of heat-flow maximum (T_{max}) shifts to higher values, indicating the need for higher energy of activation to mobilize the structurally relaxed segments of the polymer. These results are consistent with the results published by other groups [21]. The enthalpy recovery values were obtained by integrating the area under the curve and were plotted as a function of aging time (Fig. B-V-6). No significant differences were seen in the enthalpy recovery values for a corresponding aging time and temperature for the samples with different molecular weights.

Estimation of relaxation time constants:

From the enthalpy relaxation measurements, it appears that significant molecular mobility exists below the glass transition temperature. In order to compare the degree of molecular mobility between different polymers, it is necessary to calculate their relaxation time constants (τ). Relaxation time constants (τ) is the average time taken for one relaxation event. These constants can be calculated by fitting the enthalpy recovery data to stretched-exponential equation known as Kolrausch-William-Watts equation [22, 23] and obtaining adjustable relaxation time constants τ and β as follows:

$$\Phi_t = \exp\left(-\left(\frac{t}{\tau}\right)^\beta\right) \quad (1)$$

where Φ is a distribution function of different relaxation times occurring for a specific molecular relaxation process, t is the storage period, τ is the mean relaxation time constant and β is the relaxation time distribution parameter with a values between 0 and 1.

The relaxation distribution function can be obtained from the enthalpy recovery measurements by using the relationship:

$$\Phi_t = 1 - \left(\frac{\Delta H_t}{\Delta H_\infty}\right) \quad (2)$$

where Φ_t is the extent to which the material relaxes; ΔH_t is the experimentally measured enthalpy recovery and ΔH_∞ is the enthalpy recovery of a fully relaxed material. ΔH_∞ is calculated as:

$$\Delta H_x = (T_g - T)\Delta C_p \quad (3)$$

where T_g is the glass transition temperature, T is the experimental storage temperature and ΔC_p is the heat capacity step-change at the glass transition.

By rearranging and equating equation 1-3, an expression to estimate the relaxation time constant can be obtained as follows:

$$\Delta H_t = \Delta H_x \left(1 - \exp\left(-\left(\frac{t}{\tau}\right)^\beta\right) \right) \quad (4)$$

The experimental enthalpy recovery values were then fit to equation 4, using MicroMath[®] Scientist software (version 2.0) to obtain τ and β values (Table B-V-1). The initial values of τ and β were taken as 100 hours and 0.5 respectively as performed similarly elsewhere [24].

The empirical KWW function has been shown to describe the various relaxation processes of amorphous materials during enthalpy relaxation process [25]. However data interpretation should be done cautiously, because distribution of the relaxation time constants is as much important as the average relaxation time constants to access information pertaining to molecular mobility and associated stability. In Table B-V-II the average relaxation time constants along with their distribution have been reported for average of triplicate measurements for different molecular weight grade samples at different aging temperatures. A plot of logarithm of relaxation time constants (hr^{-1}) vs. ratio of T_g and storage temperature (T_a) is shown in Fig. B-V-7. As seen from the figure, mean relaxation times are non-exponential and decrease non-linearly with an increase in

storage temperature for all the polymers. This agrees with the literature findings for the non-linear dependency of relaxation time to temperature below the glass transition temperature [26]. Similarly a decrease in the mean relaxation time indicates an increase in the molecular mobility. Such a pattern is expected since the molecular mobility is known to increase with an increase in temperature. Further, the relaxation time constant for all the polymers tend to approach each other near the T_g .

Enthalpy relaxation measurements using TSPC:

Since the electric field was turned off in TSPC measurements during sample aging, a comparison of enthalpy relaxation measurements between the two techniques is valid. When the samples were heated following the protocol described in Fig. B-V-2, a series of relaxation process generate the electrical signal. In step 1 and 2, heating the samples to temperatures above T_g removes any electric and/ or mechanical stress, which otherwise would have produced noise peaks in TSC analysis. Also the thermal history of the samples was erased in steps 1 and 2 to generate 'fresh' amorphous samples. In step 3, the samples were stored at very low temperatures, and hence the dipoles were kinetically frozen. The mean relaxation time (τ) (i.e. average time taken for one molecular motion to occur) is very large at low temperatures and thereby no molecular mobility and hence polarization current was generated. As the samples were heated in step 4, the relaxation time of the dipoles decreases, and at a given temperature domain, the rate of molecular relaxation matches the experimental time scales thus producing polarization current. The temperature where the polymer main chain exhibits maximum mobility (i.e. peak

polarization current) is the glass transition temperature. In step 5, beyond the glass transition temperature, the average relaxation time of the molecules exceeds the heating rate and the motion of dipoles cancel out. The net current thereby lowers and eventually decays to the baseline.

The TSPC scans of PVP K17 and PVP K30 that were aged at 15°C below their respective T_g for a period of up to 8 hours are shown in Fig. B-V-8. The TSPC scan demonstrates two distinct global relaxation peaks analogous to the TSDC scans except for the negative sign. As a trend, for either polymers, the peak area at P1 decreased in magnitude whereas the peak area at P2 increase with aging time. However, the total area under the peaks at P₁ and P₂ remained constant.

Polarization current at P₁ and P₂:

The reduction in the area of current at P₁ was observed in case of all different molecular weight grades of PVP. Since the aging temperature (T_a) was always greater than the temperature domain corresponding to P₁, the dipoles responsible for producing current at P₁ could always be considered to be in a state of sufficient mobility so that aging does not influence them. Hence one would expect no change in their polarization current intensity with aging time, when compared to that of a freshly prepared amorphous sample. However a decrease in the polarization current peak suggesting a progressive decrease in the molecular mobility of dipoles was observed. An explanation to such behavior could be the possible entrapment of side chains of the polymer with the main chain upon

densification. Upon subsequent heating of sample at the end of aging, cooperative molecular motions between the molecular side chains and the main chain could possibly explain the reduced mobility and hence polarization current. When the samples are heated above their T_g , the main chain and side chains are free of conformational restrictions and could be considered 'fresh'.

The area under the polarization current peak at P_2 was seen to increase with aging period unlike the peak at P_1 . Also an increase in T_{max} (i.e. temperature corresponding to peak maximum intensity) at P_2 was seen as function of aging time (Figure B-V-8). The increase in the area under signal at P_2 is analogous to the increase in the enthalpy relaxation endotherm that is obtained at T_g from MDSC measurement. Since the aging temperature is below the temperature domain corresponding to P_2 , as the sample ages, it undergoes structural relaxation to attain the equilibrium state. The density of sample increases with an associated decrease in the free-volume. When the sample is reheated, the densified molecules regain their super-cooled state at their T_g . During this process, an increase in the molecular mobility, most likely due to a "burst effect", causes an increase the area of current at P_2 . This increase in the area at P_2 was found proportional to the aging time.

Polarization current peak cleaning (P_1):

Based on the data generated so far it was not possible to obtain the enthalpy relaxation due to aging at the T_g , primarily due to interference from peak P_1 . Therefore the

polarization peak at P₁ was 'removed' by modifying the experimental protocol. The modified protocol is shown in Fig. B-V-9. As seen from the protocol, a polarization step for (T_p) 15 min. was added at the end of each aging period (step 6) to polarize the dipoles responsible for peak P₁. Since the samples were rapidly cooled (step 7) in the presence of electric field, the now polarized dipoles responsible for P₁ remained in a frozen polarized state. Upon subsequent heating, the polarized dipoles would not produce any significant polarization current in the presence of electric field and the motion of main chain alone could be characterized.

Following this protocol, the modified TSPC plots of PVP samples after aging for periods up to 8 hours are shown in Fig. B-V-10. No polarization current peak at P₁ was seen in these scans when compared with TSPC plots in Fig. B-V-8. Favorably, the area under the polarization current peak at P₂ could now be integrated. This area when subtracted from the area of polarization current due to freshly prepared amorphous sample provided the cumulative molecular mobility of all the dipoles that underwent enthalpy recovery.

Correlation of TSPC and MDSC results to estimate molecular mobility:

Plots of cumulative normalized area of PVP samples after aging for a period up to 8 hrs following modified TSPC method are shown in Fig. B-V-11. Similar to the MDSC experiments, an initial increase in the polarization current followed by a plateau in the cumulative area under the peak at P₂ was observed with the TSPC (modified) experiments. This indicated that the heat flow involving and non- heat flow involving techniques characterize the same phenomenon however in a different fashion. In MDSC

experiments, the heat input that is necessary to bring the structurally relaxed state of material to its super cooled state is measured. Whereas in TSPC, the molecular mobility generated when the structurally relaxed material regains its equilibrium state is obtained from the polarization current. Therefore, the two techniques correlate in principle. In order to investigate if the experimental results correlated a plot of the net current generated at peak P₁ of structurally relaxed material and the enthalpy of recovery of the material that were aged for the same duration at a given aging temperature was constructed (Fig. B-V-8). An empirical linear relationship was observed between the data generated from the enthalpy recovery (MDSC) and the molecular mobility recovery (TSPC) techniques.

The slope of the linear line should then represent the rate of enthalpy relaxation, which indicates the extent of molecular mobility. Therefore, the relative extent of molecular mobility of a polymer at a specified storage temperature below its respective glass transition temperature could be obtained. From Fig. B-V-8, the slope of linear equation for the polymer samples decreases in the order PVP K17 > PVP K90 > PVP K30. This suggests that the molecular mobility is highest for PVP K17 (M_w ~ 10 KDa ± ~5KDa) and least for PVP K30 (M_w ~ 58 KDa ± ~5KDa). Although it is intuitive to expect a decrease in the molecular mobility between PVP K17 and PVP K90 (M_w ~ 130KDa ± ~5KDa), due to a reduction in the molecular weight, it is counter-intuitive to expect PVP K90 to have higher degree of mobility when compared to PVP K30. The mean relaxation time data (Fig. B-V-5) also suggest the rank order for decrease in the molecular mobility as PVP K17 > PVP K90 > PVP K30, which agrees with TSPC results. It is not

completely clear as to why there is such a trend in the results. One possible explanation for such a behavior could be the heat capacity step-change (ΔC_p) at the T_g for the polymer, which is the indicator of the non-equilibrium state of the amorphous phase with reference to its extrapolated supercooled liquid state (Fig. B-V-1). A larger heat capacity step-change (ΔC_p) at T_g would imply a greater driving force for the sample to reach equilibrium and hence a greater degree of molecular mobility. The higher (ΔC_p) values for PVP K90 when compared to PVP K30, could possibly explain for the higher degree of mobility in the former. However, there seems to be a balance between the two factors of molecular weight and heat capacity change at T_g , since although the (ΔC_p) values for PVP K90 is greater than PVP K17, the large differences in their molecular weights could potentially guide the extent of molecular mobility.

CONCLUSIONS

In this study, we have estimated the relative extent of molecular mobility as a function of molecular weights for three different grades of PVP. Two analytical instruments which measure on different principles, one that involves heat-flow measurements and the other that involves a direct measurement of molecular motions, were compared.

MDSC was used to perform enthalpy relaxation measurements to gain insight into the extent of molecular mobility of PVP at different aging temperatures immediately below their respective glass transition temperatures. The mean relaxation time constants were obtained by fitting the experimental results to the William-Watts equation using non-

linear regression analysis. The mean relaxation time decreased, indicating an increase in the molecular mobility, as the storage temperature was approaching the T_g .

TSC measurements revealed presence of two different global relaxation peaks in the polymer. The peak at lower temperatures was considered as the sub-glass transition peak due to the motions of the side-chain of the polymer. The intensity of current at T_g increased in proportion with aging of the samples analogous to the MDSC results. A linear empirical relation was established between the enthalpy recovery measurements (MDSC) and the molecular mobility recovery experiments (TSPC). To conclude, TSC can be used as a sensitive complimentary tool to characterize the molecular mobility of drug substance, polymers and their solid dispersions.

ACKNOWLEDGMENTS

This study is a part of Ph.D. research of Mr. Vasanthavada who is a Novartis Graduate Research Fellow and has conducted his research at Novartis R&D facility. He wishes to acknowledge the fellowship and also thank Dr. Zeren Wang, presently at Boehringer Ingelheim, for his helpful discussions.

REFERENCES

1. A. Wade, and P. J. Weller. *Handbook of pharmaceutical excipients. Second edition.* The Pharmaceutical Press, London. 1994.
2. T. W. Lee, and J. R. Robinson. Controlled-release drug delivery systems. In *Remington. The science and practice of pharmacy, 20th edition.* Lippincott Williams and Wilkins, Maryland. 903-929.
3. A. P. Simonelli, S. C. Mehta, and W. I. Higuchi. Dissolution rates of high energy polyvinylpyrrolidone(PVP)-sulfathiazole co precipitates. *Journal of Pharmaceutical Sciences.* 58:538-549 (1969).
4. G. M. Khan, and Z. Jiabi. Preparation, characterization and dissolution of ibuprofen solid dispersions using polyethylene glycol (PEG), talc, and PEG-talc as dispersion carriers. *Drug development and Industrial Pharmacy.* 24:455-462 (1998).
5. K. P. R. Chowdary, and P. V. Rao. Evaluation of some modified starches as carriers for solid dispersions. *Indian Drugs.* 29:224-227 (1991).
6. M. Yoshioka, B. C. Hancock, and G. Zografi. Inhibition of indomethacin crystallization in poly(vinylpyrrolidone) coprecipitates. *Journal of Pharmaceutical Sciences* 84:983-986 (1995).
7. T. Matsumoto, and G. Zografi. Physical properties of solid molecular dispersions of indomethacin with poly(vinylpyrrolidone) and poly(vinylpyrrolidone-co-vinylacetate) in relation to indomethacin crystallization. *Pharmaceutical Research* 16:1722-1728 (1999).
8. C. A. Angell. Formation of glasses from liquids and biopolymers. *Science.* 267:1924-1935 (1995).
9. P. H. Poole, T. Grande, C. A. Angell, and P. F. McMillan. Polymorphic phase transitions in liquids and glasses. *Science.* 275:322-323 (1997).

10. H. Sasabe, and C. T. Moynihan. Structural relaxation in poly(vinylacetate). *Journal of Polymer Science: Polymer Physics Edition*. 16:1447-1457 (1978).
11. J. M. G. Cowie, S. Harris, and I. J. McEwen. Physical ageing in poly(vinylacetate) I. enthalpy relaxation. *Journal of Polymer Sciences B: Polymer Physics* 35:1107-1116 (1997).
12. S. L. Shamblin, and G. Zografi. Enthalpy relaxation in binary amorphous mixtures containing sucrose. *Pharmaceutical research*. 15:1828-1834 (1998).
13. S. P. Duddu, and T. D. Sokoloski. Dielectric analysis in the characterization of amorphous pharmaceutical solids. I. Molecular mobility in poly(vinylpyrrolidone)-water systems in the glassy state. *Journal of Pharmaceutical Sciences*. **84**:773-776 (1995).
14. V. Andronis, and G. Zografi. Molecular mobility of supercooled amorphous indomethacin, determined by dynamic mechanical analysis. *Pharmaceutical Research*. 14:410-414 (1997).
15. C. A. Oksanen, and G. Zografi/ Molecular mobility in mixtures of absorbed water and solid poly(vinylpyrrolidone). *Pharmaceutical Research*. 10:791-799 (1993).
16. Y. Aso, S. Yoshioka and S. Kojima. Explanation of the crystallization rate of amorphous nifedipine and Phenobarbital from their molecular mobility as measured by ¹³C nuclear magnetic resonance relaxation time and the relaxation time obtained from the heating rate dependence of the glass transition temperature. *Journal of Pharmaceutical Sciences*. 90:798-806 (2001).
17. L. Goitiandia, and A. Alegria. Physical aging of poly(vinylacetate). A thermally stimulated depolarization current investigation. *Journal of Non-Crystalline Solids*. 287:237-241 (2001).
18. S. P. Duddu, and T. D. Sokoloski. Dielectric analysis in the characterization of amorphous pharmaceutical solids. I. Molecular mobility in poly(vinylpyrrolidone)-

- water systems in the glassy state. *Journal of Pharmaceutical Sciences*. **84**:773-776 (1995).
19. S. K. Jain, and G. P. Johari. *Journal of Physical Chemistry*. **92**:5851-5854 (1988).
 20. G. Collins and B. Long. A thermally stimulated current/relaxation map analysis of the relaxation process in aromatic polyester, liquid crystal polymer film. *Journal of Applied Polymer Science*. **53**:587-608 (1994).
 21. B. C. Hancock, S. L. Shamblin, and G. Zografi. Molecular mobility of amorphous pharmaceutical solids below their glass transition temperatures. *Pharmaceutical Research*. **12**:799-806 (1995).
 22. S. Montserrat. Physical aging studies in epoxy resins. 1. Kinetics of the enthalpy relaxation process in a fully cured epoxy resin. *Journal of Polymer Science (Polymer Physics Edition)* **32**:509-522 (1994).
 23. G. Williams and D. C. Watts. Non-symmetrical dielectric relaxation behavior arising from a simple empirical decay function. *Transactions in Faraday Society*. **66**:80-85 (1970).
 24. B. C. Hancock, S. L. Shamblin, and G. Zografi. Molecular mobility of amorphous pharmaceutical solids below their glass transition temperatures. *Pharmaceutical Research*. **12**:799-806 (1995).
 25. S. L. Shamblin, B. C. Hancock, Y. Dupuis, and M. J. Pikal. Interpretation of relaxation time constants for amorphous pharmaceutical systems. *Journal of Pharmaceutical Sciences*. **89**:417-427 (2000).
 26. S. L. Shamblin, B. C. Hancock, Y. Dupuis, and M. J. Pikal. Interpretation of relaxation time constants for amorphous pharmaceutical systems. *Journal of Pharmaceutical Sciences*. **89**:417-427 (2000).

Table B-V-I: Characterization of relaxation temperatures in PVP

Polymer	T _g (°C)		Sub-T _g (°C)		Δ C _p at T _g (J/g/°C) (x 10)
	MDSC	TSC	MDSC	TSC	
PVP K17	117 ± 0.6	138-141	N/D*	80-85	2.560 ± 0.22
PVP K30	165 ± 0.7	175-179	N/D*	130-135	2.658 ± 0.017
PVP K90	176 ± 0.4	178-182	N/D*	140-145	2.818 ± 0.058

* Not Detected

Table B-V-II: Average relaxation time constants obtained from enthalpy relaxation measurements

Super-cooling	Polymer	Average relaxation time constant (τ)	Distribution parameter of relaxation time (β)	ΔH_{∞} (J/g)
T _g -5°C	PVP K17	9.8008	0.37724	1.28
	PVP K30	10.2705	0.3943	1.2911
	PVP K90	12.192	0.18899	1.3885
T _g -15°C	PVP K17	25.879	0.33294	3.8400
	PVP K30	57.660	0.23877	3.8733
	PVP K90	12.704	0.42671	4.1655
T _g -30°C	PVP K17	443.59	0.39169	7.6800
	PVP K30	2473.0	0.39514	7.7466
	PVP K90	829.00	0.42273	8.331

Figure B-V-1

Schematic representation of the glass transition temperature (T_g) and loss in enthalpy during aging studies

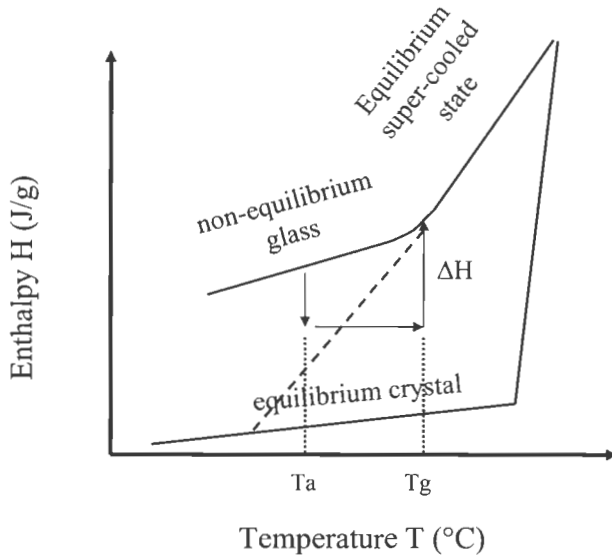


Figure B-V-2

Experimental protocol for conducting enthalpy relaxation (MDSC) and mobility recovery (TSPC) experiments. The bold lines indicate zones where the data are recorded. For TSPC measurements, the electric field is turned on during this period. The dotted line is the T_g of the polymer. T_o is the initial temperature (150°C below T_g); T_a is the aging temperature (varies from 5° to 30°C below T_g); and T_f is the final temperature (15°-20°C above the T_g). The significance of numbers is provided in the text.

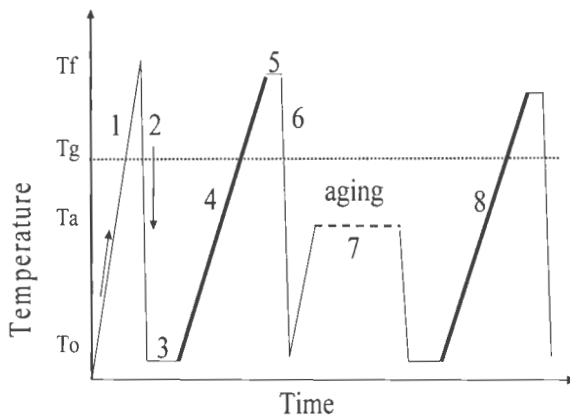


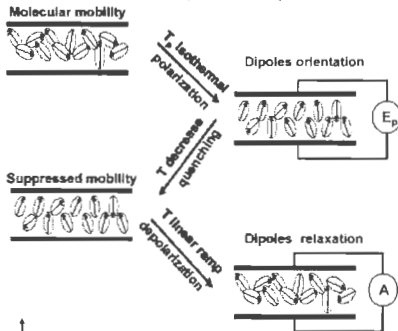
Figure B-V-3

(a) Schematic demonstration of the principle of Thermally Stimulated Currents. Reproduced from www.setaram.com (b) Schematic demonstration of the glass transition phenomenon in typical thermally stimulated depolarization current experiment.

(a)

Origin of TSC Phenomena

The motion of the dipoles as they relax produces a depolarization current that is detected by the TSC-RMA instrument ($\bullet 10^{-15}$ Amp)



(b)

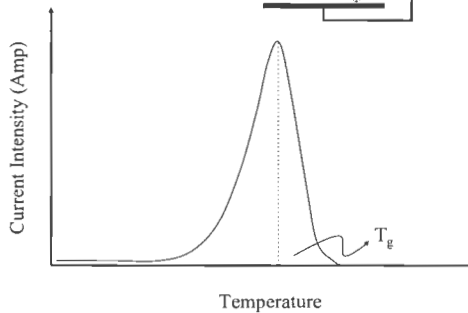


Figure B-V-4.a

(a) MDSC heat capacity scans of PVP demonstrating the T_g and the heat-capacity step change at T_g . A single T_g is noticed for all the three molecular weight grades of PVP.

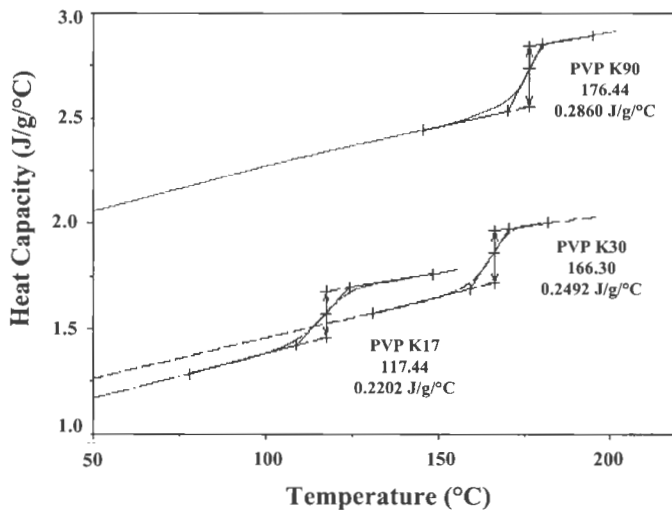


Figure B-V-4.b

(b) Thermally Stimulated Depolarization Currents of PVP K30 demonstrating two different global relaxation peaks: P_1 and P_2 .

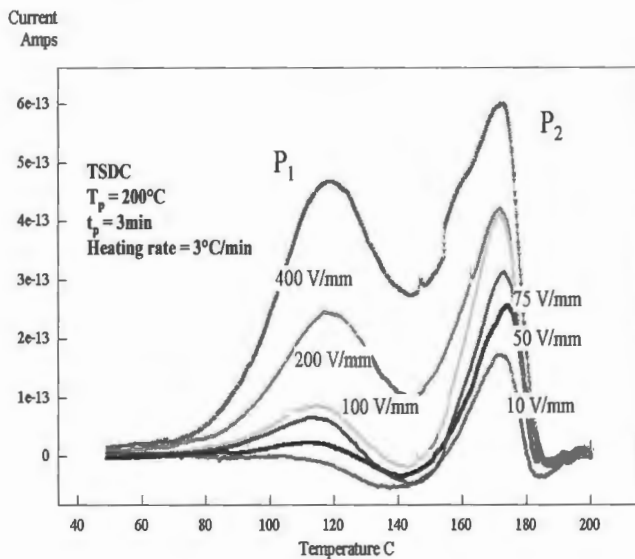


Figure B-V-5.a

MDSC non-reversing heat flow scans demonstrating the enthalpy relaxation of PVP with storage time at 15°C below the respective T_g ; for PVP K17;

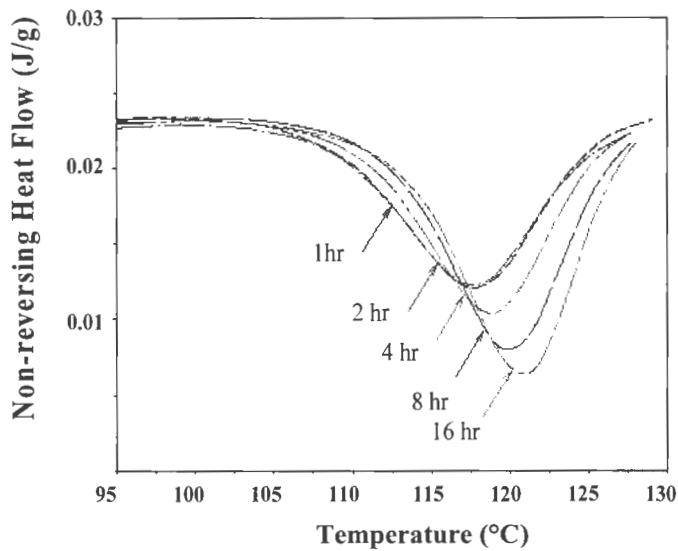


Figure B-V-5.b

MDSC non-reversing heat flow scans demonstrating the enthalpy relaxation of PVP with storage time at 15°C below the respective T_g ; for PVP K30;

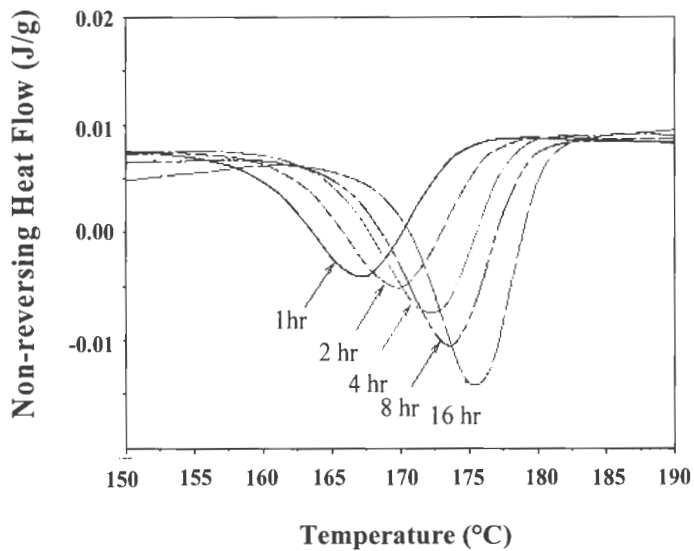


Figure B-V-5.c

MDSC non-reversing heat flow scans demonstrating the enthalpy relaxation of PVP with storage time at 15°C below the respective T_g ; for PVP K90;

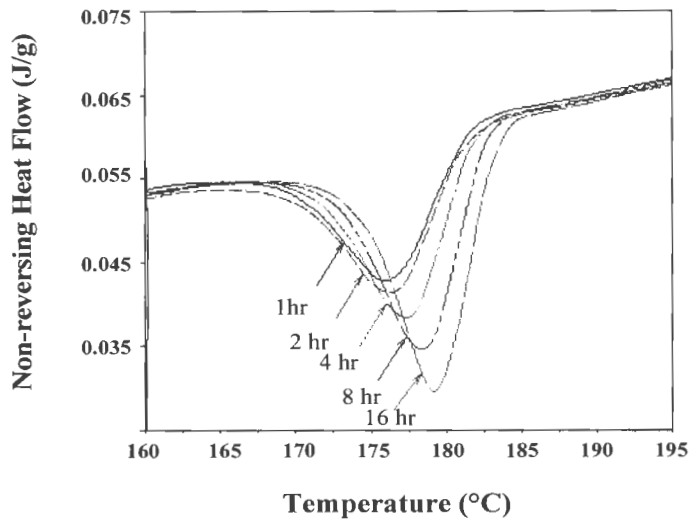


Figure B-V-6

Enthalpy relaxation of PVP obtained using MDSC with storage time at 15°C below the respective T_g. (a) PVP K17; (b) PVP K30; and (c) PVP K90

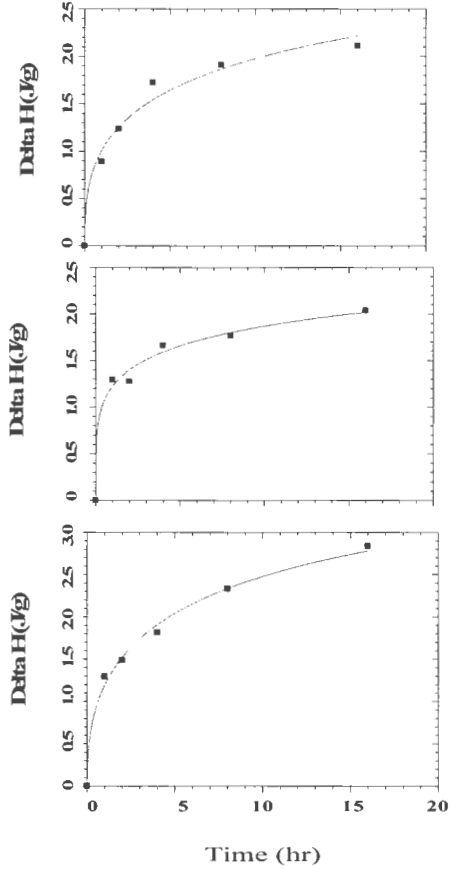


Figure B-V-7

Variation of logarithm of relaxation time constant (τ) with scaled temperature T_g/T_a , obtained using fitting the enthalpy relaxation data to the empirical KWW stretched non-exponential equation. \blacktriangle PVP K17; \bullet PVP K30; and \blacksquare PVP K90.

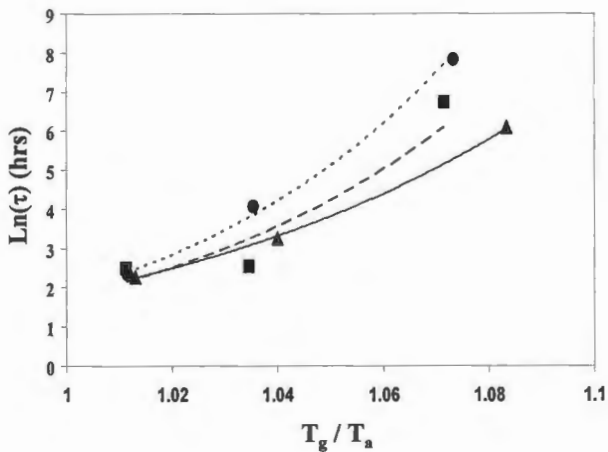


Figure B-V-8

Thermally stimulated polarization currents of (a) PVP K17; and (b) PVP K30 undergoing structural relaxation at $T_g-15^\circ\text{C}$. With storage time, the sub- T_g peak decreases in its area while the T_g peak increases for both the polymers.

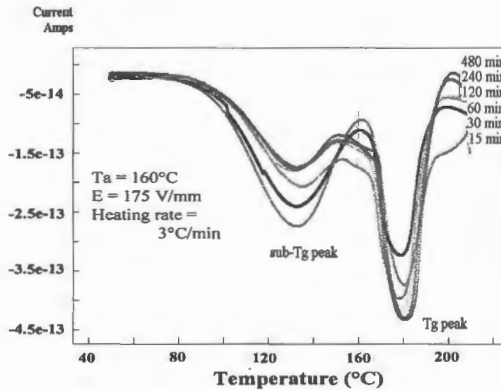
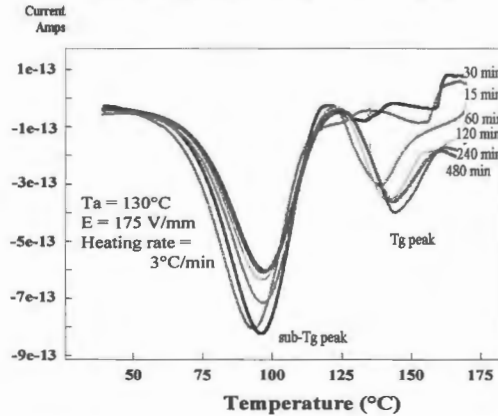


Figure B-V-9

Modified experimental protocol for structural relaxation of thermally stimulated polarization currents. An additional isothermal step # 6 for 15 min. is added at the end of aging period with the electric field turned ON.

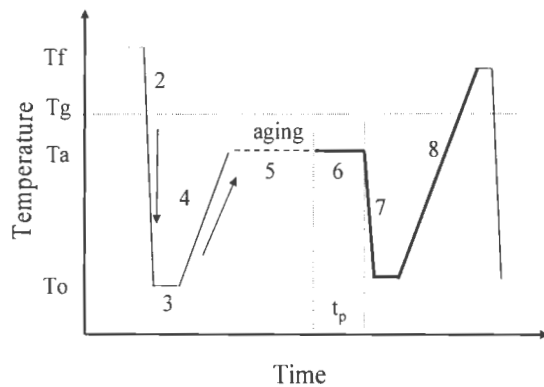


Figure B-V-10.a

Thermally stimulated polarization currents following the modified experimental protocol for PVP K17 that was aged at $T_g-15^\circ\text{C}$. Using the modified protocol, the sub- T_g peak is not produced (compare with Fig. B-V-8).

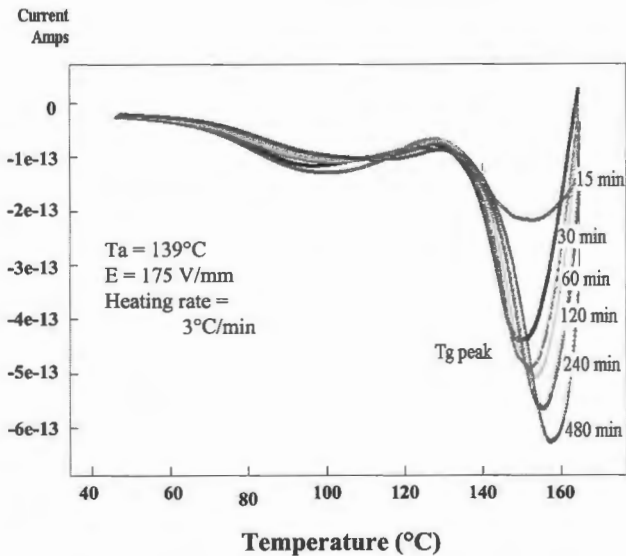


Figure B-V-10.b

Thermally stimulated polarization currents following the modified experimental protocol for PVP K30 that was aged at $T_g-15^\circ\text{C}$. Using the modified protocol, the sub- T_g peak current peak is not produced (compare with Fig. B-V-8).

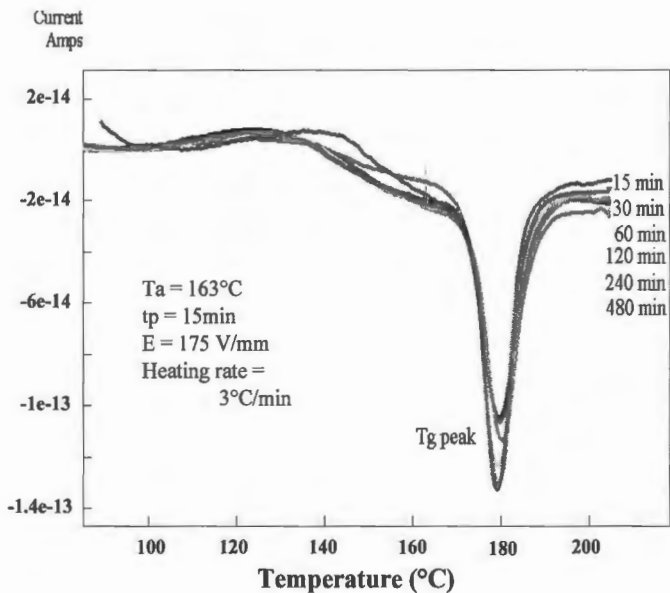


Figure B-V-10.c

Thermally stimulated polarization currents following the modified experimental protocol for PVP K90 that was aged at $T_g-15^\circ\text{C}$. Using the modified protocol, the sub- T_g peak is not produced (compare with Fig. B-V-8).

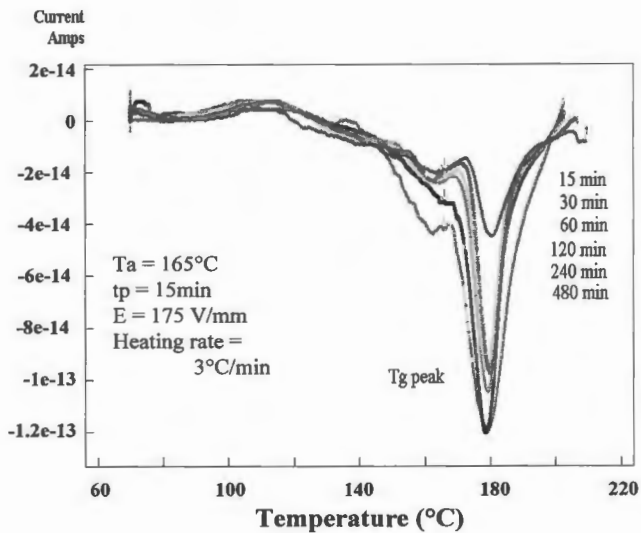


Figure B-V-11

Net current (i.e. difference in the area under current at T_g peak of structurally relaxed sample and fresh sample) plotted against the storage time for PVP aged at respective T_g-15°C. (a) ▲ PVP K17; (b) ■ PVP K30; and (c) ● PVP K90.

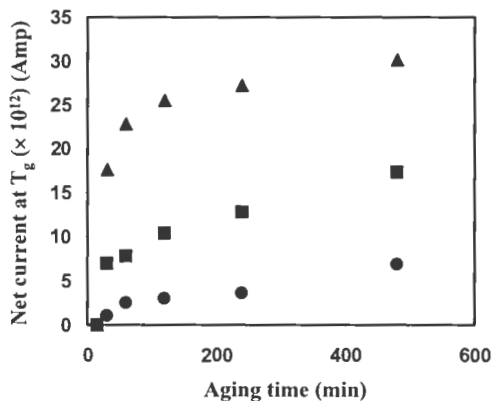
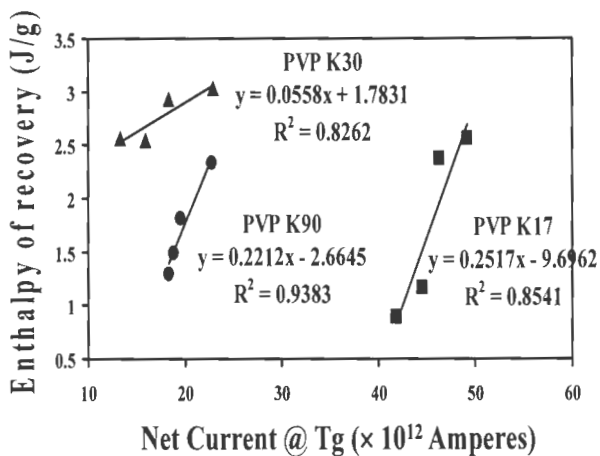


Figure B-V-12

Relationship between the enthalpy recovery measurements from MDSC and mobility recovery measurements from modified TSPC. The slope of line is indicative of relative rate of relaxation and hence molecular mobility.



SECTION C

APPENDIX A

Principles of Modulated Differential Scanning Calorimeter

Differential Scanning Calorimeter (DSC):

The principle of DSC is to heat the sample and reference pan at a linear rate and measure the heat flow absorbed by the sample (endothermic) or liberated from the sample (exothermic) when it undergoes a physical or chemical transformation. Thermal events like melting, glass transition, enthalpy relaxation and dehydration are some of the endothermic events; whereas recrystallization and most decomposition are part of exothermic processes. The heat flow differences between the sample and empty pan are accurately measured (expressed in mW) and are used to quantify the magnitude of transformation.

One of the limitations of DSC is the difficulty in interpreting the heat flow if multiple processes are involved over the same temperature range. For instance, a moisture removal and glass transition processes can occur between 60° - 100°C, and hence it is not possible to resolve the two signals. The sensitivity of the experiment can however be improved by decreasing the sample mass or heating rate; whereas the resolution to separate transitions

can be increased by increasing the sample mass or heating rate. Therefore to obtain a balance between the sensitivity and resolution is challenging.

Modulated Differential Scanning Calorimeter (DSC):

Modulated Differential Scanning Calorimeter (MDSC, trade mark of TA Instruments Inc.,) has developed a technique that heats the sample by applying sine wave modulations to an underlying standard linear heating rate. By choosing a suitable modulation parameter that includes an amplitude and period of oscillation, complex heat flow processes can be resolved with greater sensitivity. The heat flow data is deconvoluted into reversing and non-reversing heat flow signals using a discrete Fourier Transform algorithm [1]. The reversing heat flow involves transformations like glass transition phenomenon, melting, and dehydration whereas the non-reversing heat flow signal detects enthalpy relaxation, recrystallization, moisture loss, and decomposition. The other advantages of MDSC include the measurement of heat capacity and heat flow in a single experiment; separation of complex transitions into more easily interpreted components and increased sensitivity and resolution for detection of weak transitions with accuracy for measurement of crystallinity and amorphous contents.

Principles of Operation:

In DSC, the differential heat flow or heat flux is expressed using the thermal equivalent of Ohm's Law as:

$$\frac{dQ}{dt} = \frac{\Delta T}{R_D} \quad (1)$$

where $\frac{dQ}{dt}$ = heat flow

ΔT = temperature difference between the reference and sample

R_D = thermal resistance of constantan disc

In MDSC, the same heat flux is modified using sinusoidal temperature oscillation. The heating rate is dependent upon three experimental variables: underlying heating rate, the amplitude of modulation and the period (frequency) of modulation.

A different way of expressing equation 1 is as follows:

$$\frac{dQ}{dt} = C_p \left(\frac{dT}{dt} \right) + f(t, T) \quad (2)$$

where $\frac{dQ}{dt}$ = heat flow

$\frac{dT}{dt}$ = heating rate

C_p = thermodynamic heat capacity

t = time; T = absolute temperature

$f(t, T)$ = function of time and temperature which governs the calorimetric response of kinetically controlled chemical or physical phenomenon.

In equation 2, the heat capacity term is expressed as the reversing heat flow and the kinetic events are expressed as the non-reversing heat flow.

Discrete Fourier Transformation [2] is used to deconvolute the heat flow signals as follows:

$$C_p = K_{C_p} * \left(\frac{Q_{amp}}{T_{amp}} \right) * \left(\frac{Period}{2\pi} \right)$$

where C_p = Heat capacity (J/g/°C)

K_{C_p} = Heat capacity calibration constant

Q_{amp} = Heat flow amplitude (mW)

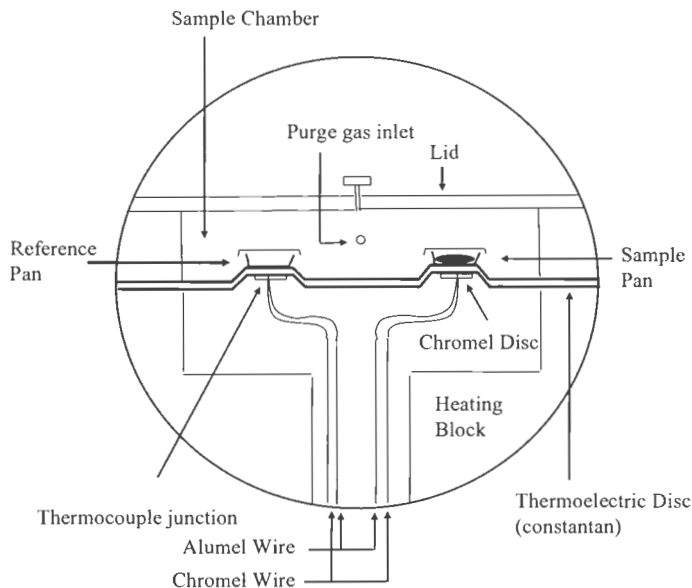
T_{amp} = Temperature amplitude (°C)

Period = Modulation period (sec).

The heat capacity term multiplied by underlying heating rate gives the reversing heat flow. The non-reversing heat flow is obtained from the difference between the total heat flow and the reversing heat flow signals.

Figure A-1

A schematic of the cross-section of a typical MDSC sample cell is reproduced from the operating manual TA Instruments for Modulated DSC.



REFERENCES

1. M. Reading, A. Luget and R. Wilson. Modulated differential scanning calorimetry. *Thermochimica Acta*. 238:295-307 (1994)
2. W. H. Press, B. P. Flannery, S. A. Teukolsky, and W. T. Vetterling. Numerical recipes. The art of scientific computing. Cambridge University Press, Cambridge, pp. 386-390 (1986).

APPENDIX B

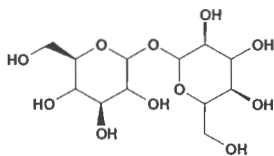
Phase Behavior of Amorphous Molecular Dispersions: Determination of the Degree and Mechanism of Solid Miscibility

(Supporting data to chapter I)

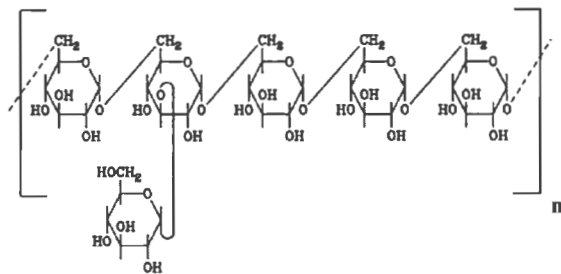
Figure B-1

Chemical structures of (a) Trehalose; (b) Dextran and (c) PVP

(a)



(b)



(c)

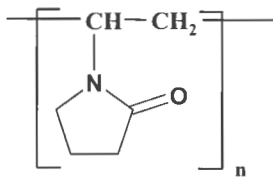


Figure B-2

(a) X-ray diffraction patterns of trehalose dihydrate untreated and lyophilized. Lyophilized trehalose is rendered amorphous. (b) X-ray diffraction patterns of lyophilized dextran and solid dispersions of dextran containing 50% and 90%w/w trehalose showing their amorphous nature.

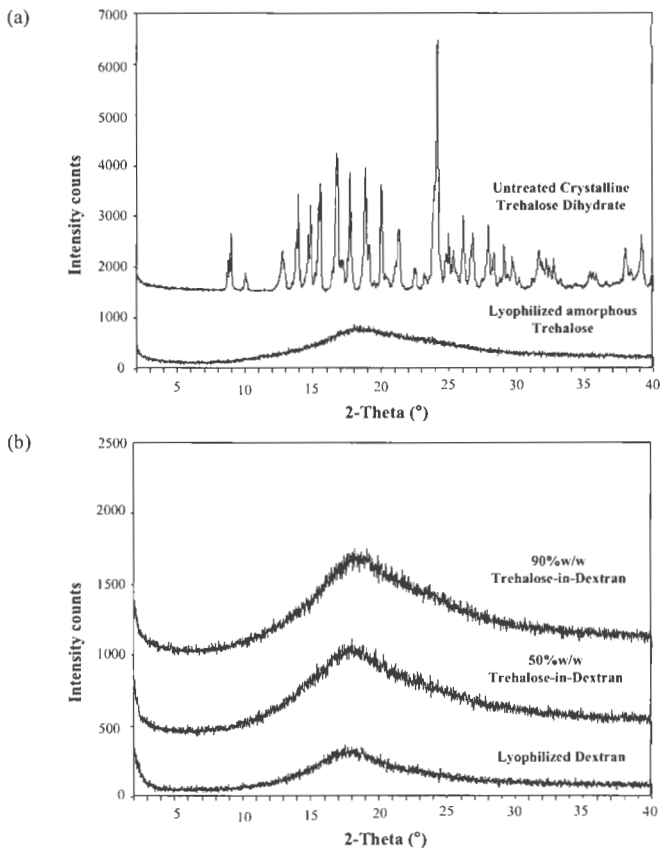


Figure B-3

Moisture sorption and de-sorption profile of trehalose at 25°C [sorption (O); de-sorption (○)]. The sudden change in the rate of moisture uptake of trehalose at relative humidity greater than 45% indicates the crystallization. Recrystallized trehalose is very stable even at 5%RH since no significant weight loss is observed in the de-sorption profile.

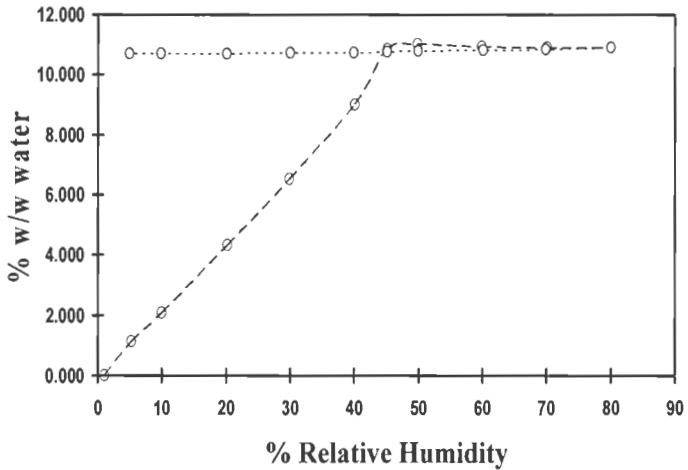


Figure B-4

Reproducibility MDSC reversing heat flow of 40%w/w trehalose-in-dextran showing the phase separation and crystallization of trehalose 4 days storage at 50°C / 75%RH

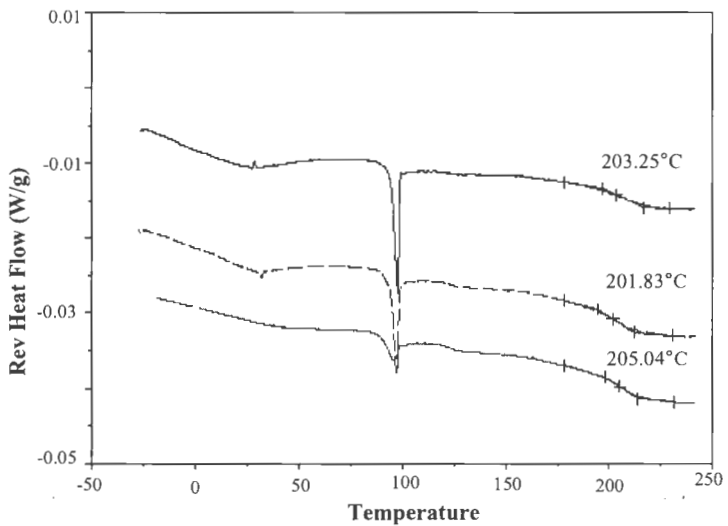


Figure B-4

Reproducibility MDSC reversing heat flow of 40%w/w trehalose-in-dextran showing the phase separation and crystallization of trehalose 13 days storage at 50°C / 75%RH

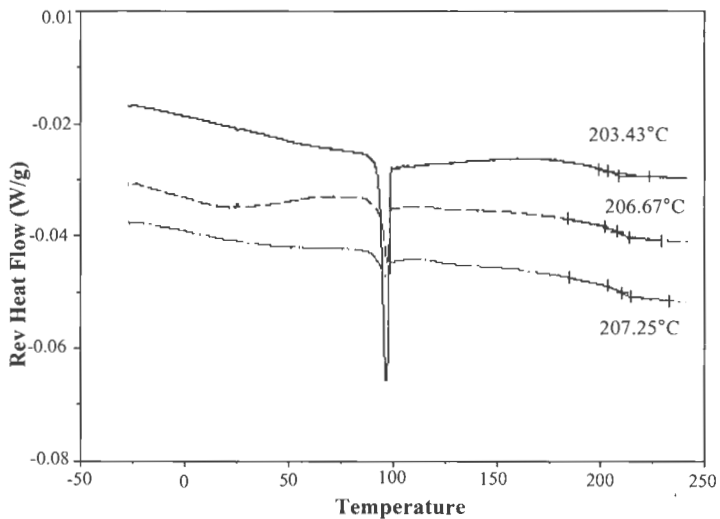


Figure B-5

Reproducibility MDSC reversing heat flow of 40%w/w trehalose-in-dextran showing the phase separation and crystallization of trehalose 23 days storage at 50°C / 75%RH

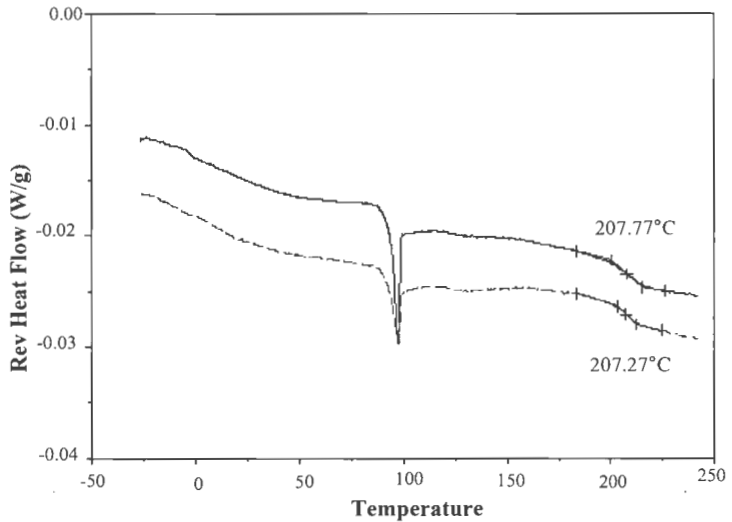


Figure B-6

Reproducibility MDSC reversing heat flow of 40%w/w trehalose-in-dextran showing the phase separation and crystallization of trehalose 34 days storage at 50°C / 75%RH

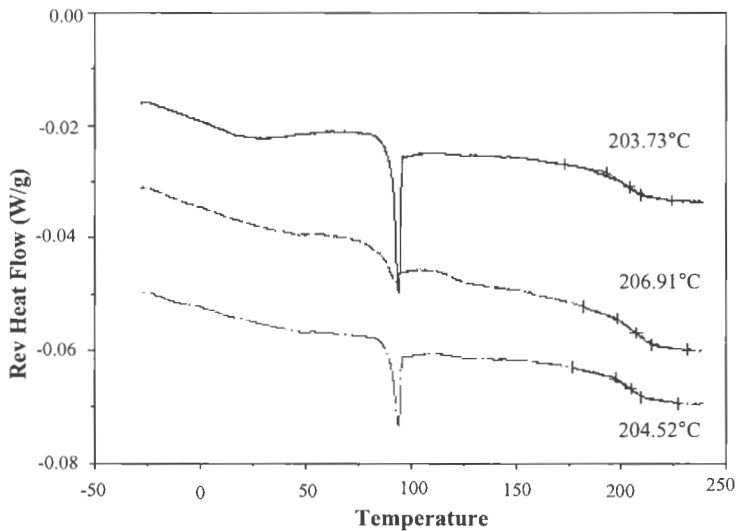


Figure B-7

MDSC reversing heat flow of 40%w/w trehalose-in-dextran showing the phase separation and crystallization of trehalose stored at 23°C / 75%RH

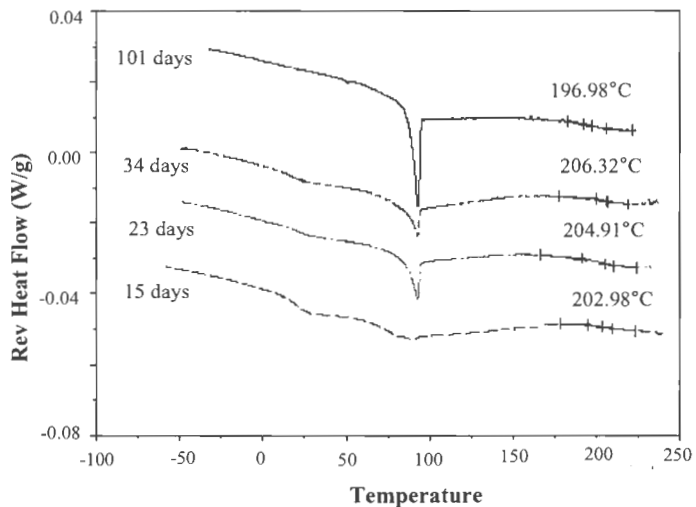


Figure B-8

MDSC total heat flow of 40%w/w trehalose-in-dextran showing the plasticized T_g and crystallization of trehalose when stored at 40°C / 75%RH

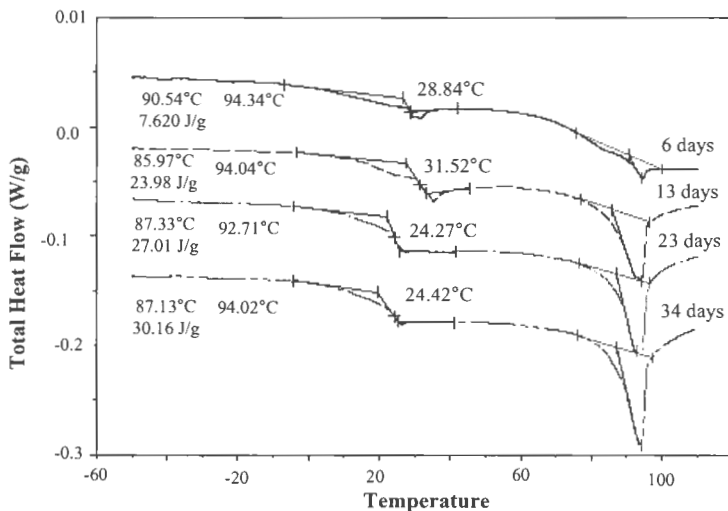


Figure B-9

MDSC reversing heat flow of 30%w/w trehalose-in-dextran showing the phase separation and crystallization of trehalose stored at 40°C / 75%RH

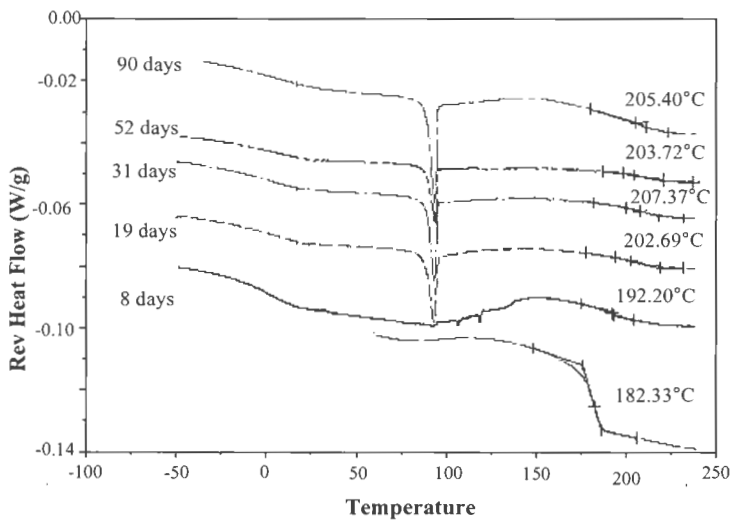


Figure B-10

MDSC total heat flow of 30%w/w trehalose-in-dextran showing the plasticized T_g and crystallization of trehalose when stored at 40°C / 75%RH

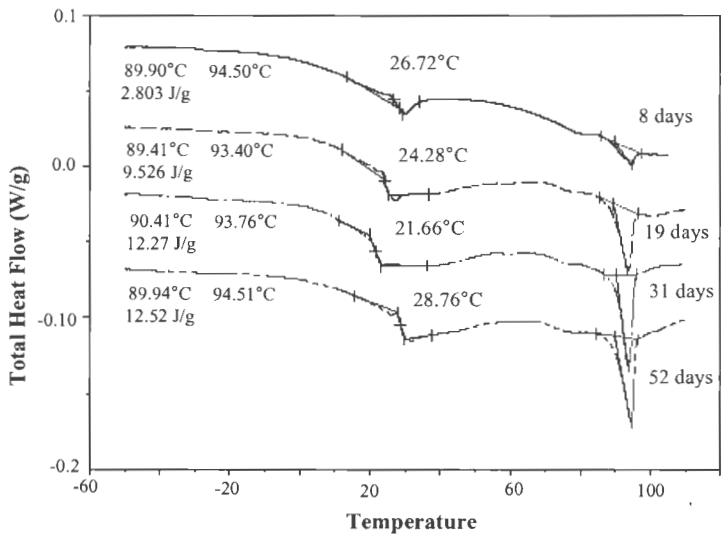


Figure B-11

MDSO total heat flow of 30%w/w trehalose-in-dextran showing the plasticized T_g and crystallization of trehalose when stored at 50°C / 75%RH

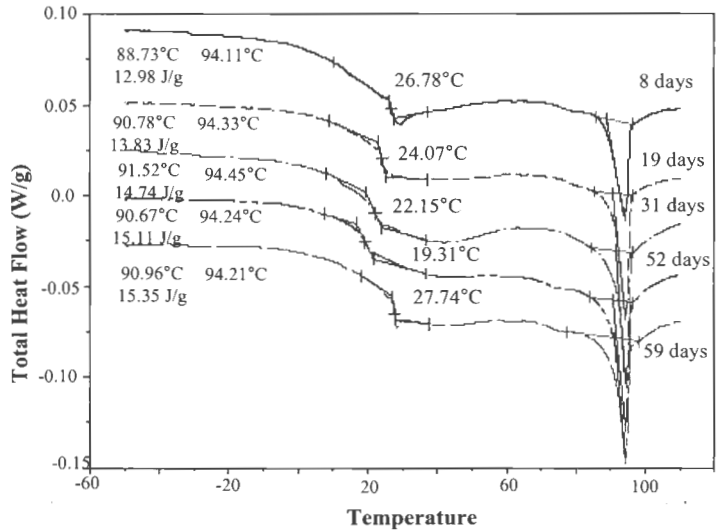


Figure B-12

MDSC reversing heat flow scans of physical mixture (1:1) of amorphous trehalose and dextran showing that liquefied trehalose does not plasticize dextran by mixing with it during heating at 1°C/min.

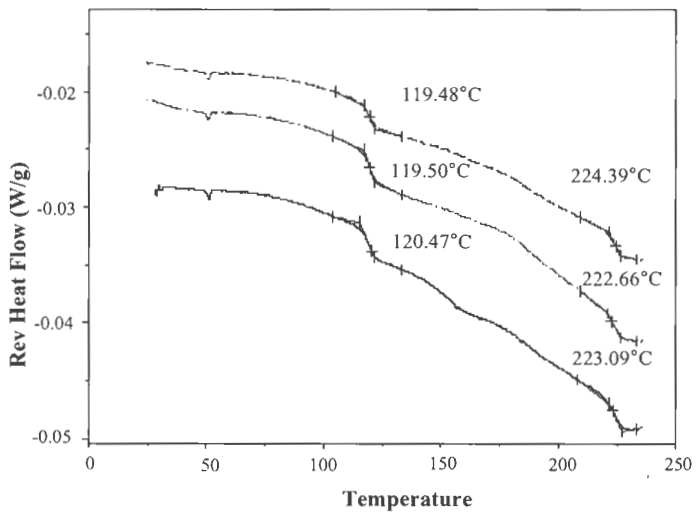
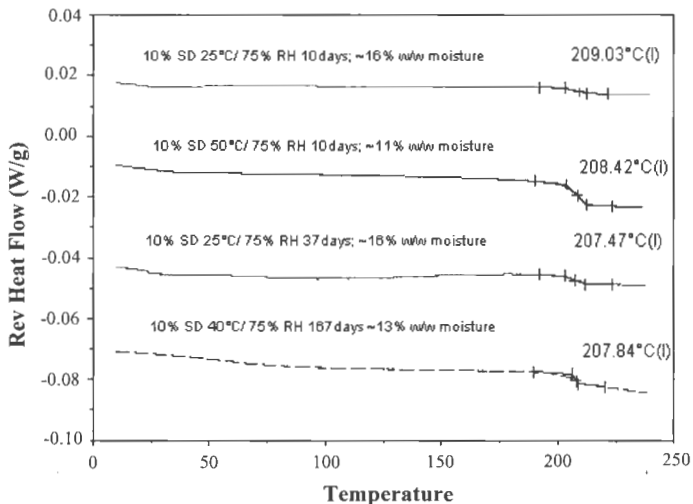


Figure B-13

MDSC reversing heat flow scans of 10%w/w trehalose-in-dextran solid dispersions prepared below the solid solubility limit. Physical stability is observed by the absence of melting endotherm of crystalline dihydrate at 96°C or increase in the T_g value to 225°C from the initial value of 210°C for freshly prepared sample.



Below are some of the comments (bold) of the anonymous reviewers when the manuscript was submitted to Pharmaceutical Research. Our response follows. The manuscript was accepted for publication.

“There is no conclusive evidence to show that water is not responsible for T_{g2} reduction. It is a well known plasticizer. Perhaps, an experiment with different RH values and same temperature would have delineated this effect. How do you explain the reduction of T_{g2} (207 - 210) at 40/75 as compared to 196-203 at 23/75? Also, in the dextran-trehalose mix, the solid solubility decreased from 18 to 12% when the water content decreased from 16.5 to 11%. Therefore, moisture also does seem to have an effect on T_{g2} reduction.”

Response: We also demonstrated that water acts as a plasticizer. It reduces the T_g of the mixtures to 22-25°C as shown in Fig. B-14. However, the reduction that we see in the T_g values in our experiments is due to the “solubilized” trehalose.

During the DSC experiments, water is driven away from the sample (8-12 mg), when it is slowly heated at 1°C/min rate, at temperatures above 100°C.

To test whether the reduction in T_{g2} values was the result of the moisture retained in the dispersions, dextran (containing no trehalose), which was previously exposed to 50°C / 75% RH for a month and contained 11% w/w water, was heated. Its T_{g2} was 225°C (Fig.B-15); which was identical to the T_g of original sample that had ~ 3% w/w moisture content. This finding indicates that water did not influence the T_{g2} values during the heating scan in DSC.

Secondly, the T_{g2} values of heat flow scans of 10% w/w trehalose-dextran mixtures that were exposed to various stability conditions and contained varying levels of moisture are demonstrated in Fig B-16. They all are consistent with that of the freshly prepared samples (Fig. 2a in the manuscript) indicating that moisture did not influence T_{g2}.

Reduction in T_{g2} (from 225°C) can be explained by the solubilization of trehalose in the polymer. For instance, trehalose mixtures above their solubility limit (i.e. 20%, 30%, 40% and 70%) were crystallized when they were exposed to stability conditions and their T_{g2} values increased to 207-210°C (at 50°C/75% RH). On the other hand, the samples containing 10 % trehalose (the concentration below the solubility limit), showed no crystallization and T_{g2} changes confirming that, reduction in T_{g2} values reflects the complete miscibility of trehalose with the polymer.

Water however, seems to impact T_{g2} by facilitating the phase separation and crystallization of trehalose, as described in detail on P12, under “*Mechanism of phase separation and solid solubility*”. Our data demonstrates that T_{g2} values of the samples were 196-203°C at 23°C / 75% RH and 207-210°C at 40°C / 75% RH. Such a change in T_{g2} values, which corresponded to a decrease in solid solubility from 18% to 12%, is probably due to the increase in storage temperature as described on P15 under “*Effect of temperature and moisture on solid solubility*”. Nevertheless, the temperature cannot be the only factor since no significant difference in solubility, was noticed between 40°C / 75% RH and 50°C/ 75% RH given the RSD. Therefore, water may have an affect on the T_{g2} values by altering solid solubility.

We have ongoing studies specifically addressing the impact of temperature and moisture on the solid solubility. We plan to submit that work to this journal as a follow up study.

Figure B-14

MDSC scans showing the plasticized T_g values of 40% w/w trehalose in dextran mixtures that were exposed to 50°C/ 75%RH conditions.

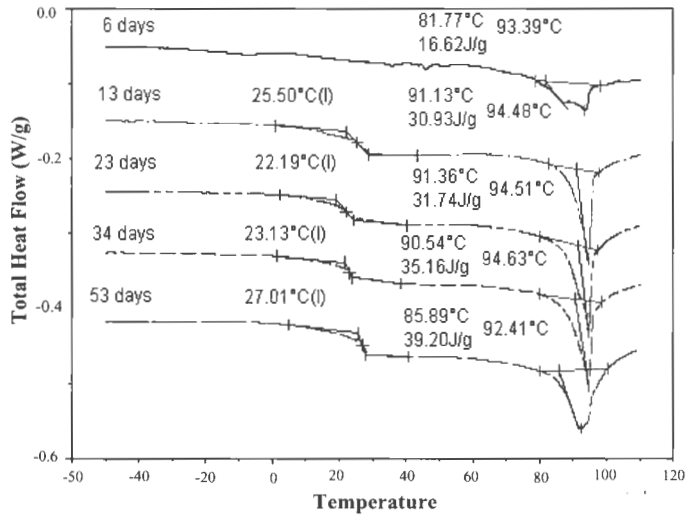


Figure B-15

DSC scans of dextran that was exposed to 50°C/75%RH for one month and containing 11% w/w moisture. The sample was heated in MDSC at the rate of 1°C/min, with $\pm 0.266^\circ$ every 50seconds to 240°C.

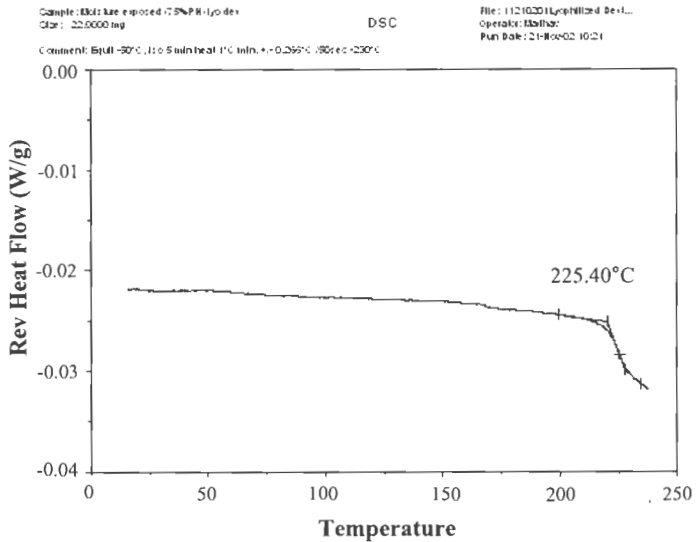
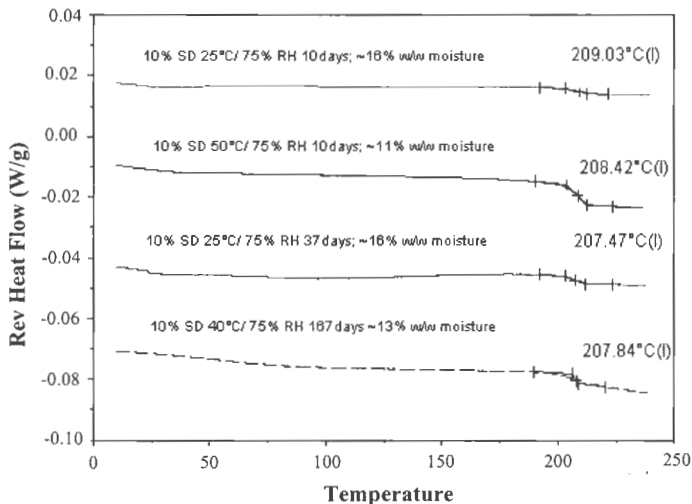


Figure B-16

MDSC reversing heat flow scans of 10% w/w trehalose-dextran mixtures that were exposed to stability conditions. No crystallization of trehalose was observed. Also the

T_{g2} values were consistent with T_g of freshly prepared sample (~210°C).



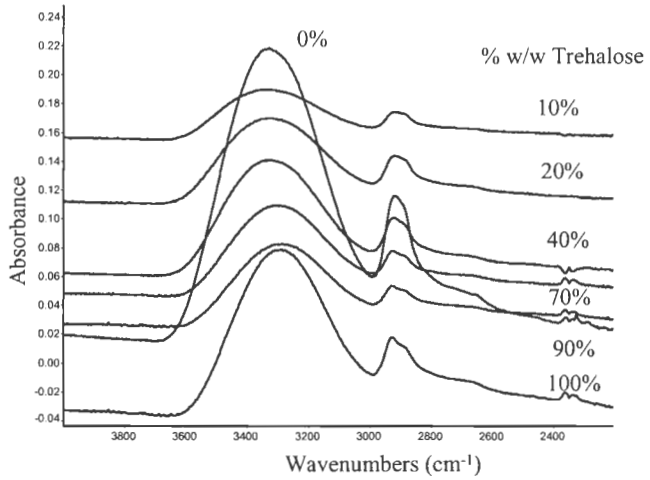
“It would always be good to support the DSC characterization with other methods such as X-ray diffraction, NMR, FTIR etc. Is it possible to show any evidence of H2 bonding for the reduction of Tg2 as claimed? The deviations in fig 2 are not conclusive.”

Response: The FTIR spectroscopy was performed on the freshly prepared samples to determine the nature of interactions between trehalose and dextran. However, no meaningful interpretation of the –OH stretch (free vs. bound), could be made as a result of the presence of multiple hydroxyls of trehalose, dextran and water (Fig. B-17). XRD and NMR were not used for these mixtures due to accessibility problems. Currently we have easier access to XRD and are using it as the supporting tool in the remaining studies.

Regarding the concerns that you raised about the certainty of deviations in Fig. 2, we can only say that the experiments were carried out with three batches and our standard deviations were very small.

Figure B-17

Hydroxyl stretches of freshly prepared trehalose-dextran amorphous mixtures as obtained with FT-IR.



“It is so easy to identify T_g in Figs. 2a & 2b. However, it is not so apparent to believe T_{g1} and T_{g2} in Figs 3a & 3b. Can a raw MDSC heat flow plot be shown to demonstrate the existence of T_g in those cases?”

Response: Thank you. A raw MDSC heat flow plot is now shown.

Figure B-18

MDSC raw heat flow scans to depict the presence of T_{g1} and T_{g2} values

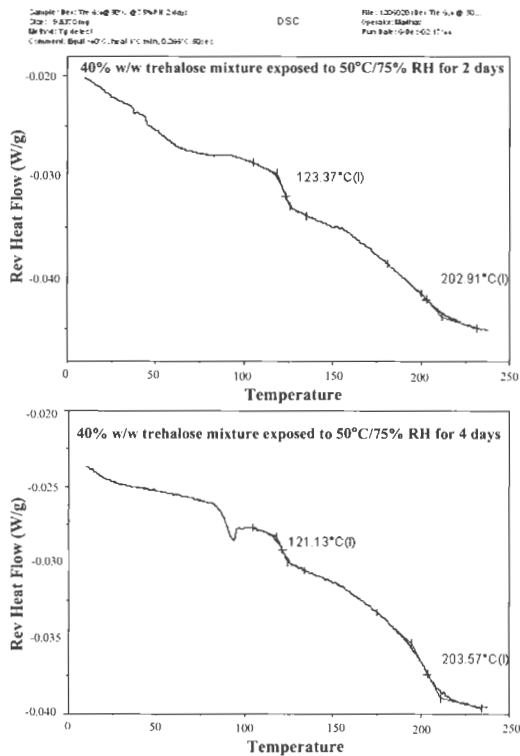
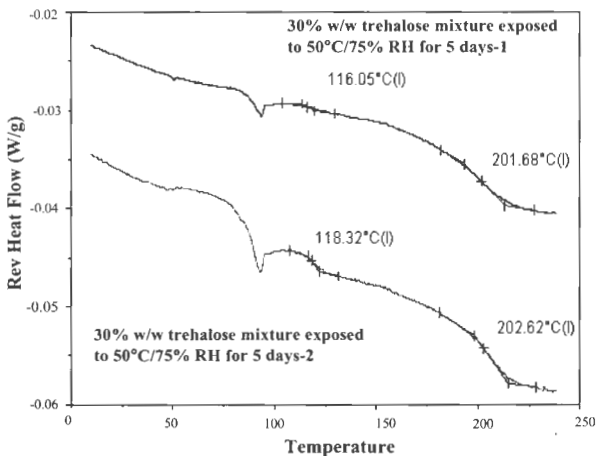
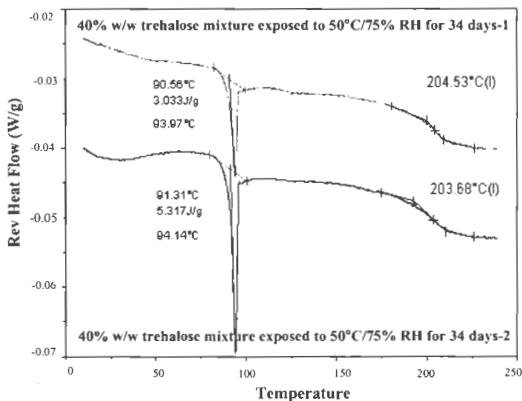


Figure B-19



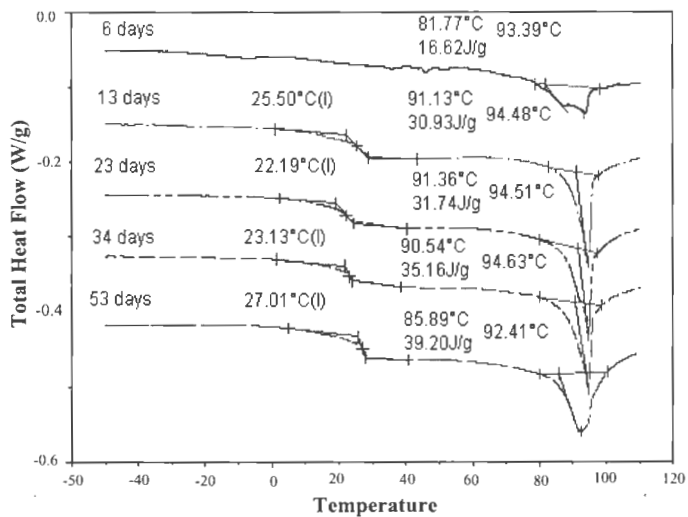
MDSC raw heat flow scans to depict the reproducibility of T_{g1} and T_{g2} values



MDSC raw heat flow scans to depict the reproducibility of T_h and T_{g2} values

Figure B-20

MDSC scans showing the plasticized T_g values of 40% w/w trehalose in dextran mixtures that were exposed to 50°C/ 75%RH



“Why there are no recrystallization/melting peaks in Fig. 3? If the phase segregation happened as illustrated in Fig. 7, anhydrate form could be formed. Why not?”

Response: Yes it could. However, under hot-stage microscope, we observed that trehalose undergoes the glass transition and subsequently liquefies before nucleating to anhydrate form. The presence of polymer is likely to inhibit the nucleation of anhydrate form and as the result; no recrystallization/melting peaks are seen.

“Is there any fundamental difference between dextran-trehalose and PVP-trehalose? T_g (eq) of the former case is so close to the melting point of trehalose, but not for the PVP dispersed system.”.

Response: The difference between trehalose-dextran and trehalose-PVP mixtures is, the most likely, the extent of miscibility of the sugar and the respective polymers.

In general, the degree of miscibility of the components may depend upon factors including (1) molecular sizes of two components i.e. two sugars are easy to mix when compared to two polymers; (2) the differences in the T_g of individual components i.e. the smaller the differences in T_gs, the lower is the difference in their relative molecular mobility at mixing temperature; (3) structural similarities between two components i.e. like dissolves like; and (4) potential for interactions between the components i.e. interactions promotes mixing.

The chemical structure of trehalose and the dextran repeat unit are very similar and also there is a potential for hydrogen bonding between the two components. For PVP mixtures the difference between the T_g of PVP (167°C) and trehalose (119°C) is less when compared to dextran (225°C) and trehalose. Also, the interactions between trehalose –OH and the basic C=O of PVP is considered stronger than trehalose –OH and dextran –OH.

The T_g^{eq} found in the trehalose-dextran mixture was lowered from 225°C to the values that happen to coincide with the melting temperature of anhydrous trehalose for samples

that were stored at 40°C and 50°C/75%RH storage conditions. This was a coincidence! Similar reduction in T_g values for PVP mixtures was seen from 168°C to 158°C due to trehalose dissolution in PVP.

Calculations of the thermodynamic parameters

The excess enthalpy, entropy and free energy of mixing of trehalose with dextran and PVP were calculated using the theoretical equations provided below. The calculation involves binary mixtures and their phase stability behavior. In the presence of water, the mixtures are however considered as ternary. Although there is a difference between a two-phase mixing and three-phase mixing, the free energy minimum of mixing (Fig. 7; manuscript 1), shows that the thermodynamic stability of the system is expected at its maximum around 20%w/w trehalose-concentration. Our observations showed that T_{g2} values reached a plateau suggesting “equilibrium” of the three phase system that corresponded to 12-18% trehalose concentration, i.e. values closer for the predicted system with no water. Although the calculations are made based on the trehalose-polymer interactions, it may be more than a coincidence.

The molar enthalpy of polymer 1, having glass transition temperature T_{g1} , in its glassy state, at a temperature T , is given as:

$$H_1^s(T) = H_1^s(T_{g1}) + \int_{T_{g1}}^T \bar{C}_{p1}^s dT \quad (1)$$

Similarly, the molar enthalpy in liquid state $H_1^l(T)$ can be described as:

$$H_1^l(T) = H_1^l(T_{g1}) + \int_{T_{g1}}^T \bar{C}_{p1}^l dT \quad (2)$$

According to Ehrenfest's theory of second-order transition; $H_1^l(T_{g1}) = H_1^g(T_{g1})$, and so equations (1) and (2) can be equated at T_{g1} .

For a miscible blend containing polymer P_1 and sugar S_2 with weight fractions w_1 and w_2 respectively, and undergoing a single glass transition temperature T_{g12} , the enthalpy of mixture, H_{12} (J/g) can be described by the relation (30):

$$H_{12} = w_1 H_1 + w_2 H_2 + \Delta H_{mix} \quad (3)$$

where H_1 and H_2 are the enthalpy in either liquid or glassy states of polymer and sugar respectively, and ΔH_{mix} is the enthalpy of mixing.

The enthalpy of mixing can be described as a function of temperature (T) and weight fraction (w), in the liquid or glassy states. By following Ehrenfest's theory, the function $H(T, w)$ is continuous at T_{g12} , (i.e. $H_{12}^l(T_{g12}) = H_{12}^g(T_{g12})$), and hence the following equations can be given:

$$H_{12}^l(T_{g12}, w) = w_1 \int_{T_{g1}}^{T_{g12}} \bar{C}_{p1}^l dT + w_2 \int_{T_{g2}}^{T_{g12}} \bar{C}_{p2}^l dT + \Delta H_{mix}^l \quad (4)$$

$$H_{12}^g(T_{g12}, w) = w_1 \int_{T_{g1}}^{T_{g12}} \bar{C}_{p1}^g dT + w_2 \int_{T_{g2}}^{T_{g12}} \bar{C}_{p2}^g dT + \Delta H_{mix}^g \quad (5)$$

Also, since $\Delta H_{mix} = \Delta H_{mix}^E + \Delta H_{idealmix}$ and $\Delta H_{idealmix} = 0$, rearranging equations (4) and (5) at T_{g12} , we have:

$$-\Delta H_{mix}(J/g) = -\Delta H_{mix}^E = \Delta H_{mix}^g - \Delta H_{mix}^l = w_1 \int_{T_{g1}}^{T_{e1}} \Delta C_{p1} dT + w_2 \int_{T_{g2}}^{T_{e2}} \Delta C_{p2} dT \quad (6)$$

where $\Delta H_{mix}^E(J/g) = \Delta H_{mix}^l - \Delta H_{mix}^g$; $\Delta C_p = C_p^l - C_p^g$; ΔH_{mix} is the enthalpy of mixing, and T_{g1} and T_{g2} are the glass transition temperatures of polymer and sugar respectively.

The entropy of mixing can also be calculated in a manner similar to the above performed calculations, and is described as:

$$-\Delta S_{mix}(J/g/^\circ K) = \Delta S_{mix}^g - \Delta S_{mix}^l = w_1 \int_{T_{e1}}^{T_{e1}} \Delta C_{p1} d \ln T + w_2 \int_{T_{e2}}^{T_{e2}} \Delta C_{p2} d \ln T - R \sum X_i \ln X_i \quad (7)$$

where $\Delta S_{mix} = \Delta S_{mix}^E + \Delta S_{ideal\ mix}$; $\Delta S_{ideal\ mix} = -R \sum X_i \ln X_i$; R is the gas constant and X_i is the mole fraction of component i of the mixture. X_i has been converted to weight fractions to adjust the units for $\Delta S_{ideal\ mix}$ to $J/g/^\circ K$.

In order to numerically calculate the thermodynamic functions, it is necessary to obtain the heat capacity of individual components of the mixture as a function of temperature in their glassy and liquid states. The heat capacity function of a polymer is typically of the form $C_p = a + bT$, where a and b are constants.

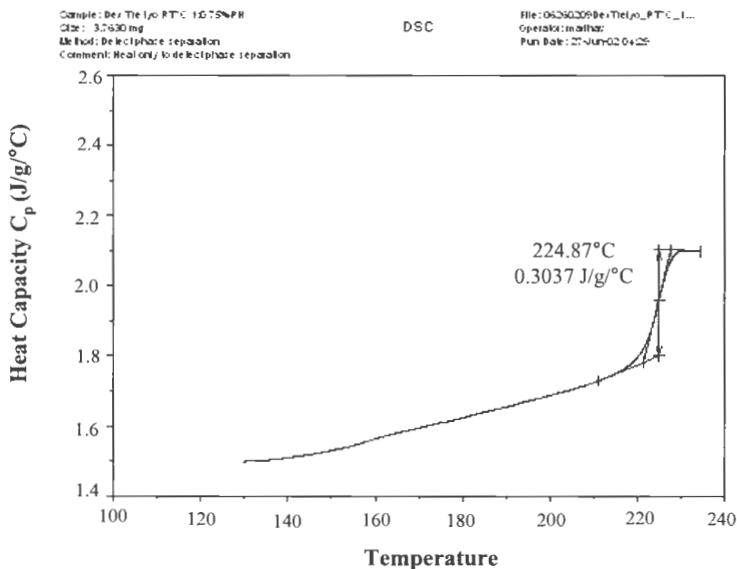
By substituting the expression for C_p in equations (6) (or (7)), the enthalpy (or the entropy) of mixing can be calculated:

$$-\Delta H_{mix} = w_1 \int_{T_{e1}}^{T_{e1}} [(a_1 + b_1 T)^l - (a_1 + b_1 T)^g] dT + w_2 \int_{T_{e2}}^{T_{e2}} [(a_2 + b_2 T)^l - (a_2 + b_2 T)^g] dT \quad (8)$$

Upon calculating the enthalpy and entropy, the free energy of mixing can be calculated using the following equation:

$$\Delta G_{mix} = \Delta H_{mix} - T_{gl2} \Delta S_{mix} \quad (9)$$

Heat capacity-Temperature scans of lyophilized dextran



Heat capacity values of dextran at different temperatures

File: C:\...\06260209DexTrelyo_1,0.001 Run Date: 27-Jun-02 04:29
Program: Universal V2.6D Run Number: 274

TA Instruments Thermal Analysis -- DSC Standard - Modulated
Sample: Dextran lyophilized
Size: 3.7630 mg
Cell Constant: 1.0689
Operator: Madhav
Method: Heat capacity changes
Comment: Heat only
Exotherm: Up

Temperature °C	Complex Cp J/g/°C	Temperature °C	Complex Cp J/g/°C
36.85	1.815	161.85	1.570
41.85	1.842	166.85	1.585
46.85	1.867	171.85	1.600
51.85	1.883	176.85	1.614
56.85	1.886	181.85	1.630
61.85	1.872	186.85	1.645
66.85	1.843	191.85	1.660
71.85	1.806	196.85	1.677
76.85	1.765	201.85	1.694
81.85	1.723	206.85	1.711
86.85	1.681	211.85	1.733
91.85	1.640	216.85	1.763
96.85	1.603	220.85	1.812
101.85	1.572	221.85	1.834
106.85	1.545	222.85	1.867
111.85	1.525	223.85	1.910
116.85	1.511	224.85	1.960
121.85	1.503	225.85	2.008
126.85	1.499	226.85	2.049
131.85	1.499	227.85	2.078
136.85	1.504	228.85	2.093
141.85	1.512	229.85	2.099
146.85	1.521	230.85	2.101
151.85	1.534	231.85	2.100
156.85	1.550	232.85	2.099
		233.85	2.099

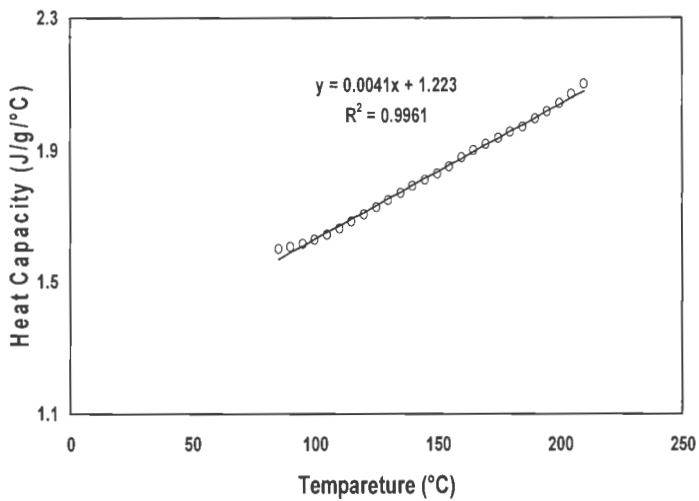
Heat capacity equations for dextran:

Supercooled state (C_p^l) = 1.7894 + 0.00196 T

Glassy state (C_p^g) = 1.223 + 0.0041 T

$\Delta C_p(C_p^l - C_p^g) = 0.5664 - 0.00214 T$

Plot of C_p^* vs. Temperature for lyophilized dextran



Heat Capacity – Temperature scans of Lyophilized PVP

Sample: PVP 130 C The Up 10

Size: 2.6410 mg

Method: EM1: C2

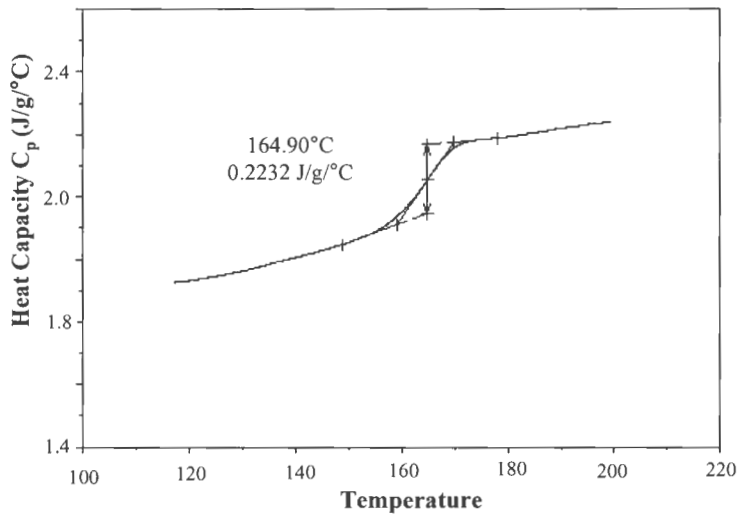
Comments: Therm. Treat still not given, heat only

DSC

File: 061702SP v P_The_Lyo_10.D01

Operator: mshahar

Run Date: 18-Jun-02 14:11



Heat capacity values of lyophilized PVP at different temperatures

File: C:\...\0617025PVP_Tre_Lyo_1,0.001 Run Date: 18-Jun-02 14:11
Program: Universal V2.6D Run Number: 237

TA Instruments Thermal Analysis -- DSC Standard - Modulated

Sample: Lyophilized PVP
Size: 2.8410 mg
Cell Constant: 1.0689
Operator: Madhav
Method: Mdsc2
Comment: Heat only
Exotherm: Up

Temperature °C	Complex Cp J/g/°C
36.85	2.170
41.85	2.192
46.85	2.229
51.85	2.269
56.85	2.285
61.85	2.276
66.85	2.256
71.85	2.222
76.85	2.174
81.85	2.122
86.85	2.070
91.85	2.018
96.85	1.979
101.85	1.948
106.85	1.930
111.85	1.923
116.85	1.925
121.85	1.936
126.85	1.950
131.85	1.968
136.85	1.992
141.85	2.013
146.85	2.037
151.85	2.065
156.85	2.106
161.85	2.183
166.85	2.301
171.85	2.373
176.85	2.387
181.85	2.397
186.85	2.409
191.85	2.423
196.85	2.435

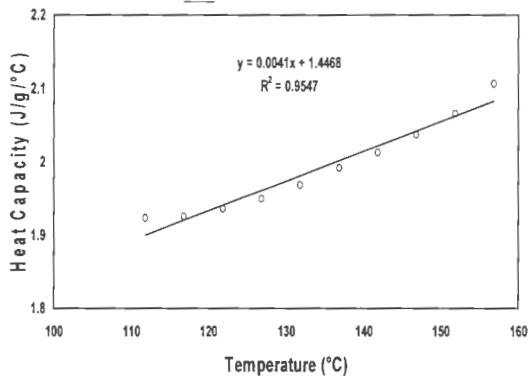
Heat capacity equations for PVP:

Supercooled state (C_p^l) = 1.951 + 0.0025 T

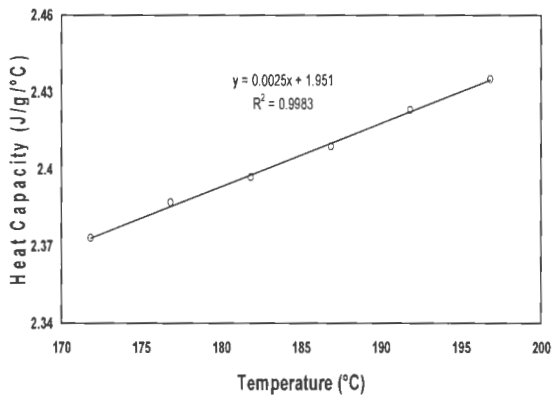
$$\text{Glassy state } (C_p^g) = 1.4468 + 0.0041 T$$

$$\Delta C_p (C_p^l - C_p^g) = 0.5042 - 0.0016 T$$

Plot of C_p^g vs. Temperature for lyophilized PVP



Plot of C_p^l vs. Temperature for lyophilized PVP

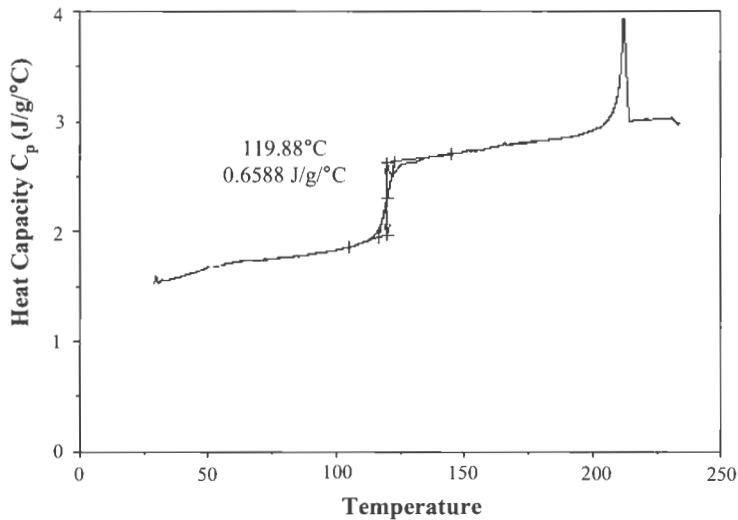


Heat Capacity - Temperature scans of Lyophilized Trehalose

Sample: De-The 0.1_Tg_detect1
Size: 7.8960 mg
File: De-The 0.1_Tg_detect1.dsc
Comment: To detect Tg of trehalose

DSC

File: 3030360e-The 0.1_Tg_detect1...
Operator: Mallikarjuna
Print Date: 17-Mar-03 12:16



Heat capacity values of lyophilized trehalose at different temperatures

File: C:\...\303039DexTre0,1_Tg-detect_1.001 Run Date: 7-Mar-03 12:16
Program: Universal V2.6D Run Number: 93

TA Instruments Thermal Analysis -- DSC Standard - Modulated

Sample: Lyophilized Trehalose Size: 7.8980 mg
Cell Constant: 1.0742
Operator: Madhav
Method: MDSC 2
Comment: Detect Heat capacity
Exotherm: Up

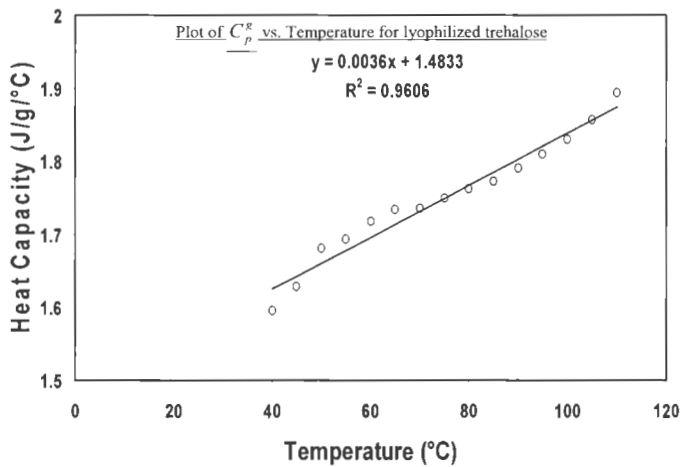
Temperature °C	Complex Cp J/g/°C	Temperature °C	Complex Cp J/g/°C
36.85	1.576	121.85	2.499
41.85	1.606	126.85	2.620
46.85	1.643	131.85	2.638
51.85	1.686	136.85	2.685
56.85	1.704	141.85	2.693
61.85	1.723	146.85	2.714
66.85	1.741	151.85	2.736
71.85	1.742	156.85	2.743
76.85	1.757	161.85	2.773
81.85	1.766	166.85	2.785
86.85	1.781	171.85	2.806
91.85	1.795	176.85	2.821
96.85	1.817	181.85	2.826
101.85	1.838	186.85	2.846
106.85	1.870	191.85	2.861
111.85	1.912	196.85	2.895
116.85	2.031	201.85	2.941
		206.85	3.045

Heat capacity equations trehalose:

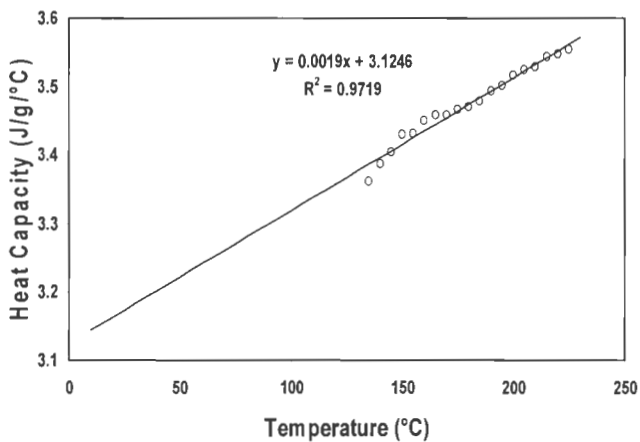
Supercooled state (C_p^l) = 3.1246 + 0.0019 T

Glassy state (C_p^g) = 1.4833 + 0.0036 T

$\Delta C_p (C_p^l - C_p^g) = 1.6413 - 0.0017 T$



Plot of C_p^l vs. Temperature for lyophilized trehalose



Sample calculation for the enthalpy of mixing:

$$-\Delta H_{mix} = w_1 \int_{T_{g12}}^{T_{g1}} [(a_1 + b_1 T)^l - (a_1 + b_1 T)^g] dT + w_2 \int_{T_{g12}}^{T_{g2}} [(a_2 + b_2 T)^l - (a_2 + b_2 T)^g] dT$$

where w_1 = weight fraction of trehalose,

w_2 = weight fraction of polymer,

T_{g1} = glass transition temperature for trehalose,

T_{g2} = glass transition temperature for polymer,

T_{g12} = glass transition temperature for trehalose-polymer mixture,

a_1 = y-intercept of linear equation of heat capacity vs. temperature for trehalose,

b_1 = slope of linear equation of heat capacity vs. temperature for trehalose,

a_2 = y-intercept of linear equation of heat capacity vs. temperature for polymer,

b_2 = slope of linear equation of heat capacity vs. temperature for polymer.

To calculate the enthalpy of mixing for a 40%w/w trehalose - in - dextran mixture:

Supercooled state (C_p^l) = 3.1246 + 0.0019 T

Glassy state (C_p^g) = 1.4833 + 0.0036 T

$\Delta C_{p1} (C_p^l - C_p^g) = 1.6413 - 0.0017 T$

Supercooled state (C_p^l) = 1.7894 + 0.00196 T

Glassy state (C_p^g) = 1.223 + 0.0041 T

$\Delta C_{p2} (C_p^l - C_p^g) = 0.5664 - 0.00214 T$

$-\Delta H_{mix} = (0.4 * (1.6413 * (391 - 442)) - 0.4 * (0.0017) * ((391 * 391) / 2 - (442 * 442) / 2)) +$

$0.6 * (0.5664 * (497 - 442)) - 0.6 * (0.00214) * ((497 * 497) / 2 - (442 * 442) / 2))$

Enthalpy of mixing for trehalose – dextran mixtures

Trehalose Wt. fraction	Dextran Wt. fraction	T _g mixture (°K)	ΔH_{mix}^E (J/g)
0	1	497	0
0.1	0.9	482.36	14.55
0.2	0.8	467.50	24.93
0.3	0.7	454.41	31.01
0.4	0.6	442.33	33.54
0.5	0.5	431.01	32.93
0.6	0.4	421.22	29.85
0.7	0.3	412.40	24.68
0.8	0.2	403.97	17.41
0.9	0.1	397.21	9.32
1	0	391	0

Since, the enthalpy of mixing, $\Delta H_{mix} = \Delta H_{idealmix} + \Delta H_{mix}^E$, and $\Delta H_{idealmix} = 0$, the excess enthalpy of mixing is equal to total enthalpy of mixing as given in the above table.

Excess entropy of mixing for trehalose – dextran mixtures

Trehalose Wt. fraction	Dextran Wt. fraction	T _g mixture (°K)	ΔS_{mix}^E (X 10 ³) (J/g/K)
0	1	497	0
0.1	0.9	482.36	31.88
0.2	0.8	467.50	55.42
0.3	0.7	454.41	69.94
0.4	0.6	442.33	76.66
0.5	0.5	431.01	76.20
0.6	0.4	421.22	69.88
0.7	0.3	412.40	58.37
0.8	0.2	403.97	41.54
0.9	0.1	397.21	22.43
1	0	391	0

To calculate the entropy of mixing, the ideal entropy of mixing is added to the excess entropy as described by the equations below;

$\Delta S_{mix} = \Delta S_{mix}^E + \Delta S_{ideal\ mix}$; $\Delta S_{ideal\ mix} = -R \sum X_i \ln X_i$; R is the gas constant and X_i is the mole fraction of component i of the mixture. X_i needs to be converted to weight fractions to adjust the units for $\Delta S_{ideal\ mix}$ to J/g³K as conducted below.

Calculation of ideal and total entropy of mixing:

Wt. Trehalose	Mol. Wt Trehalose	Wt. Dextran	Mol. Wt Dextran
0	342	1	71000
0.1	342	0.9	71000
0.2	342	0.8	71000
0.3	342	0.7	71000
0.4	342	0.6	71000
0.5	342	0.5	71000
0.6	342	0.4	71000
0.7	342	0.3	71000
0.8	342	0.2	71000
0.9	342	0.1	71000
1	342	0	71000

Term A* (X 10 ²)	ln (term A) (X 10 ³)	Term B ⁵ (X 10 ²)	ln (term B)	$\Delta S_{ideal\ mix}$	$\Delta S_{ideal\ mix}$ (corrected) [§] (X10 ⁵)	ΔS_{mix} (X10 ³)
0	-	100	0	0	1.48	0
95.84	-42.43	4.15	-3.18	1.436833	1.56	31.90
98.10	-19.08	1.89	-3.96	0.779261	1.75	55.43
98.88	-11.17	1.11	-4.49	0.507611	2.00	69.95
99.28	-7.19	0.71	-4.93	0.353851	2.33	76.67
99.52	-4.80	0.47	-5.34	0.252576	2.80	76.21
99.67	-3.20	0.32	-5.74	0.179422	3.49	69.88
99.79	-2.06	0.20	-6.18	0.123032	4.64	58.37
99.87	-1.20	0.12	-6.72	0.077215	6.90	41.55
99.94	-0.53	0.053	-7.53	0.037945	13.49	22.44
1	0	0	-	0	292.39	0

*Term A =

$$\left(\frac{\left(W_{Trehalose} MW_{Trehalose} \right)}{W_{Trehalose} MW_{Trehalose} + W_{Dextran} MW_{Dextran}} \right)$$

‡Term B =

$$\left(\frac{\left(W_{Dextran} MW_{Dextran} \right)}{W_{Trehalose} MW_{Trehalose} + W_{Dextran} MW_{Dextran}} \right)$$

§ $\Delta S_{ideal\ mix}$ (corrected for units to J/g/°K) = $\Delta S_{ideal\ mix}^*$

$$\left(\frac{1}{W_{Trehalose}^* MW_{Trehalose} + W_{Dextran}^* MW_{Dextran}} \right)$$

Free energy of mixing for trehalose – dextran mixtures

Free energy of mixing, $\Delta G_{mix} = \Delta H_{mix} - T_{g12} \Delta S_{mix}$

ΔH_{mix} (J/g)	ΔS_{mix} ($\times 10^3$) (J/g/°K)	T_{g12} (°K)	ΔG_{mix} (J/g)
0	0	497	0
14.55	31.90	482.36	-0.83
24.93	55.43	467.50	-0.98
31.01	69.95	454.41	-0.77
33.54	76.67	442.33	-0.37
32.93	76.21	431.01	0.082
29.85	69.88	421.22	0.4180
24.68	58.37	412.40	0.60
17.41	41.55	403.97	0.63
9.32	22.44	397.21	0.41
0	0	391	0

Enthalpy of mixing for trehalose – PVP mixtures

Trehalose Wt. fraction	PVP Wt. fraction	T _g mixture (°K)	ΔH_{mix}^E (J/g)
0	1	441	0
0.1	0.9	430.21	5.80
0.2	0.8	424.05	9.14
0.3	0.7	420.61	11.43
0.4	0.6	415.8	12.58
0.5	0.5	411.33	12.74
0.6	0.4	406.38	11.62
0.7	0.3	401.41	9.34
0.8	0.2	398.15	7.18
0.9	0.1	395.09	4.44
1	0	391	0

Since, the enthalpy of mixing, $\Delta H_{mix} = \Delta H_{idealmix} + \Delta H_{mix}^E$, and $\Delta H_{idealmix} = 0$, the excess enthalpy of mixing is equal to total enthalpy of mixing as given in the above table.

Excess entropy of mixing for trehalose – PVP mixtures

Trehalose Wt. fraction	PVP Wt. fraction	T _g mixture (°K)	ΔS_{mix}^E (X 10 ³) (J/g/K)
0	1	441	0
0.1	0.9	430.21	13.86
0.2	0.8	424.05	22.04
0.3	0.7	420.61	27.77
0.4	0.6	415.8	30.74
0.5	0.5	411.33	31.32
0.6	0.4	406.38	28.75
0.7	0.3	401.41	23.24
0.8	0.2	398.15	17.95
0.9	0.1	395.09	11.17
1	0	391	0

To calculate the entropy of mixing, the ideal entropy of mixing is added to the excess entropy as described by the equations below;

$\Delta S_{mix} = \Delta S_{mix}^E + \Delta S_{ideal\ mix}$; $\Delta S_{ideal\ mix} = -R \sum X_i \ln X_i$; R is the gas constant and X_i is the mole fraction of component i of the mixture. X_i needs to be converted to weight fractions to adjust the units for $\Delta S_{ideal\ mix}$ to J/g^oK as conducted below.

Calculation of ideal and total entropy of mixing:

Wt. Trehalose	Mol. Wt Trehalose	Wt. PVP	Mol. Wt PVP
0	342	1	58000
0.1	342	0.9	58000
0.2	342	0.8	58000
0.3	342	0.7	58000
0.4	342	0.6	58000
0.5	342	0.5	58000
0.6	342	0.4	58000
0.7	342	0.3	58000
0.8	342	0.2	58000
0.9	342	0.1	58000
1	342	0	58000

Term A* (X 10 ²)	ln (term A) (X 10 ³)	Term B ^E (X 10 ²)	ln (term B)	$\Delta S_{ideal\ mix}$	$\Delta S_{ideal\ mix}$ (corrected) ^S (X10 ⁵)	ΔS_{mix} (X10 ³)
0	-	100	0	0	0	0
94.96	-51.70	5.03	-2.98	1.65	3.17	13.82
97.69	-23.31	2.30	-3.77	0.91	1.96	22.02
98.64	-13.66	1.35	-4.29	0.59	1.46	27.75
99.12	-8.80	0.87	-4.73	0.41	1.19	30.73
99.41	-5.87	0.58	-5.13	0.29	1.02	31.31
99.60	-3.92	0.39	-5.54	0.21	0.90	28.74
99.74	-2.52	0.25	-5.98	0.14	0.82	23.23
99.82	-1.47	0.14	-6.52	0.09	0.77	17.94
99.93	-0.65	0.06	-7.33	0.04	0.74	11.16
1	0	0	-	0	0	0

$$*\text{Term A} = \left(\frac{\left(\frac{W_{t_{\text{Trehalose}}}}{MW_{\text{Trehalose}}} \right)}{W_{t_{\text{Trehalose}}} / MW_{\text{Trehalose}} + W_{t_{\text{PVP}}} / MW_{\text{PVP}}} \right)$$

$$\xi \text{Term B} = \left(\frac{\left(\frac{W_{t_{\text{PVP}}}}{MW_{\text{PVP}}} \right)}{W_{t_{\text{Trehalose}}} / MW_{\text{Trehalose}} + W_{t_{\text{PVP}}} / MW_{\text{PVP}}} \right)$$

$$\begin{aligned} & \S \Delta S_{\text{ideal mix}} \text{ (corrected for units to J/g}^\circ\text{K)} = \\ \Delta S_{\text{ideal mix}} * & \left(\frac{1}{W_{t_{\text{Trehalose}}} * MW_{\text{Trehalose}} + W_{t_{\text{PVP}}} * MW_{\text{PVP}}} \right) \end{aligned}$$

Free energy of mixing for trehalose – PVP mixtures

Free energy of mixing, $\Delta G_{\text{mix}} = \Delta H_{\text{mix}} - T_{g12} \Delta S_{\text{mix}}$

ΔH_{mix} (J/g)	ΔS_{mix} ($\times 10^3$) (J/g $^\circ$ K)	T_{g12} ($^\circ$ K)	ΔG_{mix} (J/g)
0	0	441	0
5.80	13.82	430.21	-0.16
9.14	22.02	424.05	-0.21
11.43	27.75	420.61	-0.24
12.58	30.73	415.8	-0.20
12.74	31.31	411.33	-0.14
11.62	28.74	406.38	-0.06
9.34	23.23	401.41	0.015
7.18	17.94	398.15	0.033
4.44	11.16	395.09	0.027
0	0	391	0

APPENDIX C

Phase Behavior of Amorphous Molecular Dispersions: Role of Hydrogen Bonding in Solid Solubility and Kinetics of Phase Separation

(Supporting data to Manuscript II)

Physical stability of amorphous drug substance

It is seen from Fig. C-1, that both the amorphous drugs undergo recrystallization after glass transition phenomenon while heating in DSC. This indicates the instability of drugs in their amorphous phases. Based on the DSC scans it is inferred that indoprofen is a relatively stable crystalline molecule due to its high heat of fusion. Also it is expected to be relatively unstable in its amorphous phase due to its lower T_g (50°C) and lower recrystallization temperature (72°C).

Figure C-1

Heat flow scans of amorphous and crystalline griseofulvin exhibiting the physical transitions

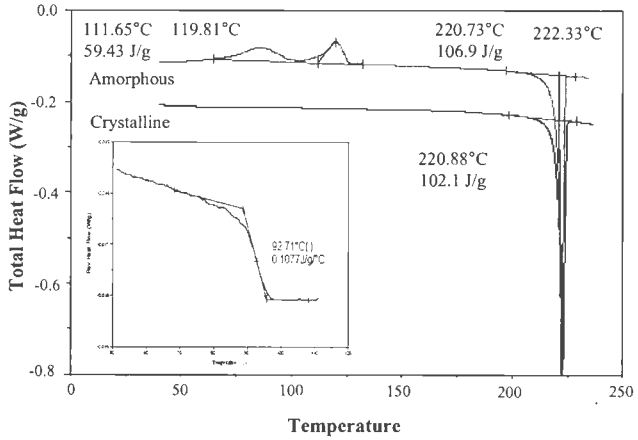
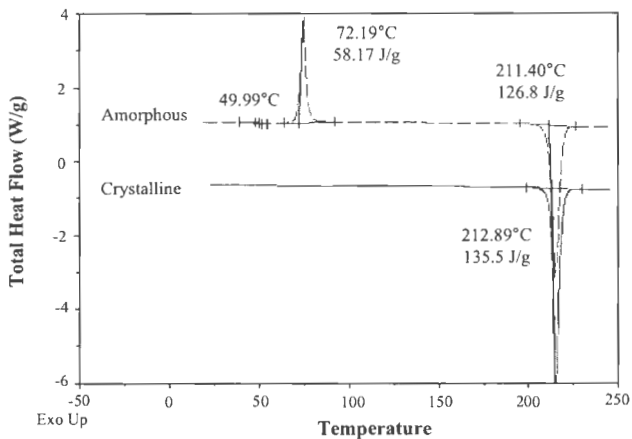


Figure C-2

Heat flow scans of amorphous and crystalline indoprofen exhibiting the physical transitions



Spectroscopic investigation of drug crystallization patterns:

In order to understand the nature of interactions between drug molecules in their amorphous and crystalline forms a spectroscopic investigation was conducted. Such a study would provide information on the various routes through which the drug molecules crystallize. Vibrational spectroscopy is a technique that is well established and is typically used to study specific interactions. FT-IR spectroscopy was used in this study to probe into the state of functional groups of drugs in their amorphous and crystalline states and the spectra are shown in Fig. C-3. Differences are evident

between the two forms of both the drugs in the carbonyl stretch region of 1750 cm^{-1} and 1600 cm^{-1} .

Griseofulvin has three methoxy units and two carbonyl groups as shown in Fig. 1a (chapter 2). On its FT-IR spectra, in addition to broadening of peaks in the amorphous sample, a weak peak at 1739 cm^{-1} was seen for crystalline form indicating the presence of unbound C=O groups (Fig. C-3A). Also a strong peak at 1598 cm^{-1} presumably due to the carbon-carbon structural ordering of molecules is seen in crystalline form and is absent in amorphous phase. Since there are no significant differences in the peak pattern of carbonyl groups between the amorphous and crystalline griseofulvin, it is possible that the functional groups do not involve through interactions during drug crystallization.

Indoprofen has two carbonyl groups: a) C=O of -COOH group and b) C=O of the amide in pyrrolidone ring (Fig. C-3B). In the case of crystalline indoprofen, a weak peak at 1728 cm^{-1} and a strong peak at 1697 cm^{-1} was seen. The presence of a high intensity peak at lower wave-numbers relative to peak at 1728 cm^{-1} ($\Delta\nu=31\text{ cm}^{-1}$) indicates that the C=O of -COOH is largely present in a bound state. The band at 1681 cm^{-1} is assigned to the C=O of pyrrolidone ring. In the case of amorphous indoprofen, the peak at 1728 cm^{-1} has much higher intensity when compared to the peak at 1697 cm^{-1} , indicating that the C=O of -COOH are relatively "free". Actually, the peak at 1728 cm^{-1} is characteristic of free C=O of -COOH groups where the -OH group is hydrogen bonded to a different functional group. The carbonyl band of -COOH group where both C=O and -OH groups are free appear at 1750 cm^{-1} . In the amorphous state, in addition to band at 1681 cm^{-1} , a broad band at 1648 cm^{-1} was

observed. This band was assigned to the hydrogen bonded C=O the pyrrolidone ring ($\Delta\nu=33\text{cm}^{-1}$). The C=O of pyrrolidone ring could most likely be bonded to $-\text{OH}$ group of $-\text{COOH}$. This would agree with previous observation of free carbonyl group of $-\text{COOH}$ stretch at 1728cm^{-1} instead of 1750cm^{-1} . Therefore it can be concluded that indoprofen molecules crystallize by forming cyclic dimers between two $-\text{COOH}$ units of individual molecules.

Figure C-3
FTIR carbonyl stretching of amorphous and crystalline A) griseofulvin and B) indoprofen

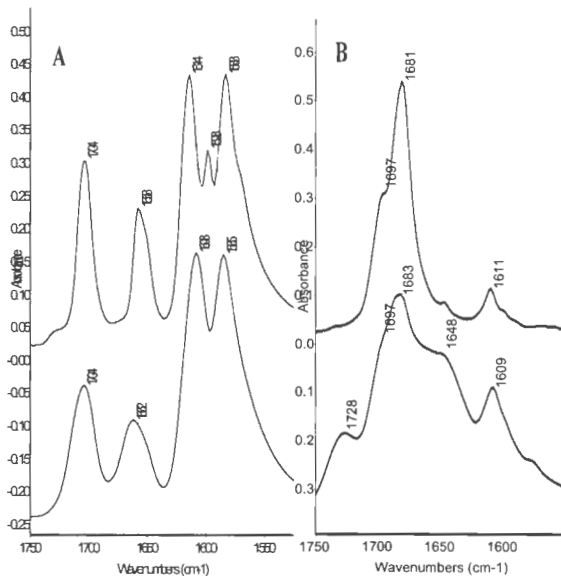


Figure C-4

MDSC reversing heat flow scans of 30%w/w griseofulvin-in-PVP solid dispersions exposed to 40°C/69%RH for (a) 2 days and (b) 4, 6, and 10 days

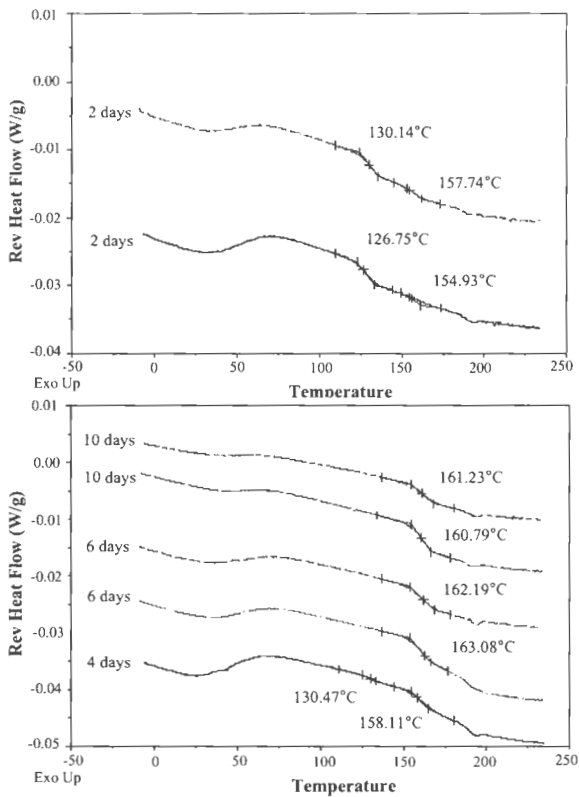


Figure C-5

MDSC reversing heat flow scans of 30%w/w griseofulvin-in-PVP solid dispersions exposed to 40°C/69%RH for (a) 11, 15 days and (b) 35 days

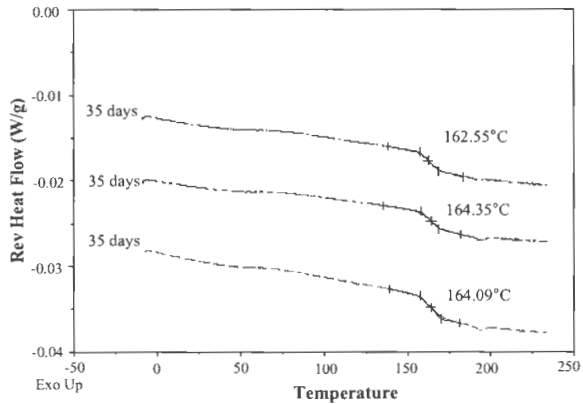
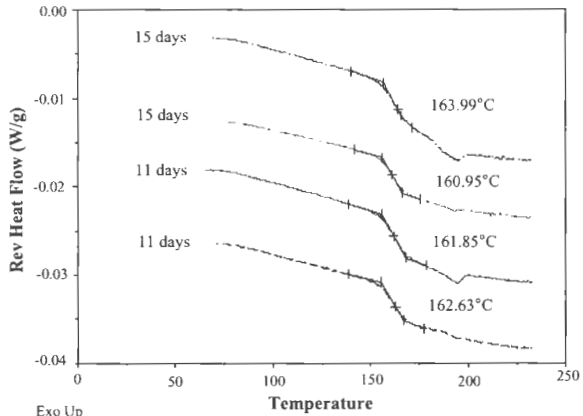


Figure C-6

MDSC reversing heat flow scans of 30%w/w griseofulvin-in-PVP solid dispersions exposed to 40°C/69%RH for 65, 75 and 90 days

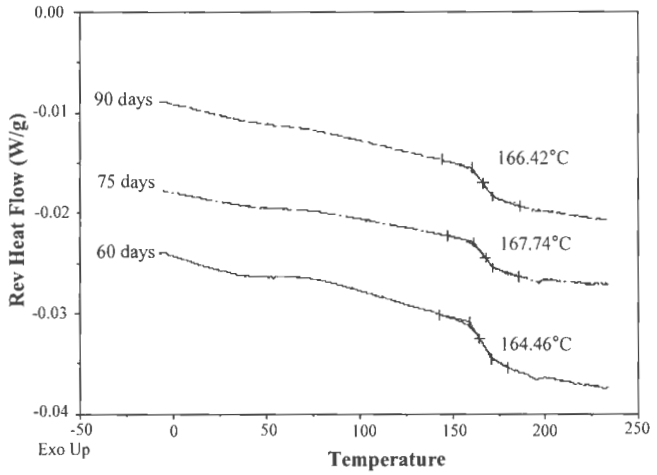


Figure C-7

MDSC reversing heat flow scans of 20%w/w griseofulvin-in-PVP solid dispersions exposed to 40°C/69%RH for (a) 2 days and (b) 6 days

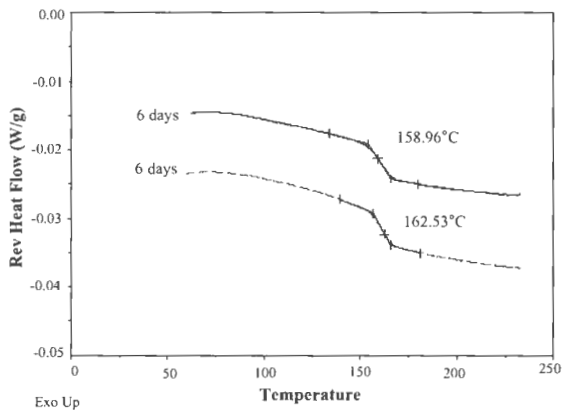
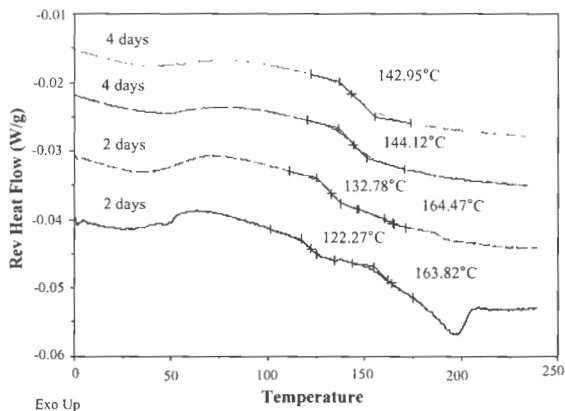


Figure C-8

MDSC reversing heat flow scans of 20%w/w griseofulvin-in-PVP solid dispersions exposed to 40°C/69%RH for (a) 4, 6, 10 days and (b) 10, 15 days

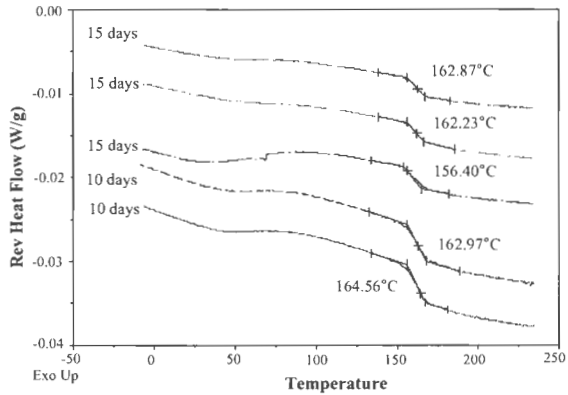
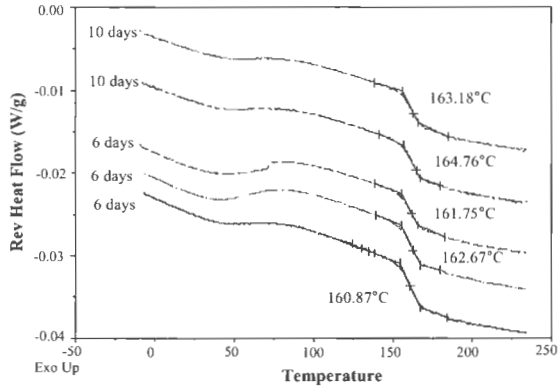


Figure C-9

MDSC reversing heat flow scans of 20%w/w griseofulvin-in-PVP solid dispersions exposed to 40°C/69%RH for (a) 50, 60, 70 days

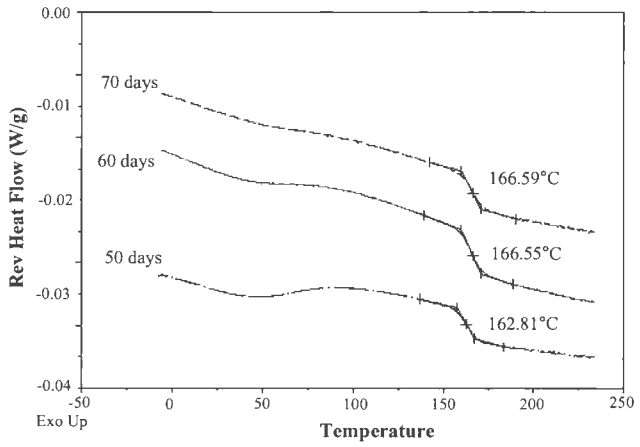


Figure C-10

MDSC reversing heat flow scans of 10%w/w griseofulvin-in-PVP solid dispersions exposed to 40°C/69%RH for (a) 2, 3, 4, 6, 10 days and (b) 6, 10, 60 days

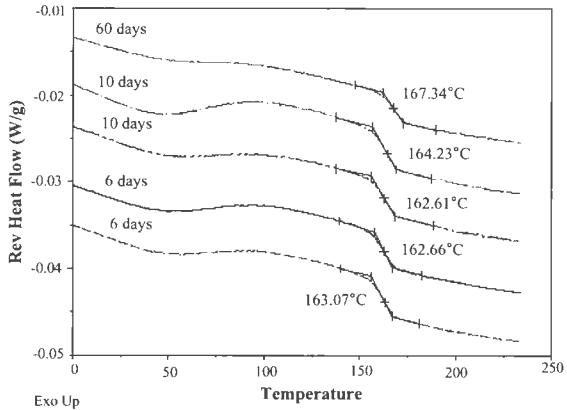
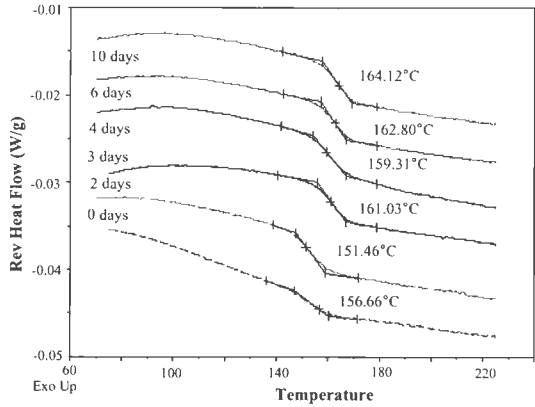


Figure C-11

MDSC reversing heat flow scans of 30%w/w indoprofen-in-PVP solid dispersions exposed to 40°C/69%RH for (a) 1, 7, 15 days and (b) 15, 36 days

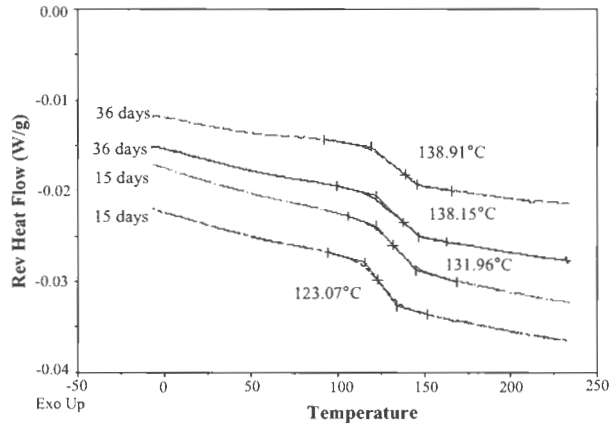
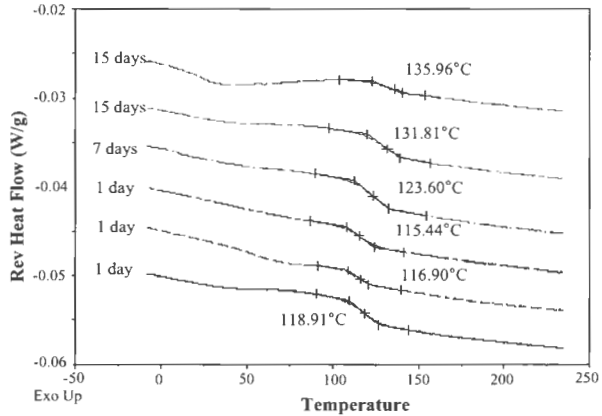


Figure C-12

MDSC reversing heat flow scans of 30%w/w indoprofen-in-PVP solid dispersions exposed to 40°C/69%RH for 50, 75, 90 days

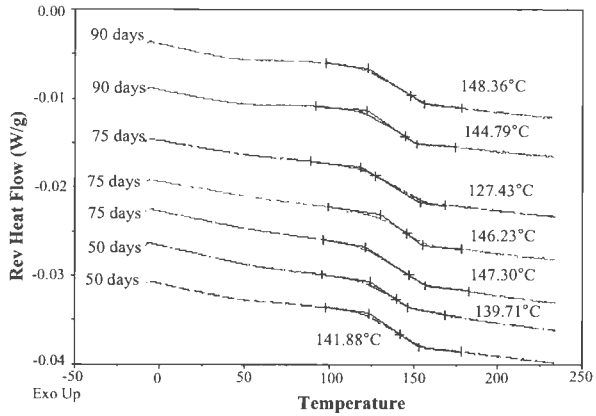


Figure C-13

MDSC reversing heat flow scans of 20%w/w indoprofen-in-PVP solid dispersions exposed to 40°C/69%RH for (a) 1, 2, 9 days and (b) 15 days

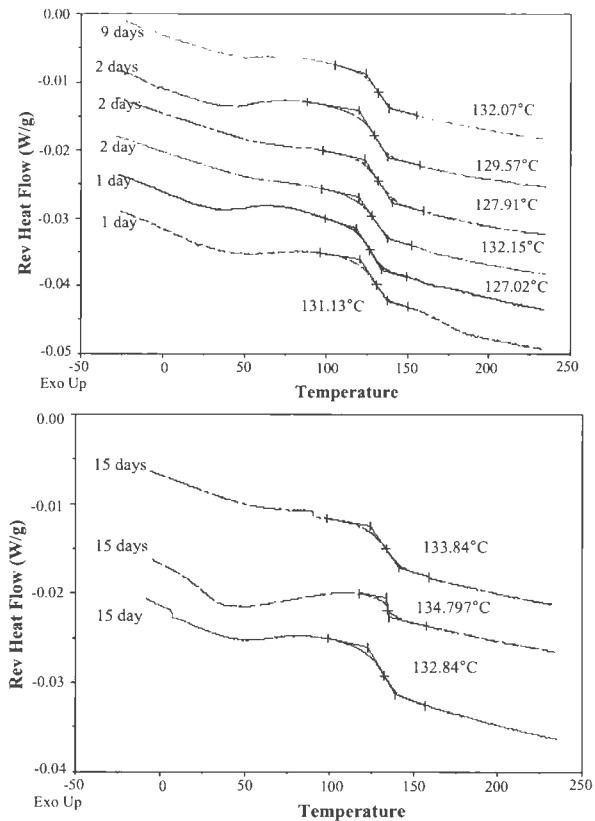


Figure C-14

MDSC reversing heat flow scans of 20%w/w indoprofen-in-PVP solid dispersions exposed to 40°C/69%RH for (a) 36, 54 days and (b) 55, 70, 90 days

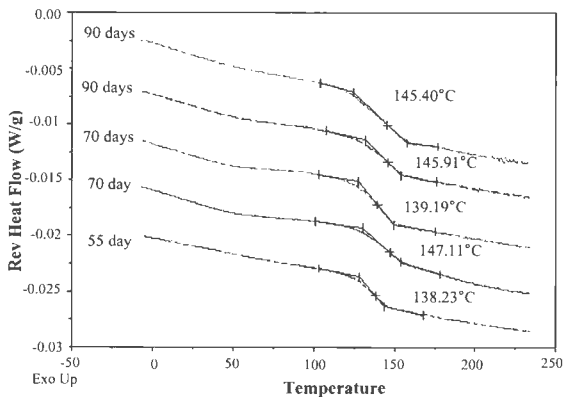
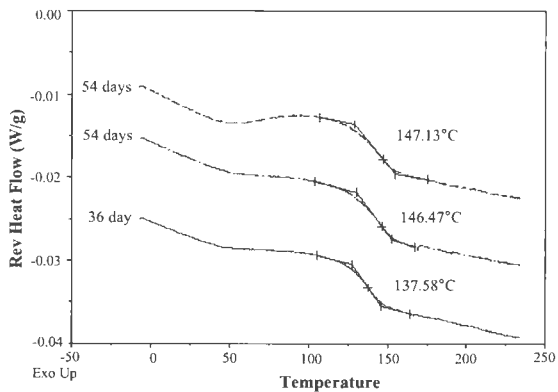


Figure C-15

MDSC reversing heat flow scans of 10%w/w indoprofen-in-PVP solid dispersions exposed to 40°C/69%RH for (a) 0, 1, 2, 16, 36, 54 days and (b) 1, 2, 9, 16 days

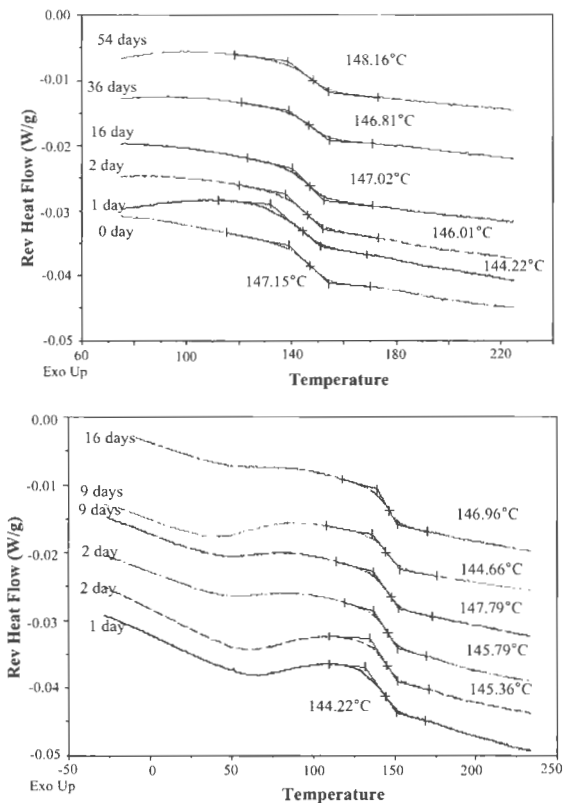


Figure C-16

MDSC reversing heat flow scans of 10%w/w indoprofen-in-PVP solid dispersions exposed to 40°C/69%RH for (a) 18, 36, 55 days and (b) 35, 55, 70 days

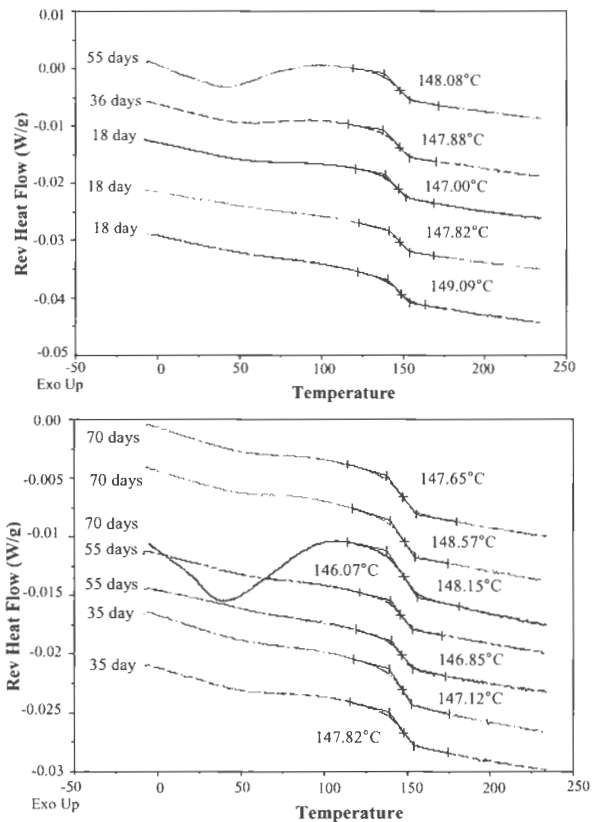


Figure C-17

MDSC reversing heat flow scans of PVP solid dispersions containing (a) 30%w/w griseofulvin and (b) 20%w/w griseofulvin, exposed to 40°C/0%RH for 34 days. No significant deviations in T_g are seen indicating that moisture is essential to cause phase-separation and crystallization of griseofulvin.

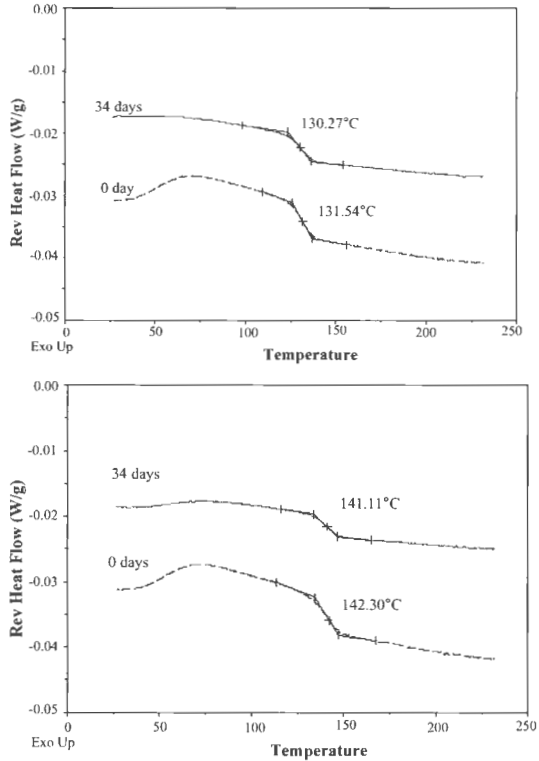


Figure C-18

MDSC reversing heat flow scans of PVP solid dispersions containing (a) 10%w/w griseofulvin exposed to 40°C/0%RH for 34 days.

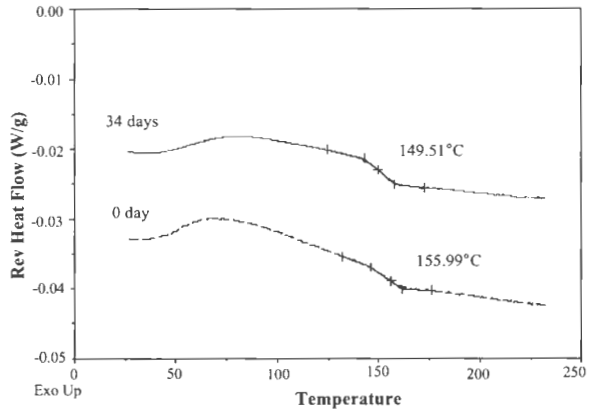


Figure C-19

MDSC reversing heat flow scans of PVP solid dispersions containing (a) 30%w/w indoprofen and (b) 20%w/w indoprofen exposed to 40°C/0%RH for 34 days.

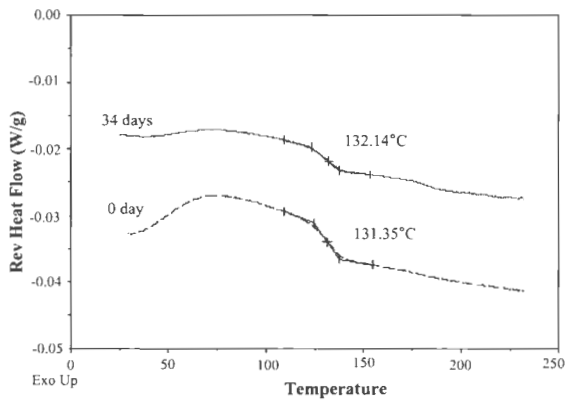
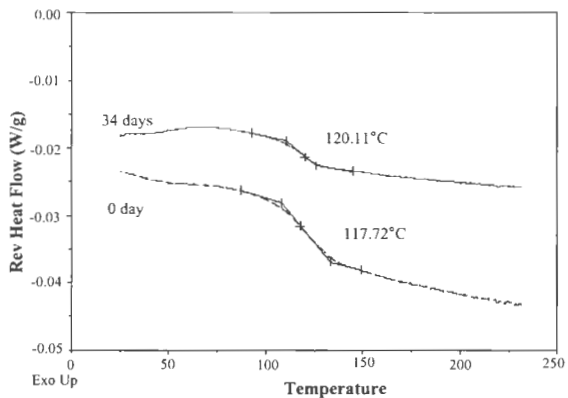
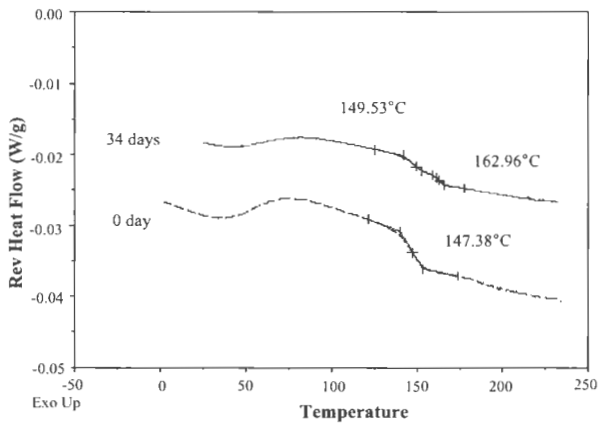


Figure C-20

MDSC reversing heat flow scans of PVP solid dispersions containing (a) 10%w/w indoprofen exposed to 40°C/0%RH for 34 days.



Estimation of the Rate of Phase Separation of Griseofulvin and Indoprofen from PVP
Solid Dispersions

To estimate the kinetic rate of phase separation of the drug from the polymers, the changes in the T_g of the mixture were utilized to calculate the fraction of the drug that had phase-separated. It is assumed that with increasing phase-separation of drug from the polymer, the T_g of the mixture would increase and eventually reach to T_g of pure polymer when no drug remains miscible.

Based on this assumption, a mixture having T_g equal to that of a freshly prepared sample was accounted as 100% miscible mixture. Likewise a T_g of 167°C indicated a 0% miscible mixture. Accordingly, the percentage of drug miscible was calculated at a specific storage time (t) as follows:

$$(1 - \alpha)_t = 1 - \frac{T_{g(\text{polymer})} - T_{g2(t)}}{T_{g(\text{polymer})} - T_{g(\text{initial})}}$$

where α is the amount of drug phase separated, T_{g(polymer)} is the 167°C, T_{g(initial)} is the T_g of freshly prepared sample and is dependent on the composition of drug present, T_{g2(t)} is the T_g of the mixture at the specified storage time t .

Upon obtaining the fraction of drug phase separated with storage time, the phase separation rate constant was estimated by using a first-order rate equation:

$$[-\ln(1 - \alpha)] = kt$$

where k is the rate constant for phase separation.

A first order rate equation was applied since it seemed to best fit the data when compared to other rate equations.

Phase separation rates were determined from average of n=3 T_g values at every time point.

Table C-I: Griseofulvin kinetics of phase separation from 30%w/w solid dispersions

Days (<i>t</i>)	T_g (°C)	167°C - T_g	a ($\times 10^2$)	1- a	-[ln(1- a)]
0	131	36	0	1	0
1	159	8	77	0.222	1.504
2	155	12	66	0.333	1.098
5	160	7	80	0.194	1.637
9	162	5	86	0.138	1.974
11	161	6	83	0.166	1.791
15	163	4	88	0.111	2.197
35	163	4	88	0.111	2.197
60	164	3	91	0.083	2.484
70	166	1	97	0.027	3.583
90	167	0	100	0	-

Table C-II: Griseofulvin kinetics of phase separation from 20%w/w solid dispersions

Days (<i>t</i>)	T_g (°C)	167°C - T_g	a ($\times 10^2$)	1- a	-[ln(1- a)]
0	142	25	0	1	0
2	164	3	88	0.12	2.120
6	161	6	76	0.24	1.427
10	163	4	84	0.16	1.832
15	160	7	72	0.28	1.272
30	164	3	88	0.12	2.120
60	166	1	96	0.04	3.218
70	166	1	96	0.04	3.218
90	167	0	100	0	-

Table C-III: Griseofulvin kinetics of phase separation from 10%w/w solid dispersions

Days (t)	T _g (°C)	167°C - T _g	a (x 10 ²)	1 - a	-[ln(1 - a)]
0	156	11	0	1	0
2	156.35	10.65	3	0.968	0.032
3	160.49	6.51	40	0.591	0.524
6	162.86	4.14	62	0.376	0.977
10	163.42	3.58	67	0.325	1.122
39	165.35	1.65	85	0.15	1.894
50	166.17	0.83	92	0.075	2.584
60	166.34	0.66	94	0.06	2.813
75	166.74	0.26	97	0.023	3.744

Figure C-21

Plot of $-\ln(1-a)$ vs. time for griseofulvin-PVP solid dispersions to obtain the rate constant for drug phase separation.

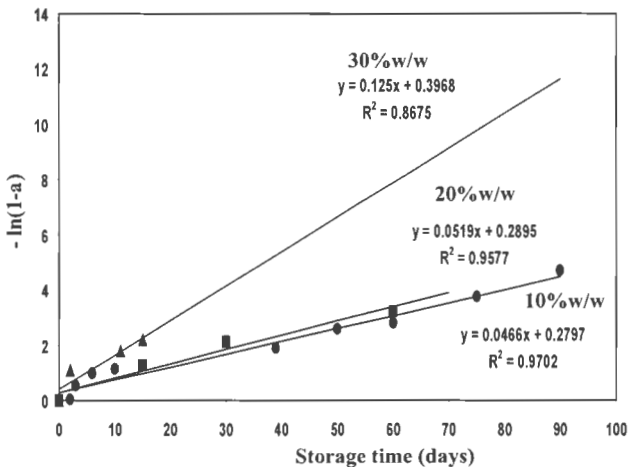


Table C-IV: Indoprofen kinetics of phase separation from 30%w/w solid dispersions

Days (<i>t</i>)	T _g (°C)	167°C - T _g	<i>a</i> (x 10 ²)	1- <i>a</i>	-[ln(1- <i>a</i>)]
1	117	50	0	1	0
7	119	48	4	0.96	0.040
15	127	40	20	0.8	0.223
36	137	30	40	0.6	0.510
50	140	27	46	0.54	0.616
75	143	24	52	0.48	0.733
90	143	25	50	0.50	0.694

Table C-V: Indoprofen kinetics of phase separation from 20%w/w solid dispersions

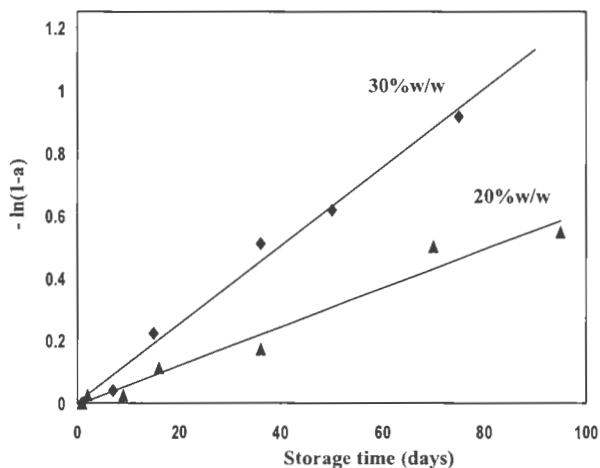
Days (<i>t</i>)	T _g (°C)	167°C - T _g	<i>a</i> (x 10 ³)	1- <i>a</i>	-[ln(1- <i>a</i>)]
1	129	38	0	1	0
2	130	37	2	0.973	0.026
9	130	37	2	0.973	0.026
16	133	34	10	0.894	0.111
36	135	32	15	0.842	0.171
54	143	24	36	0.631	0.459
70	143	24	36	0.631	0.459
95	144	23	39	0.605	0.502

Table C-VI: Indoprofen kinetics of phase separation from 10%w/w solid dispersions

Days (<i>t</i>)	T_R (°C)	167°C - T_g	a (x 10 ²)	1 - a	$-\ln(1 - a)$
1	144	23	0	1	0
2	145	22	4	0.956	0.044
9	146	21	8	0.913	0.090
16	147	20	13	0.869	0.139
36	147	20	13	0.869	0.139
54	147	20	13	0.869	0.139
70	148	19	17	0.826	0.191
90	148	19	17	0.826	0.191

Figure C-22

Plot of $-\ln(1-a)$ vs. time for indoprofen-PVP solid dispersions to obtain the rate constant for drug phase separation.



APPENDIX D

Phase Behavior of Amorphous Molecular Dispersions: Determination of Solid Solubility in Ternary Solid Dispersions

(Supporting data to Manuscript III)

Figure D-1

MDSC reversing heat flow scans of solid dispersions containing PVP, indoprofen and sugar ester O1570. A composition dependent single T_g is evident for the freshly prepared ternary solid dispersions. With an increase in the surfactant concentration, the T_g of the mixture decreases. **A** 65:30:05 (7.14%w/w); **B** 60:30:10 (14.20%w/w); **C** 70:30:15 (17.64%w/w); **D** 50:30:20 (28.5%w/w); **E** 70:30:30 (39%w/w); **F** 40:30:30 (42%w/w). The compositions are given as PVP: Indoprofen: sugar-ester. The numbers within the brackets are for the percentage surfactant in the overall mixture. The increase in the baseline at temperatures above 180°C indicates the decomposition of the surfactant.

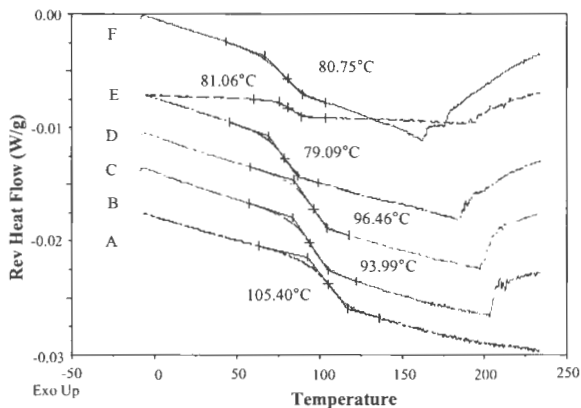


Figure D-2

MDSC reversing heat flow scans of PVP: Indoprofen: Sugar-ester in the ratio 60:30:10 that were stored at 40°C/69%RH for different storage intervals. The T_g of 114°C at the end of 15 days was less than the T_g of 123°C (see chapter 3) corresponding to solid solubility of sugar ester in PVP at 40°C/69%RH. The fraction of indoprofen dissolved in PVP was therefore not influenced (neither increased nor decreased) by the presence of sugar ester.

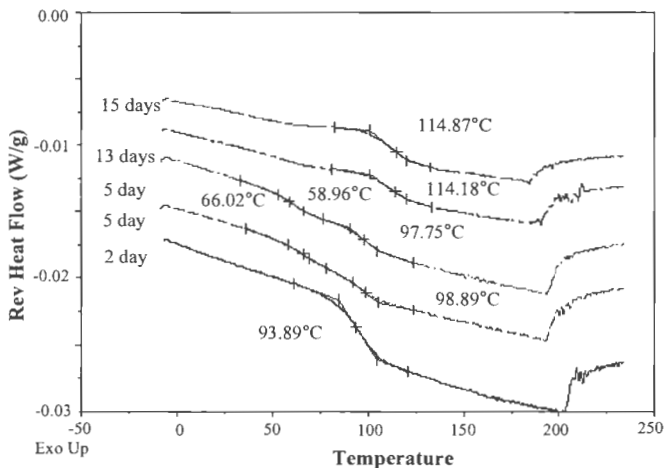


Figure D-3

MDSC reversing heat flow scans of PVP: Indoprofen: Sugar-ester in the ratio 65:30:05 that were stored at 40°C/69%RH for different storage intervals. The T_g of 114°C at the end of 7 days for this composition indicates that the final T_g value (114°C) is not influenced by the initial surfactant concentration (see Fig.A4-2). The fraction of indoprofen dissolved in PVP was not influenced (neither increased nor decreased) by the presence of sugar ester.

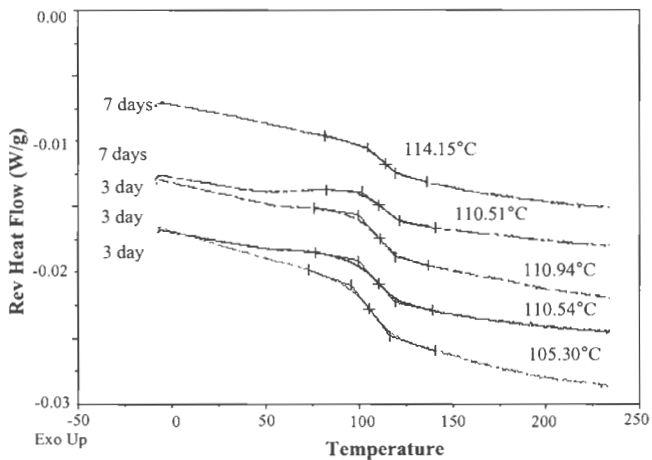
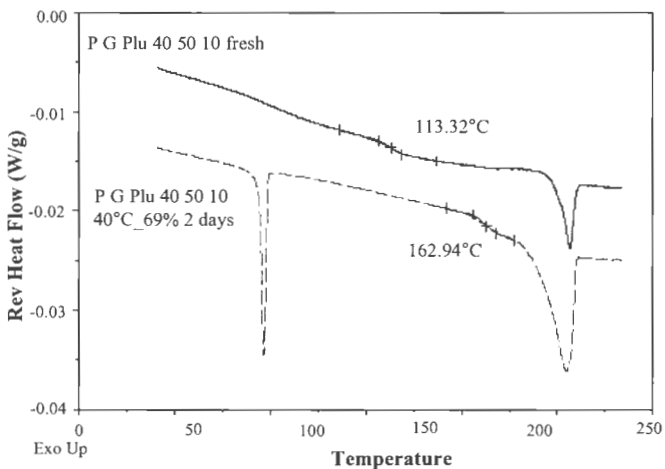


Figure D-4

MDSC reversing heat flow scans of PVP: griseofulvin: pluronic in the ratio 40:50:10 those were stored at 40°C/69%RH for 2 days. Phase separation of griseofulvin is seen from the shift in T_g from 113°C to 162°C. In addition, the surfactant – Pluronic F87 crystallizes completely as indicated by the melting at 70°C and the shift in T_g of PVP to 162°C. The approach described in this study was found useful to identify the physical stability of this product at 40°C/69%RH conditions.



APPENDIX E

Crystallization Kinetics of Amorphous Griseofulvin under Low Moisture Content

(Supporting data to Manuscript IV)

**Table E-I: XRD calibration plot to determine the kinetics of griseofulvin
crystallization.**

A physical mixture of crystalline and amorphous griseofulvin was prepared using 20%w/w of lithium fluoride (LiF) as the internal reference. The peak height of crystalline griseofulvin peak and lithium fluoride were measured and their ratios (crystalline griseofulvin: LiF) were plotted against the percentage of crystalline griseofulvin in the sample.

%w/w crystalline griseofulvin in total griseofulvin (i.e. 80% of sample)	Peak height ratio [crystalline griseofulvin/ LiF]	Average	SD
30%	0.5754	0.538575	0.151251
	0.5841		
	0.6732		
	0.3216		
50%	0.835	0.857125	0.067632
	0.928		
	0.892		
	0.7735		
70%	0.9146	0.9749	0.127906
	1.021		
	1.129		
	0.835		

Figure E-1

XRD calibration plot of peak ratio of crystalline griseofulvin and lithium fluoride

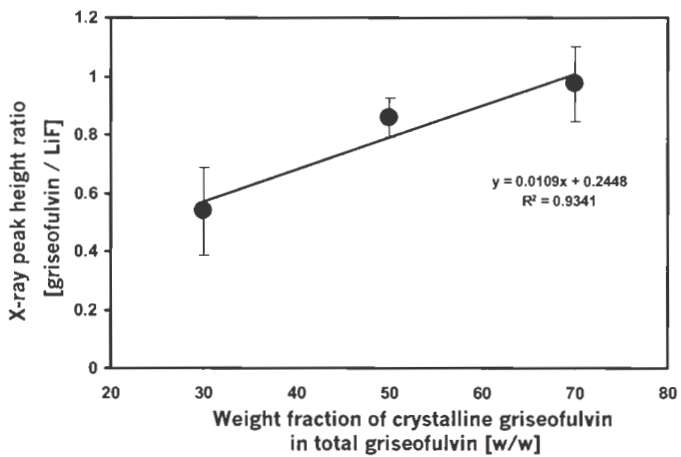
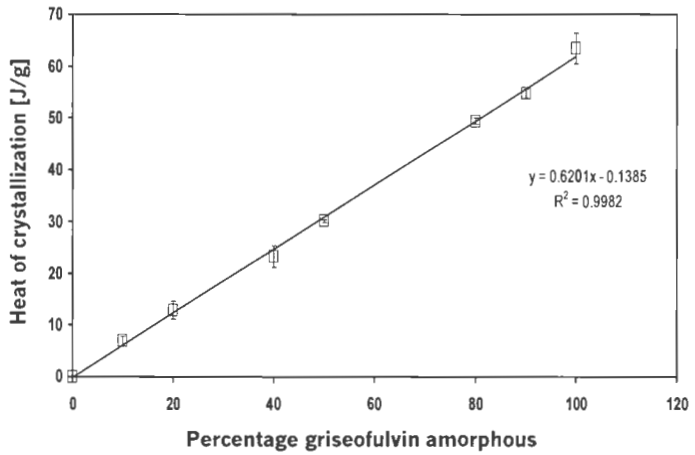


Table E-II: Heat of recrystallization of amorphous griseofulvin in physical mixtures of crystalline and amorphous griseofulvin for the construction of calibration plot

Percent Amorphous	Heat of recrystallization (J/g)			Average heat of recrystallization (J/g)	Standard deviation
	Batch 1	Batch 2	Batch 3		
100	61.38	62.36	60.31	61.35	1.025
90	54.12	53.9	55.21	54.41	0.701
80	49.9	50.26	49.98	50.04	0.189
50	29.95	29.35	30.05	29.78	0.378
40	24.74	24.53	23.92	24.39	0.425
20	14.05	13.95	14.56	14.18	0.327
10	7.554	7.378	8.04	7.657	0.342
0	0	0	0	0	0

Figure E-2

MDSC calibration plot of heat of griseofulvin crystallization and percentage of amorphous griseofulvin in the sample.



Isothermal crystallization studies

Figure AE-3

MDSC nonreversing heat flow scans of amorphous griseofulvin undergoing isothermal crystallization at 43%RH. As crystallization occurs, the amorphous fraction in the sample decreases and hence the area under the crystallization peak decreases. To quantify the percentage of griseofulvin in the amorphous state, the DSC calibration plot and the heat of crystallization (i.e. area under the crystallization curve) is used.

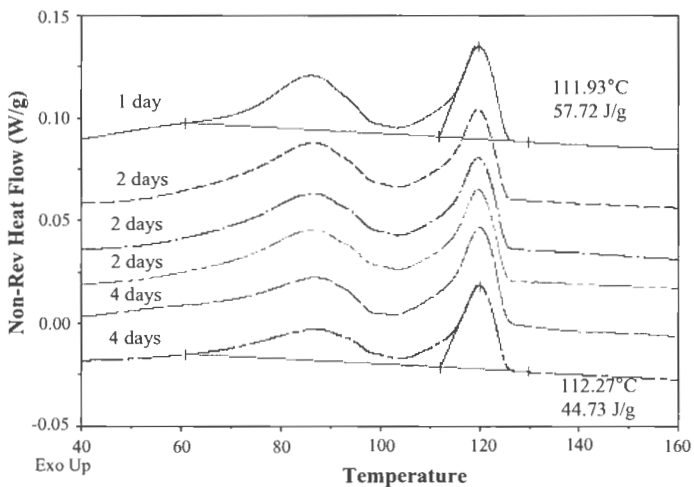


Figure E-4

MDSC nonreversing heat flow scans of amorphous griseofulvin undergoing isothermal crystallization at 43%RH.

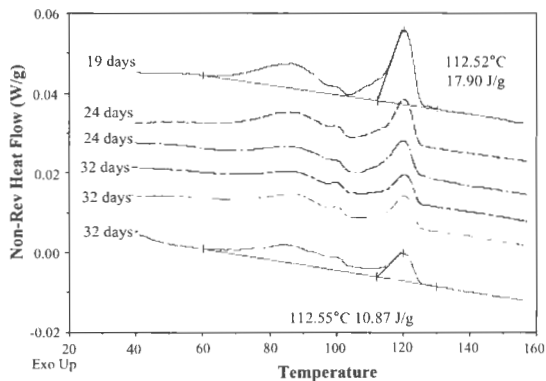
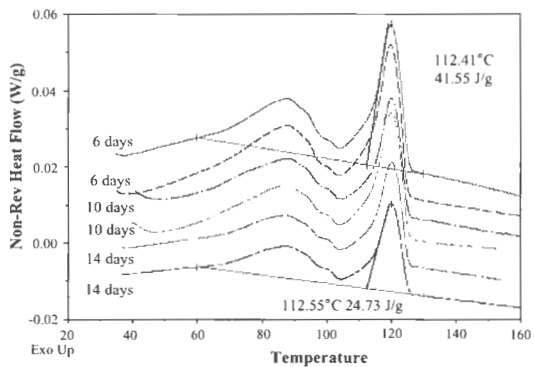


Figure E-5

MDSC nonreversing heat flow scans of amorphous griseofulvin undergoing isothermal crystallization at 32%RH.

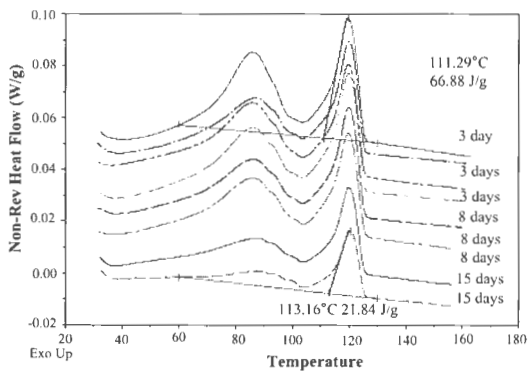
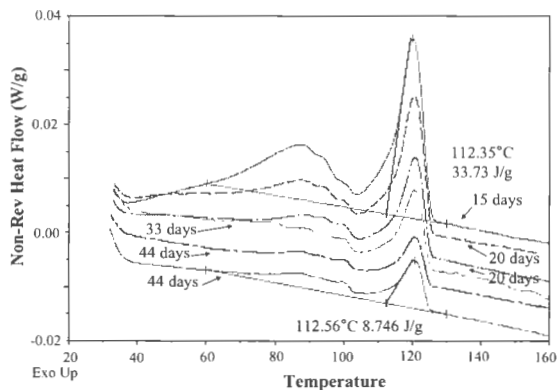
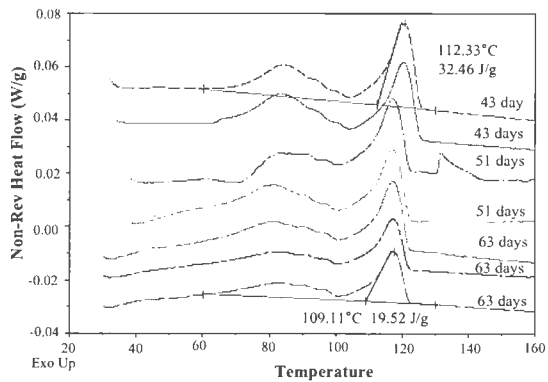
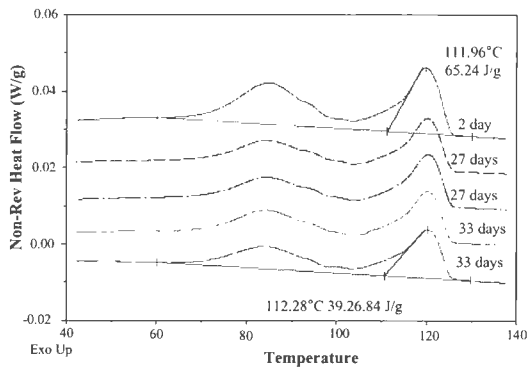


Figure E-6

MDSC nonreversing heat flow scans of amorphous griseofulvin undergoing isothermal crystallization at 0%RH.



Choosing appropriate rate equation to fit the isothermal crystallization data of amorphous griseofulvin: Hancock-Sharp equation and KJMA equation

To determine the crystallization rate constant for the isothermal griseofulvin crystallization, the fraction of griseofulvin crystallized with storage time is fit to the Hancock-Sharp equation.

$$\ln[-\ln(1-\alpha)] = \ln B + m \ln t \quad (\text{A5-1})$$

where α the fraction of drug that has crystallized, t is the storage time, B is a constant and m is a constant relating to the mechanism of griseofulvin crystallization.

The kinetic equations for the most common mechanisms that are believed to operate in solid-state alteration are presented in Table B-IV-III, chapter 4.

In order to find the equation that best fits the crystallization rate, the equation that has the m value closest to the slope obtained in the Hancock-Sharp fit was chosen, which is KJMA rate equation ($m = 1$). To counter-verify, the crystallization data obtained is fit to all the equations listed in Table B-IV-III, chapter 4.

Table E-III: Fit of crystallization data to various kinetic rate equations. KJMA; F1 - $-\ln(1-\alpha)$ rate equation was chosen since the m value from Hancock-Sharp fit was closest to 1.00. Also the R2 value with KJMA fit was 0.9918, which can be considered very well.

time	α	$1-(1-\alpha)^{1/2}$	$1-(1-\alpha)^{1/3}$	$-\ln(1-\alpha)$ KJMA	$[-\ln(1-\alpha)]^{1/2}$
0	0	0.666667	0	0	0
1	4.2	0.680667	0.021225	0.042908	0.021454
2	3.810673	0.679369	0.019238	0.038852	0.019426
4	22.70178	0.742339	0.120806	0.257499	0.12875
6	29.10884	0.763696	0.158031	0.344024	0.172012
10	41.224	0.80408	0.233345	0.531437	0.265718
14	57.15011	0.857167	0.345402	0.847467	0.423734
19	72.4521	0.908174	0.475139	1.289244	0.644622
24	83.08537	0.943618	0.588726	1.776991	0.888496
32	86.92267	0.956409	0.638374	2.03429	1.017145
40	92.89982	0.976333	0.733538	2.64505	1.322525
R²	0.9044	0.9639	0.9044	0.9918	0.9918
slope	2.502	0.0196	0.0083	0.0678	0.0339

time	$[-\ln(1-\alpha)]^{1/3}$	α^2	$(1-\alpha)\ln(1-\alpha) + \alpha$
0	0	0	0
1	0.014303	0.001764	0.000895
2	0.012951	0.001452	0.000735
4	0.085833	0.051537	0.027975
6	0.114675	0.084732	0.047205
10	0.177146	0.169942	0.099883
14	0.282489	0.326613	0.208362
19	0.429748	0.524931	0.369361
24	0.59233	0.690318	0.530282
32	0.678097	0.755555	0.603196
40	0.881683	0.863038	0.741195
R²	0.9918	0.9666	0.9775
slope	0.0226	0.0244	0.0202

time	$[1 - (1 - \alpha)^{1/3}]^2$	$(1 - 2\alpha/3) - (1 - \alpha)^{2/3}$
0	0.444444	0.666667
1	0.463307	-5.21333
2	0.461542	-4.17374
4	0.551068	-171.124
6	0.583232	-281.775
10	0.646545	-565.806
14	0.734735	-1088.04
19	0.824779	-1749.1
24	0.890415	-2300.39
32	0.914718	-2517.85
40	0.953226	-2876.13
R²	0.9249	0.9666
slope	0.0138	-81.391

Figure E-7

Demonstration of the griseofulvin crystallization data fit to various equations

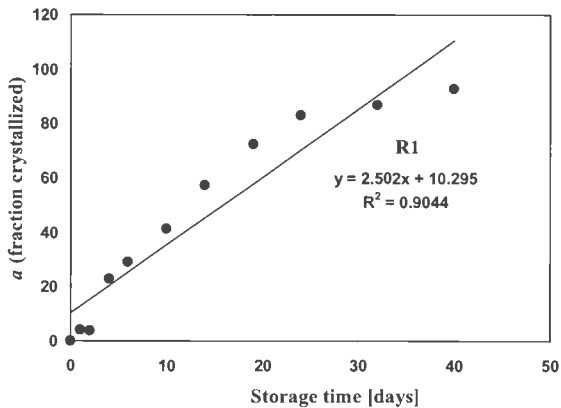
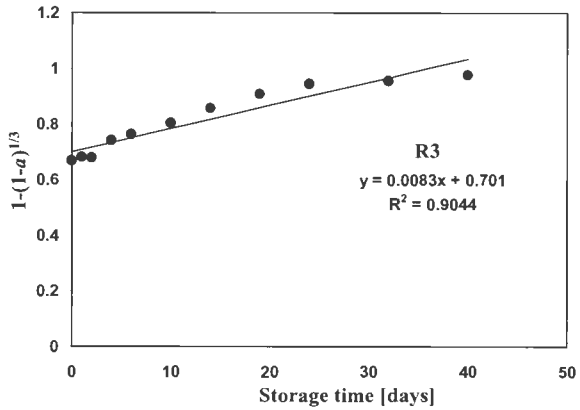
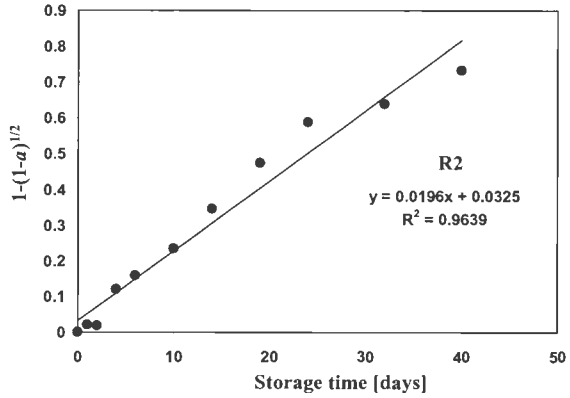
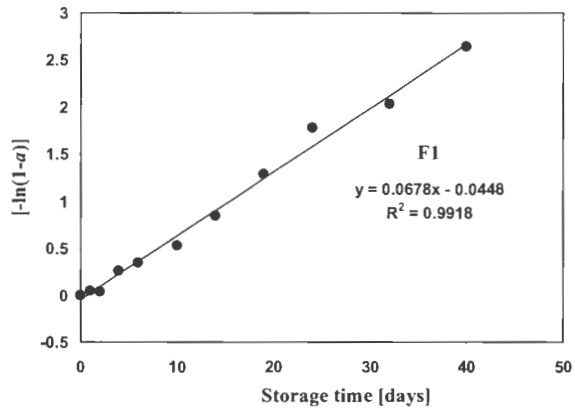
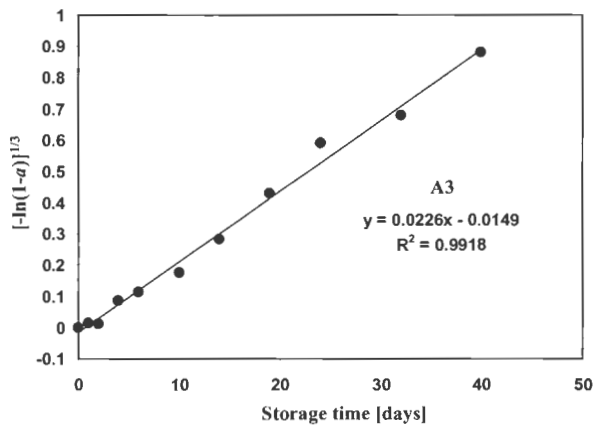
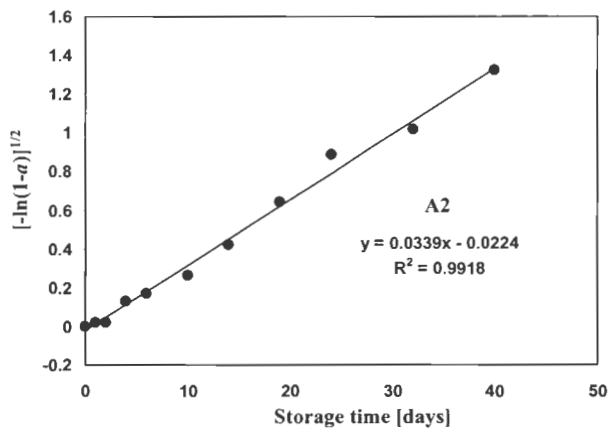
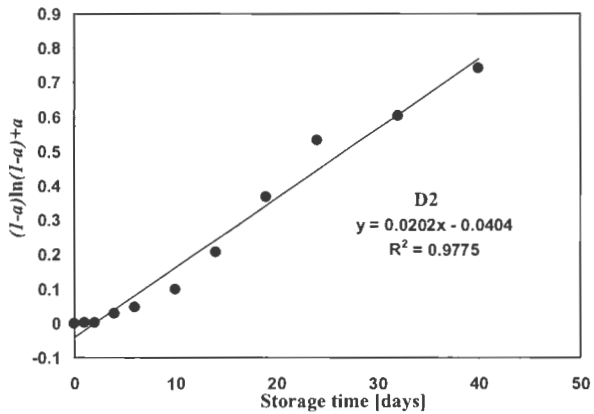
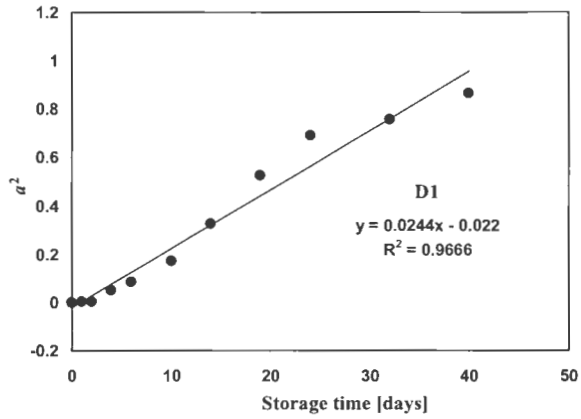


Figure E-7 (contd.)









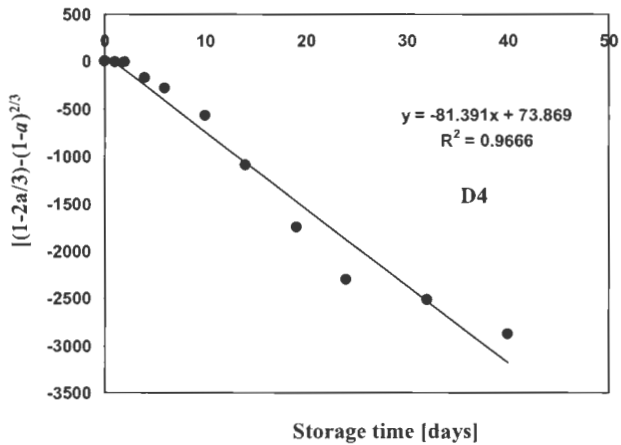
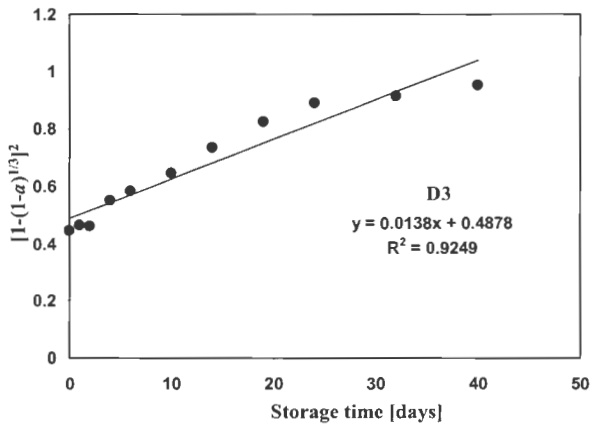


Table E-IV: Fit of griseofulvin crystallization data at 0%, 32% and 43% RH to the KJMA rate equation. Average of n=3 repetitions were fit to the equation.

0% RH			32%RH		
time	α	$-\ln(1-\alpha)$ KJMA	time	α	$-\ln(1-\alpha)$ KJMA
0	0	0	0	0	0
2	2.05	0.020713	1	0	0
26	35.97909	0.44596	3	0	0
36	38.053	0.478891	5	7.283242	0.075621
43	45.45099	0.606071	8	18.10035	0.199675
51	53.46397	0.764943	15	45.143	0.60044
63	69.22366	1.178424	20	65.146	1.054002
			25	83.152	1.321254
			33	79.82443	1.600698
			44	87.79331	2.103186
R²	0.9555		R²		0.9885
slope	0.0169		slope		0.0509

43%RH		
time	α	$-\ln(1-\alpha)$ KJMA
0	0	0
1	4.2	0.042908
2	3.810673	0.038852
4	22.70178	0.257499
6	29.10884	0.344024
10	41.224	0.531437
14	57.15011	0.847467
19	72.4521	1.289244
24	83.08537	1.776991
32	86.92267	2.03429
40	92.89982	2.64505
R²		0.9918
slope		0.0678

APPENDIX F

Measurement of sub-glass transition molecular motions of Poly (vinyl pyrrolidone): comparison of the utility of thermally stimulated current (TSC) and modulated differential scanning calorimeter (MDSC)

(Supporting data to Manuscript V)

Figure F-1

Reproducibility scans to demonstrate the heat capacity change and glass transition temperature in PVP K17

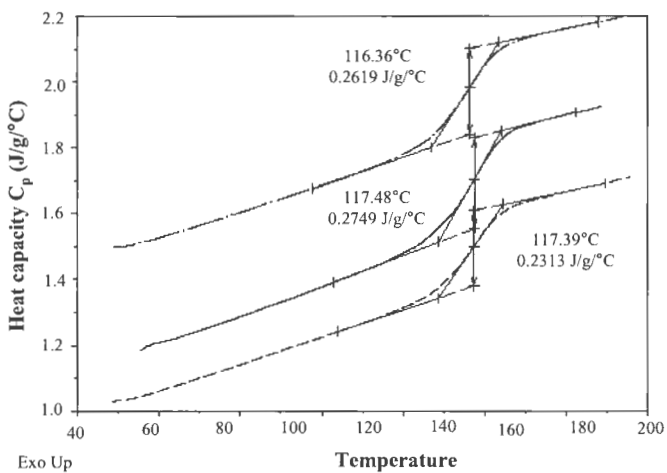


Figure F-2

Reproducibility scans to demonstrate the heat capacity change and glass transition temperature in PVP K30

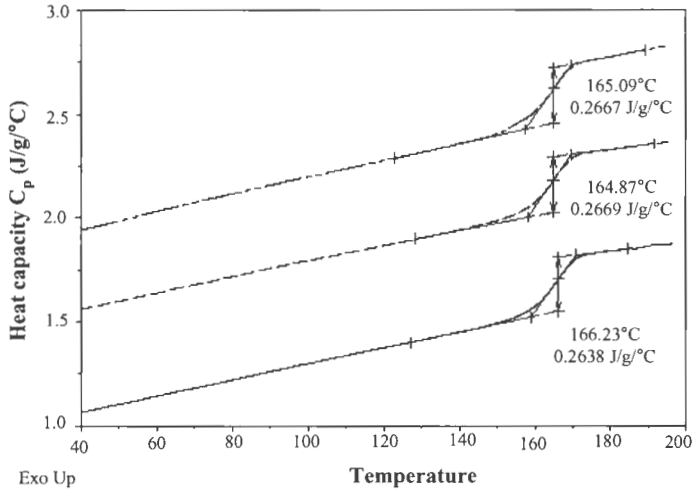


Figure F-3

Reproducibility scans to demonstrate the heat capacity change and glass transition temperature in PVP K90

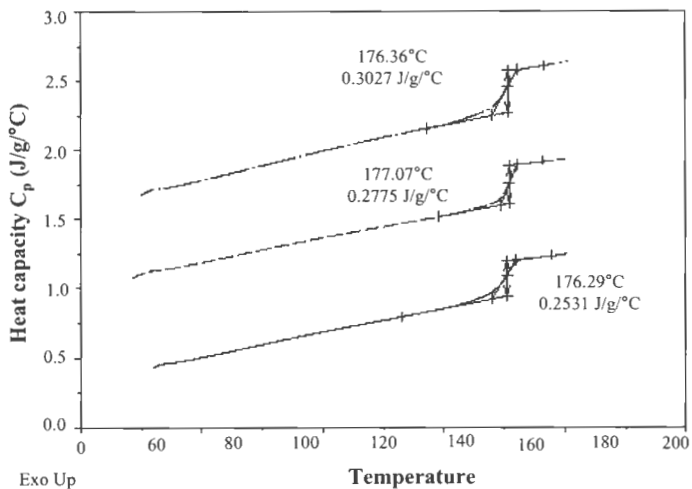


Figure F-4

MDSC non-reversing heat flow scans of PVP K17 exhibiting enthalpy relaxation when subjected to 5°C below their glass transition temperature of 117°C. The area under the non-reversing heat flow increases, indicating progressive enthalpy relaxation to the equilibrium supercooled state.

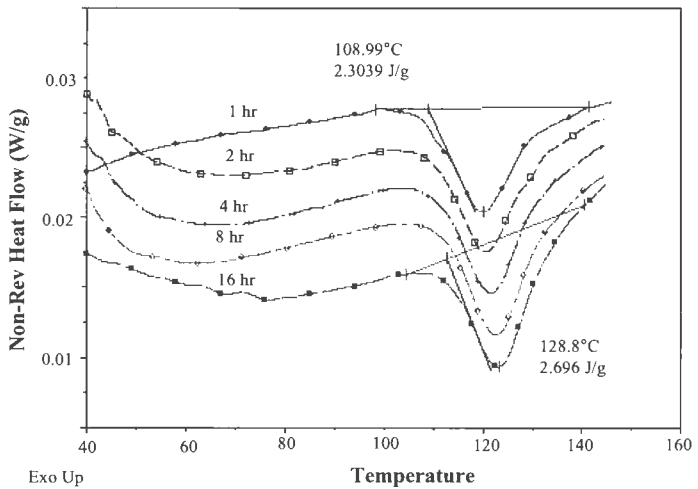


Figure F-5

MDSC non-reversing heat flow scans of PVP K17 undergoing enthalpy relaxation at storage temperature 15°C below 117°C.

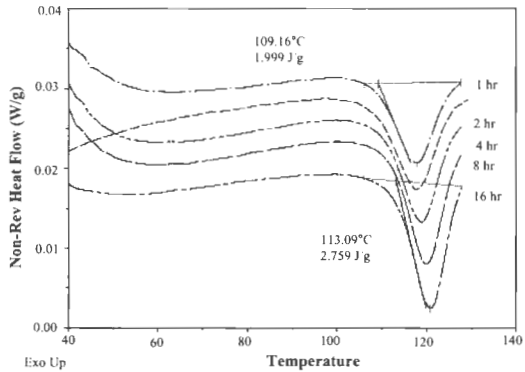


Figure F-6

MDSC non-reversing heat flow scans of PVP K17 undergoing enthalpy relaxation at storage temperature 30°C below 117°C.

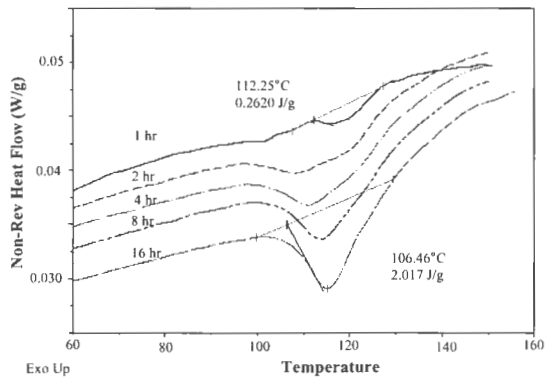


Figure F-7

MDSC non-reversing heat flow scans of PVP K30 undergoing enthalpy relaxation at storage temperature 5°C below 166°C.

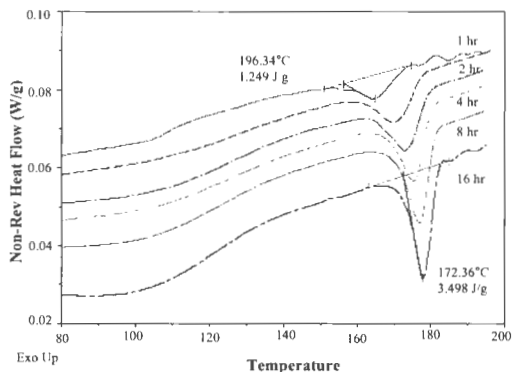


Figure F-8

MDSC non-reversing heat flow scans of PVP K30 undergoing enthalpy relaxation at storage temperature 15°C below 166°C.

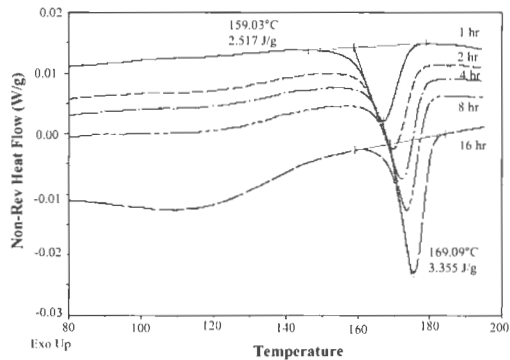


Figure F-9

MDSC non-reversing heat flow scans of PVP K30 undergoing enthalpy relaxation at storage temperature 30°C below 166°C.

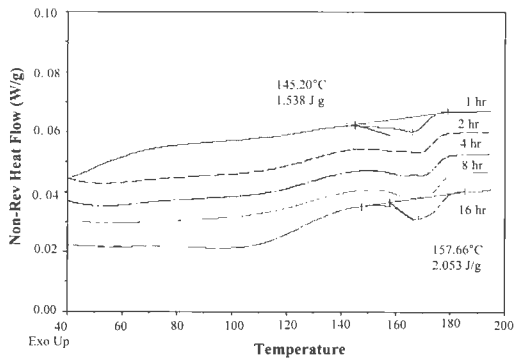


Figure F-10

MDSC non-reversing heat flow scans of PVP K90 undergoing enthalpy relaxation at storage temperature 5°C below 175°C.

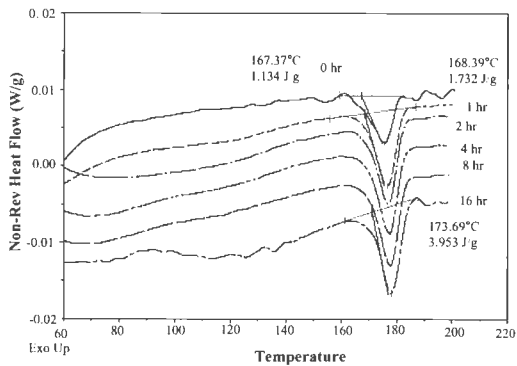


Figure F-11

MDSC non-reversing heat flow scans of PVP K90 undergoing enthalpy relaxation at storage temperature 15°C below 175°C.

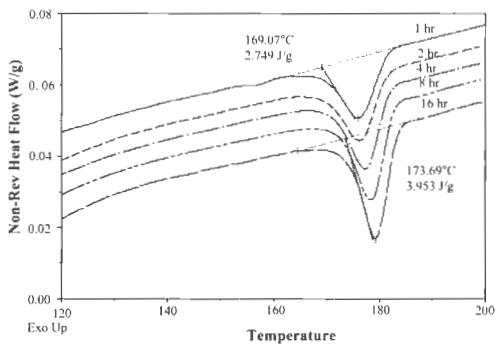
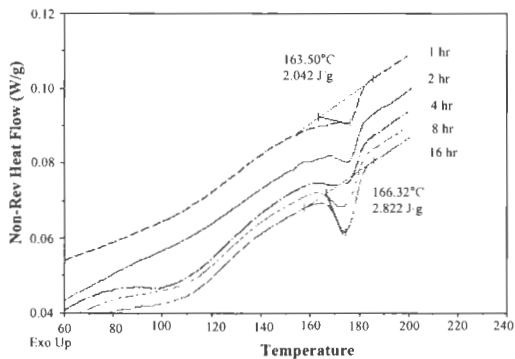


Figure F-12

MDSC non-reversing heat flow scans of PVP K90 undergoing enthalpy relaxation at storage temperature 30°C below 175°C.



BIBLIOGRAPHY

- Ahmed H., Buckton G., and Rawlins D. Crystallization of partially amorphous griseofulvin in water vapour: determination of kinetic parameter using isothermal heat conduction microcalorimetry. *International Journal of Pharmaceutics*. 167:139-145 (1998).
- Andronis V., and Zografí G. Molecular mobility of supercooled amorphous indomethacin, determined by dynamic mechanical analysis. *Pharmaceutical Research*. 14:410-414 (1997).
- Andronis V., Yoshioka M. and Zografí G. Effects of sorbed water on the crystallization of indomethacin from the amorphous state. *Journal of Pharmaceutical Sciences*. 86:346-351 (1997).
- Angell C. A. Formation of glasses from liquids and biopolymers. *Science*. 267:1924-1935 (1995).
- Aso Y., Yoshioka S. and Kojima S. Explanation of the crystallization rate of amorphous nifedipine and Phenobarbital from their molecular mobility as measured by ¹³C nuclear magnetic resonance relaxation time and the relaxation time obtained from the heating rate dependence of the glass transition temperature. *Journal of Pharmaceutical Sciences*. 90:798-806 (2001).
- Aso Y., Yoshioka S., and Kojima S. Relationship between the crystallization rates of amorphous nifedipine, Phenobarbital, and flopropione, and their molecular mobility as measured by their enthalpy relaxation and ¹H NMR relaxation times. *Journal of Pharmaceutical Sciences*. 89:408-416 (2000).
- Aso Y., Yoshioka S., Otsuka T., and Kojima S. The physical stability of amorphous nifedipine determined by isothermal microcalorimetry. *Chemical and Pharmaceutical Bulletin*. 43:300-303 (1995).
- Aungst J., Nguyen N. H., Rogers N. J., Rowe S. M., Hussain M. A., White S. J., and Shum L. Amphiphilic vehicles improve the oral bioavailability of a poorly soluble HIV protease inhibitor at high doses. *International Journal of Pharmaceutics*. 156:79-88 (1997).

- Briggner L. E., Buckton G., Bystrom K. and Darcy P. The use of isothermal microcalorimetry in the study of changes in crystallinity induced during the processing of powders *International Journal of Pharmaceutics*. **105**:125-135 (1994).
- Brunacci, Pedemonte E., Cowie J. M. G., and MeEwen I. J. The thermodynamics of mixing of polystyrene and poly(α -methylstyrene) from a calorimetric viewpoint. *Polymer*. **35**:2893-2896 (1994).
- Carstensen J. T. and Scoik K. V. Amorphous-to-crystalline transformation of sucrose. *Pharmaceutical Research*. **7**:1278-1281 (1991).
- Chang I., Fujara F., Geil B., Heuberger G., Mangel T., Sillescu H. J. Translational and rotational molecular motion in supercooled liquids studied by NMR and forced rayleigh scattering. *Journal of Non Crystalline Solids* **172-174**: 248-255 (1994).
- Chee K. K. Thermodynamic study of glass transitions in miscible polymer blends. *Polymer*. **36**:809-813 (1995).
- Chiou W. L., and Riegelman S. Pharmaceutical applications of solid dispersion systems. *Journal of Pharmaceutical Sciences*. **60**:1281-1302 (1971).
- Chowdary K. P. R., and Rao P. V. Evaluation of some modified starches as carriers for solid dispersions. *Indian Drugs*. **29**:224-227 (1991).
- Chun Y. S., Han Y. S., Hyun J. C., and Kim W. N. Glass transition temperatures and rigid amorphous fraction of poly (ether ether ketone) and polyarylate blends. *Polymer* **41**:8717-8720 (2000).
- Coleman E. A study of the crystallization of some binary metallic glasses. M. Sc. Thesis, Rutgers, The State University of New Jersey. (1979).
- Coleman M. M., Graf J. F. and Painter P. C. *Specific interactions and the miscibility of polymer blends*. Technomic Publishing, Lancaster, Basel, 1991.

- Collins G. and Long B. A thermally stimulated current/relaxation map analysis of the relaxation process in aromatic polyester, liquid crystal polymer film. *Journal of Applied Polymer Science*. 53:587-608 (1994).
- Couchman P. R., and Karasz F. E. A classical thermodynamic discussion on the effect of composition on glass-transition temperatures. *Macromolecules* 11:117-119 (1978).
- Cowie J. M. G., Harris S., and McEwen I. J. Physical ageing in poly(vinylacetate) 1. enthalpy relaxation. *Journal of Polymer Sciences B: Polymer Physics* 35:1107-1116 (1997).
- Craig D. Q. M., Kett V. L., Murphy J. R., and Price D. M. The measurement of small quantities of amorphous material – should we be considering the rigid amorphous fraction? *Pharmaceutical Research*. 18:1081-1082 (2001).
- Craig D. Q. M.. The mechanism of drug release from solid dispersions in water soluble polymers. *International Journal of Pharmaceutics*. 231:131-144 (2002).
- Crowley K. J. and Zografi G. The effect of low concentrations of molecularly dispersed poly(vinylpyrrolidone) on indomethacin crystallization from the amorphous state. *Pharmaceutical Research*. 20:1417-1422 (2003).
- Doherty C., and York P. Accelerated stability of an X-ray amorphous furosemide-poly (vinyl pyrrolidone) solid dispersion. *Drug Development and Industrial Pharmacy*. 15:1969-1987 (1989).
- Dordunoo S. K., Ford J. L., and Rubinstein M. H. Physical stability of solid dispersions containing triamterene or temazepam in polyethylene glycols. *Journal of Pharmacy and Pharmacology*. 49:390-396 (1997).
- Duddu S. P., and Sokoloski T. D. Dielectric analysis in the characterization of amorphous pharmaceutical solids. 1. Molecular mobility in poly(vinylpyrrolidone)-water systems in the glassy state. *Journal of Pharmaceutical Sciences*. 84:773-776 (1995).

- Duncan-Hewitt W. C. and Grant D. J. W. True density and thermal expansivity of pharmaceutical solids: comparison of methods and assessment of crystallinity. *International Journal of Pharmaceutics*. **28**:75-84 (1986)
- Ediger M. D., Angell C. A., and Nagel S. R. Supercooled liquids and glasses. *Journal of Physical Chemistry*. **100**:13200-13212 (1996).
- Ford J. L. The current status of solid dispersions. *Pharmaceutica Acta Helvetia*. **61**:69-88 (1986).
- Forster A., Rades T., and Hempenstall J. Selection of suitable drug and excipient candidates to prepare glass solutions by melt extrusion for immediate release oral formulations. *Pharmaceutical Technology Europe*. October:27-37 (2002).
- Galop M and Collins G. L. Thermally stimulated currents observed in pharmaceutical products. *Thermochemica Acta*. **6436**:1-5 (2000).
- Gines J. M., Veiga M. D., Arias M. J., Rabasco A. M. Elaboration and thermal study of interactions between cinnarizine and gelucire[®] 53/10 physical mixtures and solid dispersions. *International Journal of Pharmaceutics* **126**:287-291 (1995).
- Goitiandia L., and Alegria A. Physical aging of poly(vinylacetate). A thermally stimulated depolarization current investigation. *Journal of Non-Crystalline Solids*. **287**:237-241 (2001).
- Grant D. J. W. and York P. A disruption index for quantifying the solid state disorder induced by additives or impurities. II. Evaluation from heat of solution. *International Journal of Pharmaceutics*. **28**:103-112 (1986).
- Hancock B. C., and Parks M. What is the true solubility advantage for amorphous pharmaceuticals? *Pharmaceutical Research* **17**:397-404 (2000).
- Hancock B. C., and Zografi G. The relationship between the glass transition temperature and the water content of amorphous pharmaceutical solids. *Pharmaceutical Research*. **11**:471-477 (1994).

- Hancock B. C., Shamblin S. L. and Zografi G. Molecular mobility of amorphous pharmaceutical solids below their glass transition temperatures. *Pharmaceutical Research*. 12:799-806 (1995).
- Hancock C., Shamblin S. L. and Zografi G. Molecular mobility of amorphous pharmaceutical solids below their glass transition temperatures. *Pharmaceutical Research*. 12:799-806 (1995).
- Hendriksen. Characterization of calcium fenoprofen 1. Powder dissolution rate and degree of crystallinity. *International Journal of Pharmaceutics*. 60:243-252 (1990).
- Jain S. K., and Johari G. P. *Journal of Physical Chemistry*. 92:5851-5854 (1988).
- Jeffrey G. A., and Saenger W. *Hydrogen bonding in biological structures*. Springer-Verlag Berlin Heidelberg, New York. 1991.
- Khan G. M., and Jiabi Z. Preparation, characterization and dissolution of ibuprofen solid dispersions using polyethylene glycol (PEG), talc, and PEG-talc as dispersion carriers. *Drug Development and Industrial Pharmacy*. 24:455-462 (1998).
- Khougaz K., and Clas S. Crystallization inhibition in solid dispersions of MK-0591 and poly(vinylpyrrolidone) polymers. *Journal of Pharmaceutical Sciences*. 89:1325-1334 (2000).
- Kissinger H. E. Reaction kinetics in differential thermal analysis. *Analytical Chemistry*. 29:1702-1706 (1957).
- Kissinger H. E. Variation of peak temperature with heating rate in differential thermal analysis. *Journal of Research in National Bureau Standards*. 57:217-221 (1956).
- Lee H. S., and Kim W. N. Glass transition temperatures and rigid amorphous fraction of poly(ether ether ketone) and poly(ether imide) blends. *Polymer* 38:2657-2663 (1997).

- Lee T. W., and Robinson J. R. Controlled-release drug delivery systems. In *Remington, The science and practice of pharmacy, 20th edition*. Lippincott Williams and Wilkins, Maryland. 903-929.
- Leuner C. and Dressman J. Improving drug solubility for oral delivery using solid dispersion. *European Journal of Pharmaceutics and Biopharmaceutics*. 50:47-60 (2000).
- Levy G. *American Journal of Pharmaceutics*. 135:78- (1963).
- Lin C., and Cham T. Effect of particle size on the available surface area of nifedipine from nifedipine-polyethylene glycol 6000 solid dispersions. *International Journal of Pharmaceutics*. 127:261-272 (1996).
- Lu Q., and Zografi G. Phase behaviour of binary and ternary amorphous mixtures containing indomethacin, citric acid, and PVP. *Pharmaceutical Research*. 15:1202-1206 (1998).
- Lu X. and Weiss R. A. Relationship between the glass transition temperature and the interaction parameter of miscible binary polymer blends. *Macromolecules*. 25:3242-3246 (1992).
- Matsuda Y., and Kawaguchi S.. Physicochemical characterization of oxyphenbutazone and solid-state stability of its amorphous form under various temperature and humidity conditions. *Chemical and Pharmaceutical Bulletin*. 34:1289-1298 (1986).
- Matsumoto T., and Zografi G. Physical properties of solid molecular dispersions of indomethacin with poly(vinylpyrrolidone) and poly(vinylpyrrolidone-co-vinylacetate) in relation to indomethacin crystallization. *Pharmaceutical Research*. 16:1722-1728 (1999).
- Medlicott N. J., Foster K. A., Audus K. L., Gupta S. and Stella V. J.. Comparison of the effects of potential parenteral vehicles for poorly water soluble anticancer drugs (organic cosolvents and cyclodextrins solutions) on cultured endothelial cells (HUV-EC). *Journal of Pharmaceutical Sciences*. 87:1138-1143 (1998).

- Molyneux P. *Water-soluble synthetic polymer: properties and behavior*, Volume I, CRC Press, Florida. 1983.
- Montserrat S. Physical aging studies in epoxy resins. I. Kinetics of the enthalpy relaxation process in a fully cured epoxy resin. *Journal of Polymer Science (Polymer Physics Edition)* **32**:509-522 (1994).
- Moskala J., Varnell D. F., and Coleman M. M. Concerning the miscibility of poly(vinylphenol) blends – FTIR. study. *Polymer*. **26**:228-234 (1985).
- Moustafa M. A. and Carless J. E. Application of differential scanning calorimetry to the study of sulphathiazole crystal forms. *Journal of Pharmacy and Pharmacology* **21**:359-365 (1969).
- Moustafa M. A., Khalil S. A, Ebian A. R. and Motawi M. M. Succinylsulfathiazole crystal forms I: preparation, characterization, and interconversion of different crystal forms. *Journal of Pharmaceutical Sciences*. **63**:1103-1109 (1974).
- Mullin J. W. *Crystallization*; Butterworth Heinemann: Oxford, 1992.
- Mumenthaler M. and Leuenberger H. Atmospheric spray freeze-drying: A suitable alternative in freeze-drying technology. *International Journal of Pharmaceutics*. **72**:97-110 (1991).
- Nakai Y., Fukuoka E., Nakajima S. and Hasegawa J. Crystallinity and physical characteristics of microcrystalline cellulose. *Chemical and Pharmaceutical Bulletin*. **25**:96-101 (1977).
- Nakamachi H., Wada Y., Aoki I., Kodama Y. and Kuroda K. Effect of a minor component on thermal transformation of crystalline 6-mercaptopurine. *Chemical and Pharmaceutical Bulletin*. **29**:2956-2965 (1981).
- Nyqvist H. Saturated salt solutions for maintaining specified relative humidities. *International Journal of Pharmaceutical Technology and Production Manufacturers*. **4**:47-48 (1983).

- Oksanen C. A., and Zografi G. Molecular mobility in mixtures of absorbed water and solid poly(vinylpyrrolidone). *Pharmaceutical Research*. 10:791-799 (1993).
- Otsuka M. and Kaneniwa N. A kinetic study of the crystallization process of noncrystalline indomethacin under isothermal conditions. *Chemical and Pharmaceutical bulletin*. 36:4026-4032 (1988).
- Painter P. C., Park Y., and Coleman M. M. Hydrogen bonding in polymer blends. 2. Theory. *Macromolecules*. 21:66-72 (1988).
- Peng Y., Kerney A. S., Patel K., Palepu N. R., and Zuber G. Investigation of formulation approaches to improve the dissolution of SB-210661, a poorly water soluble 5-lipoxygenase inhibitor. *International Journal of Pharmaceutics*. 176:31-38 (1998).
- Pikal M. J. and Shah S. The collapse temperature in freeze drying: dependence on measurement methodology and rate of water removal from the glassy phase. *International Journal of Pharmaceutics*. 62:165-186 (1990).
- Pikal M. J., Lukes A. L., Lang J. E. and Gaines K. Quantitative crystallinity determinations for β -lactam antibiotics by solution calorimetry: correlations with stability. *Journal of Pharmaceutical Sciences*. 67:767-773 (1978).
- Poole P. H., Grande T., Angell C. A., and McMillan P. F. Polymorphic phase transitions in liquids and glasses. *Science*. 275:322-323 (1997).
- Saleki-Gerhardt and Zografi G. Non-Isothermal and Isothermal Crystallization of Sucrose from the Amorphous State. *Pharmaceutical Research*. 11:1166-1173 (1994).
- Saleki-Gerhardt, Ahineck C. and Zografi G. Assessment of disorder in crystalline solids. *International Journal of Pharmaceutics*. 101:237-247 (1994).
- Sasabe H., and Moynihan C. T. Structural relaxation in poly(vinylacetate). *Journal of Polymer Science: Polymer Physics Edition*. 16:1447-1457 (1978).

- Schmitt E. A., Law D. and Zhang G. Z. Nucleation and crystallization kinetics of hydrated amorphous lactose above the glass transition temperature. *Journal of Pharmaceutical Sciences*. **88**:291-296 (1999).
- Sebhatu T., Angberg M. and Ahlneck C. Assessment of the degree of disorder in crystalline solids by isothermal microcalorimetry. *International Journal of Pharmaceutics*. **104**:135-144 (1994).
- Sekiguchi K., and Obi N. Studies on absorption of eutectic mixture. I. A comparison of the behavior of eutectic mixture of sulfathiazole and that of ordinary sulfathiazole in man. *Chemical and Pharmaceutical Bulletin*. **9**:866-872 (1961).
- Serajuddin A. T. M. Recent advances in the formulation of solid dispersion systems for poorly water-soluble drugs. Abstract for symposium at the 2004 *American Association of Pharmaceutical Scientists Annual Meeting and Exposition*, Baltimore, MD November 7-11, 2004.
- Serajuddin A. T. M. Solid dispersion of poorly water-soluble drugs: early promises, subsequent problems, and recent breakthroughs. *Journal of Pharmaceutical Sciences*. **88**:1058-1066 (1999).
- Serajuddin A. T. M., Sheen P. C., Augustine M. A. Improved dissolution of a poorly water-soluble drug from solid dispersions in poly(ethylene glycol) polysorbate 80 mixtures. *Journal of Pharmaceutical Sciences*. **79**:463-464 (1990).
- Serajuddin A. T. M., Sheen P. C., Mufson D., Bernstein D. F., Augustine M. A. Effect of vehicle amphiphilicity on the dissolution and bioavailability of a poorly water-soluble drug from solid dispersions. *Journal of Pharmaceutical Sciences*. **77**:414-417 (1988).
- Serajuddin A. T. M., Sheen P. C., Mufson D., Bernstein D. F., Augustine M. A. Physicochemical basis of increased bioavailability of a poorly water-soluble drug following oral administration as organic solutions. *Journal of Pharmaceutical Sciences*. **77**:325-329 (1988).
- Sethia S., and Squillante E. Physicochemical characterization of solid dispersions of carbamazepine formulated by supercritical carbon dioxide and conventional solvent evaporation method. *Journal of Pharmaceutical Sciences*. **91**:1948 (2002).

- Shalaev E. Y., and Zografi G. How does residual water affect the solid-state degradation of drugs in the amorphous state? *Journal of Pharmaceutical Sciences*. **85**:1137-1141 (1996).
- Shamblin S. L., and Zografi G. Enthalpy relaxation in binary amorphous mixtures containing sucrose. *Pharmaceutical Research*. **15**:1828-1834 (1998).
- Shamblin S. L., and Zografi G. The effects of absorbed water on the properties of amorphous mixtures containing sucrose. *Pharmaceutical Research*. **16**:1119-1124 (1999).
- Shamblin S. L., Hancock B. C., Dupuis Y., and Pikal M. J. Interpretation of relaxation time constants for amorphous pharmaceutical systems. *Journal of Pharmaceutical Sciences*. **89**:417-427 (2000).
- Shamblin S. L., Taylor L. S., and Zografi G. Mixing behavior of colyophilized binary systems. *Journal of Pharmaceutical Sciences*. **87**:694-701 (1998).
- Shami E. G., Bernardo P. D., Rattie E. S. and Ravin L. J. Kinetics of polymorphic transformation of sulfathiazole form I. *Journal of Pharmaceutical Sciences*. **61**:1318-1320 (1972).
- Sheen P. C., Khetarpal V. K., Cariola C. M., and Rowlings C. E. Formulation studies of a poorly water soluble drug in solid dispersion to improve bioavailability. *International Journal of Pharmaceutics*. **118**:221-227 (1995).
- Shen S. and Torkelson J. M. Miscibility and phase separation in poly(methyl methacrylate)/Poly(vinyl chloride) blends: study of thermodynamics by thermal analysis. *Macromolecules*. **25**:721-728 (1992).
- Simonelli A. P., Mehta S. C., and Higuchi W. I. Dissolution rates of high energy polyvinylpyrrolidone(PVP)-sulfathiazole co precipitates. *Journal of Pharmaceutical Sciences*. **58**:538-549 (1969).

- Six K., Berghmans H., Leuner C., Dressman J., Werde K. V., Mullens J., Benoist L., Thimon M., Meublât L., Verreck G., Peeters J., Brewster M., and Mooter G. V. Characterization of solid dispersions of itraconazole and hydroxypropylmethylcellulose prepared by melt extrusion, part II. *Pharmaceutical Research*. **20**:1047-1054 (2003).
- Sugimoto I., Kuchiki A., and Nakagawa H. Stability of nifedipine-polyvinylpyrrolidone coprecipitate. *Chemical and Pharmaceutical Bulletin*. **29**:1715-1723 (1981).
- Sussuch F., Urbani R., Princivale F., and Cesaro A. Polymorphic amorphous and crystalline forms of trehalose. *Journal of American Chemical Society*. **120**:7893 – 7899 (1998).
- Suzuki H., and Sunanda H. Some factors influencing the dissolution of solid dispersions with nicotinamide and hydroxypropylmethylcellulose as combined carriers. *Chemical and Pharmaceutical Bulletin*. **46**:1015-1020 (1998).
- Tang X. C., Pikal M. J., and Taylor L. S. The effect of temperature on hydrogen bonding in crystalline and amorphous phases in dihydropyridine calcium channel blockers. *Pharmaceutical Research* **19**:484-490 (2002).
- Taylor L. S. and York P. Characterization of phase transitions of trehalose dihydrate on heating and subsequent dehydration. *Journal of Pharmaceutical Sciences*. **87**:347-355 (1998).
- Taylor L. S. and Zografi G. Spectroscopic characterization of interactions between PVP and indomethacin in amorphous molecular dispersions. *Pharmaceutical Research*. **14**:1691-1698 (1997).
- Taylor L. S. and Zografi G. Sugar-polymer hydrogen bond interactions in lyophilized amorphous mixtures. *Journal of Pharmaceutical Sciences*. **87**:1615-1621 (1998).
- Torrado S., Torrado S., Torrado J. J., and Cadorniga R. Preparation, dissolution and characterization of albendazole solid dispersions. *International Journal of Pharmaceutics*. **140**:247-250 (1996).

- Turnbull D., Fisher J. C. Rate of nucleation in condensed systems. *Journal of Chemical Physics*. 17:71-73 (1949)
- Vasanthavada M., Tong W., Joshi Y. and Kislalioglu M. S. Phase behavior of amorphous molecular dispersions: determination of the degree and mechanism of solid miscibility. *Pharmaceutical Research*. Accepted. In press.
- Verreck G., Six K., Mooter G. V., Baert L., Peeters J., and Brewster M. E.. Characterization of solid dispersions of itraconazole and hydroxypropylmethylcellulose prepared by melt extrusion-part I. *International Journal of Pharmaceutics*. 251:165-174 (2003).
- Vudatha G. K., and Rogers J. A. Oral bioavailability of griseofulvin from aged griseofulvin-lipid co-precipitates: *in vitro* studies in rats. *Journal of Pharmaceutical Sciences*. 81:1166-1169 (1992).
- Wade A., and Weller P. J. *Handbook of pharmaceutical excipients*. Second edition. The Pharmaceutical Press, London. 1994.
- Williams G. and Watts D. C. Non-symmetrical dielectric relaxation behavior arising from a simple empirical decay function. *Transactions in Faraday Society*. 66:80-85 (1970).
- Woldt E. The relationship between isothermal and nonisothermal description of Johnson-Mehl-Avrami-Kolmogorov kinetics. *Journal of Physical and Chemical Solids* 53:521-527 (1992).
- Wulff M., Alden M., and Craig D. Q. M. An investigation into the critical surfactant concentration for solid solubility of hydrophobic drug in different polyethylene glycols. *International Journal of Pharmaceutics*. 142:189-198 (1996).
- Wulff M., and Alden M. Phase equilibria in drug-polymer-surfactant systems. *Thermochimica Acta*. 256:151-165 (1995).
- York P. Solid-state properties of powders in the formulation and processing of solid dosage forms. *International Journal of Pharmaceutics*. 14:1-28 (1983).

- Yoshioka M., Hancock B. C. and Zografi G. Crystallization of indomethacin from the amorphous state below and above its glass transition temperature. *Journal of Pharmaceutical Sciences*. **83**:1700-1705 (1994).
- Yoshioka M., Hancock B. C. and Zografi G. Inhibition of indomethacin crystallization in poly(vinylpyrrolidone) coprecipitates. *Journal of Pharmaceutical Sciences*. **84**:983-986 (1995).
- Yoshioka M., Hancock B. C., and Zografi G. Crystallization of indomethacin from the amorphous state below and above its glass transition temperature *Journal of Pharmaceutical Sciences*. **83**:1700-1705 (1994).
- Yu L. Amorphous pharmaceutical solids: preparation, characterization and stabilization. *Advanced Drug Delivery Reviews* **48**:27-42 (2001).